

**Energy Transfer and –Conversion by Functionalized
Nano-Bio-Fibers for Biomedical Applications**

Von der Naturwissenschaftlichen Fakultät der
Gottfried Wilhelm Leibniz Universität Hannover

zur Erlangung des Grades

Doktor der Naturwissenschaften (Dr. rer. nat.)

genehmigte Dissertation

von

Manish Kumar,

Master of Technology

Date of birth: 08.01.1990

2017

Referent: Prof. Dr. Franz Renz
Korreferent: Prof. Dr. –Ing. Ralf Franz Sindelar
Korreferent: Prof. Dr. Jürgen Caro
Vorsitzender: Prof. Dr. Jens-Uwe Grabow
Tag der Promotion: 18.10.2017

Abstract

Nanostructured bio-fibrous membranes prepared by electrospinning (ESP) technique, offer unique properties, such as large specific surface area, high porosity, excellent flexibility and the ability to incorporate selectively reactive molecules. These enable such nano-bio-fibrous membranes to have wide biomedical applications.

In this work, Polylactic acid (PLA)-, Polyethylene glycol (PEG)-, Hydroxypropyl cellulose (HPC)- and N-Vinylcaprolactam (NVCL)- molecules have been combined. Pre-studies on PLA-HPC thin-film membranes have been done, before producing fibrous membranes. Thin-film membranes have the advantage of unified surface in comparison of fibrous membranes. PLA-HPC membranes (thin-film and fibers) show volume-phase transition, proposing pulsatile model drug release under changes in temperature effect.

PLA-PEG-NVCL composite fibrous membranes are functionalized with magnetic nanoparticles (MNPs) and therapeutic effective molecules. Such membranes behave like actuators, controlled by external magnetic stimuli, proposing triggered drug release at a specific time and location.

Biotinylated bovine serum albumin (BSA) is embedded in PLA-PEG composite fibrous membranes and attached via the biotin-streptavidin interaction. Its specific immobilization is validated by the added fluorescent-labeled avidin molecules. This idea demonstrates the suitability of the material for biosensor applications.

Therefore, smart nano-fibrous membranes are developed today for smart nanomedicine of tomorrow.

Keywords: Electrospinning, Nano-Bio-Fibers, Composite-Fibrous-Membranes, Biomedical Applications

Zusammenfassung

Nanostrukturierte Bio-Faser-Membranen, hergestellt durch Elektrospinning (ESP) zeigen außergewöhnliche Eigenschaften, wie eine hohe spezifische Oberfläche, hohe Porosität, hervorragende Flexibilität und die Fähigkeit, reaktive Moleküle selektiv einzubauen. Dadurch wird für Nano-Bio-Faser-Membranen ein breites biomedizinisches Anwendungsfeld geschaffen.

In der vorliegenden Arbeit werden folgende Moleküle: Polymilchsäure (PLA), Polyethylenglykol (PEG), Hydroxypropylcellulose (HPC) und N-Vinylcaprolactam (NVCL) unterschiedlich miteinander kombiniert. Vor der Herstellung der Fasermembranen sind Vorstudien mit Dünnschicht-Membranen aus PLA, kombiniert mit HPC in unterschiedlichen Gewichtsanteilen, durchgeführt worden. Der Vorteil dieser Dünnschicht-Membrane im Vergleich zu den Fasermembranen liegt in ihrer einheitlichen Oberfläche. PLA-HPC-Membranen (Dünnschicht und Fasern) zeigen bei Temperaturänderungen einen Phasen-Volumen-Übergang mit einer pulsierenden Freisetzung von Modellarzneistoffen.

PLA-PEG-NVCL-Verbundfasermembranen sind mit magnetischen Nanopartikeln (MNPs) und therapeutisch wirksamen Molekülen funktionalisiert worden. Solche Membranen verhalten sich wie Aktuatoren, die durch externe magnetische Reize gesteuert werden, wodurch eine Arzneimittelfreisetzung lokal zu einem bestimmten Zeitpunkt ausgelöst werden kann.

Rinderserumalbumin mit Biotin (BSA) wird in PLA-PEG-Verbundfaser-Membranen eingebettet und über die Biotin-Streptavidin-Wechselwirkung angebunden. Die spezifische Immobilisierung des BSA wird durch die zugegebenen fluoreszenzmarkierten Avidin-Moleküle nachgewiesen. Mit dieser Idee wird die Eignung des Materials für Biosensor-Anwendungen demonstriert.

So können heute intelligente Nanofaser-Membrane für die intelligente Nanomedizin von morgen entwickelt werden.

Stichwörter: Elektrospinning, Nano-Bio-Fasern, Komposite-Faser-Membrane, Biomedizinische Anwendungen

Acknowledgement

This project has been made possible by the Lower Saxony PhD programme (Hannover School for Nanotechnology) and Graduiertenakademie scholarship, for this I sincerely thank **Dr. Fritz Schulze Wischeler** and **Dr. Meike Huntebrinker**.

First of all, my deep sense of gratitude and heartfelt thanks to my first research supervisor **Prof. Dr. Franz Renz**, for his outstanding guidance, kind encouragement and parental affection for his involvement with the research work. There is no doubt in my mind that I will be a student of his group for the remainder of my life.

I take immense pleasure in expressing my deep sense of gratitude and thanks to my second research supervisor **Prof. Dr.-Ing. Ralf Sindelar**, for introducing me to this exciting field of electrospinning and drug delivery systems.

My project involved active collaboration with **Associate Prof. Dr. Vesa Hytönen**, BioMediTech, University of Tampere, Finland. I have learnt a lot from him, especially how to do things better and improve to the best. I thank him for his input in my results. His collaboration has proven to be the most fruitful gift of my life.

I would like to thank **Prof. Dr.-Ing. Hans-Josef Endres**, Institute for Bioplastics and Biocomposites (Ibb), HsH, for providing Polylactic acid (PLA) samples. I would also like to thank **Dr.-Ing. Marc Christopher Wurz**, Institute of Micro Production Technology (IMPT), LUH, for his support with the VSM equipment at his laboratory. I would like to thank **Prof. Dr. Andreas Kirschning**, Institute of Organic Chemistry, LUH, for allowing me to work in his lab.

I thank to **Ms. Dagmar Wengerowsky**, for her moral support and inspiration, which always helped me to keep going.

I express my sincere thanks to **M.Sc. Folke Dencker**, **M.Sc. Fabian Zimmermann**, **M.Sc. Niklas Burblied**, **M.Sc. Mona Oltmanns**, **M.Sc. Francesco Trenti**, **M.Sc. Rolle Rahikainen** and **Cesare Delbrück von Borke** for their expertise and effort. I also wish to express my thanks to past and present members of Prof. Renz working group.

Finally, I wish to thank **my family** and **friends** for their encouragement, motivation, and caring through these years.

Hannover, 2017

Manish Kumar

Table of Contents

Abstract	i
Zusammenfassung	ii
Acknowledgement	iii
Table of Contents	iv
1. Introduction	1
1.1 Nano-Bio-Fibers and Biocomposites	2
1.2 Objectives and Methodology.....	4
2 State-of-the-Art of Electrospinning Process	6
2.1 Fundamental of Electrospinning.....	6
2.2 Typical Electrospinning Setup	9
2.3 Electrospinning Experimental Setup Type.....	12
2.3.1 Single Nozzle Spinning	12
2.3.2 Coaxial Spinning	13
2.3.3 Side-by-side Spinning	14
2.4 Different Morphology of Nanofibers	16
2.5 Factors Affecting Electrospinning.....	17
2.6 Possibility of Errors during the Electrospinning	17
2.7 Advantage of Using Nanofibers	18
3 Theoretical Background	19
3.1 Drug Delivery Systems.....	19
3.2 Mechanism of Drug Release	21
3.3 Advantages of Synthetic Polymers over Natural Polymers	24
3.4 Fabrication of Different Stimuli Responsive Systems for On-Demand Drug Release.....	25
3.5 Development of Stimuli-Responsive Nanofibers.....	26
3.5.1 Magnetically-Sensitive Release System.....	29
3.5.2 Temperature-Sensitive Release System	30
3.6 Present Challenge and their Solutions.....	31
4 Materials and Methods	32
4.1 Materials	32
4.2 General Analytical Methods.....	35
4.2.1 Scanning Electron Microscopy (SEM).....	35
4.2.2 Ultraviolet-Visible (UV-Vis) Spectroscopy	35

4.2.3	Thermogravimetric Analysis (TGA)	35
4.2.4	Differential Scanning Calorimetry (DSC).....	36
4.2.5	Micro Raman Spectroscopy (MRS)	37
4.2.6	Contact Angle (CA).....	38
5	Biopolymers.....	39
5.1	Classification of Biopolymers	40
5.2	Poly(lactic acid) (PLA).....	41
5.3	PLA Advantages and Disadvantages.....	45
5.4	Polyethylene Glycol	46
5.5	N-vinyl Caprolactam	47
5.6	Hydroxypropyl Cellulose	48
6	Electrospinning of PLA.....	50
6.1	PLA Solution Property	50
6.1.1	PLA Solubility.....	50
6.1.2	PLA Miscibility	51
6.2	PLA Fiber Formation by Electrospinning	51
6.2.1	Concentration Effects	54
6.2.2	Voltage Effects	54
6.2.3	Feed Rate Effects.....	55
6.3	Surface Modification of PLA Electrospun Fibers	56
6.4	BET Surface Area.....	57
6.5	PLA Electrospun Fibers: Crystallinity	58
7	Preparation of Magnetic PLA Fibrous Membranes	59
7.1	Abstract.....	59
7.2	Introduction	59
7.3	Experimental.....	60
7.3.1	Materials Used.....	60
7.3.2	Material Charecterization	61
7.3.2.1	Scanning Electron Microscopy (SEM).....	61
7.3.2.2	Thermogravimetric Analysis (TGA)	61
7.3.2.3	X- ray Diffractometer (XRD).....	61
7.3.2.4	Vibrating Sample Magnetometer (VSM)	61
7.3.3	Synthesis of PLA, PLA-PEG and PLA-PEG-MNPs Composite Fibers	61
7.4	Results and Discussion of Magnetic PLA Fibrous Membranes.....	62
7.4.1	Scanning Electron Microscopy (SEM).....	62
7.4.2	Energy Dispersive X-ray (EDX)	64
7.4.3	Thermal Analysis.....	65

7.4.4	X-ray Diffractometer Analysis	66
7.4.5	Magnetic Properties of Fibers	67
7.5	Conclusions of Magnetic PLA Fibrous Membranes	68
8	Preparation of PLA-PEG-NVCL Fibrous Membranes	69
8.1	Abstract.....	69
8.2	Introduction	69
8.3	Experimental.....	70
8.3.1	Materials Used.....	70
8.3.2	Material Characterization	71
8.3.2.1	Scanning Electron Microscopy (SEM).....	71
8.3.2.2	Micro Raman Spectroscopy (MRS)	71
8.3.2.3	Differential Scanning Calorimetry (DSC).....	71
8.3.2.4	Contact Angle (CA).....	71
8.3.2.5	UV-VIS Spectrophotometry	72
8.3.2.6	Microbiological Tests	72
8.3.3	Synthesis of PLA, PLA-PEG and PLA-PEG-NVCL Composite Fibrous Membranes	72
8.4	Results and Discussion of PLA-PEG-NVCL Fibrous Membranes	73
8.4.1	Scanning Electron Microscopy (SEM).....	73
8.4.2	Micro Raman Spectroscopy (MRS)	75
8.4.3	Differential Scanning Calorimetry (DSC).....	77
8.4.4	Contact Angle (CA).....	79
8.4.5	Biological Properties of PLA-PEG-NVCL and PLA-PEG-NVCL-TCH Composite Fibrous Membranes.....	80
8.4.6	Magnetically-Triggered Drug Release.....	81
8.5	Conclusions of PLA-PEG-NVCL Fibrous Membranes	84
9	Preparation of PLA-HPC Thin Film Membranes.....	85
9.1	Abstract.....	85
9.2	Introduction	85
9.3	Experimental.....	90
9.3.1	Materials Used.....	90
9.3.2	Material Characterization	90
9.3.2.1	UV-VIS Spectrophotometry	90
9.3.3	Synthesis of PLA-HPC Thin-film Membranes	90
9.4	Results of PLA-HPC Thin-film Membranes	91
9.4.1	Results from the Side-by-Side Franz Cell	91

9.4.2	Results from the Modified Vertical Franz Cell Simulating Simplified Blood Pressure Conditions	93
9.5	Discussion of PLA-HPC Thin-film Membranes	94
9.6	Conclusion of PLA-HPC Thin-film Membranes	96
10	Preparation of PLA-HPC Fibrous Membranes.....	97
10.1	Abstract.....	97
10.2	Introduction	97
10.3	Experimental.....	100
10.3.1	Materials Used.....	100
10.3.2	Material Characterizations.....	100
10.3.2.1	Scanning Electron Microscopy (SEM)	100
10.3.2.2	In vitro Release Profile of MEB	100
10.3.3	Synthesis of PLA, PLA-MEB and PLA-MEB-HPC Composite Fibrous Membranes	101
10.4	Results and Discussion of PLA-HPC Composite Fibrous Membranes.....	101
10.4.1	Scanning Electron Microscopy (SEM).....	101
10.4.2	In-vitro Release of MEB	102
10.5	Conclusions of PLA-HPC Fibrous Membranes	104
11	Preparation of PLA-PEG-BSA Fibrous Membranes.....	105
11.1	Biosensors.....	105
11.2	Avidin-Biotin.....	106
11.3	Advantages of Avidin-Biotin	107
11.4	Challenges	107
11.5	Results of PLA-PEG-BSA Fibrous Membrane	108
12	Conclusions	117
	Literature Cited	119
	Symbols and Abbreviations	133
	Figures List.....	135
	Tables List	140
	List of Journal Publications (2013-2017).....	141
	Supporting Information	144
	Declaration	152
	Curriculum Vitae.....	153

1. Introduction

Energy transfer and –conversion exists in many fold-ways. In fact, it is the essence of life. In the present work, the focus is on energy transfer and –conversion in functional nanofibrous membranes for biomedical applications. Such membranes may be used for on-demand drug delivery and biosensors in daily life applications. Figure 1.1 shows energy transfer and –conversion scheme and biomolecule detection.

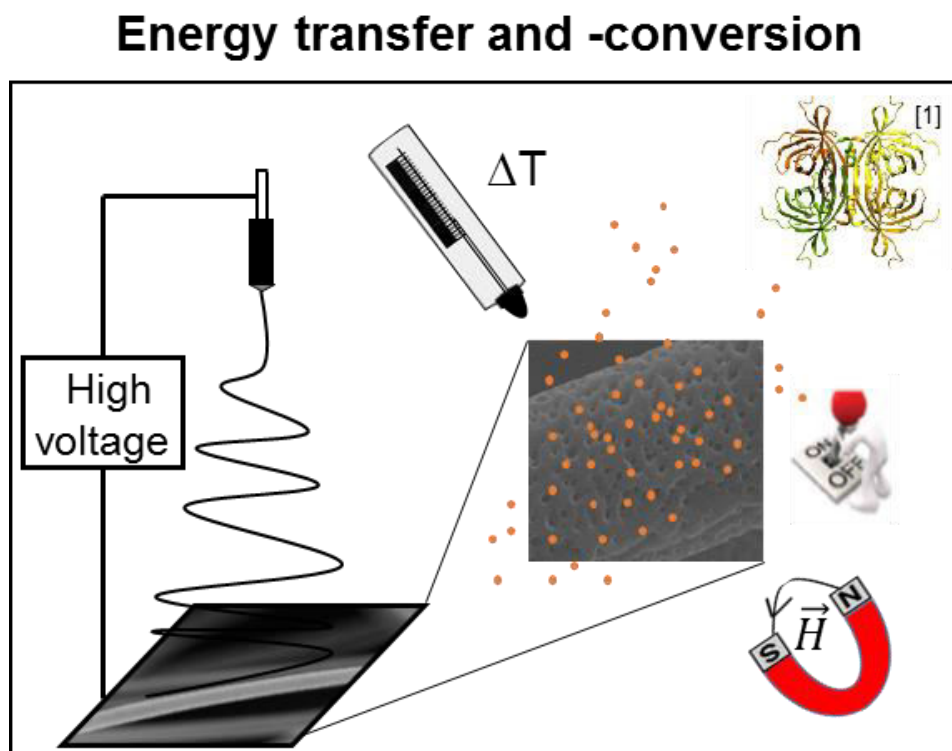


Figure 1.1: Schematic illustration of the energy transfer and –conversion scheme. First functional nanofibers with tailored properties are fabricated by electrospinning technique. After this, the functionalized nanofibers are treated with an external energy source and stimulated (on-demand) therapeutic release is measured. The functionalized nanofibers are treated with biological samples [1] and their binding ability is demonstrated (Picture: M. Kumar).

A global increasing pressure in achieving better quality of life with decreasing costs of healthcare, provide the ideal framework to explore the new possibilities created by nanotechnology and biomaterials science, to tackle these demanding health-related problems from a radical new angle [2]. One key issue is the materials being used in biomedical field called biomaterials. It is predicted that nanotechnological approaches of biomaterials in medical fields will have a long lasting impact on safety, accuracy and efficacy of currently available medical devices [3][4][5]. The major target areas are drug delivery, tissue engineering as well as biosensors [6][7].

Synthetic biopolymer have captured the interest to fabricate electrospun biofibrous membranes of different size (micro- or nano sized) and surface functionality [8][9]. These membranes have been routinely used as vehicles for drug delivery, due to their ability to

protect the encapsulated drug, the ease of fabrication, tunable degradation kinetics and high surface to volume ratio [10]. Different synthetic biofibers have proved their potential for efficient controlled delivery of drug [11]. However, some diseases require, that drug level should be accelerated within the therapeutic index (the difference between minimum effective level and the toxic level) to treat complex diseases such as cancer with better performance. This need catalyzed the development of “stimuli-responsive” nano-bio-fibrous membranes, which will be able to measure minute changes in the heterogeneity of the system and subsequently provide responses.

Taking inspiration from mother nature for stimuli-responsive materials, for examples the leaves of *Mimosa pudica* collapse suddenly when touched, sunflowers turn toward the sun and chameleons change color according to their environment [12][13]; scientists have succeeded to synthesize stimuli-responsive polymers, that can be switched by using temperature, light, ultrasound, electromagnetic fields, pH and biomolecules. This trigger a corresponding change in the polymer’s physical properties such as size, shape, hydrophobicity and degradation rate [14]. These switching properties of the polymer have a significant effect on the vast area of biomedical applications [12]. Stimuli-responsive polymers have been variously called stimuli-sensitive [15], intelligent [16], smart [17][18] and environmentally-sensitive polymers [19]. Fabricating such stimuli-responsive materials in nano-bio-fibers, also called stimuli-responsive fibers (SRFs) become possible due to the major advancement in nanotechnology [20].

At the nanoscale, materials exhibit novel or improved chemical, thermal, and biological properties. Combining these unique properties with their remarkable recognition capabilities have resulted in systems with significantly improved performance and novel applications. An important use of nanomaterials is in composites, materials that combine one or more separate components, which are designed to exhibit overall the best properties of each component. This occurs because nano-size composites have the much higher surface area and the number of defects might be reduced at the nano level [21].

1.1 Nano-Bio-Fibers and Biocomposites

Nano-bio-fibers developed from biopolymers become an important resource for energy saving materials, which have the advantages of energy recovery, good biodegradability, sustainability and are less hazardous to health [22]. Biopolymers are the diverse and versatile class of materials that have potential applications in virtually all sectors of the economy. For example, they can be used as energy storage, drug delivery vehicles, cosmetics, biosensors, and even switching devices. Currently, many biopolymers are still in the developmental stage, but various opportunities are arising in the areas of biomedical applications, from sensing (such as biosensors) to diagnostics (such as on-demand drug

delivery). Figure 1.2 shows exponential rise of journal articles published on use of nanofibers for biomedical applications for the past 12 years.

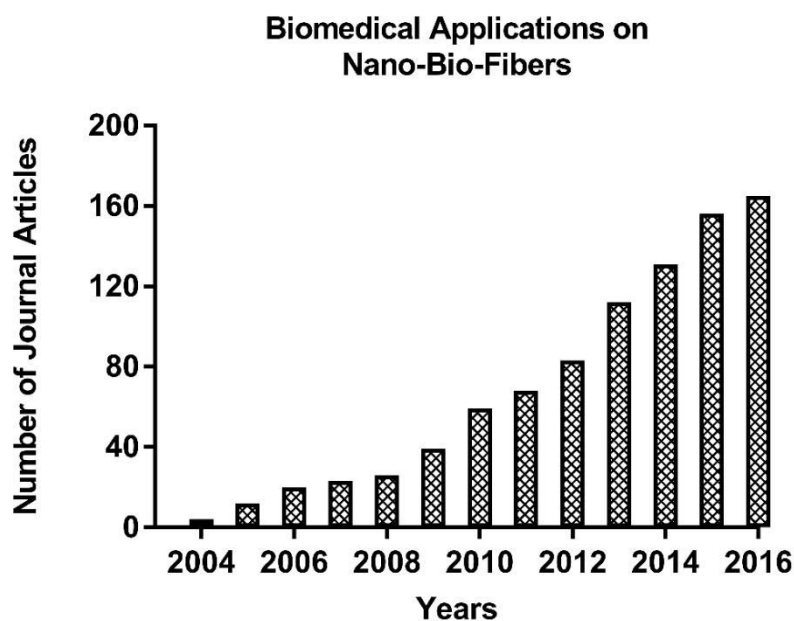


Figure 1.2: Number of publication related to nanofibers for biomedical applications (Source: Web of Science accessed on 6 March 2017).

Several materials, that are used in biomedical applications lack certain characteristics such as chemical nature, biodegradability and renewability [23][24], for these reasons, use of biocomposite materials improved their tailor-made characteristics and properties. In this way, biocomposite enhance material properties and reduce energy needs [25]. Composite materials are attractive because they combine material properties in ways not found in nature. The purpose of composite is the manipulation of properties to produce result in biocomposites. Fabrication of nano-bio-fibers from biocomposites could produce smart fibers which have the advantages of low density, biodegradability, structural and functional stability.

1.2 Objectives and Methodology

Nano-bio-fibers developed from biopolymers attracted significant attention because of its wide biomedical applications. Within the presented work, the aim was to explore and establish suitable electrospinning conditions for several biocompatible polymers (e.g. PLA, PEG, and HPC). The basic studies on these fibrous membranes were investigated and applied to technical biomedical applications.

The main objectives of this thesis were divided into the following parts:

Objective I: To explore the efficient routes for production of polylactic acid (PLA) electrospun fibers. The study investigates how PLA fibers diameter vary by changing electrospinning parameters. PLA fibers were further functionalized with polyethylene glycol (PEG) and magnetic nanoparticles (MNPs) to provide the resulting material magnetic properties. The study investigates how magnetic properties were influenced by a change in concentration of MNPs.

Objective II: To study magnetic stimulated on-demand drug delivery, PLA-PEG-NVCL composite fibrous membranes were fabricated. An antibiotic was embedded into these composite membranes, and their antimicrobial properties were investigated. The study evaluate how on-off conditions of magnetic field affect drug release.

Objective III: To study temperature induced on-demand drug delivery, PLA-HPC membranes were fabricated. Pre-studies on PLA-HPC thin film were also done. The study investigates how drug release influence under temperature stimuli.

Objective IV: To develop a suitable material for paper based biosensors, biotinylated bovine serum albumin (BSA) was incorporated into PLA-PEG composite membranes. These membranes were examined for their binding ability towards fluorescently labelled avidin. The study investigates biotin-avidin binding and blocking on fiber surface.

[Figure 1.3](#) and [Figure 1.4](#) show working plans for the development of functional nano-bio-fibrous membranes and their use for biomedical applications.

Abbreviations used: PLA: Polylactic acid; PEG: Polyethylene glycol; NVCL: N-vinylcaprolactam; HPC: Hydroxypropyl cellulose.

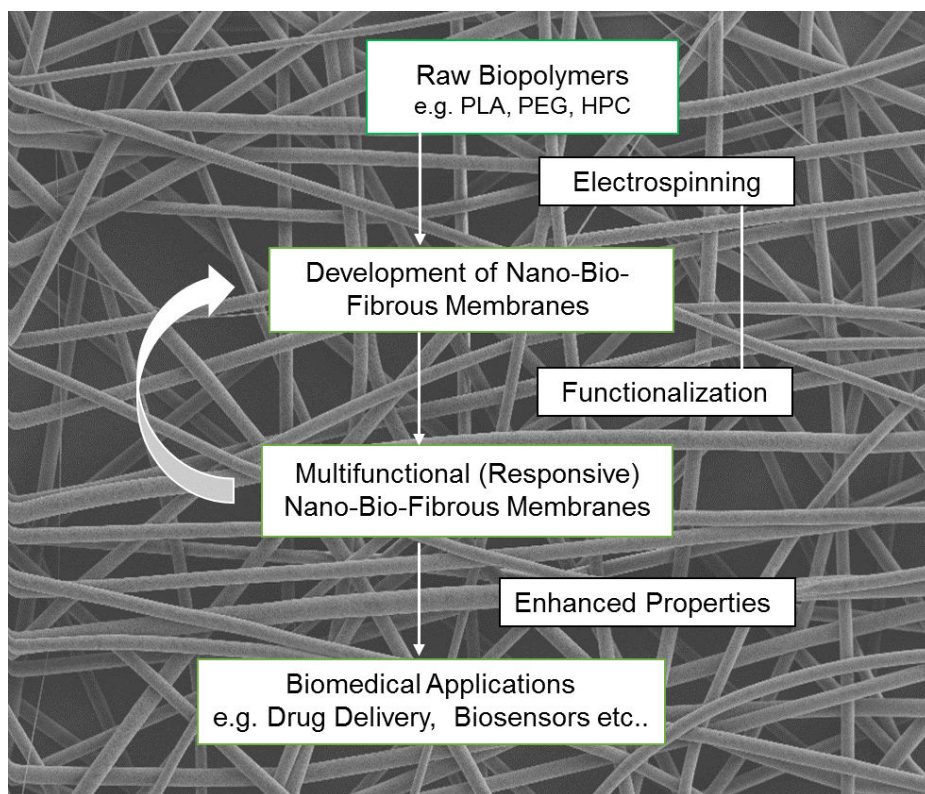


Figure 1.3: From raw materials to functional nano-bio-fibrous membranes by electrospinning technique and their potential biomedical applications (Picture: M. Kumar).

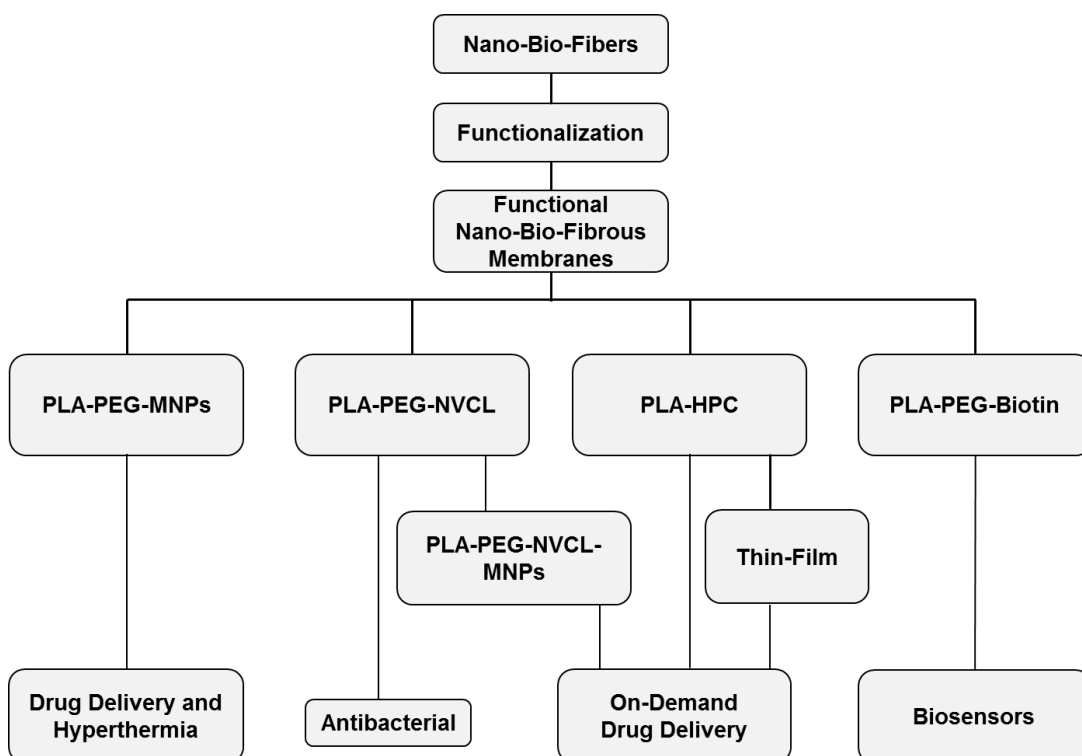


Figure 1.4: Working package for the development of functional nano-bio-fibrous membranes and their potential biomedical applications (Picture: M. Kumar).

2 State-of-the-Art of Electrospinning Process

2.1 Fundamental of Electrospinning

Electrospinning (ESP) becomes a fascinating technique for research activity worldwide [26]. It is an effective technique to produce micro/nano-sized polymer fibrous membranes [27]. These membranes have significant advantages due to their large surface-area-to-volume ratio, high porosity, flexibility and the ability to incorporate selectively reactive molecules. Fibers with a complex architecture such as randomly oriented, aligned fibers, core-shell fibers, hollow fibers, porous fibers, side-by-side structures can be easily produced with this technique [28].

There are several techniques for obtaining nanofibers such as drawing with a micropipette, template synthesis, phase separation, self-assembly and electrospinning. However, out of all available techniques, electrospinning is the only technique in which the process can be scaled to a commercial level [29]. Therefore, huge interest has been shown in the last fifteen years and there are many companies build across the world. Table 2.1 shows some of the electrospun companies with their product/service offer and web address. This table shows rising market demand of electrospun fibers.

Table 2.1: Some of the electrospun production sites.

Company	Country	Product/Service	Website
PolyNanoTec	Germany	Formulation of electrospinning material	http://www.polynanotec.com/
Bioinicia	Spain	Nanofibers	http://www.bioinicia.com/
Nano-FM	Netherlands	Biomaterials company	http://nano-fm.nl/
Pardam nanotechnology	Czech Republic	Inorganic and polymer nanofibers	http://pardam.cz/
Elmarco	Czech Republic	Industrial production of nanofibers	http://www.elmarco.com
Kato Tech Co. Ltd.	Japan	Equipment manufacturers	http://www.keskato.co.jp
Hirose Paper Mfg Co., Ltd	Japan	Nanofiber coated paper	http://www.hirose-paper-mfg.co.jp/english/pdct_nanofiber.html

Finetex Technology	Korea	Nanofibers	http://www.finetextech.com
Nanofiber Future Technologies Corp.	Canada	Polymer based nanofibers	http://www.nftc.cc
eSpin Technologies Inc.	U.S.	Nanofibers	http://www.espintechologies.com
BioSurfaces Inc.	U.S.	Drug loaded electrospun fibers for medical applications	http://www.biosurfaces.us/
RevolutionFibres	New Zealand	Nanofiber	http://www.revolutionfibres.com/

Most nanofiber producers as well as research institutes have constructed their own electrospinning equipment, because of its simplicity. Mechanical and bioprocess research institute, University of applied science and arts also has its own, as shown in Figure 2.1.

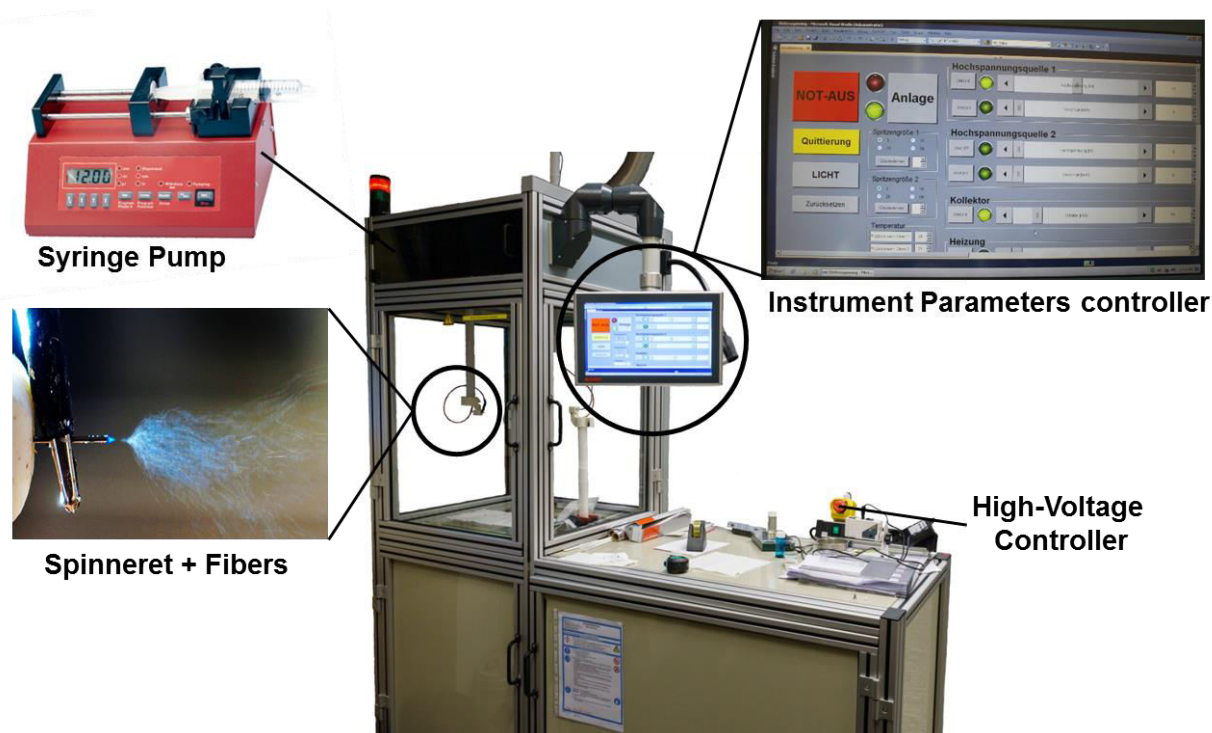


Figure 2.1: Electrospinning lab set-up (Picture:F. Böttcher and M. Kumar).

The first patent on electrospinning was issued by Formhals in 1934 [30] and since then hundreds of patents have been done in over eighty two years. Although the term "electrospinning," derived from "electrostatic spinning", was used relatively recently (in around 1994), its fundamental idea dates back more than 70 years earlier. From 1934 to 1944 Formhals published a series of patents [30][31][32][33][34] describing an experimental setup to produce polymer filaments using an electrostatic force. Table 2.2 shows the history of electrospinning.

Table 2.2: History of electrospinning.

Year	Scientist	Work	Reference
1934	Formhals	The first U.S. patent on electrospinning	[30]
1939	Formhals	Revised the disadvantages of the earlier setup by altering the distance between the spinneret and the collection device	[31][32]
1952	Vonnegut and Neubauer	Produce streams of highly-electrified uniform droplets of about 0.1 mm in diameter	[35]
1955	Drozin	Investigated the dispersion of a series of liquids into aerosols under high electric potentials	[36]
1960	Taylor	Showed that as the intensity of the electric field is increased, the hemispherical surface of the fluid at the tip of the capillary tube elongates to form a conical shape known as the Taylor cone	[37]
1966	Simons	Patented an apparatus to produce nonwoven fabrics of ultra-thin and very light weight with different patterns using electrical spinning	[38]
1971	Baumgarten	Design an apparatus to electrospin acrylic fibers with diameters in the range of 0.05–1.1 μm	[39]
Up till now		Electrospinning processes are like that described by Baumgarten	

2.2 Typical Electrospinning Setup

A typical setup for traditional electrospinning consists of four key components [28]:

1. A high voltage power supply (10-30 kV);
2. A polymer reservoir that can maintain a constant flow rate of solution, commonly a syringe connected to either a mechanical or a pneumatic syringe pump;
3. A conductive dispersing needle
4. A conductive substrate serves as collector.

When high voltage is applied to the needle, the polymer solution at the needle tip become unstable and a jet is issued [40][41]. The jet flows away from the needle initially in a nearly straight line, then it bends in a complex path during which electrical forces stretch and thin it to the nanometer scale [42][43]. The initial straight section of the jet is the “Near Field regime region” [44]. The area, where the electrical instabilities dominate creating a whipping motion of the jet, is called “Far Field regime region” [45].

The main parameters, involved in electrospinning that can be varied to optimize the results for specific applications, are listed in [Table 2.3](#).

Table 2.3: Important parameters for electrospinning experiments

S. No.	Parameters	Effects
1	Polymer precursor material	The material, that is electrospun, affects the final fibers morphology.
2	Polymer solution concentration	This parameter mainly influences the thickness of the fibers. The more diluted solutions generally lead to thinner fibers and vice versa. When the solution is too concentrated, electrospinning might not be possible.
3	Needle-to-collector- distance	The typical electrode-to-collector distance can vary from 8 cm to 30 cm and can influence fibers distribution, density, thickness and homogeneity.
4	Flow rate	Similarly, to the needle-to-collector distance, the flow rate can influence fibers distribution, density, thickness and homogeneity.
5	Voltage	The intensity of the applied voltage mainly influences the thickness of the fibers, which decreases when a higher voltage is applied.

-In the first step, the polymer droplet would assume spherical-like shape as controlled by the surface tension of the solution. With the introduction of high voltage, the polymer droplet stretches more and more, until it gets close to a critical potential acquiring the characteristic conical shape, referred to as Taylor cone [46]. The fibers are produced when the voltage crosses this critical point. The resulting fibers come from evaporation of the solvents from the polymer solution and stretching deformations due to applied electric field.

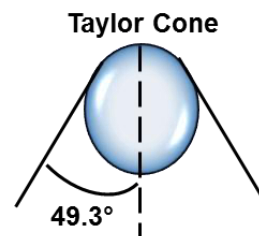
There are several theories on ESP process [47], three are given as below,

1. Theory on the fluid charging;
2. Theories on the liquid droplet under high voltage—Taylor Cone theory;
3. Theories on the jet in flight—Instability Theories.

1. Theory on the fluid charging: A high voltage power is applied to the viscous fluid, which generate charges. The generated charge carriers as free electron, ions or ion pairs form double layer in the fluid owing to the ion mobility.

2. Taylor Cone theory: It describe the deformation of one-drop of viscous fluid under the high voltage power supplied.

- (I) The stable shape of viscous fluid could be acquired owing to the equilibrium of the electric forces and the surface tension of viscous fluid;
- (II) When the voltage is further increased, the equilibrium will be abolished, resulting a conical shape from the viscous fluid. The conical shape has a half angle of 49.3 (a whole angle of 98.6), referred to as the Taylor Cone.



3. Instability Theories: Initially, the fibrous jet is nearly in a straight line then it formed into a complex path known as whipping instability. Whipping instability is the reason for the formation of nano dimension fibrous structures. The following forces are acting on the whipping charged jet;

- (I) Gravitational force, F_G (towards the collector plate in a vertically arranged apparatus). $F_G = \rho\pi r^2g$, where ρ is the density of the liquid and g is the acceleration due to gravity.
- (II) The electrostatic force, F_E , which extends the jet and propels it towards the grounded collector.

- (III) Coulombic repulsion forces F_c on the surface of the jet, which introduce instability and whipping motions.
- (IV) Viscoelastic forces, which work against elongation of the jet in the electric field.
- (V) Surface tension forces, which work against the stretching of the jet.

The specific surface area of these electrospun fibers is high, due to the small fiber diameter, the length can be many kilometers [48]. There inherent property of the electrospun fiber makes suitable for advanced biomedical applications [49] [50], such as (Figure 2.2): drug delivery, wound dressing, medical implants, biosensors and much more.

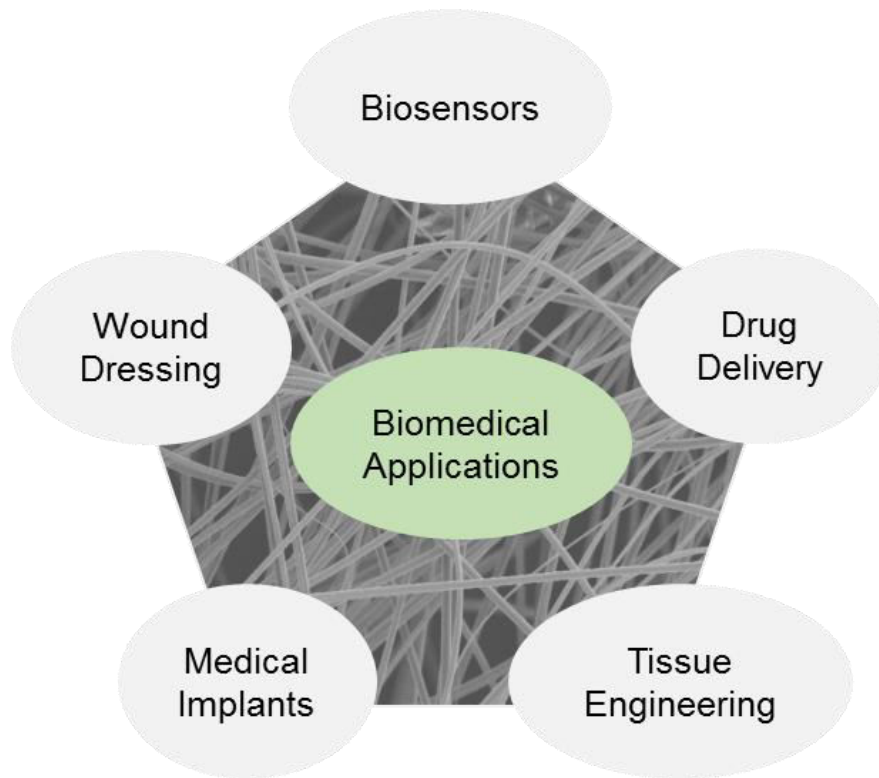


Figure 2.2: Some of the advanced biomedical applications of electrospun nanofibers (Picture: M. Kumar)

2.3 Electrospinning Experimental Setup Type

2.3.1 Single Nozzle Spinning

As the name suggest, in single nozzle electrospinning (ESP) system the polymer solution is forced from a single nozzle syringe, connected with the electrospinning set-up (as shown in Figure 2.3). This one is the simplest technique for fabricating one-dimensional nanofibers. The working principle is same, as described in section 2.2. Here, only one type of polymers solution or one mixture of two or more different types of polymer solutions can be spun. In the experiments, the needle used was the blunt-tip type with a diameter of 0.80 x 22 mm (21G x 7/8”). One example of single nozzle fiber (PLA fiber) is shown in Figure 2.6.

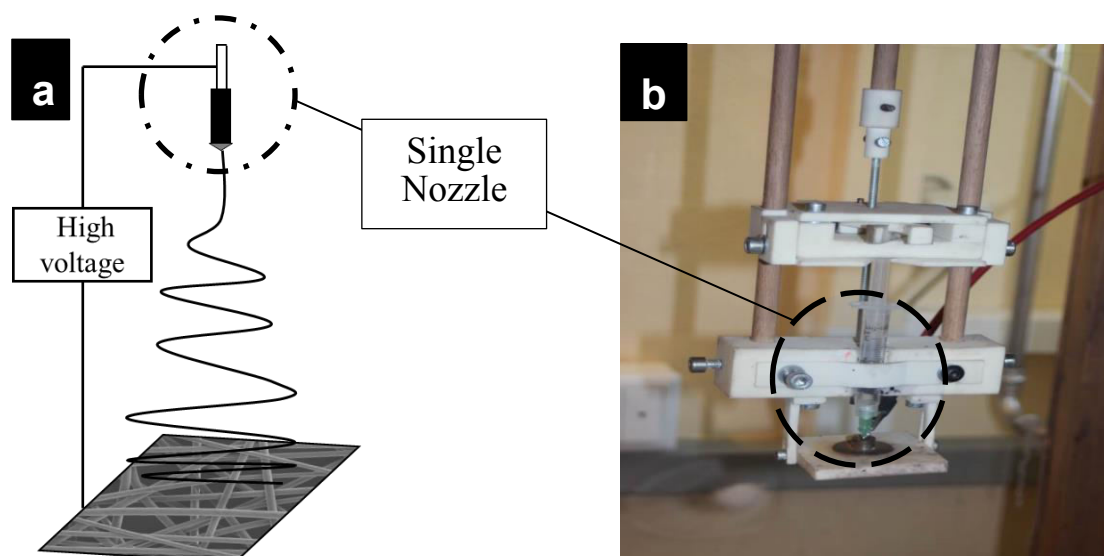


Figure 2.3: (a) Schematic illustration of single nozzle electrospinning setup and (b) designed lab apparatus displaying the single nozzle system (Pictures: M. Kumar).

2.3.2 Coaxial Spinning

Coaxial spinning (co-electrospinning) is an expansion of the single nozzle spinning. In this, core fiber could consist of a material which cannot be electrospun to fibers such as low molecular weight polymer, oil or even water molecules [51][52][53]. In this case, two polymers (containing different spinning solutions) are arranged in a concentric configuration and are connected to two reservoirs, as shown in Figure 2.4. In the experiments, the needle used was the blunt-tip type with an outer diameter of 1.37 mm, inner diameter of 0.51 mm. In this technique, drug molecules can be coated with the polymer shell which provides temporal protection for drug molecules and offers their controlled release [54][55]. Coaxial electrospinning has been applied so far for the preparation of polymer core-shell fibers as well as hollow fiber. The mechanism by which the two layers hollow fiber is prepared is based on the evaporation of the core solution through the shell yielding the deposition of the core material onto the shell layer [56]. These methods are directly integrated into the production process and reduce the effort for post process coatings massively. One example of coaxial fiber (Cellulose acetate-PLA) is shown in Figure 2.6.

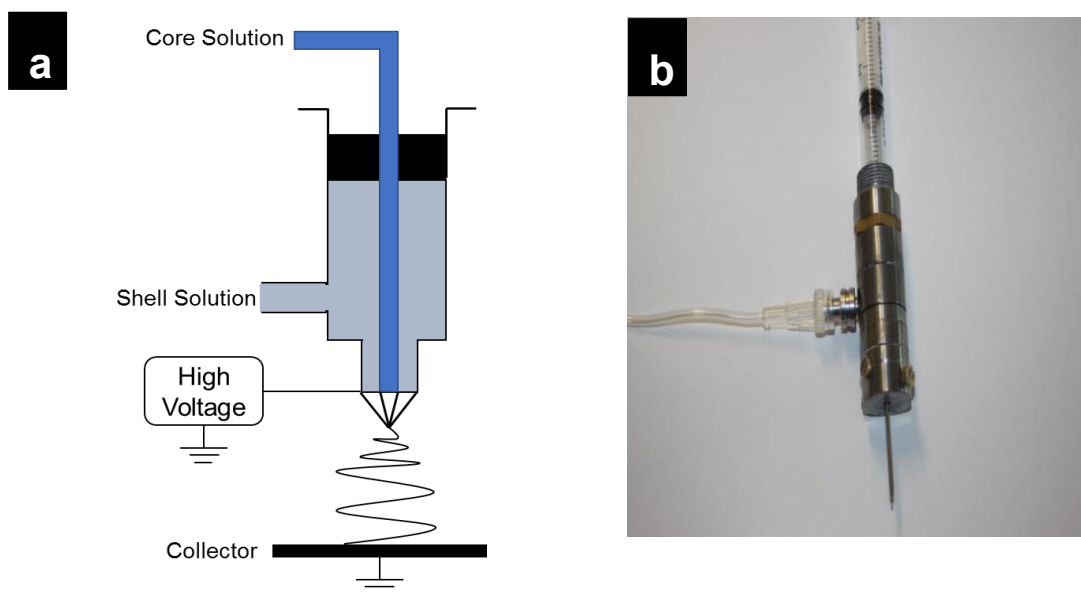


Figure 2.4: (a) Schematic illustration of coaxial electrospinning setup and (b) designed lab apparatus displaying the core-shell system (Pictures: M. Kumar).

2.3.3 Side-by-side Spinning

To enhance the production and functionality of nanofibers, the side-by-side spinning technique is used as shown in Figure 2.5. This is an advanced ESP technique, in which two different kinds of the polymer solution can be easily fabricated. In such kind of advanced ESP technique, it is possible to spray one type of polymer/drug over another kind of polymer fiber surface. One example of side-by-side spun fiber (PLA-Cellulose acetate) is shown in Figure 2.6.

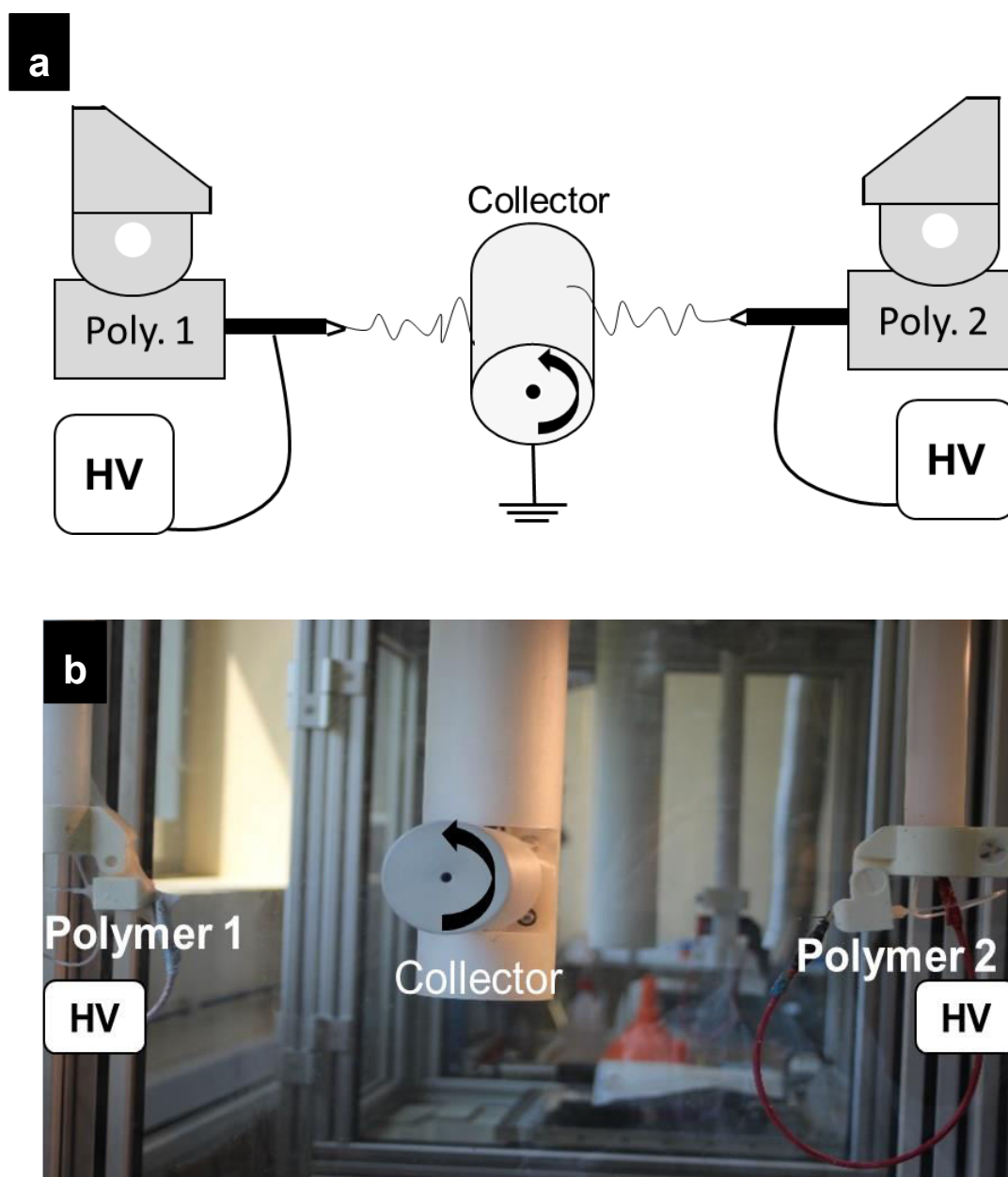


Figure 2.5: (a) Schematic illustration of side-by-side electrospinning setup (b) designed lab apparatus displaying the two side on single collector (Pictures: M. Kumar)

Figure 2.6 shows SEM micrographs of PLA fibers fabricated using these three techniques (single nozzle spinning, coaxial spinning and side-by-side spinning).

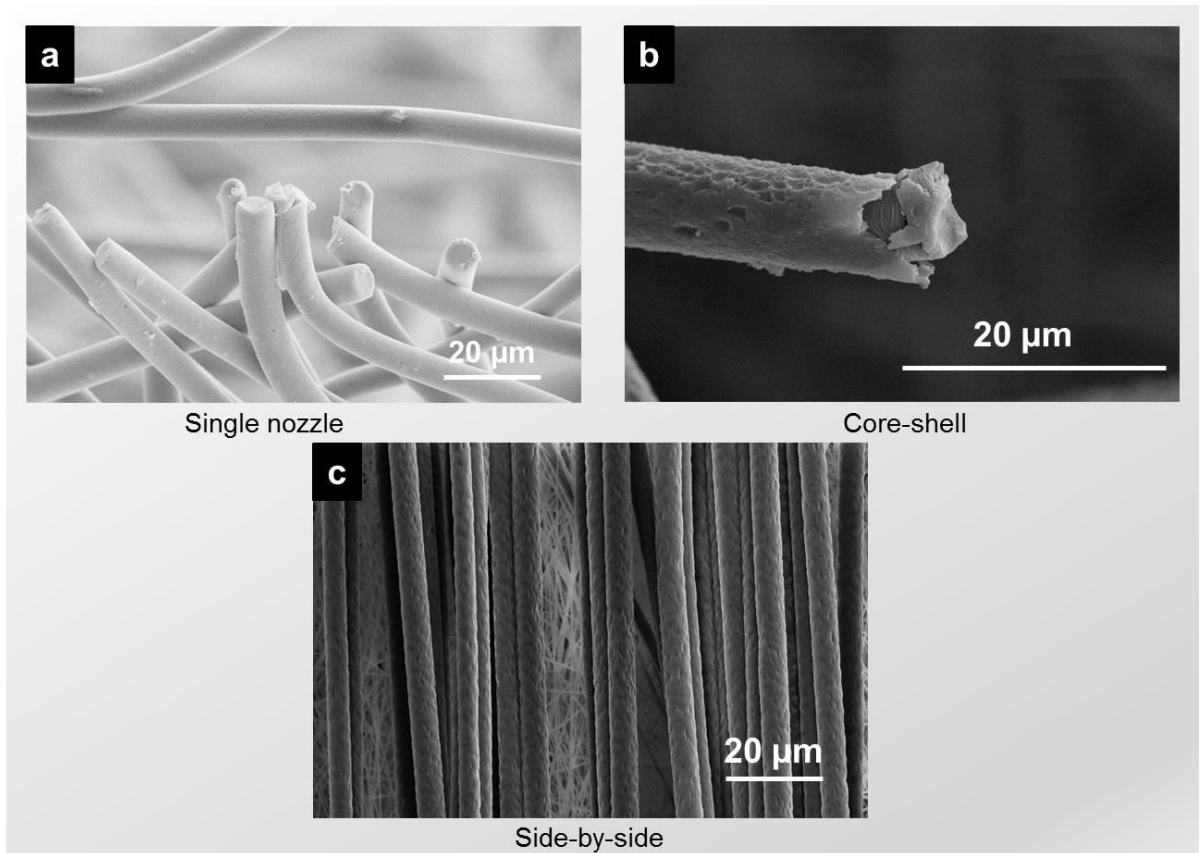


Figure 2.6: SEM micrographs of electrospun PLA fibers fabricated by using (a) Single nozzle spinning (b) coaxial spinning [Cellulose acetate (core) – PLA (shell)] (c) side-by-side spinning [PLA (one side) – cellulose acetate (second side)]. (Pictures: F. Dencker)

2.4 Different Morphology of Nanofibers

Depending on the polymer characteristics, the process parameters, and the ambient conditions, the generated fibers can vary vastly in diameter and morphology [57] (smooth and circular, flat ribbon-like structure, fibers with beads, highly porous, hollow fibers and core-shell fibers) (as shown in Figure 2.7). The reasons for such phenomena were explained in different ways by various authors [58][59][60]. This method presents an outstanding possibility to adjust the fibers morphology for the enhancement in advanced biomedical applications.

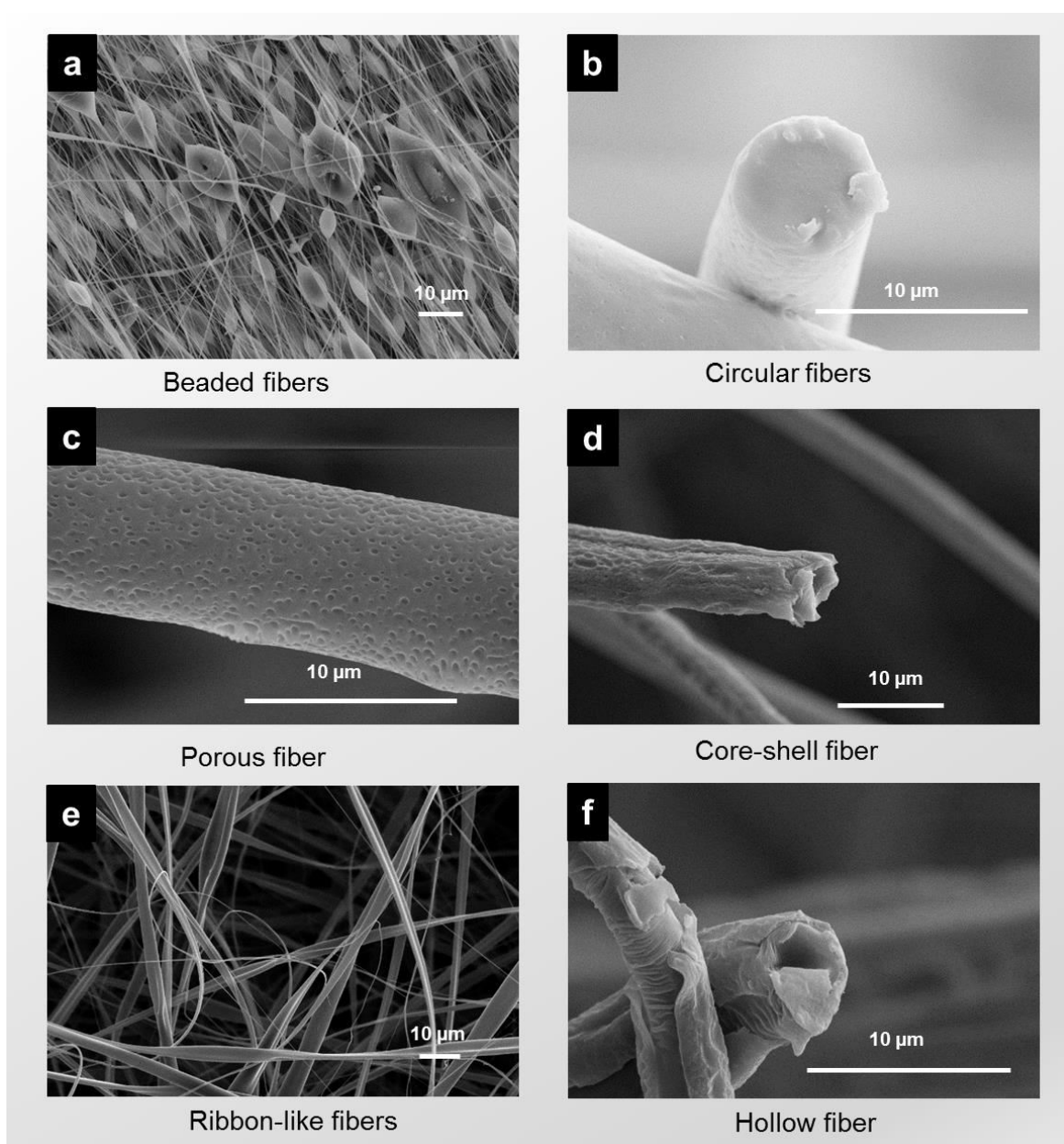


Figure 2.7: SEM micrographs of different morphologies of fibers (a) beaded PLA fibers (b) circular PLA fibers (c) porous PLA fibers (d) core-shell (Cellulose acetate-PLA) fibers (e) ribbon-like cellulose acetate fibers (f) hollow PLA fibers. (Pictures: F. Dencker)

2.5 Factors Affecting Electrospinning

There are several important parameters (process-, physical-, systemic- and solution-) which affect the fiber morphology and properties of electrospun fibers [29]. Table 2.4 shows a list of key factors affecting electrospun fibers [61].

Table 2.4: List of variable parameters affecting the characteristics of electrospun fibers

Process Parameters	Systemic Parameters	Solution Parameters	Physical Parameters
Voltage	Polymer type	Viscosity	Humidity
Flow rate	Molecular weight	Concentration	Temperature
Collector	Solvent used	Dielectric constant	Air velocity
Distance	--	Surface tension	--
Angle	--	Charge of jet	--
Rotar Speed	--	Conductivity	--

2.6 Possibility of Errors during the Electrospinning

In the electrospinning technique, several procedures are important to have consistent results. Some are listed as below:

1. Accuracy in the sample weighing measurement
2. Temperature in which solution was prepared
3. Room temperature and humidity also affect the fibers
4. Air bobble in the syringe should be avoided
5. Once-injects should be used

In the following Table 2.5, some hints are listed for what can be done in typical situations facing problems during electrospinning experiments.

Table 2.5: Typical problems and their solutions during electrospun fiber formation

Problems	Solutions	
	Increase the following values	Decrease the following values
Beads formation	Applied electric field; conductivity of the solution	Surface tension of the solution (e.g., addition of surfactants)
Deposition of fragments	Applied electric field, homogeneity of the solution	Weight concentration of the polymer; solution flow rate
Spraying	Molecular weight of the polymer; viscosity	Applied electric field

2.7 Advantage of Using Nanofibers

Polymer nanofibers have many advantages; some of these are as follow:

1. Large specific surface area and active reaction sites
2. Possibility of hosting functional molecules
3. Ability to protect from the outside environment (Core-shell)

The large specific surface area, i.e. the surface of a unit area of a nanofiber becomes higher, so, it is possible to collect more foreign objects, which lead to improving the properties of the existing device. It is also possible to integrate functionalities to nanofibers by chemical and physical technique. The sensitive molecules can also be protected from the environment by using core-shell fiber structure, as describe in section 2.3.2. In nanofibers, molecules are arranged in places, so there are improved properties that were not possible to obtain from micro or bigger scale of fibers before. For example, higher strength and higher heat-resistance properties are expected. Also, high conductivity can be obtained like carbon nanofibers. In addition to this, fibers generated from ESP technique do not require further purification.

3 Theoretical Background

3.1 Drug Delivery Systems

At present, the global advanced drug delivery market is forecast to grow at a compound annual growth rate (CAGR) of 4.9% from roughly \$-178.8 billion in 2015 to nearly \$ 227.3 billion by 2020, according to recent BCC Research [62]. One reason for this rapid growth is many genetically engineered protein drugs that are now being introduced. Encapsulation of protein in biopolymer materials prevent from being prematurely destroyed by attacking enzymes. The major area of application for these novel sustained-release systems is in the treatment of cancers and geriatric diseases.

In general, drug delivery systems (DDS) are engineered technologies for administering pharmaceutical compounds in the living body [63]. Therapeutic drugs play an important role in almost all aspects of medical treatment. However, when the drug is conventionally administered as a single dose and is metabolized rapidly inside the living body, resultant in a peak-to-valley concentration in blood plasma. This concludes to a poor patient response since the time frame over which the drug concentration is above the minimum effective level may not be long enough to produce a significant effect in a single dose. Low concentrations of drugs in the target tissues will lead to the suboptimal therapeutic effects and require more frequent administration and more side-effects. Albeit this situation can be improved by increasing the amount of dose, this quickly raises the drug level to the toxic region [64]. Figure 3.1 shows hypothetical drug delivery profiles, which shows an immediate drug release profile in the systemic circulation, resulting from the consecutive administration of multiple doses.

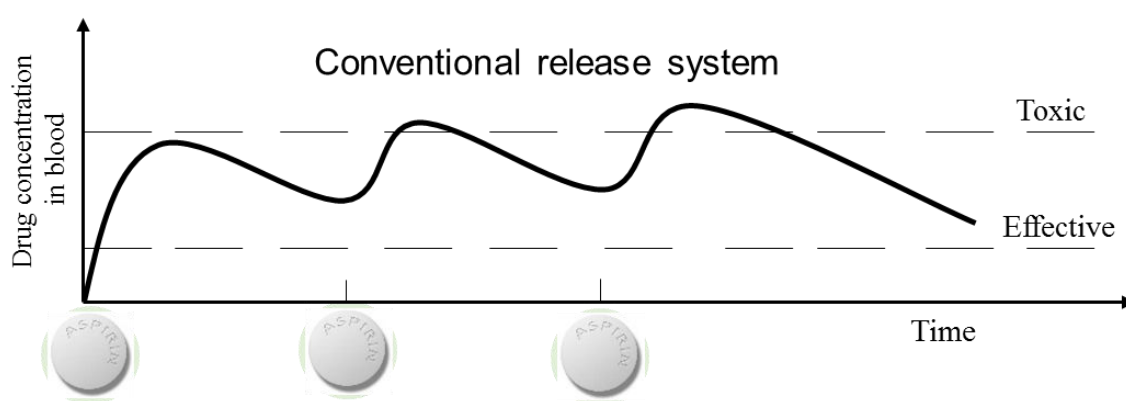


Figure 3.1: Drug concentration level in blood showing conventional release system (Multiple dosing at regular intervals leads to oscillating drug concentrations, which may fall outside the therapeutic range for significant time periods). (Picture: M. Kumar).

So, there is a great need to develop controlled release systems. A century had been devoted in developing those kinds of system.

Controlled drug delivery systems are an extensively investigated research area due to several advantages, e.g. they preserve drugs that are rapidly destroyed by the living body and maintain the drug within the desired therapeutic range as shown in Figure 3.2(a), hence reducing toxicity and improving patient comfort [65]. However, challenges in this area still remain such as overcoming biological barrier owing to the structures of the materials, the solubility of many small-molecule drugs, the difference between *in-vitro* and *in-vivo* conditions, the assessment of device stability and the complexity of the regulatory issues. Even, many useful drugs are hydrophobic in nature, therefore it is difficult to solubilize in an aqueous environment. In order to address some of these challenges, following area should be improved:

- (1) Enhanced efficacy,
- (2) Reduced side-effects,
- (3) Increased ease of use,
- (4) Polymeric material properties

Therefore, the current demand for sophisticated drug delivery devices continues to drive this development.

In addition to this, 95% of all newly developed therapeutics have poor pharmacokinetics and biopharmaceutical properties [66]. Therefore, there is a great desired to tune the DDS that distribute the therapeutically active drug molecule only to the site of action, without affecting healthy organs and tissues. The solution of the presented problem is the incorporation of therapeutics molecules to the “Biomaterials”. Biomaterial is defined as “Any substance (other than a drug) or combination of substances, synthetic or natural in origin, which can be used as a whole or as a part of system which treats, augments or replaces any tissue, organ, or function of the body” [67]. Biomaterials used in drug delivery systems are mainly focused on natural biopolymer-based biometrics, as such as collagen, chitosan and hyaluronic acid; synthetic biodegradable polymers, as such as poly-lactic acid / poly-glycolic acid (PLA/PGA) copolymers, polyanhydrides and synthetic non-biodegradable polymers, like silicone, cellulose derivatives etc.

For *in-vivo* applications, controlled release means once a drug which includes the active ingredient and polymers for delivery, enters the living body and delivers the active ingredient at a precise rate. The therapeutic range is the concentration needed in the plasma for effective treatment. In certain cases, it is preferred that the drug is expected to release upon external stimuli, as the exact time and dosing can be adjusted to match the

patient's needs e.g. for pain control or treatment of infections, as shown in Figure 3.2(b). Several years of research has shown that these controlled release systems can be triggered by environmental conditions. There are two ways to trigger release. One is an environmental response inside the body and the other is a response externally triggered outside the body. As the drug is released over an external triggered period, less frequent dosing is required, resulting in an enhanced safety of the system and better patient compliance [68].

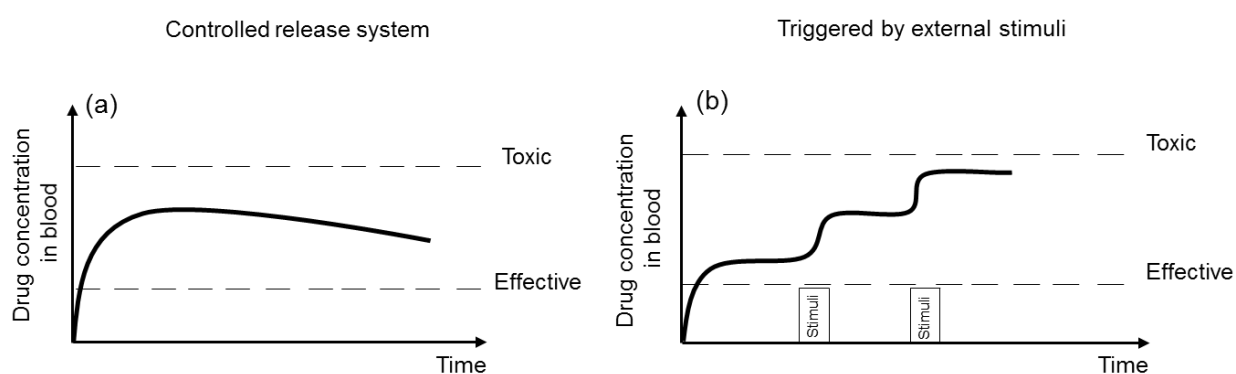


Figure 3.2: Drug concentration level in blood showing (a) controlled release system (drug concentration in blood lies within the therapeutic range, which is bounded below by the minimum toxic concentration and above by the minimum effective concentration) and (b) triggered release system. (Pictures: M. Kumar).

3.2 Mechanism of Drug Release

Drug release from biodegradable polymers is controlled by: (i) erosion and (ii) diffusion, or a combination of these mechanism [69]. These mechanisms are shown below in Figure 3.3. They depend on the nature of the encapsulated drugs, the nature of the polymer materials and the site of interest. Diffusion-controlled release from polymer membrane often occurs in combination with erosion/degradation processes [70]. There is no reported evidence for significant PLA degradation in an initial period of time corresponding to two-three months [71]. Therefore, it can be assumed that diffusion through the PLA fiber membranes would be the predominant mechanism for drug release during an initial period of time [72]. The second mechanism which is mainly governed by polymer degradation can occur after a period of two-three months or even a couple of years, thus making PLA based polymeric material, ideal for biomedical applications [73].

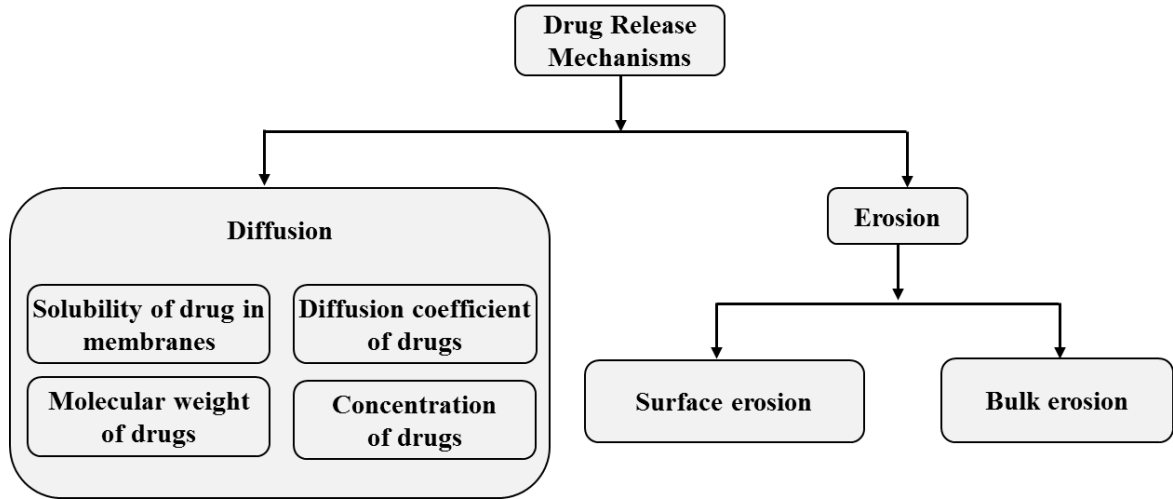


Figure 3.3: Different mechanisms of drug release

As it is mentioned above, diffusion is the main initial mechanism that occurs when PLA fiber membranes are used for drug delivery [71]. Diffusion is especially high for hydrophilic drugs, since they have a strong affinity towards aqueous physiological environments [64]. The flux (movement) of the drug across the membrane is governed by Fick’s first and second law of diffusion [74], which is directly proportional to the concentration gradient that takes places from a region of higher drug concentration to a region of lower concentration, as shown in Equation 3.1 (steady state diffusion).

$$J = -D \frac{dc}{dx} \quad \text{Equation 3.1}$$

where, J is the flux across a surface of per unit area (mol/m²sec); D is the diffusion coefficient of the drug in the membrane (m²/sec); dc/dx is the concentration gradient of the drug molecule across a diffusional path with thickness dx ; and a negative sign is used to define the direction of diffusion from a region with high concentration to a region with low concentration [75].

The second law of diffusion is the extension of Fick’s I law to a non-steady state. Here, at any given instant, the flux is not the same at different cross- sectional planes along the diffusion direction x .

Let consider a slab of unit area, having thickness Δx along the diffusion distance x . The volume of the slab is then Δx . In a non-steady state conditions, the flux is not equal to in (J_x) and out ($J_{x+\Delta x}$) of the slab. The rate of depletion of the diffusing atoms within this elemental volume is $(\partial c/\partial t)\Delta x$. This can be expressed as:

$$\left(\frac{\partial c}{\partial t}\right) \Delta x = J_x - J_{x+\Delta x} = J_x - \left\{J_x + \left(\frac{\partial J}{\partial x}\right) \Delta x\right\} \quad \text{Equation 3.2}$$

$$J_{x+\Delta x} = \left\{ J_x + \left(\frac{\partial J}{\partial x} \right) \Delta x \right\} \quad \text{Equation 3.3}$$

$$\left(\frac{\partial c}{\partial t} \right) \Delta x = J_x - J_{x+\Delta x} - \left(\frac{\partial J}{\partial x} \right) \Delta x \quad \text{Equation 3.4}$$

$$\left(\frac{\partial c}{\partial t} \right) \Delta x = - \left(\frac{\partial J}{\partial x} \right) \Delta x \quad \text{Equation 3.5}$$

Therefore,

$$\left(\frac{\partial c}{\partial t} \right) = - \left(\frac{\partial J}{\partial x} \right) \quad \text{Equation 3.6}$$

Now considering Equation 3.1

$$J = -D \frac{dc}{dx}$$

Substituting Equation 3.1 in Equation 3.6,

$$\left(\frac{\partial c}{\partial t} \right) = - \frac{\partial}{\partial x} \left(-D \frac{\partial c}{\partial x} \right) \quad \text{Equation 3.7}$$

$$\left(\frac{\partial c}{\partial t} \right) = \frac{\partial}{\partial x} \left(D \frac{\partial c}{\partial x} \right) \quad \text{Equation 3.8}$$

This is Fick's second law of diffusion under unsteady state conditions. If D is independent of concentration then Equation 3.8 becomes,

$$\left(\frac{\partial c}{\partial t} \right) = D \left(\frac{\partial^2 c}{\partial x^2} \right) \quad \text{Equation 3.9}$$

where, c is the concentration (mol.m⁻³); x is the length (m) and t is the time (Sec.).

In order to further understand the mechanism of drug release, Korsmeyer and Peppas developed a general model for drug release [76] [77] as shown in Equation 3.10:

$$\frac{M_t}{M_\infty} = kt^n \quad \text{Equation 3.10}$$

Taking log both the side (Equation 3.10):

$$\log \frac{M_t}{M_\infty} = \log k + n \log t \quad \text{Equation 3.11}$$

where, $\frac{M_t}{M_\infty}$ is the fractional release of the drug, t is the drug release time, k is a constant related to the drug diffusion coefficient and n is the diffusional exponent, which is an indication for the drug release mechanism (Table 3.1).

Table 3.1: Analysis of diffusional release mechanisms [76]

Diffusional release exponent (n)	Time-dependence of solute release rate (dM _t /dt)	Overall solute diffusion mechanism
0.5	$t^{-0.5}$	Fickian diffusion
$0.5 < n < 1.0$	t^{n-1}	Anomalous (non-Fickian) diffusion
1.0	Zero-order (time-independent) release	Case-II transport
$n > 1.0$	t^{n-1}	Super Case II transport

When fiber membranes are used for drug release measurements, there are several assumptions to be considered [78]; (1) the electrospun fibrous membranes, that are randomly arranged and constitute of three-dimensional macrostructures with large voids among them; (2) the randomly oriented fibrous membranes, could prevent the uniform soaking and wetting from the surrounding medium in the first stage. On considering these assumptions and following above mentioned mechanism, the diffusion coefficient can be determined [79].

3.3 Advantages of Synthetic Polymers over Natural Polymers

Synthetic polymers are prepared in a controlled platform with a fixed quantity of monomers. Whereas natural polymer productions depends upon environmental and seasonal factor [80], so there is a large batch-to-batch variation in the reproducibility of polymers. The rate of hydration is nearly uncontrollable because of the difference in collection time, region, species and environment condition of the natural polymers. The degradation of naturally occurring polymers almost always relies on enzymatic processes. There will inevitably be some patient to patient variation in the degradation rate depending on the activity of the specific degradative enzyme in each individual. In addition to this, natural polymers are exposed to natural environment which lead to microbial contamination because of the presence of moisture. Therefore, it is widely proposed to use synthetic polymers for biomedical applications [81].

3.4 Fabrication of Different Stimuli Responsive Systems for On-Demand Drug Release

In certain cases, it is preferred, that the drug is released upon external stimuli, as the exact time and dosing can be adjusted to match the patient's needs. Different types of external stimuli (physical, chemical and biological) can also be applied to provide a means for controlling “on-off” -release of the encapsulated therapeutic reagents within the fibrous membranes. The physical stimuli include e.g. temperature, electric field, magnetic field, solvent compositions, light, pressure and sound; while the chemical stimuli consist of e.g. pH-value, ions and various “signaling” molecules. Biological stimuli consist of e.g. specific biomolecules, like enzymes, amino acids, nucleotides, sugars, fatty acids, proteins, and lipids (Table 3.2). These stimuli-responsive systems, which can undergo an abrupt volume change in response to small changes in external parameters, such as temperature, pH, irradiation, and so on, lead to controlled on-demand drug release. One important feature of this type of material is reversibility, i.e. the ability of the polymer to return to its initial state upon application of a counter-trigger. They are also termed ‘smart’ [82], ‘intelligent’ [83], or ‘environmentally sensitive’ polymers. Figure 3.4 shows classification of stimuli of stimuli-responsive polymers.

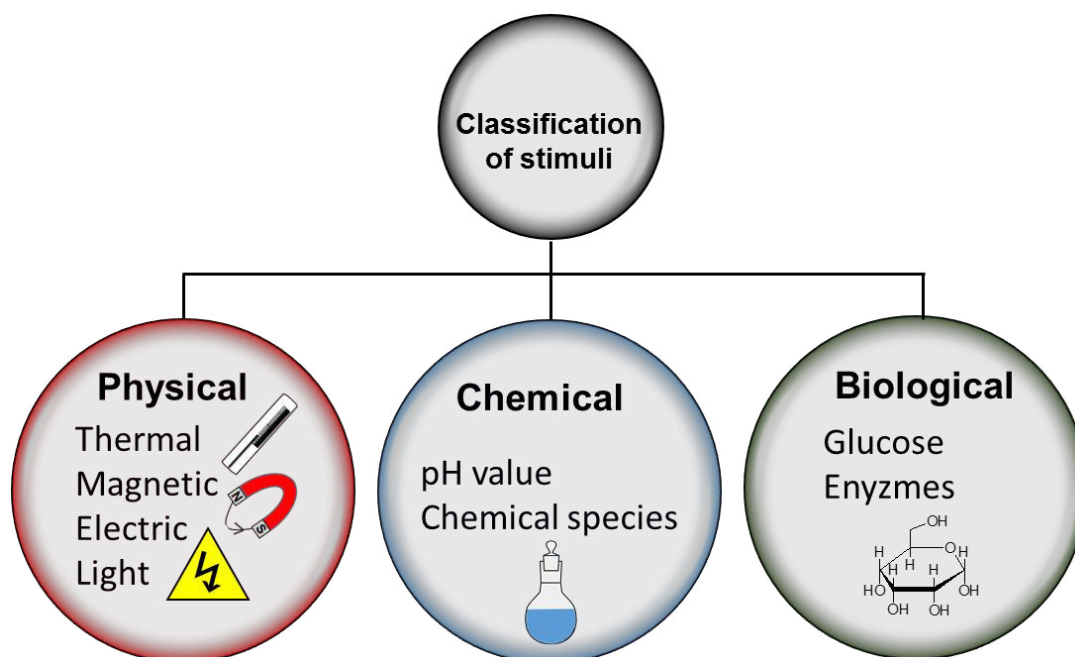


Figure 3.4: Classification of stimuli of stimuli-responsive polymers (Picture: M. Kumar)

3.5 Development of Stimuli-Responsive Nanofibers

Synthetic biodegradable polymers have proved their potential for efficient drug delivery systems. They are efficient at delivering controlled drug release. But some disease requires, that the drug level should be accelerated within the therapeutic index (the difference between minimum effective level and the toxic level), to treat complex disease with ever better performance such as cancer, tumor etc. To do this, we need to design a very sensitive stimuli-responsive nanofibrous surface, which will be able to measure minute changes in the heterogeneity of the system and subsequently provides a response. Figure 3.5 shows a symmetric diagram of stimuli-responsive drug-release from fibrous membranes. The amount of active substance transported and dispersed by the fibrous membranes can be controlled and externally triggered. This makes now possible to use even highly toxic drugs, which can't be used directly.

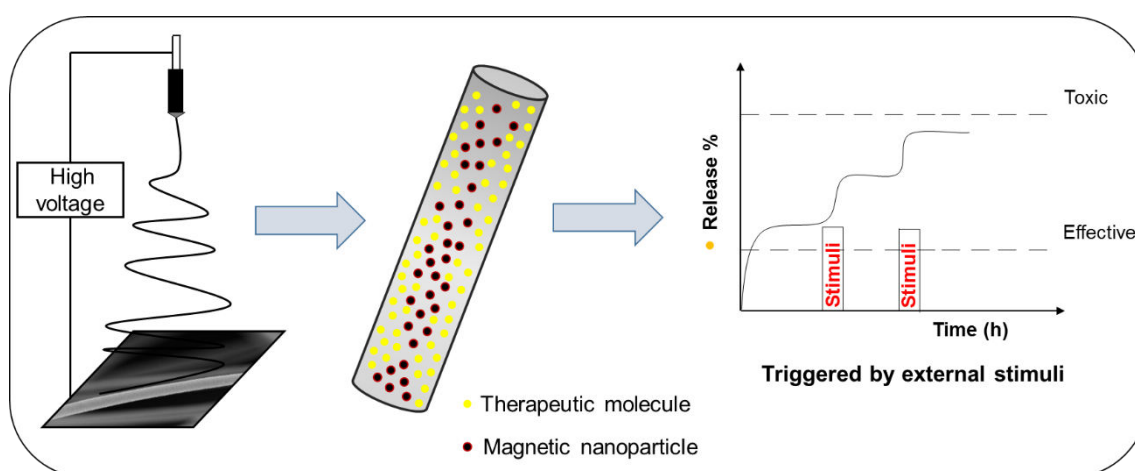


Figure 3.5: A symmetric diagram shows a stimuli-responsive drug-release system (Picture: M. Kumar)

Recent advancement in material chemistry and nanotechnology, makes externally triggered drug release possible by using functional nano-bio-fibers. Implementation of such fibers requires the use of biocompatible materials that are susceptible to a change in conformation, solubility or alternation of the hydrophilic-hydrophobic balance and consequently release of therapeutic molecules. Stimulus responsive polymeric nanofibers have the capability to respond to external stimuli by changing their physico-chemical properties, such as e.g. volume, water content, refractive index, permeability, and hydrophilicity–hydrophobicity balance [84][85]. Table 3.2 shows the effect of various external-internal stimuli, release mechanism, advantages, limitations, and their examples [12][86].

Table 3.2: Some effects of various external stimuli, release mechanisms, advantages, limitations and examples

Stimulus	Release Mechanism	Advantages	Limitations	Examples
Thermal	Intermolecular and intramolecular hydrogen bonding below and above the LCST	Ease of incorporation of active molecules	Injectability issues under application conditions	Poly(<i>N</i> -isopropylacrylamide) (PNIPAAm)
		Simple manufacturing and formulation	Low mechanical strength, biocompatibility issues and instability of thermolabile drugs	
Magnetic	Forces acting on the magnetic nanoparticles are changing the shape of polymer network	Magnetic nanoparticles are used as drug carrier and stimuli for drug–release	Magnetic field need to be focused in deep tissue	Iron oxide particles, NdFeB particles
Electrical	Electrophoresis of charged drugs; diffusion of drug from the electro-erodible polymers.	Pulsative release with changes in electric current	Difficulty in optimising the magnitude of electric current	Vinyl alcohol, Allyl amine, Acrylonitrile
			Surgical implantation required	
Light	Photodynamic release in which low energy light is used to generate reactive oxygen species from the combination of	Ease of controlling the trigger mechanism	Tissue penetration depth	Doxorubicin (DOX) loaded hollow gold nanospheres (HAuNSs) coated with
		Accurate control over the stimulus	Inconsistent responses to light	

Theoretical Background

	light, a photosensitizer (PS), and oxygen.			polyethylene glycol (PEG)
Ultrasound	Microbubbles break down faster with exposure of ultrasound	Controllable release	Optimal ultrasound sensitivity to allow reduction of transmitted energy	10 – Hydroxycamptothecin loaded PLA microbubbles
Mechanical stress	Applied mechanical stress deforms the structures	Possibility to achieve the drug release	Difficulty in de-stress and therefore in controlling the release profile	Alginate
pH-value	Diffusion – controlled; Swelling – controlled	Suitable for thermolabile drugs	Lack of toxicity data	Poly(methacrylic acid)
Chemical species	Electron-donating compounds cause charge transfer.	Easy to apply	Difficulty in controlling the release profile	N, N-diethylacrylamide (DEAA)
Enzymes	Physical entanglements between chemically different polymer networks	Wide variety of enzymes are available, which can be used as important signals for site-specific delivery	<i>In-vivo</i> conditions differ person-to-person, therefore difficult to optimize	Interpenetrating polymer network of oligopeptide-terminated poly(ethylene glycol) and dextran
	Physical stimuli	Chemical stimuli	Biological stimuli	

3.5.1 Magnetically-Sensitive Release System

Magnetic-sensitive release system is an efficient method of delivering drug to a localized disease site. This method can also be applied to fibrous membranes. For this, membranes are loaded with magnetic nanoparticles (MNPs) and interacts with an oscillating magnetic field. This results in the generation of local heat within the nanocarriers, which in turn enhance release of the drug. Magnetic nanoparticles are used to generate heat, either from hysteresis losses or from Néel or Brownian relaxation processes [87].

Applying high intensity magnetic field (amplitude \gg kA/m) around the MNPs can cause thermally induced damages to the surrounding tissues, resulting in pain in the living body because of high local heat generation. These thermal effects can be accepted in cancer therapy (i.e. cell apoptosis), but they may be not still accepted for a chronic disease treatment, such as inflammatory diseases. Therefore, it is recommended to use the lower intensity magnetic field (amplitude \ll kA/m). Hence, induced drug release is controlled by a mechanical oscillation, instead of heat generation. In this way, on-demand drug release can be obtained without a macroscopic heat generation, thus preventing damage from temperature and eddy current loss and safety secondary effect [88]. Figure 3.6 shows a symmetric diagram of the magnetically controlled drug release system.

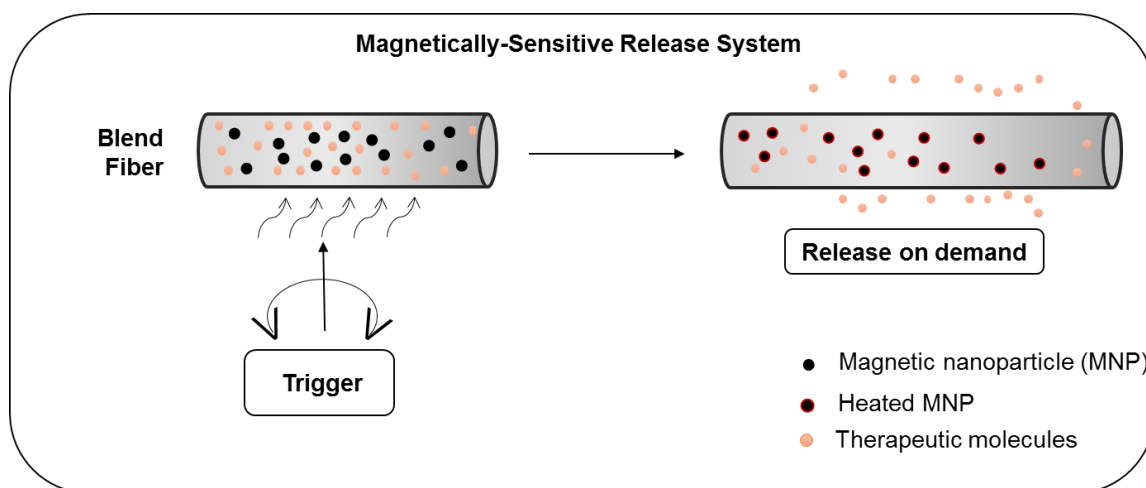


Figure 3.6: Symmetric diagram shows magnetically-sensitive release system (Picture: M. Kumar)

3.5.2 Temperature-Sensitive Release System

Some polymers change their solubility behavior upon heating and cooling [89]; they show phase separation at a certain temperature, known as lower critical solution temperature (LCST). Polymers, which become insoluble upon heating, have a so-called LCST, and which become soluble upon heating, have an UCST. The phase diagram of a polymer/solvent mixture vs. temperature shows both: a one-phase and a two-phase region, as depicted in Figure 3.7. One can be identified as the critical solution temperature: the UCST or LCST; it is the maximum (UCST) or the minimum (LCST) of the phase diagram [90]. The LCST is mainly dependent on the hydrogen bonding between water molecules and the structure of functional monomer unit of polymers.

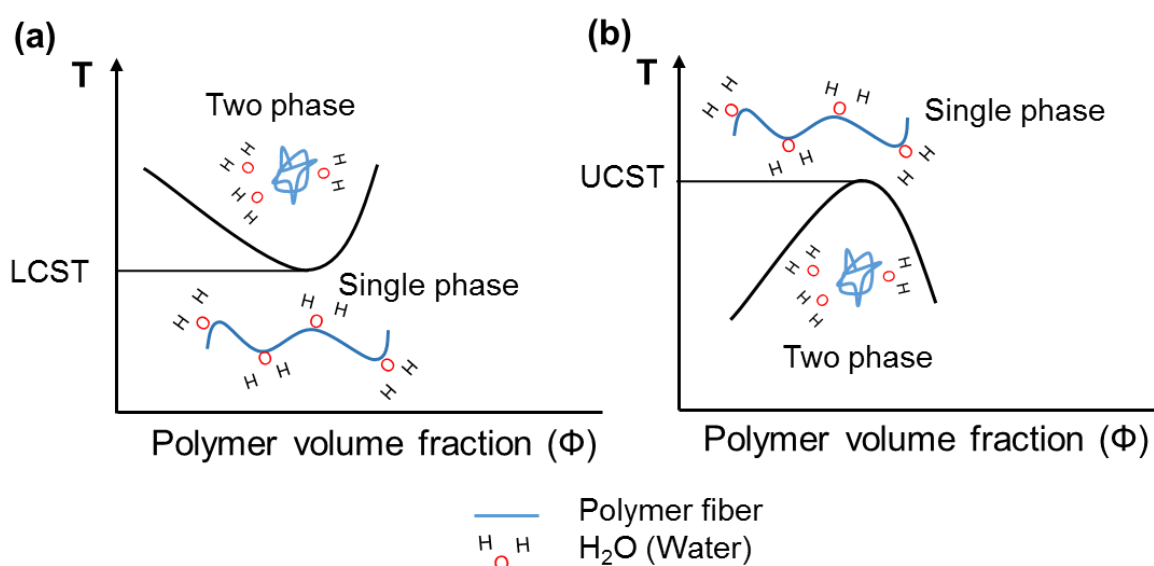


Figure 3.7: Schematic illustration of phase diagram for polymer/solvent mixture (a) lower critical solution temperature (LCST) behavior and (b) upper critical solution temperature (UCST) behavior (Pictures: M. Kumar).

The temperature-sensitive polymers generally consist of hydrophobic groups, such as methyl-, ethyl- and propyl-group. The common examples are; Poly(N-isopropylacrylamide) (PNIAAm), Poly(N,N-diethylacrylamide) (PDEAAm) and Pluronics. These materials have a lower critical solution temperature (LCST) in the range of 25 – 34°C. The temperature sensitivity of polymers is associated with the temperature dependence of hydrogen bonding and hydrophobic interactions [91]. At lower temperature, the polymer chains dissolve or swell in water because hydrophobic polymer chains are highly hydrogen bonded which lower the free energy of mixing. At higher temperatures, the hydrogen bonds weaken. At the same time, the tendency of the system to minimize the contact between water and hydrophobic surfaces, i.e., the hydrophobic interaction, increases [92]. As a result, on heating a polymer solution, a transition from swollen to collapsed state occurs at a critical temperature.

3.6 Present Challenge and their Solutions

Because of the adverse side-effect of therapeutic molecules during treatment, there is a dire need to change the approach of diagnosis. Even some of the disease treatment requires that drugs should be delivered in the feedback controlled loop system. This is possible by developing stimuli responsive drug delivery system.

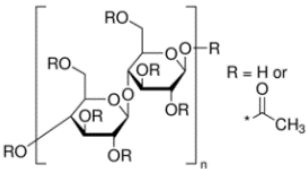
It is always better to precisely detect and quantify levels of disease by understanding their molecular heterogeneity and then accordingly provide treatment. This is a truly complex challenge. To do this, it is needed to design a very sensitive functional nano-bio surface, which will be able to measure minute changes in the heterogeneity of the system. This could be possible by incorporating the temperature sensitive molecules in the nanofibers. This leads to the development of functional nano-fibrous membranes, which permit rapid detection in the change of biological environments and provide an effective requirement for drug release.

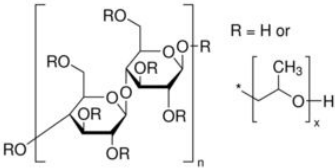
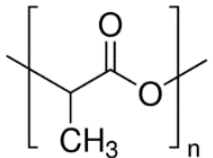
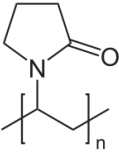
4 Materials and Methods

An exhaustive list of utilized chemicals and solvents including their suppliers is provided in Table 4.1. General analytical techniques are described below in Section 4.2. More specialized procedures relevant for the single parts of this work can be found in the respective experimental sections (Sections 7.3, 8.3, 9.3 and 10.3).

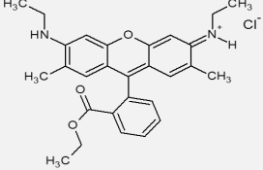
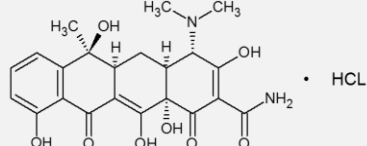
4.1 Materials

Table 4.1: Utilized chemicals, their abbreviation used and suppliers

Chemicals	Average Mw g/mol and density (d)	Abbreviation	Supplier; Grade/Purity
2,2,2-Trifluoroethanol (CF ₃ CH ₂ OH)	100.04	TFE	Carl Roth, Germany, 99.8%
Biotin-XX-NHS	--	BTN	Sigma Aldrich, Finland
Cellulose acetate 	50,000; d-1.3	CA	Sigma Aldrich, Germany
Dichloromethane (CH ₂ Cl ₂)	84.93; d-1.33	DCM	Carl Roth, Germany, 99.95%
Di-sodium hydrogen phosphate dihydrate (Na ₂ HPO ₄ · 2 H ₂ O)	177.99, d-2.1	--	Carl Roth, Germany, 99.5%
<i>Escherichia coli</i>	--	<i>E. coli</i>	Institute of organic chemistry; LUH

Hydroxypropyl cellulose 	1,000,000, powder, 20 mesh particle size	HPC	Sigma Aldrich, 99%
Iron(II) acetate anhydrous (C ₄ H ₆ FeO ₄)	173.95	FeAce	Abcr, Germany, 97%
MagSilica (Fe ₃ O ₄ @SiO ₂)	--	MagSilica®	Evonik formally Degussa AG, Germany
Methanol (CH ₃ OH)	32.04; d-0.79	MeOH	Carl Roth, Germany, 99.95%
Methylene blue trihydrate (C ₁₆ H ₁₈ ClN ₃ S · 3H ₂ O)	319.85	MEB	Sigma Aldrich
N-Vinylcaprolactam (C ₈ H ₁₃ NO)	139.2; d - 1.029	NVCL	Sigma Aldrich, Germany
Polyethylene glycol, (C ₂ H ₄ O) _n H ₂ O	1500, d-1.07	PEG 1500	abcr, Germany
Polylactic acid 	--	PLA	Ingeo™ biopolymer NatureWorks USA
Polyvinylpyrrolidone 	360,000	PVP	Sigma Aldrich, Germany
Potassium chloride (KCl)	74.56, d- 1.984	--	Carl Roth, Germany, 99%
Potassium dihydrogen phosphate (KH ₂ PO ₄)	136.09, d- 2.34	--	Carl Roth, Germany, 99%

Materials and Methods

<p>Rhodamine 6G</p>  <p>The structure shows a central xanthene ring system with two dimethylamino groups (-N(CH₃)₂) at the 6 and 7 positions, a methyl group at the 2 position, and a phenylacetate group (-OCH₂CH₂Ph) at the 10 position. A chloride ion (Cl⁻) is shown as a counterion.</p>	<p>479.02</p>	<p>Rh6G</p>	<p>Sigma Aldrich, Germany</p>
<p>Sodium chloride (NaCl)</p>	<p>58.44; d-2.17</p>	<p>--</p>	<p>Carl Roth, Germany, 99.8%</p>
<p>Tetracycline hydrochloride</p>  <p>The structure shows the tetracycline core with a dimethylamino group at C4, a methyl group at C5, and a primary amide group (-CONH₂) at C6. It is shown as a hydrochloride salt with a chloride ion (Cl⁻).</p>	<p>480.90</p>	<p>TCH</p>	<p>Carl Roth, Germany</p>
<p>Trichloromethane (CHCl₃)</p>	<p>119.38; d- 1.48</p>	<p>TCM</p>	<p>Carl Roth, Germany, 99%</p>
<p>Tetrahydrofuran (C₄H₈O)</p>	<p>72.11;d-0.89</p>	<p>THF</p>	<p>Carl Roth, Germany, 99.9%</p>

4.2 General Analytical Methods

4.2.1 Scanning Electron Microscopy (SEM)

To study specimen morphology scanning electron microscope (SEM) (Zeiss Leo VP 1455, Germany) is used. In SEM, an electron beam is generated by a filament in a vacuum chamber and is focused by electromagnetic lenses to form a beam point. When the primary electron beam impinges on the specimen surface, secondary electrons are emitted and collected by a detector to generate an image [93]. The high radiation density of the electron beam leads to static charges, which can contradict the measurements. This happens due to electrons accumulation at the measuring spot interacting with the electron beam. These charges occur in non-conductive samples, which can be prevented. For this purpose, all samples are coated with a conductive layer of platinum or gold of about 10 nm thickness (SC7620 Mini Sputter Coater, Quorum Technologies). This coating step is very important for obtaining high quality pictures with low noise interference. For the measurements, all specimens are operated on an accelerating voltage of 10 KV in high vacuum.

4.2.2 Ultraviolet-Visible (UV-Vis) Spectroscopy

To study the unknown concentration of a releasing compound in solution ultraviolet-visible spectroscopy (UV-Vis) (PerkinElmer, Lambda 650 S, Germany) is used. The basic theory behind this is the relationship between the absorbance of a species of interest and its concentration in a solution. The theory follows Beer's Lambert Law as shown below in Equation 4.1.

$$A = \varepsilon \cdot l \cdot C \quad \text{Equation 4.1}$$

where, A is the absorbance, ε is the absorbance constant, l is the cell path length and C is the concentration of the analyte of solution [94][95].

The concentration of a compound of interest in a sample can be determined using the linear relationship between absorption and concentration in a calibration graph of the compound of interest. For the measurements with methylene blue the maximum absorption of light was determined at a wavelength of 664 nm. Similarly, for tetracycline hydrochloride the wavelength for the maximum absorption of light is located at 358 nm.

4.2.3 Thermogravimetric Analysis (TGA)

To study the thermal degradation, moisture absorbance, the level of inorganic and organic components and solvent residues of the specimen thermogravimetric analysis (TGA)

(NETZSCH STA 409, Germany) were conducted. TGA examines the mass change of a material as function of temperature in the scanning mode or as a function of time in the isothermal mode [96][97]. It can also be used to identify types of polymers in polymer blends or mixtures by comparison of degradation curves, as well as to identify and quantify additives and also give an indication of thermal stability.

A TGA curve consist of two portions: 1. Horizontal and 2. slanting portion. Horizontal portion indicates the region where there is no mass change. This state thermal stability of the materials. It reveals the temperature in which substances like polymer, packing materials and alloys may be safely used. Whereas the slanting downward portion indicates the region which represents weight loss, due to dehydration/rupture/formation of volatile products, due to decomposition or dissociation etc.. Hence, the qualitative and/or quantitative information regarding the substance can be obtained from thermogram.

In qualitative analysis:

- Stability of the substance at elevated temperature
- Identification of the substances and their purity determinations
- Decomposition mechanisms of polymers, inorganic salts etc.

In quantitative analysis:

- How much of a substance is present in the sample
- To find out the amount of filler in a polymeric sample

T_g values also depend on the molecular weight of polymers according to the Flory-Fox equation [98].

$$T_g = T_g^* - \frac{K}{M_n} \quad \text{Equation 4.2}$$

where, T_g^* is the glass transition temperature at infinite molecular weight and K is a constant [98].

4.2.4 Differential Scanning Calorimetry (DSC)

To study fusion and crystallization events as well as to identify the glass transition (T_g) temperature and melting temperature (T_m), differential scanning calorimetry (DSC) (NETZSCH STA 409, Germany) was used. In DSC technique, the difference in the amount of heat required to increase the temperature of a sample and reference is measured as a function of temperature. As the temperature increases, an amorphous polymer will become less viscous and at some stage, the polymer chains may obtain a freedom of motion to rearrange themselves into crystalline domains. This is known as the

crystallization temperature (T_c). The transition of crystalline to amorphous forms is an exothermic process seen as an exothermic peak in the DSC curve. A further increase in the temperature causes the polymer to reach its melting temperature [97].

A considerable amount of PLA properties depends on its degree of crystallinity. Different grade (molecular weight) has a considerable influence on the melting temperature (T_m) of polymeric crystals. One of the most generally employed methods to determine the crystallinity of PLA is DSC by the following equation.

$$\text{Crystallinity (\%)} = \frac{\Delta H_m}{\Delta H_{m^\circ}} \quad \text{Equation 4.3}$$

Where, ΔH_m is the enthalpy of fusion of the studied sample and ΔH_{m° is the enthalpy for 100% crystalline PLA samples being equal to 93.7 J/g [99] assuming no cold crystallization taking place during the heating run, otherwise the cold-crystallization enthalpy should be subtracted from the melting enthalpy.

4.2.5 Micro Raman Spectroscopy (MRS)

To study molecular information on the specimen, micro Raman spectroscopy (MRS) (Bruker Optik GmbH, Germany) was used. In Raman spectroscopy the frequency changes arises in molecules, when exposed to electromagnetic radiation [100]. Raman spectroscopy provides complementary information on the sample to infrared spectroscopy, as the selection rules involved mean that some bands visible in Raman are not seen in the infrared and vice versa. One of the important advantages of Raman spectroscopy is that the symmetrical bonds such as C-C, C=C and C≡C manifest themselves by giving the most intensive bands in the Raman spectra, while being inactive in the infrared [101][96]. In this study, such information is important because very small amount of TCH is incorporated in nanofibers (see Chapter 8). The exact molecular composition, quantitatively and qualitatively can be determined with the MRS.

4.2.6 Contact Angle (CA)

To study wetting behavior of a specimen by a liquid, contact angle (CA) (Universal, Surftens, OEG GmbH, Germany) measurements were performed. In CA measurements, a drop of liquid (water) is laid on a nanofibrous membrane. The drop will be in an equilibrium position where the three forces involved known as the interfacial tensions between solid and liquid are balanced. The interfacial tension between solid, liquid, and gas is described by the relationship between the cosine of the drop/surface contact angle and the three surface tensions, given by Young's equation, as follows:

$$\gamma_{SV} = \gamma_{SL} + \gamma_{LV} (\cos\theta) \quad \text{Equation 4.4}$$

where, γ_{SV} is interfacial energy between solid and vapor, γ_{SL} is interfacial energy between solid and liquid and γ_{LV} is interfacial energy between liquid and vapor, respectively [102]. If the substrate is hydrophobic, then $\theta > 90^\circ$, since the droplet does not wet the surface. On a hydrophilic substrate ($\theta < 90^\circ$), the droplet partially or fully wets the surface. Figure 4.1 shows components of a three phase system for contact angle measurements.

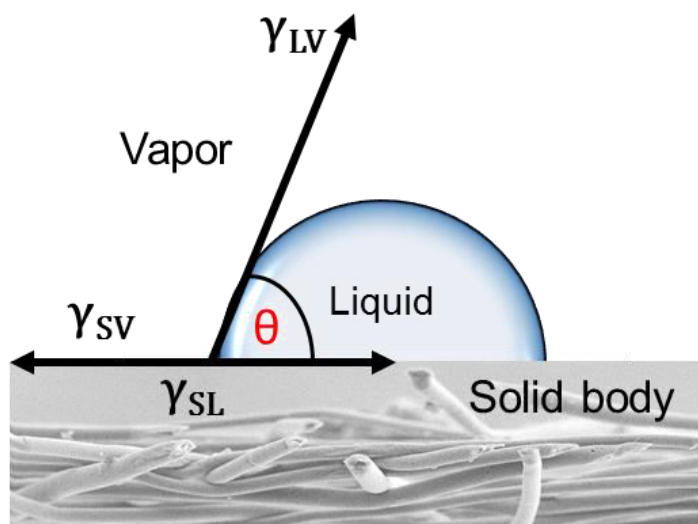


Figure 4.1: Schematic illustration of the contact angle measurements on fibrous membranes (Picture: M. Kumar)

5 Biopolymers

In literature and patents there is no consensus on the exact definition of the generic terms biopolymers and bio-based which appear to have multiple and overlapping meanings. The term “biopolymers” has been defined in a variety of ways by researchers in different disciplines. In general, biopolymers fall into two principal categories [103]:

- (1) Polymers that consist (partly) of bio-based (renewable) raw materials, for example plants, animals, microorganisms etc.
- (2) Materials, that are in some way biodegradable

Bio-based term applies to polymers which derive from renewable resources. ASTM (American Society for Testing and Materials) defines a bio-based material as “an organic material in which carbon is derived from a renewable resource via the biological process”. Currently, there are no standards on what can be called “bio-based product”. However, there are objective ways to quantify the bio-based content of a product. The bio-based content of a biopolymer can be determined by calculating the number of carbon atoms that come from the short CO₂ -cycle, that is, from biomass as raw material. It is known that carbon-14 (¹⁴C), which has a half-life of about 5700 years, found in bio-based materials but not in fossil fuels. Thus, “bio-based materials” refer to organic materials in which the carbon comes from non-fossil biological sources. The detection of ¹⁴C is indicative of a bio-based material.

Biopolymer is a current trending topic in research as confirmed by the increasing number of scientific publications as reported by ISI Web of knowledge. Figure 5.1 shows the exponential trend of the scientific publications from the year 2000 up to 2016.

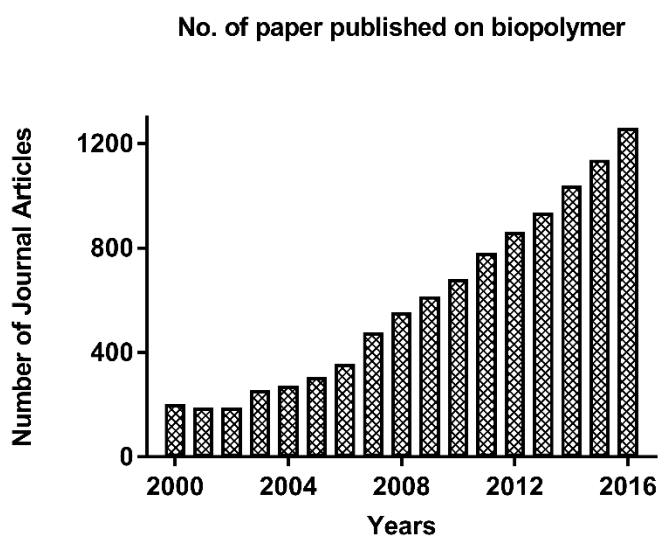


Figure 5.1: Number of scientific papers published on biopolymers (Source: Web of Science accessed on 6 March 2017)

5.1 Classification of Biopolymers

Biopolymers can be divided also into two broad groups, namely biodegradable and non-biodegradable polymers. Biodegradable polymers are further categorized in two main groups, 1) agro-polymers 2) biopolyesters. A broad classification of biopolymers is shown in Figure 5.2 [104]. Examples of biodegradable polymers are cellulose, wheat and PLA and examples of non-biodegradable polymers are Epoxy, PU (Polyurethane), PVC (Polyvinyl chloride) etc. Further classifications of biodegradable polymers are shown in Figure 5.3.

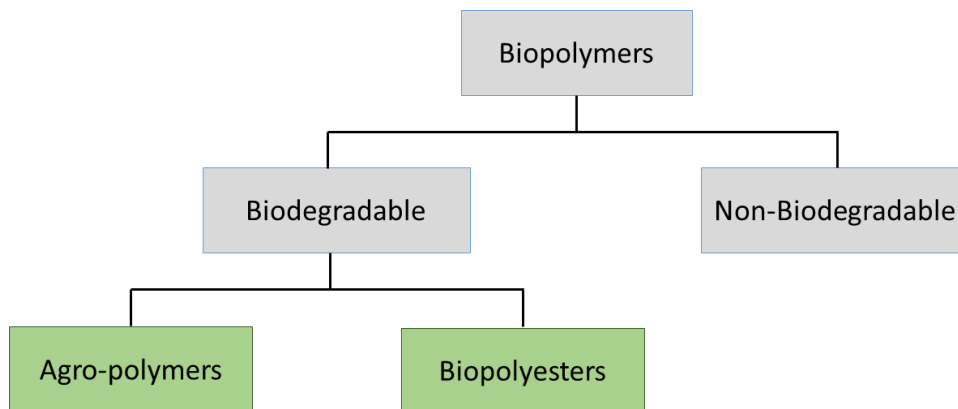


Figure 5.2: A broad classification of biopolymers

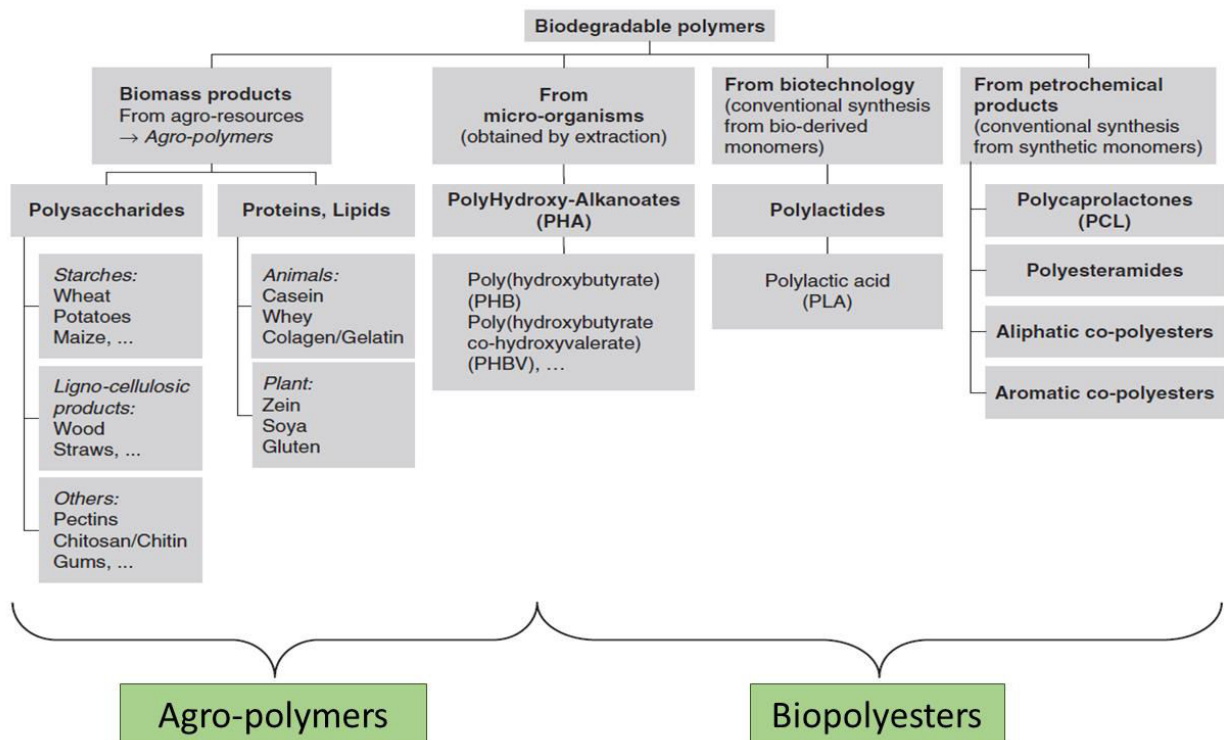


Figure 5.3: Classification of the biodegradable polymers (Adapted from Reference [105].)

Some of the mentioned biopolymers can be derived from both agro-polymers and biopolyesters resources, such as PLA (Polylactic acid). Although PLA is largely produced by fermentation from renewable resources such as starch and sugarcane, it can be synthesized also from fossil fuels.

5.2 Poly(lactic acid) (PLA)

In today's world of "green chemistry", polymers from renewable resources are attracting increasing interest as potential substitutes for petrochemical-based materials in many applications [106]. The most attractive and commonly used synthetic polymers are polylactic acid (PLA), polyglycolide (PGA) and polylactic-co-glycolic acid (PLGA), which carry all important characteristic properties of a biodegradable biomaterial [107]. Furthermore, these materials are commercially available in different compositions and molecular weights, which allow the control of polymer degradation [108].

Polylactic acid (PLA) is at present, represents front-runner biocompatible thermoplastic aliphatic polyester [98], as an alternative to conventional polymers, such as polypropylene (PP), polyethylene terephthalate (PET) and polystyrene (PS). PLA offers environmental benefits, such as low energy to produce and reduced green-house gas production. It belongs to polyester family, characterized by their potentially hydrolysable ester bonds. The building block, or monomer, for PLA synthesis is lactic acid. Lactic acid is a chiral molecule, this means that two optical isomers or enantiomers exists. One is known as L-(+)-lactic acid and the other is as the D-(-)-lactic acid, and a mixture of both, the racemic lactic acid as shown in Figure 5.4.

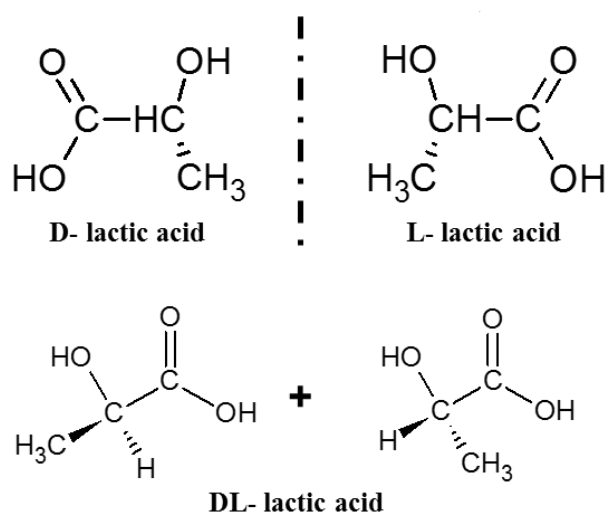


Figure 5.4: Structures of mono D-, L- and DL-lactic acid

Lactic acid (2-hydroxypropionic acid), is synthesized by fermentation process using renewable resources such as glucose. These sugar feedstocks are drawn from agricultural (potato skins and corn) and dairy wastes. The lactic acid monomers produced by fermentation can be used to create either low or high molecular weight polylactide polymers. Variation of the reaction conditions, such as temperature and choice of catalyst, provides control over the molecular weight of the polymer. Figure 5.5 shows the life cycle of PLA.

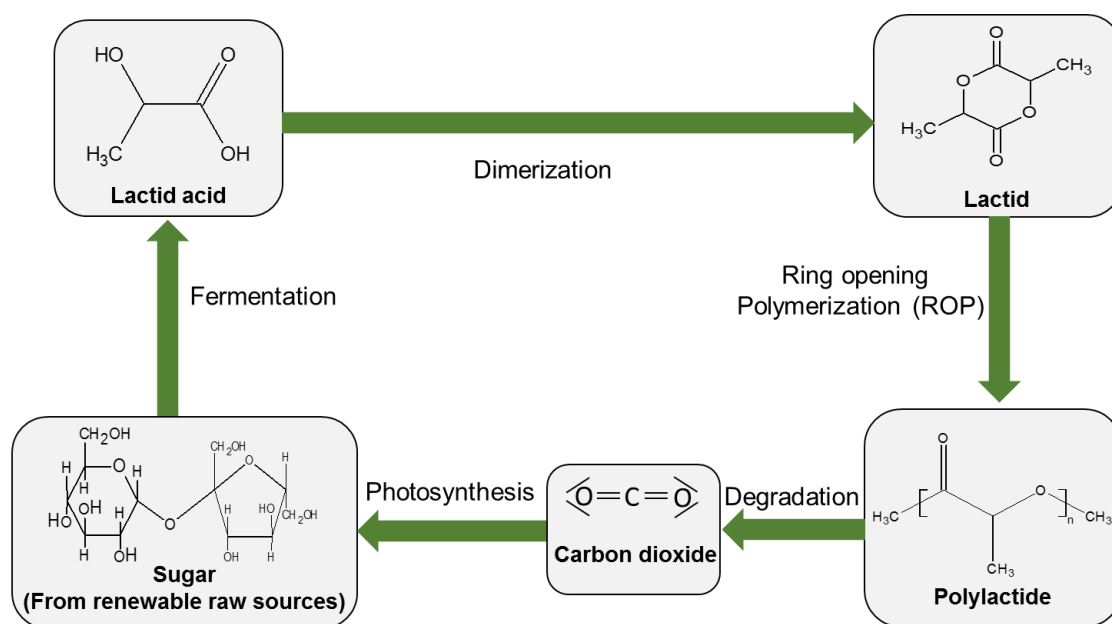


Figure 5.5: PLA life cycle

PLA can be prepared by (a) direct condensation of lactic acid and (b) ring-opening polymerization [109] of the cyclic lactide dimer. Direct condensation route of lactic acid limits the high molecular weight PLA, because of the difficulty in removing trace amount of water in late stage of polymerization. Therefore, ring-opening polymerization (ROP) of lactic acid is favorable by using different initiator such as Sn(II)_2 -ethylhexanoate (Sn(Oct)_2) [110], Zn-Lactat [111], Al-Isopropoxid [112] etc. Out of these initiator, Sn(Oct)_2 is preferred because of the high reaction rate of the polymerization, the low degree of racemization, solubility in common organic solvents and its commercial availability [113][114]. Several mechanisms have been proposed for the Sn(Oct)_2 induced polymerization [115]. According to the most recent results [116], the polymerization mechanism of PLA using Sn(Oct)_2 initiator is shown below in Figure 5.6.

PLA Production Mechanisms

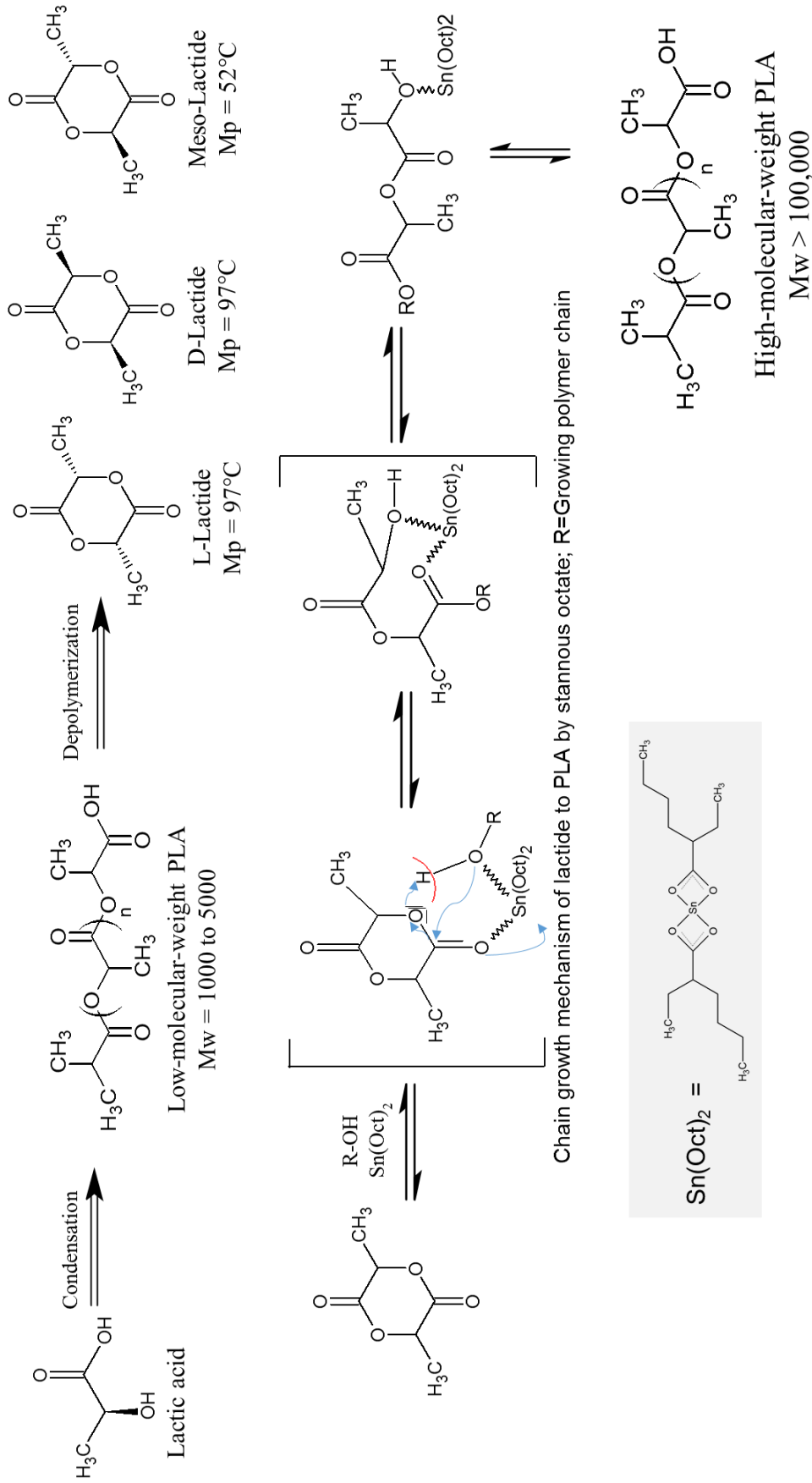


Figure 5.6: Current production steps for PLA.

PLA-based materials have been extensively investigated for biomedical applications, such as controlled drug release, packaging materials and biosensors, as shown in Figure 5.7. The reason for this is, that the final degradation product of PLA, lactic acid, is a metabolite and can be easily eliminated from the human body via the Krebs cycle. Even lactic acid is biodegraded by microbes into carbon dioxides, methane and water [117]. The use of PLA is interesting due to its hydrolytic degradability and low toxicity [118]. Figure 5.8 show digital image of PLA pellets. In this thesis, the focus is in the development of PLA based fibrous membranes with on-demand drug delivery capability and biosensors applications.

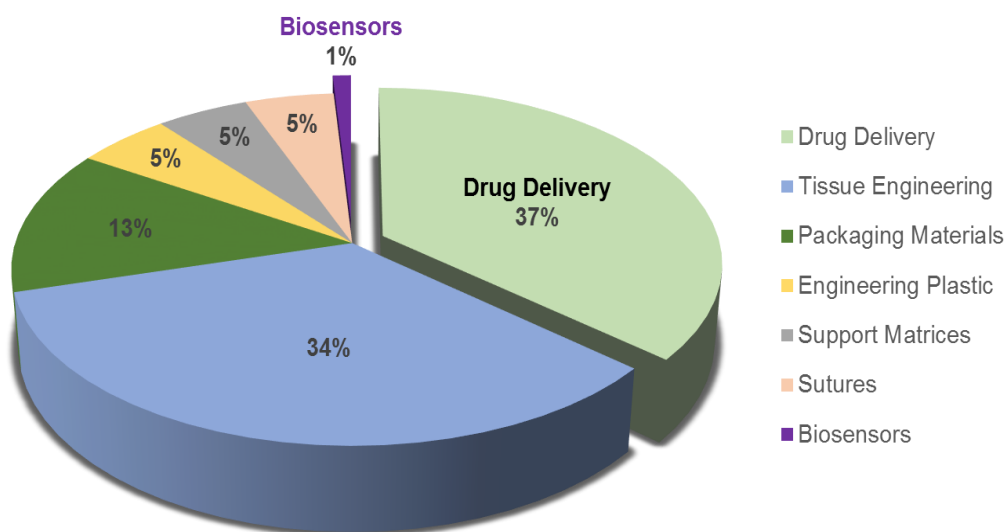


Figure 5.7: Some of the biomedical applications of PLA (Source: Web of Science accessed on 20 Dec 2016)

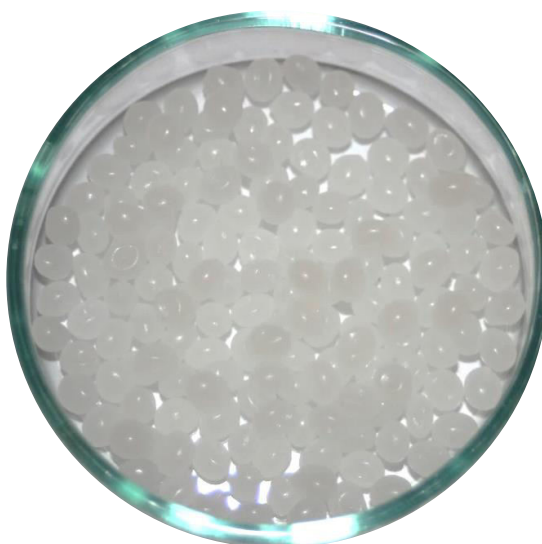


Figure 5.8: PLA 6202 pellets (Picture: M. Kumar).

5.3 PLA Advantages and Disadvantages

The properties of PLA can be tailored by the ratio of lactic acid isomers (L and D lactic acid) used.

Essential advantageous properties of PLA are:

1. It is obtained from a renewable agricultural source (corn).
2. Its production consumes quantities of carbon dioxide (low environmental impact).
3. It is recyclable and compostable.
4. It is degraded by the human body.
5. It has high modulus of elasticity.
6. It has high transparency (low degree of crystallinity).
7. It is water, oil, fat, and some alcohol resistance.

However, PLA has some disadvantageous properties:

1. It is strong hydrophobic.
2. It has poor thermal stability (glass transition temperature 45-65°C, melting temperature 150-160°C).
3. It is low resistance to solvents, acids, and bases.

There are several approaches to improving hydrolysis resistance and/or chemical resistance in PLA materials, such as:

1. End group modification
2. Blending
3. Co-monomer
4. Minimizing residual monomer

5.4 Polyethylene Glycol

Polyethylene glycol (PEG) is a hydrophilic, non-ionic polyether. It is synthesized from ethylene oxide via an anionic ROP in the presence of small amount of water and metal hydroxides (MOH). Synthesis of PEG is shown in [Figure 5.9](#). PEG is widely resistant to hydrolytic and enzymatic degradation, yet susceptible to oxidation of its terminal hydroxyl group and subsequent chain shortening by a single oxyethylene unit. PEG influences the pharmacokinetic properties of a multitude of drugs and biologically active compounds such as proteins, DNA, and also small molecules. Therefore, it play a key role in many biomedical applications [119].

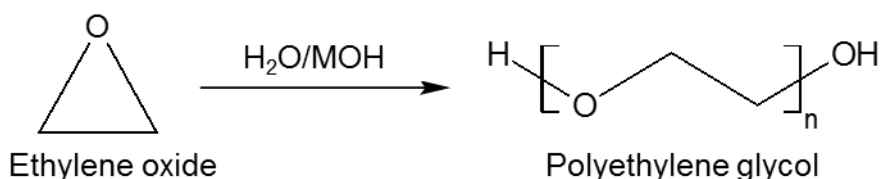


Figure 5.9: Polyethylene glycol preparation by using ethylene oxide polymerization

PEG is one of the most widely used biocompatible polymers. It is mainly used because it improved solubility, controlled permeability through biological barriers and longevity in the blood stream [120]. It is used for surface modification, to provide protein- and cell-rejecting properties, and to control electro-osmosis. The main property of PEG is its “exclusion effect” or “steric stabilization effect”. It is well accepted that heavy hydration, good conformational flexibility and high chain mobility are principally responsible for the exclusion effect [121][122]. PEG work only as a hydrogen bond acceptor, not as a donor [123].

PEG molecules are completely soluble in water at low temperature, whereas it loses its solubility at elevated temperatures [124]. This happens because at lower temperatures, the solubility of non-polar substances is increased due to a formation of a relatively ordered water layer around the non-polar substance. The structure is preserved to maintain as many hydrogen bonds between the water molecules as possible, despite the presence of the solute. At higher temperatures, where entropy becomes more important, the solubility decreases [124].

PEG is most popularly used polymer because of many advantages, such as good hydrophilicity, flexibility, antiphagocytosis against macrophages, nontoxicity and biocompatibility [125].

5.5 N-vinyl Caprolactam

N-vinylcaprolactam (NVCL) is one of an important group of vinyl compounds. It is a non-ionic, nontoxic, water soluble, thermosensitive and biocompatible monomer. NVCL finds wide applications for biomedical applications. NVCL shows of its stability against hydrolysis, which makes it more biocompatible than other existing thermo-responsive polymer such as (N-isopropylacrylamide, (NIPAA_m)). It is dissolved in both polar and non-polar organic substances. Solvents such as benzene, hexane, isobutanol, isopropanol are used with a free radical initiator for the solution polymerization of N-vinylcaprolactam [126]. The mechanism for the synthesis of NVCL is shown in Figure 5.10. Table 5.1 shows physical properties of NVCL monomers.

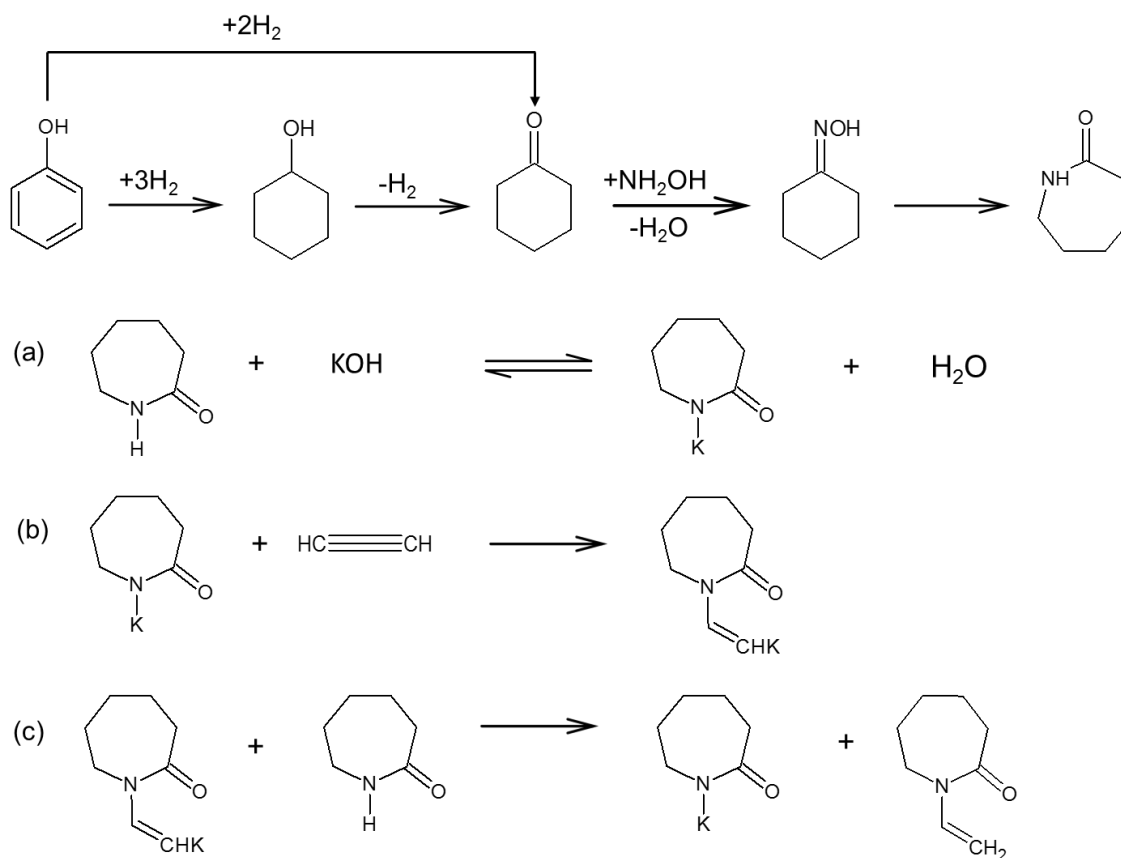


Figure 5.10: Mechanism for the preparation of NVCL (Adapted from Reference [127])

Table 5.1: Characteristics of N-Vinylcaprolactam NVCL.

Molecular Formula	C ₈ H ₁₃ NO
Appearance	White Crystals
Melting point	35-38°C
Density, g/mL at 25°C	1.029 g/mL
Viscosity	6.16 mm ² /s
Stability	Stable at RT
Solubility	Water, alcohols (methanol, ethanol, propanol, etc.), amides (DMF), chlorinated hydrocarbons (CH ₂ Cl ₂) and aromatic hydrocarbons (toluene, benzene, xylol).

5.6 Hydroxypropyl Cellulose

Hydroxypropyl cellulose (HPC) is a non-ionic cellulose derivative which can be synthesized by substituting with hydroxypropyl ether groups [128]. HPC could also be used in the field of biomedical application such as drug delivery [129][130], because it is a physiologically inert substance and is considered to be non-toxic. A mechanism for the preparation of HPC is shown in Figure 5.11.

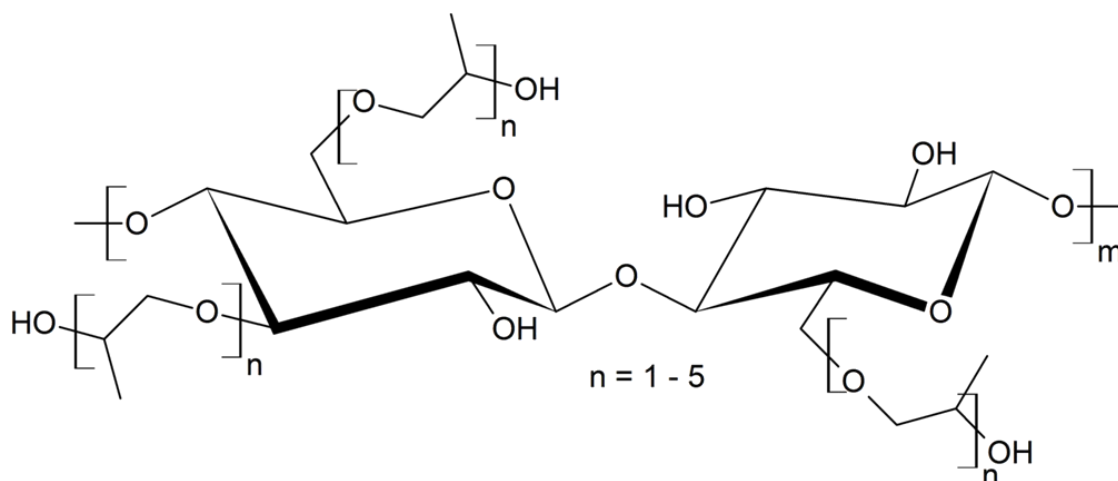


Figure 5.11: Structure of Hydroxypropyl cellulose (HPC) (Adapted from Reference [131])

HPC- molecule is more lipophilic than other water-soluble cellulose ethers. This makes it compatible with a large number of anionic, cationic, non-ionic, and amphoteric surfactants. It shows an unusual combination of properties such as [132]:

1. Solubility in organic solvents at any temperature
2. Hydration in cold water
3. Insolubility in hot water
4. Thermoplasticity

The stability of HPC against process-related changes of temperature, pH value and shear force is high. The HPC- molecules react to these parameters by temporary and reversible changes in its physical state. Upon removal of these factors, the original texture can be retained. Table 5.2 shows some of the characteristics of HPC molecule.

Table 5.2: Characteristics of Hydroxypropyl cellulose (HPC)

Origin	Wood pulp or cotton
Chemical composition	Linear molecule of β -D-glucose with uncharged hydrophilic ($\text{CH}_2\text{CHOHCH}_3$) substituents
Fiber content	97% soluble dietary fiber
Toxicology	No
Solubility in H_2O	T = 0-38°C: high, 100% soluble T > 40-45°C: insoluble (precipitation of dissolved HPC)
Solubility in other solvents	e.g. Methanol, Ethanol, Propylene glycol
Appearance of an aqueous solution	Water-clear, transparent
pH stability	High (from pH 2-11)
Film formation	High
Gelation	No
Emulsion stabilization	Support of emulsifiers
Surface activity	High, good foam generator
Protein activity	Low

6 Electrospinning of PLA

The transformation of PLA into fibers structures depends on structural changes in the polymer during processing (physical, systemic and solution). There are distinct features of each of these properties, subsequently reflected in fiber morphologies.

6.1 PLA Solution Property

6.1.1 PLA Solubility

The solubility of a biopolymer is determined by its morphology (polarity, presence or absence of crystallinity, etc.) and composition. Generally, biopolymers with low crystallinity are easy to dissolve than those of high crystallinity. A good solvent for PLA is Dichloromethane (DCM) and trichloromethane (TCM). PLA is also soluble in some other organic solvents like tetrafluoroethylene (TFE), tetrahydrofuran (THF). PLA is insoluble in water, some alcohols (e.g. ethanol, methanol) and alkanes [133]. Table 6.1 shows solubility of PLA with different solvent and their fiber formation ability [134].

Table 6.1: Solubility of PLA with different solvent.

Biopolymer	Product Code	Solvent	Mol. Mass of Solvent (g/mol)	Solubility	Fibers formation
PLA	6202	Dichloromethane (DCM), CH ₂ Cl ₂	84.9	Soluble and transparent	Yes
		Trichloromethane (TCM), CHCl ₃	119.4	Soluble and transparent	Yes
		Tetrahydrofuran (THF), C ₄ H ₈ O	72.1	Partially Soluble	Yes
		2,2,2-Trifluoroethanol (TFE), C ₂ H ₃ F ₃ O	100	Soluble and opaque	Yes
		Methanol (CH ₃ OH),	32	Not soluble	No
		Ethanol (C ₂ H ₅ OH)	46	Not soluble	No
		Water (H ₂ O)	18	Not soluble	No

6.1.2 PLA Miscibility

For the development of functional biodegradable materials, the two most important issues should be satisfied: (1) miscibility or compatibility of the biopolymer blend, and (2) suitable solvent. The miscibility of PLA biopolymer with another biopolymer is presented in Table 6.2. These functional materials improve the end-use properties of biodegradable polymers.

Table 6.2: Miscibility of PLA (6202) with other biopolymers

PLA (6202) + polymers	Molecular weight	Provider	Solvent	Miscibility
Polyethylene glycol (PEG)	1500	abcr	TCM (CHCl ₃)	Miscible (transparent)
N-vinylcaprolactam	139.19	Sigma Aldrich	TCM (CHCl ₃)	Miscible (transparent)
Hydroxypropyl cellulose (HPC)	1,000,000	Sigma Aldrich	TFE (C ₂ F ₄)	Miscible (opaque)
Cellulose acetate (CA)	50,000	Sigma Aldrich	TFE (C ₂ F ₄)	Miscible (opaque)
TCM: Trichloromethane (CHCl ₃); TFE: Tetrafluoroethylene (C ₂ F ₄).				

6.2 PLA Fiber Formation by Electrospinning

8 wt% PLA was dissolved in chloroform (CHCl₃) solvent at room temperature and stirred for 10 hours to obtain a uniform viscous solution. The used concentration of 8 wt% was an experience value (choice) of author, which was obtained from more than 100 PLA electrospun samples. PLA electrospun fibers were possible to fabricate at concentration range between 1 wt% to 20 wt%. This 8 wt% of PLA viscous solution was filled in a 3mL plastic syringe equipped with a blunt end stainless steel needle having a size of 0.80×22 mm² (21×7/8 G’’).

During electrospinning at room temperature, a positive high voltage was maintained between needle (as a positive terminal) and stainless steel flat surface covered with aluminum foil (as negative terminal). Under this applied electrostatic field, the polymeric hemi-sphere droplet surface gets elongated to form the “Taylor cone” and when it reaches the critical point, the repulsive force overcomes the surface tension of the polymeric solution. Hence, the charged jet was emitted from the end of Taylor cone and converted

into a web of fibrous material which is collected on the grounded substrate. In this experiment, single-nozzle electrospinning apparatus was used as described in section 2.3.1. An electrode distance of 12 cm, a flow rate of 1 ml/h, and a voltage of 10 KV (at the syringe) gives PLA fibers with diameters approximately of 6 μm . These electrospun membranes were then peeled off from the collector and kept for drying at room temperature to remove the residual solvent [135]. Figure 6.1 show 3 D image of the PLA electrospun fibrous membrane in CHCl_3 solvent. Figure 6.2 shows SEM image of a single PLA fiber.

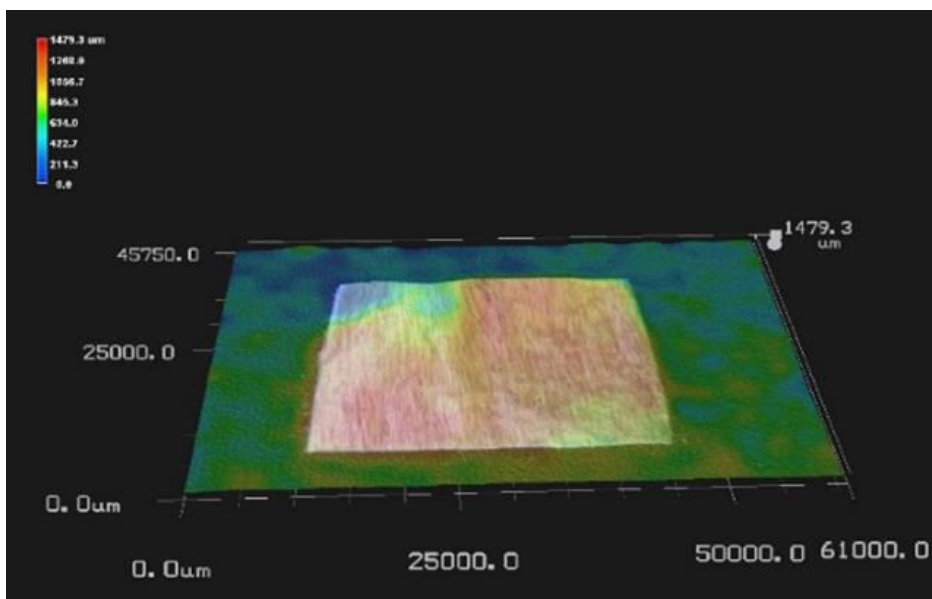


Figure 6.1: 3D image of PLA electrospun fibrous membrane (Picture: M. Kumar)

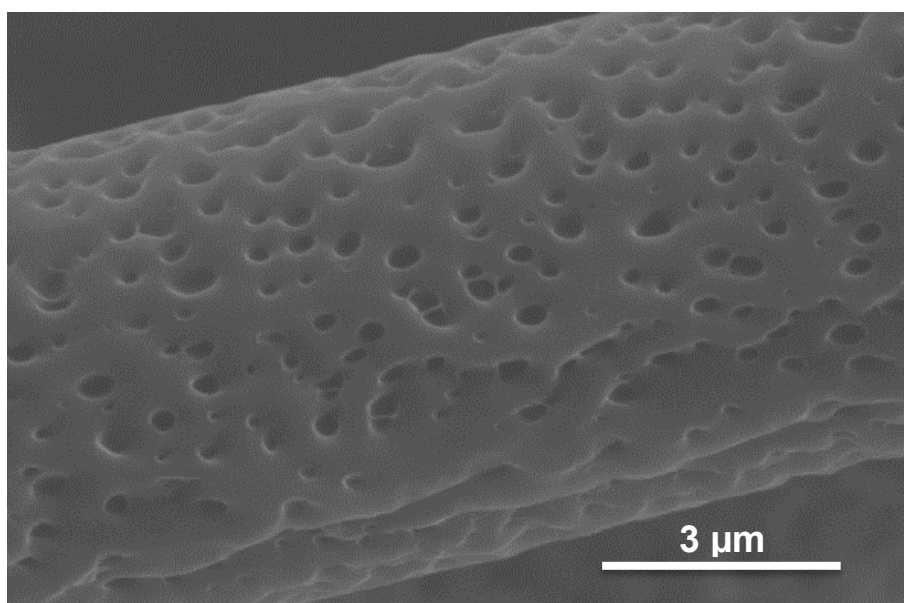


Figure 6.2: SEM image of single PLA fiber in chloroform solvent (Picture: F. Dencker)

The choice of solvent, polymer molecular weight, and parameters of electrospinning, strongly influences the fibers diameter and their morphology. Another organic solvent like, DCM, THF and TFE can also be used for electrospinning of PLA but the morphology of the fibers will be different. For example, 8 wt% PLA fibers in DCM solvent are porous because the applied voltage is low enough and the solvent is more volatile (Figure 6.3 a), [136], whereas PLA fibers pores are covered in THF solvent (Figure 6.3 b).

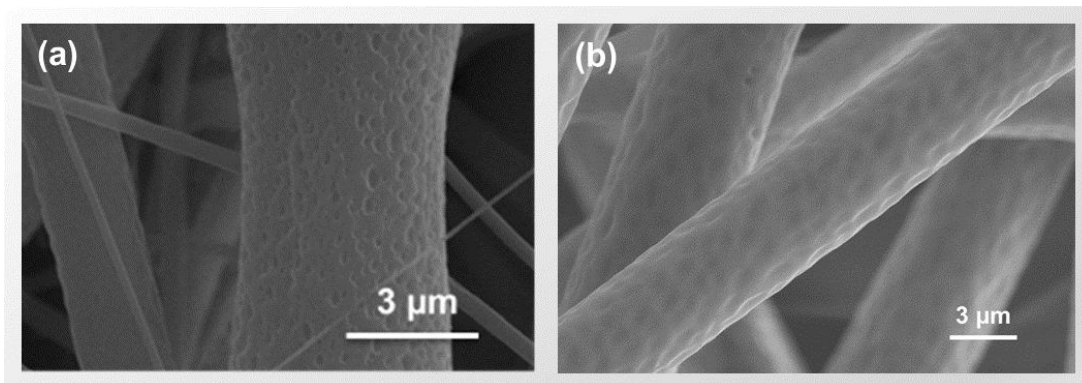


Figure 6.3: SEM micrograph of PLA electrospun fiber in (a) DCM solvent and (b) THF solvent

For average fibers diameter more than 50 measuring points per fibrous membrane are used. As discussed above, PLA fibers are porous, which provide additional sites for adsorption. The porosity is induced as a result of condensation of moisture in the air.

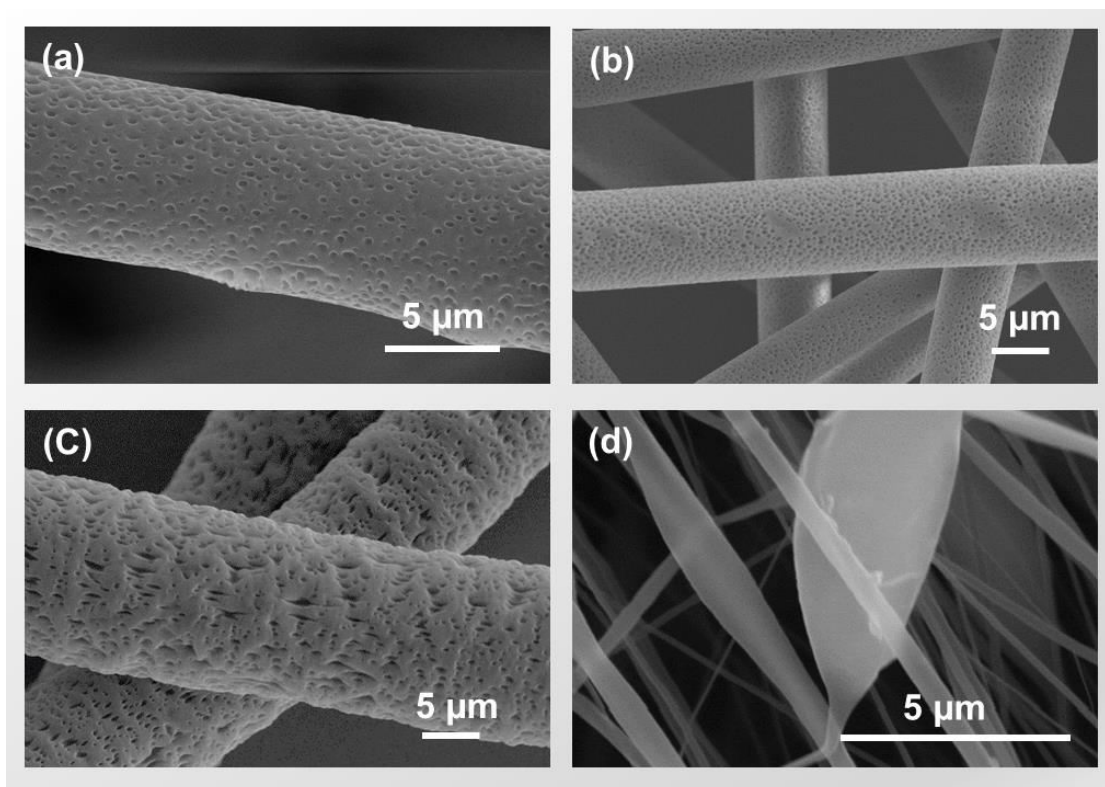


Figure 6.4: SEM micrograph shows electrospun fiber of (a) 8 wt% PLA in DCM (b) 8 wt% PLA in TCM (c) 20 wt% PLA in TCM and (d) 0.1 g/mL PLA in TFE solvent

Figure 6.4 shows the effect of different solvents (DCM, TCM and TFE) on PLA fibers porosity. It is observed that 8 weight% of PLA in DCM and TCM solvent have an ability to form spherical-like pores, whereas pores of 20 weight% of PLA in TCM solvent changed from spherical to spindle-like shape because of increased concentration. It is also observed that pores of 0.1 g/mL PLA in TFE solvent are vanished [137].

6.2.1 Concentration Effects

By analyzing different concentration of PLA samples (8 wt% in CHCl_3 , 8 wt% in C_2F_4 , 10 wt% in CHCl_3 and 20 wt% in CHCl_3), where the distance between the tip of the needle and collector was 20 cm, applied voltage was 15 KV and the feed rate was 1 ml/h, it was found that, by increasing the concentration, fibers with higher diameters were obtained, as shown in Figure 6.5. Increased concentration means that the viscosity is strong, which brings greater resistance of the solution to be stretched by the charges on the jet [29]. Optimal concentration is required to yield fibers without beads. Higher concentration => higher diameter.

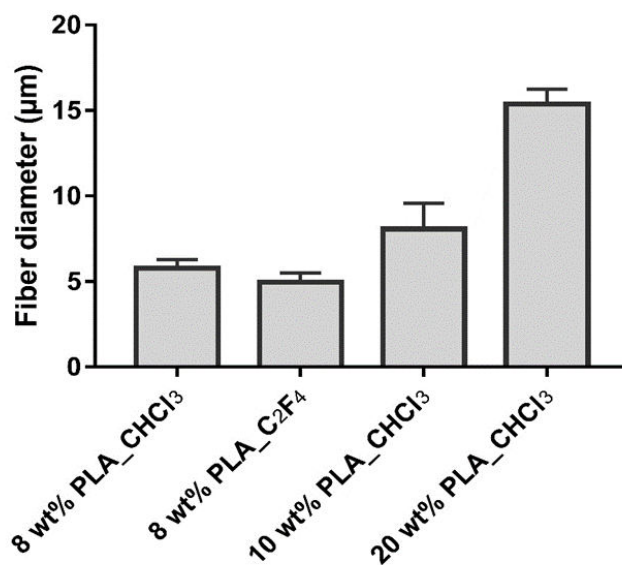


Figure 6.5: Average fibers diameter distribution v/s concentration of PLA

6.2.2 Voltage Effects

By analyzing 8 wt% PLA sample, where the distance between the tip of the needle and collector was 20 cm and the feed rate was 1 ml/h, applied voltage was varied (10 KV, 15 KV, 18 KV, 20 KV and 22 KV), it was found that by increasing the applied voltage, fibers with lower diameters were obtained, as shown in Figure 6.6. This effect occurs because the fibers were more stretched, due to high electric field strength (greater columbic forces) between the needle tip and collector, and also encourage faster solvent evaporation [29].

If the voltage applied is too high, the increased instability of the jet can result in beads formation. Higher voltage => lower diameters.

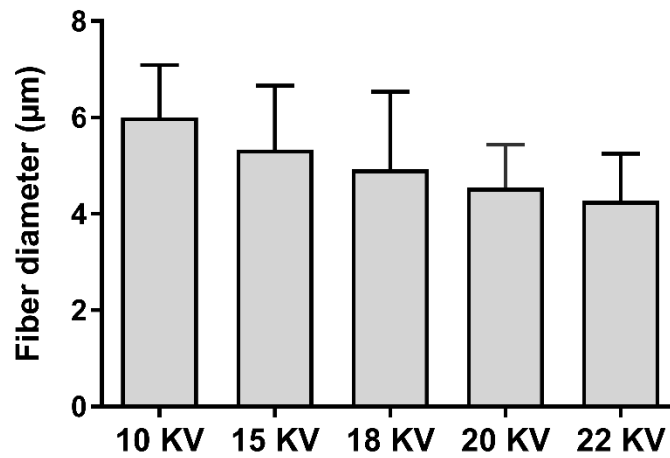


Figure 6.6: Average fibers diameter distribution v/s applied voltage for PLA

6.2.3 Feed Rate Effects

By analyzing 8 wt% PLA sample, where the distance between the tip of the needle and collector was 15 cm, applied voltage was 15 KV and the feed rate was varied (0.5 ml/h, 1 ml/h, 2 ml/h and 2.5 ml/h), it was found that, the average fiber diameters were increased, as shown in Figure 6.7. When the feed rate is increased, there is a greater volume of solution that is drawn away from the tip of the needle, which increasing the fiber diameter [29]. More solution => higher diameter.

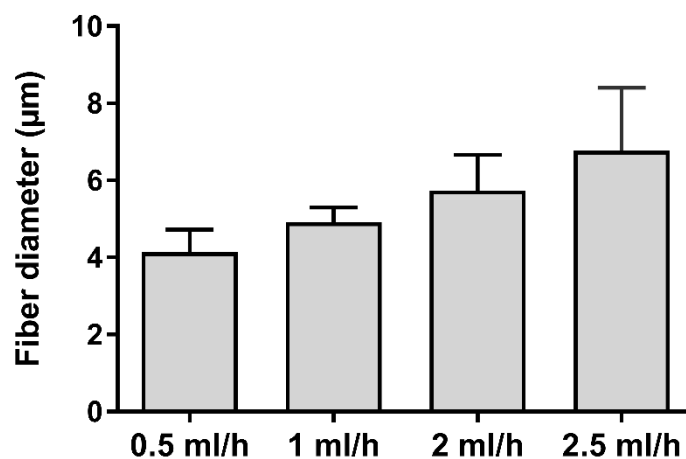


Figure 6.7: Average fiber diameter distribution v/s PLA flow rate

6.3 Surface Modification of PLA Electrospun Fibers

In general, surface properties can be divided into two major groups: (1) physical and (2) chemical. Physical properties include the morphology (roughness and smoothness), specific surface area and surface polarity. Chemical properties include elemental, molecular and functional group composition. In term of PLA fibers surface modification, the use of a surface treatment is desirable to promote wettability and increase the interfacial bonding by removing native surface material and hence leave behind a more active functional group.

Therefore, two methods are adopted to alter the surface of PLA electrospun fibers: (1) Plasma treatment and (2) blending, as shown in Figure 6.8.

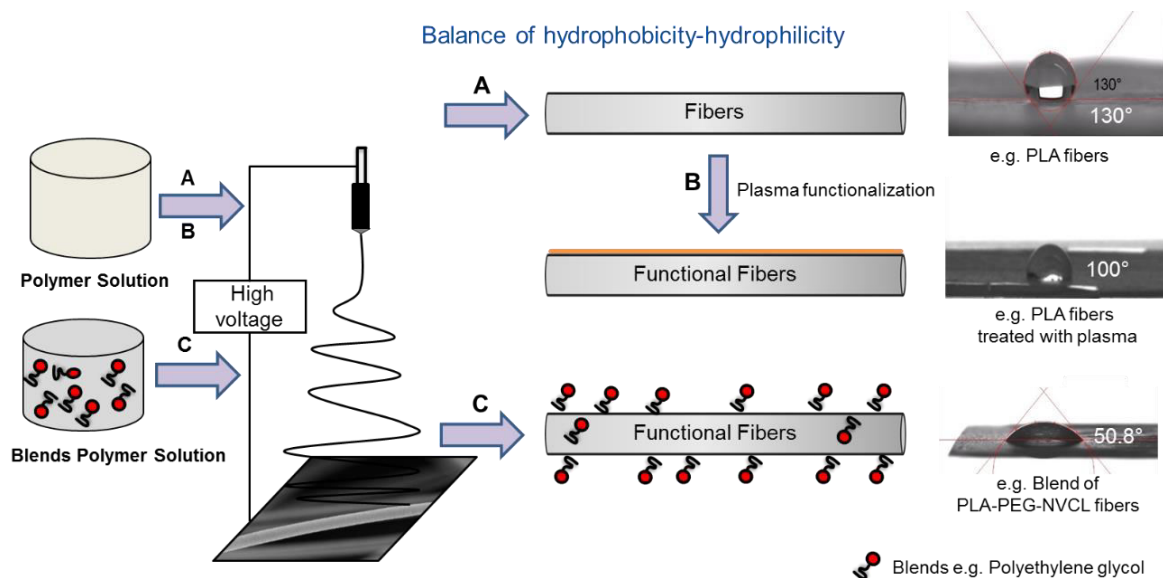


Figure 6.8: Surface modification technique applied on PLA electrospun fibers (A, C) Co-electrospinning and (B) Plasma treatment (Picture: M. Kumar)

Plasma jet is applied on PLA fibrous membranes. The distance between the plasma needle and sample (PLA membranes) is 6 centimeters. PLA fiber decreases their hydrophobicity as shown by a decrease in water contact angle from 130° to 100°. SEM analysis showed morphology of PLA fiber retained even after plasma etching (Figure 6.9). In order to further decrease in hydrophobicity, blending of PEG and NVCL to PLA is applied. PLA-PEG-NVCL fibrous membrane became hydrophilic as shown by a decrease in water contact angle from 130° to 50.8°. Therefore, blending method is applied for the further development of nano-bio-fibrous materials.

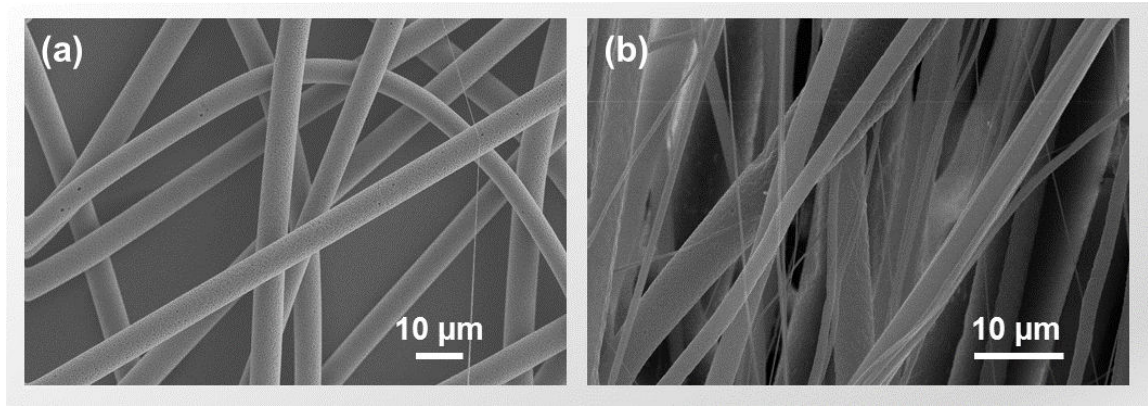


Figure 6.9: SEM micrograph of PLA electrospun fibers (a) before plasma treatment and (b) after plasma treatment

6.4 BET Surface Area

The BET surface area of the PLA pellets (bulk) is $0.3 \text{ m}^2/\text{g}$, however, PLA fibers in TCM solvent have 86% increase in surface area from 0.3 to $2.1 \text{ m}^2/\text{g}$. PLA-PEG composite fibers in TCM solvent shows 93% increase in surface area from 0.3 to $4.5 \text{ m}^2/\text{g}$ compared to PLA pellets. The characteristic of fibrous structure consists of interparticle spacing and more number of voids distribution which leads to increase in surface area. Figure 6.1 shows increment in surface area from PLA pellets to PLA fibers to PLA-PEG composite fibrous membrane.

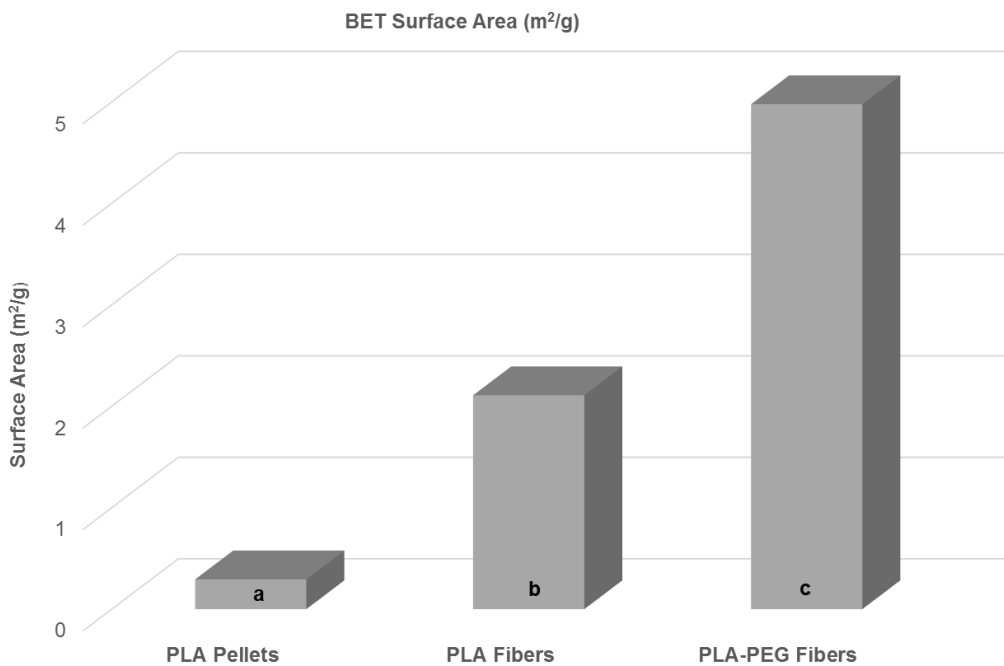


Figure 6.10: BET surface area of PLA (a) Pellets, (b) PLA fibers and (c) PLA-PEG composite fibers

6.5 PLA Electrospun Fibers: Crystallinity

The control of the polymer fiber crystallinity is important, because it can strongly affect the solubility as well as degradation rate, which are vitally important for the biomedical applications. By changing the morphology of PLA, it is possible to tune the degree of its crystallinity [138]. The crystalline structure of PLA is investigated by X-ray diffraction (XRD) analysis. The diffraction pattern of PLA pellet and its fiber is illustrated in Figure 6.11. A diffuse peak close to $2\theta = 17.8^\circ$ is observed for the crystalline part of PLA pellets, whereas PLA fibers does not show sharp peak. These results suggest that PLA fibers are amorphous in nature, whereas PLA pellets are semi-crystalline.

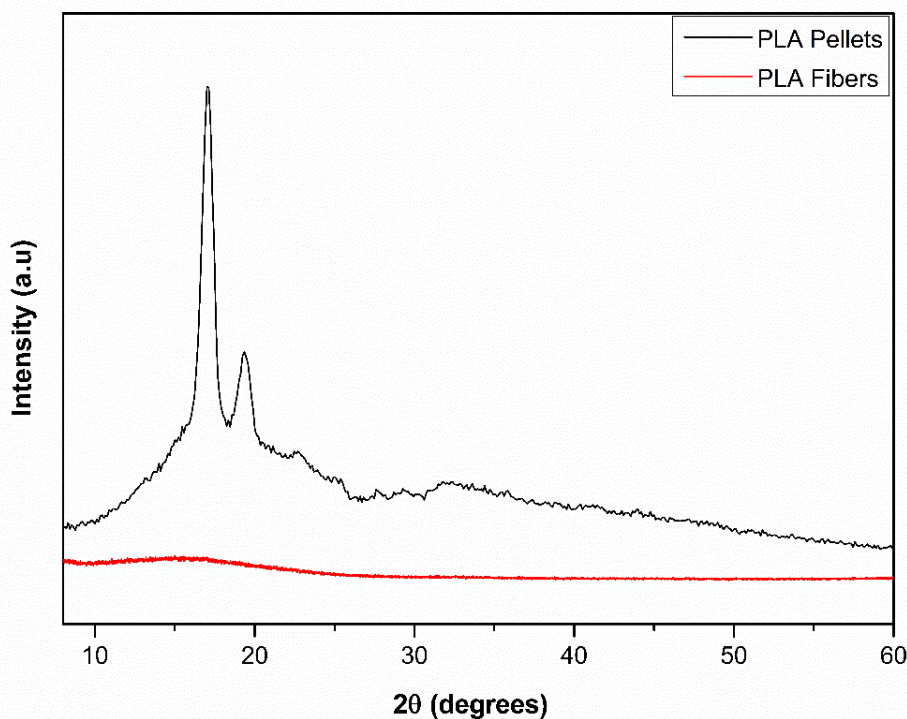


Figure 6.11: XRD spectrum of PLA fibers show amorphous nature whereas PLA pellet show semi-crystalline

7 Preparation of Magnetic PLA Fibrous Membranes

7.1 Abstract

Poly(lactic acid) (PLA) is blended with Poly(ethylene glycol) (PEG) and magnetic nanoparticles (MNPs). A series of mixtures are converted to fibers via electrospinning at room temperature. The fiber diameter of PLA decreases on blending with PEG from 6 down to 3 micrometers and with PEG + MNPs down more ca. 1 micrometer. The thermogravimetric study confirms the effect of blending, enhancing the stability on adding PEG to PLA. The magnetic properties of polymer fibers containing different concentrations of MNPs are studied by vibrating sample magnetometer (VSM). The fiber blends show proportionally reduced saturation magnetization compared to pure magnetic nanoparticles. The MNPs incorporated PLA-PEG nanocomposite mat show magnetization and therefore promise the possibility for temperature effects, such as hyperthermia treatment.

7.2 Introduction

Polymer fiber containing magnetic nanoparticles (MNPs) open novel opportunities in the biomedical field such as hyperthermia treatments [139], biosensors [140], magnetically triggered drug delivery [141][142][143] and beyond. This is the one most promising strategies, as a system consists of magnetic nanoparticles and suitable therapeutic agent into a biocompatible polymer composite [144][145][146]. Designing such composites to be nontoxic with a proper degree of degradability and having an active responses are considered to be a primary requirement [147]. For this purpose, biopolymer-based fibers prepared by the electrospinning technique have been most widely studied because of high aspect ratio, high surface area, high porosity and outstanding properties [148].

Due to good biocompatibility, biodegradability and nontoxicity, poly(lactic acid) (PLA) is being used in biomedical and ecological applications [149][150][151]. Poly(lactic acid) electrospun mats are porous and cylindrical [152] and it is well known, that they are hydrophobic [153], because of the presence of methyl groups in its chemical structure. Hendrick and Fey also found, that water contact angle can be decreased by blending with a water-soluble polymer such as poly(ethylene glycol) (PEG) which further increases solubility [154]. The magnetic property is a vital requirement for the use of the material in biomedical applications, especially for hyperthermia therapy. Therefore, MagSilica® is carefully chosen as nanometric heat-generating sources, which can be triggered remotely by the utilization of an external alternating magnetic field. Silica-coated magnetic nanoparticles ($\text{Fe}_3\text{O}_4@\text{SiO}_2$ core-shell NPs) are hydrophilic, nontoxic and

provide good stability under aqueous conditions [155]. The main advantage of such magnetic polymer fibers is local and precise heating of the membranes, which is ideal for hyperthermia treatment. Such advanced materials could also be used as “smart” fibers and fabrics for protective clothing and in first-response personnel health care [156]. Figure 7.1 shows magnetisation of PLA-PEG-MNPs3 composite fibrous membrane.

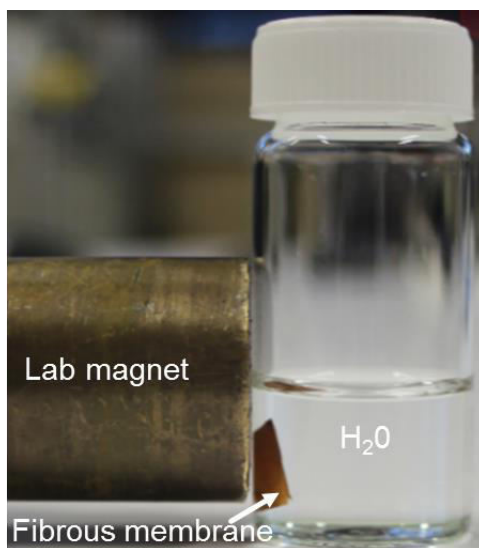


Figure 7.1: PLA-PEG-MNPs3 composite fibrous membrane in distilled water shows the magnetic attraction by the lab magnet [155]

With this in mind, here magnetic polylactic acid fiber membrane by means of electrospinning technique is developed. To enhance the hydrophilicity, PEG is incorporated. And to gain the magnetic properties MagSilica® is incorporated. The processing tools to produce magnetic fibers are described and their magnetic properties are investigated for biomedical applications.

7.3 Experimental

7.3.1 Materials Used

All chemicals were of analytical grade and used without prior treatment. Polylactic acid 6202 (PLA) was provided by Prof. Dr. –Ing. Hans-Josef Endres, Institute for Bioplastics and Biocomposites (Ifbb) Hannover, Germany. MagSilica® 50 ($\text{Fe}_3\text{O}_4@\text{SiO}_2$) was purchased from Evonik formally Degussa AG, Germany. Poly(ethylene glycol) 1500 was purchased from Abcr, Germany and chloroform from Roth, Germany.

7.3.2 Material Characterization

7.3.2.1 Scanning Electron Microscopy (SEM)

Scanning Electron Microscopy (SEM) (Zeiss Leo VP 1455) was used to analyze the surface morphology and diameter of the prepared fibers. Three samples were prepared; in the first sample PLA fibrous mat, in the second sample PLA-PEG blends fibrous mat and in the third sample PLA-PEG-MNPs fibrous mat. All specimens were vacuum coated with gold/platinum before taking SEM image to minimize sample charging.

7.3.2.2 Thermogravimetric Analysis (TGA)

To study the thermal degradation, moisture absorbance and solvent residues of the polymer fibers TGA was conducted using thermogravimetric analyzer (NETZSCH STA 409, Germany) under argon atmosphere. The heating rate was 10 K/min, and the scanning range was from 40°C to 500°C. All specimens with a weight of approximately 8 – 10 mg were used.

7.3.2.3 X-ray Diffractometer (XRD)

X-ray powder diffraction (XRD) patterns of injected specimens were obtained using a Bruker D2 powder diffractometer with CuK α radiation ($\lambda = 1.5406 \text{ \AA}$, power = 40 KV, $2\theta = 60^\circ$).

7.3.2.4 Vibrating Sample Magnetometer (VSM)

The magnetic properties (M–H curves) of pure MNPs and PLA-PEG-MNPs composite fibers, were evaluated by Vibrating Sample Magnetometer (VSM) (EG&G Princeton Applied Research Model 4500). All the specimens were measured at a room temperature.

7.3.3 Synthesis of PLA, PLA-PEG and PLA-PEG-MNPs Composite Fibers

Three sets of viscous polymer solution were prepared, in one set, 8 wt% PLA was dissolved in trichloromethane (TCM) and stirred for 10 hours at room temperature. In the second set, PEG (1:1 wt%) was added to the prepared PLA solution and stirred for 5 hours. And in the third set, MNPs dispersed in methanol (1 mL) were made into composite solutions with PLA-PEG solution. The concentrations of MNPs in PLA-PEG were determined at 1, 2 and 3 wt% (referred as MNPs1, MNPs2 and MNPs3, respectively). The blend solution was ultrasonically agitated for 2 minutes. To obtain a homogeneous and stable nanocomposite solution, they were stirred for another 5 hours. This nanocomposite suspension was filled in a 10 mL plastic syringe equipped with a blunt

end stainless steel conducting needle having a size of $0.80 \times 22 \text{ mm}^2$ ($21 \times 7/8 \text{ G}''$) and connected to electrospinning unit. Table 7.1 shows performed parameters for electrospinning.

Table 7.1: Summary of electrospinning conditions

Sample	Concentration [wt %]	Flow rate [mL h^{-1}]	Voltage [kV]	Height [cm]	Rotor Speed [m/s]	Mean Diameter [$\mu\text{m} \pm \text{SD}$]
PLA	8	1	12	10	10	6.39 ± 0.02
PLA-PEG	8-8	1	12	12	10	2.90 ± 0.34
PLA-PEG- MNP _{s1}	8-8-1	2	15	15	12	1.12 ± 0.29
PLA-PEG- MNP _{s2}	8-8-2	2	15	15	12	0.87 ± 0.39
PLA-PEG- MNP _{s3}	8-8-3	2	15	15	12	1.33 ± 0.45

7.4 Results and Discussion of Magnetic PLA Fibrous Membranes

7.4.1 Scanning Electron Microscopy (SEM)

The morphology of the electrospun fibers (Figure 7.2) shows that prepared fibers are porous, bead-free, interconnected and smooth surface with almost uniform diameters. Figure 7.2a revealed that electrospun PLA fibers are porous and cylindrical [152]. The porous structure is induced by phase separation, resulting from the rapid evaporation of the solvent (CHCl_3) during electrospinning. The mean diameter of the fibers is $6.4 \pm 0.02 \mu\text{m}$. Figure 7.2b revealed that PLA- PEG blend fibers with a diameter of $2.9 \pm 0.3 \mu\text{m}$. A significant decrease in fiber diameter was observed when PEG copolymer is incorporated into PLA solution by physical blending. This is expected because PEG works as a plasticizer which attributes to decrease in electrospun fiber diameter [157]. In addition, incorporation of PEG to PLA decreases the viscosity of the polymer solution because of the flexible PEG chains, which led to the production of smaller fiber diameter. The resultant fiber mat shows smooth and cylindrical morphology. Figure 7.2(c-e) revealed that the PLA-PEG-MNPs blends fibers with a mean diameter of $1.1 \pm 0.3 \mu\text{m}$, $0.9 \pm 0.4 \mu\text{m}$ and $1.3 \pm 0.5 \mu\text{m}$ for MNPs₁, MNPs₂ and MNPs₃, respectively. While the addition

of MNPs up to 2% progressively and gradually decreased the fiber diameter, the addition of 3% increased the fiber diameter. It is considered that other factors such as solution electrical conductivity and viscosity should be changed with the addition of MNPs, which affected the fiber diameter significantly. Figure 7.3 revealed the mean fibers diameter distribution. It is observed that the MNPs are randomly separated into the polymeric composite fibers due to segregation effect [158].

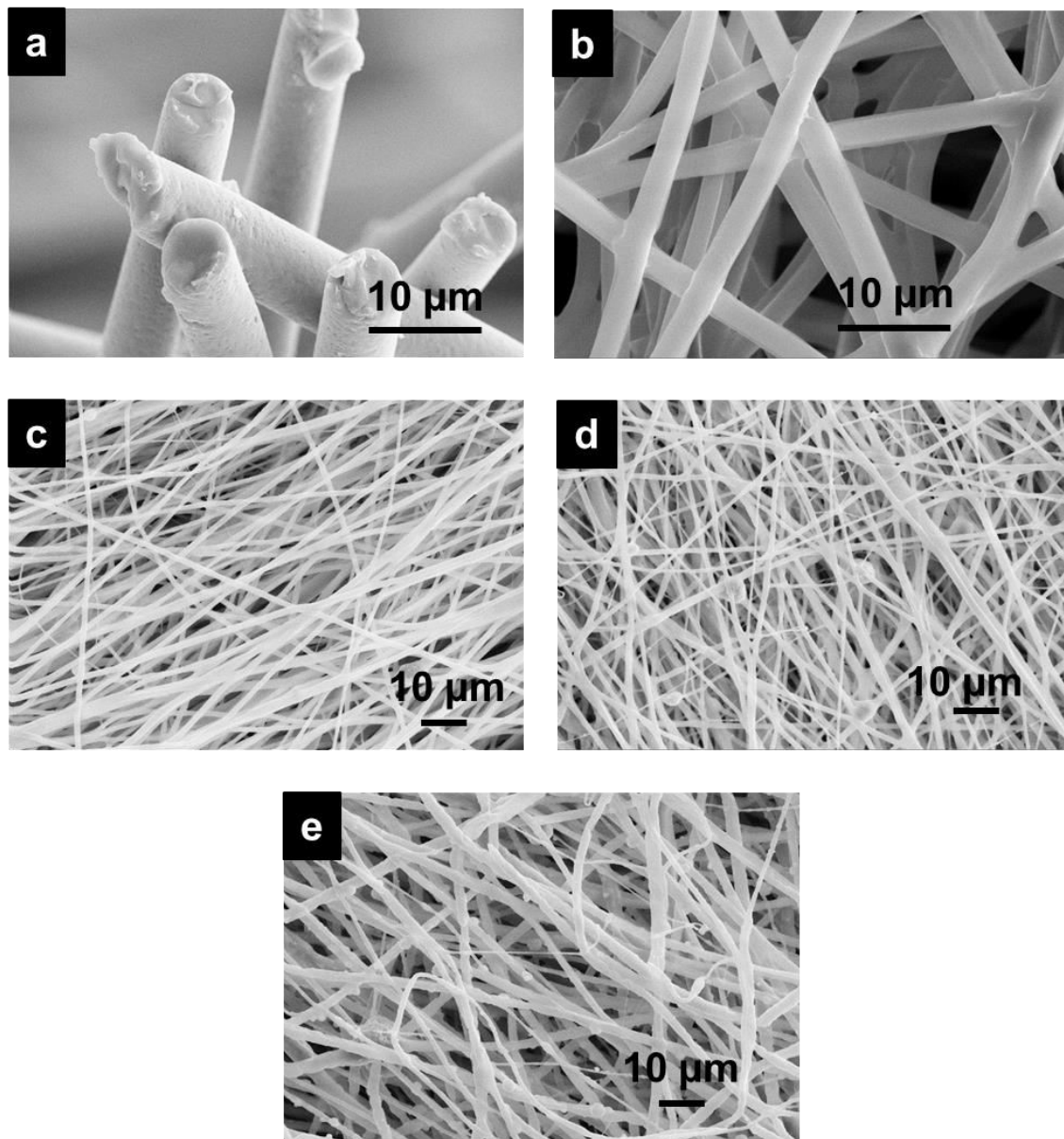


Figure 7.2: Scanning electron micrographs for electrospun (a) PLA fibers (b) PLA-PEG blend fibers (c) PLA-PEG-MNPs1 blend fibers (d) PLA-PEG-MNPs2 blend fibers and (e) PLA-PEG-MNPs3 blend fibers [159].

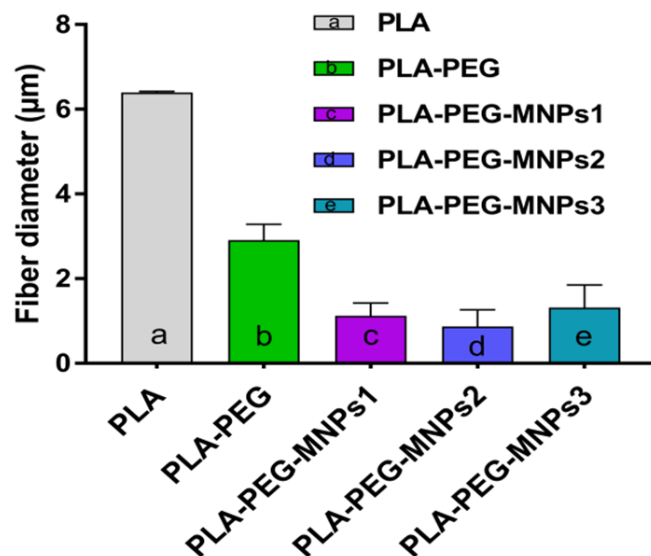


Figure 7.3: Average mean fibers diameter measurement of (a) PLA fibers (b) PLA-PEG blend fibers (c) PLA-PEG-MNPs1 blend fibers (d) PLA-PEG-MNPs2 blend fibers and (e) PLA-PEG-MNPs3 blend fibers [159].

7.4.2 Energy Dispersive X-ray (EDX)

EDX was carried out to confirm the element compositions (C, Si and Fe) of the PLA-PEG-MNPs1 fiber blends. The result is shown in Figure 7.4 and indicates the presence of MNPs in the fibers without any other impurity.

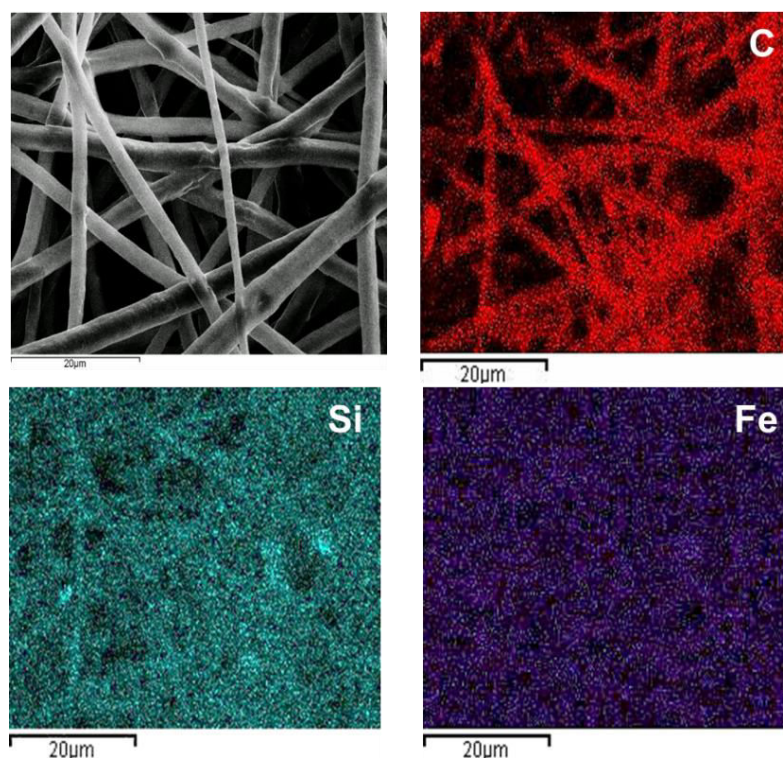


Figure 7.4: Energy dispersive x-ray micrographs for electrospun PLA-PEG-MNPs1 composite fibers

7.4.3 Thermal Analysis

The thermal behavior of electrospun fibers is investigated by TGA analysis, as shown in Figure 7.5. Figure 7.5a revealed single step weight loss of 92.1% from PLA fibers in the temperature range of 240°C and 375°C, which is in agreement with previous studies by M. Liu and co-worker [160]. The weight losses below 200°C can be assigned to physisorbed water, which is 1.2%. This result indicates that PLA has a higher decomposition temperature. In order to improve the hydrophilicity, PEG is incorporated [161] which shows two-step weight loss as shown in Figure 7.5b. In the first interval, there is 55% weight loss in the temperature region from 225°C to 370°C which is corresponding to the PLA. In the second interval, there is 39% weight loss in temperature region 370°C to 450°C which is corresponding to PEG. From TGA analysis of PLA and PLA-PEG fibers, it is observed that blend fibers of PLA-PEG are more stable than pure PLA fibers. This may be due to the plasticizer effect of PEG molecules. This could make PLA-PEG blend fibers as an ideal material for medical applications such as hyperthermia [162]. All the treatments are shown in Table 7.2.

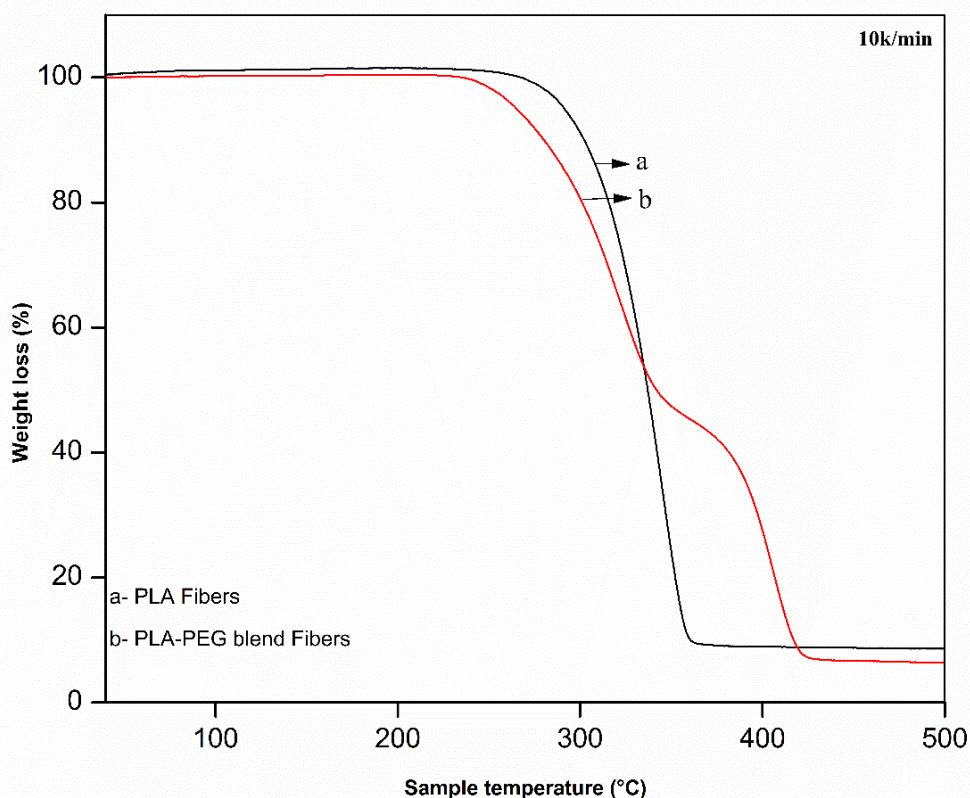


Figure 7.5: Thermal degradation of (a) PLA fibers (b) PLA-PEG blend fibers as measured through TGA [159].

Table 7.2: Thermogravimetric data table for PLA and PLA-PEG blend fibers [159]

Sample	Weight loss Interval	T _{onset} °C (±3°C)	T _{endset} °C (±3°C)	Weight Loss (%)
PLA	1	240	375	92.10
PLA-PEG	2	225	370	55.11
		370	450	38.85

7.4.4 X-ray Diffractometer Analysis

The crystalline phases present in the samples were identified by XRD. XRD patterns of the pure MNPs and different weight % of MNPs (1, 2 and 3 wt% of MNPs) composite PLA-PEG membranes as PLA-PEG-MNPs1, PLA-PEG-MNPs2 and PLA-PEG-MNPs3 are shown in Figure 7.6. The characteristic peaks in different intensities at the same 2θ – value are shown in the XRD patterns. There are no diffraction peaks of other substances observed, which clearly indicate the presence of MNPs inside the composite fibers membrane.

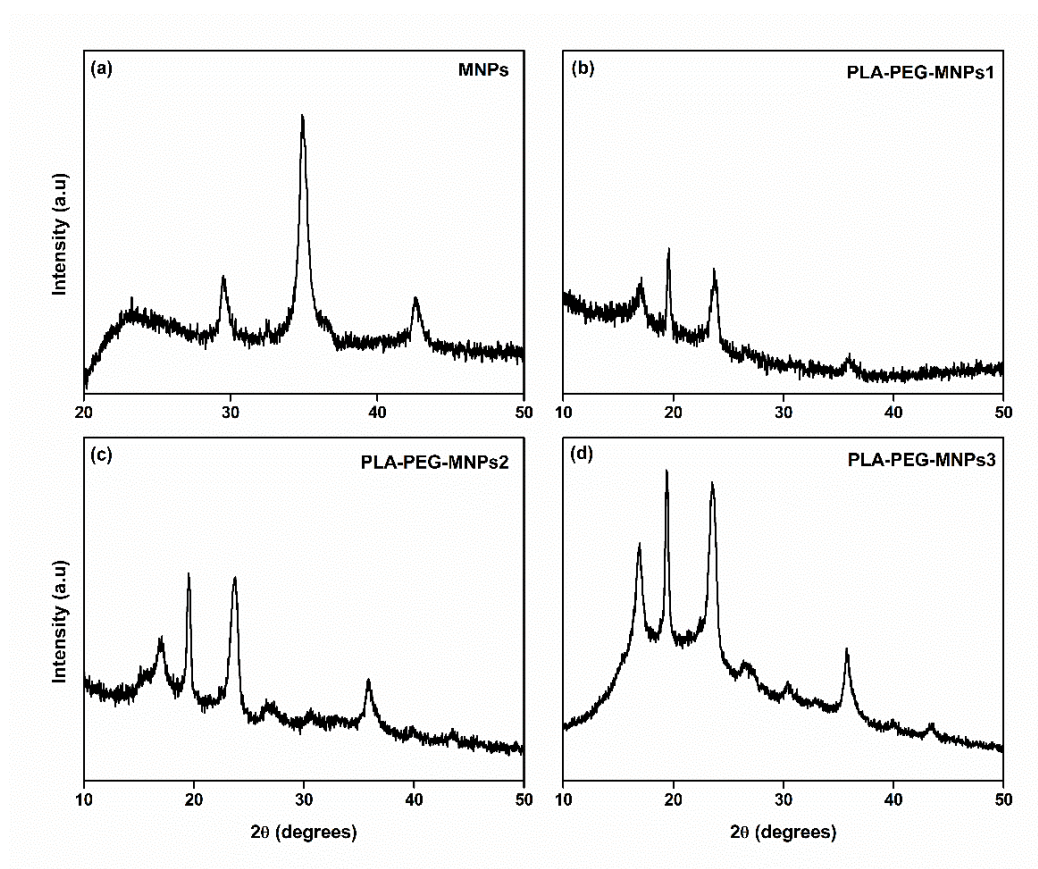


Figure 7.6: XRD pattern of (a) pure MNPs (b) PLA-PEG-MNPs1 composite fibers (c) PLA-PEG-MNPs2 composite fibers and (d) PLA-PEG-MNPs3 composite fibrous membrane

7.4.5 Magnetic Properties of Fibers

The magnetic properties of the MNPs and MNPs incorporated PLA-PEG composite fibers are determined by measuring their M-H curves (Figure 7.7). The result shows that the MNPs within the nanofibers are easily magnetized by an applied external magnetic field. Samples are measured over a range of applied fields between -6000 and +6000 G. The saturation magnetization (M_s) value reaches near to 2000 G. For pure MNPs, the M_s reached 18.58 emu g⁻¹. The PLA-PEG-MNPs composite fibers still possessed magnetism, but considerably lower than that of pure MNPs. The values measured are 1.26, 2.40, 3.37 emu g⁻¹ for the MNPs1, MNPs2 and MNPs3, respectively [163]. The M_s values are roughly proportional to the MNPs content in polymer fibers. The results clearly show that MNPs incorporated fiber produced by the electrospinning technique retained magnetic properties at room temperature which has potential for broad biomedical applications [164].

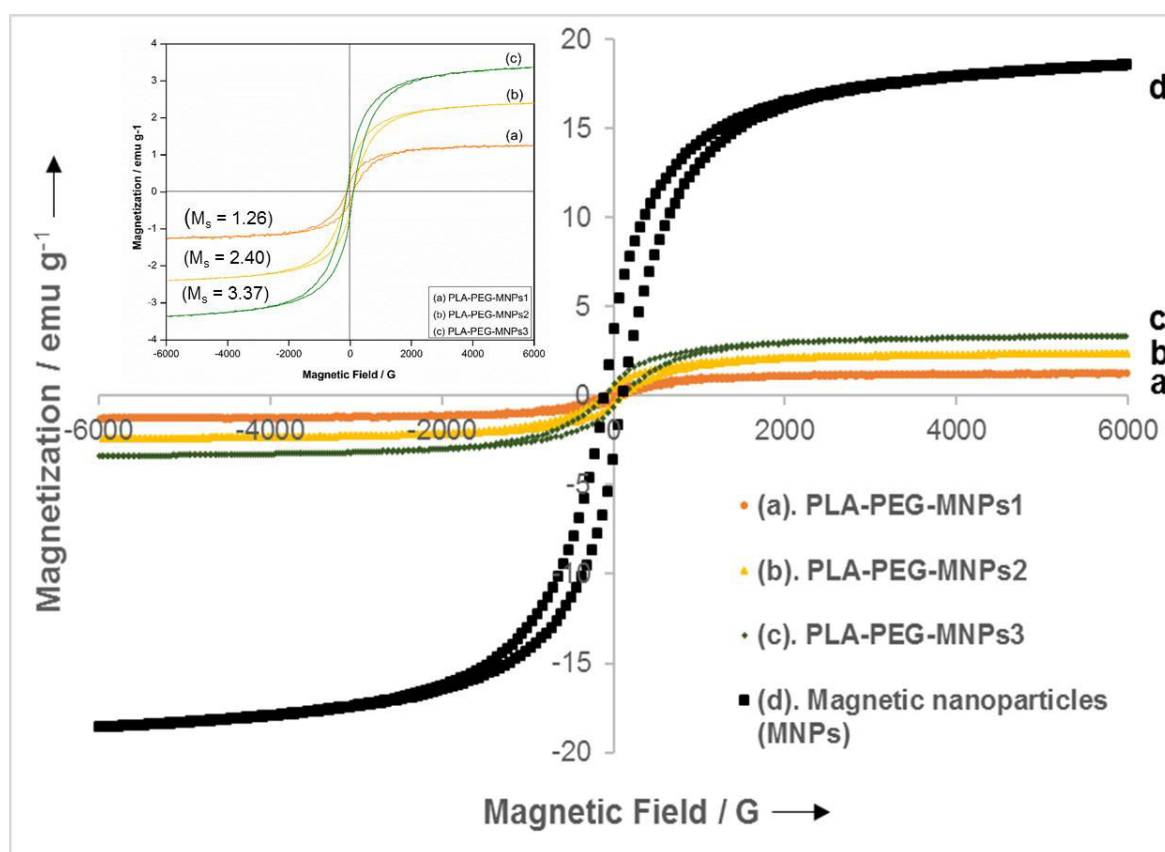


Figure 7.7: Magnetization curves measured at room temperature for (a) PLA-PEG-MNPs1 (b) PLA-PEG-MNPs2 (c) PLA-PEG-MNPs3 and (d) Pure MNPs [159].

The literature on magnetic polymer composites is exponentially increasing and the variety of materials already exists (as some are summarized in Table 7.3). However, just a few of those shows stability.

Table 7.3: Some materials based on magnetic polymer composites and their potential medical applications.

Materials	Stimuli	Medical Applications	Ref.
PCL-MNPs fibers	Magnetic field	Bone Regeneration	[165]
PVA-Fe ₃ O ₄	Magnetic field	Drug delivery	[166]
PNIPAM-MNPs	Magnetic field	On-demand drug delivery	[142]
PLGA-MNPs	Magnetic and NIR irradiation	Drug and hyperthermia therapy	[167]
PLA-MWCNT-Fe ₃ O ₄	Magnetic field	Drug delivery	[168]
PLA-PEG-MNPs	Magnetic field	Drug delivery and hyperthermia	This work
PCL: Poly(caprolactone); PVA: Poly(vinyl alcohol); PNIPAM: Poly(N-isopropylacrylamide); PLGA: Poly(lactic acid-co-glycolic acid); MWCNT: Multiwalled carbon nanotubes.			

7.5 Conclusions of Magnetic PLA Fibrous Membranes

In summary, the modifications of PLA polymer fibers to tune their properties for applications was investigated, e.g. in the present case PLA with PEG and MNPs was modified. A simple way of preparation by blending MNPs into PLA-PEG to yield magnetic composite nanofibers by electrospinning technique was presented. The thermogravimetric analysis confirmed that the PLA fiber is modified by PEG. SEM analysis showed that the fibers mean diameter decreases with blending, PEG to PLA from 6 μ m to 3 μ m and MNPs to PLA+PEG from 3 μ m to 1 μ m while all the others electrospinning parameters were kept constant. During and after synthesis the magnetization of the MNPs in the fibers is retained. The magnetic properties of the fibers could be changed by incorporating MNPs, while the topological morphology remained constant only the diameter varied slightly around 1 \pm 0.3 μ m. The saturation magnetization of the composite fibers is proportional to the amount of MNPs. The results are promising for further investigation of advanced biomedical applications.

8 Preparation of PLA-PEG-NVCL Fibrous Membranes

8.1 Abstract

In this study, Polylactic acid (PLA), Polyethylene glycol (PEG) and N-Vinylcaprolactam (NVCL) composite fibrous membranes were fabricated via electrospinning. An antibiotic was embedded into these composite membranes and used as an antimicrobial membrane. These (PLA-PEG-NVCL) composite fiber membranes were further functionalized with magnetic nanoparticles (MNPs) and employed for magnetic thermo-drug delivery system using an external magnetic field. The release rate significantly increases upon exposure to the magnetic field and can be controlled by on and off situation.

8.2 Introduction

The administration of safer drug doses using a controlled drug delivery system is an attractive alternative to the systemic treatment [169]. One of the main advantages of controlled drug delivery system is that the entrapped drug can be gradually released, achieving therapeutic levels but avoiding toxic and inefficient concentrations, which usually occurred in traditional ways of administering drugs. Therefore, undesirable effects are reduced and the efficacy of the treatment is increased with these systems [170]. By using targeted drug release with precise local administration, it is possible to use such drugs, which until now have been considered as too toxic to be used at all.

The glass transition temperature (T_g) can be used as a reversible thermoresponsive switch. Thermal switch is based on a significant change in diffusivity of a solute around the glass transition temperature (T_g) of a polymer. At a temperature below the glass transition temperature of the polymer ($T < T_g$), the polymer is in a glassy state, where polymer chain movement and hole free volume are low. Therefore, the diffusion coefficient of the incorporated drug is low, limiting drug release. Increasing the temperature to above the T_g of the polymer ($T > T_g$), it changes from the glassy to the rubbery state. In the rubbery state, polymer chain movement and hole free volume are significantly higher than in the glassy state. This significantly increases the flexibility and free volume of the polymer, resulting in several orders of magnitude higher release. Since the glass transition is a reversible transition, subsequent lowering of the temperature significantly decreases the drug release rate from the membrane, enabling pulsatile drug administration [171]. [Figure 8.1](#) shows the effect of phase transition temperature on the polymers volume and drug delivery.

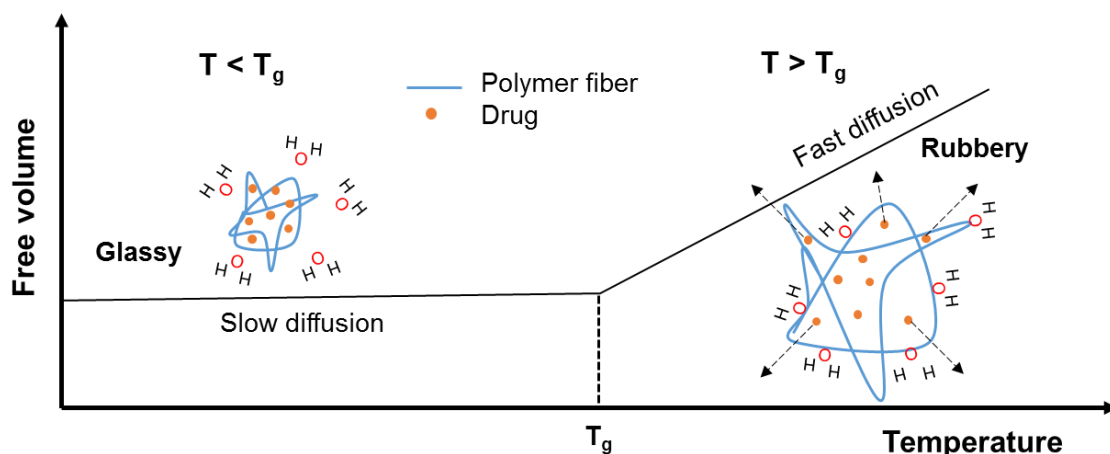
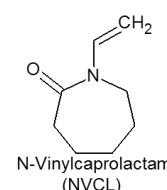


Figure 8.1: Effect of phase transition temperature on the polymer fiber volume and drug delivery (Picture: M. Kumar)

PLA-PEG composite fibrous membranes are described in chapter seven. Here, N-Vinylcaprolactam (NVCL), is incorporated into PLA-PEG. NVCL is a monomer with amphiphilic character. It possesses hydrophilic carboxylic and amide group (lactam ring), where the hydrophilic amide group is connected to the hydrophobic vinyl group and carbon-carbon backbone chain. So, its hydrolysis does not produce small amide compounds, which are undesirable for biomedical applications. Moreover, this polymer has been intensively studied because of their interesting physicochemical properties and their structural similarity to proteins [172].



In this work, PLA-PEG-NVCL composite fibrous membranes by means of electrospinning technique is developed. To provide thermo-switch ability with reduced glass transition temperature, NVCL monomer is embedded. Tetracycline hydrochloride (TCH) is used as an antimicrobial to show the antibacterial activity. Further, these composite membranes (PLA-PEG-NVCL) are functionalized by magnetic nanoparticles (MNPs). The processing tools to produce composite fibrous membranes are described and applied for on-demand drug delivery under magnetic stimuli.

8.3 Experimental

8.3.1 Materials Used

All chemicals were of analytical grade and used without prior treatment. Poly(lactic acid) 6202 (PLA) was provided by Prof. Endres, Institute for Bioplastics and Biocomposites (Ifbb) Hannover, Germany. Tetracycline Hydrochloride, TCH, ($M_w = 480.9$ g/mol) was purchased from Roth, Germany. N-Vinylcaprolactam, (NVCL) (Aldrich) was used as a monomer (NVCL, $FW = 139.2$, $d = 1.029$ g/mL). Rhodamine 6G (Rh6G), ($M_w = 479.02$

g/mol) was purchased from Sigma. The solvent used in this study was chloroform from Roth, Germany.

8.3.2 Material Characterization

8.3.2.1 Scanning Electron Microscopy (SEM)

Scanning Electron Microscopy (SEM) (Zeiss Leo VP 1455) was used to analyze the surface morphology and diameter of the prepared fibers. All specimens were vacuum coated with gold/platinum before taking SEM image to minimize sample charging.

8.3.2.2 Micro Raman Spectroscopy (MRS)

Raman spectra were scanned on a SENTERRA Dispersive Raman Microscope Spectrometer (Bruker Optik GmbH, Germany) with a thermoelectrically cooled CCD detector (charge-coupled device). For the analysis, a diode laser with the excitation wavelength of 785 nm was used. All specimens were analyzed with an Olympus LWD 50× (NA = 0.50) microscope in a spectral range from 90 to 3500 cm^{-1} (2 s integration time, 5 accumulations, 100 mW laser power). All samples were measured at a controlled temperature of $(22 \pm 1)^\circ\text{C}$.

8.3.2.3 Differential Scanning Calorimetry (DSC)

DSC data were obtained using NETZSCH STA 409, Germany under argon atmosphere. Temperature and enthalpy calibration was performed using indium and lead. The heating rate was 10 k/min and the scanning range was from 40°C to 500°C . All specimens with a weight of 8 – 10 mg were used. From thermograms glass transition (T_g), melting point (T_m) and degree of crystallinity were estimated.

8.3.2.4 Contact Angle (CA)

The contact angle measurements of the designed composite membranes were performed by Universal, Surftens, OEG GmbH, Germany. The syringe full of water was connected with the instrument on a balance table. Slowly, a drop of water was placed on the sample and contact angle measurement was automatically controlled through the software. The contact angles were determined by the Wilhelmy technique.

8.3.2.5 UV-VIS Spectrophotometry

Ultraviolet-visible spectrophotometry measurements were taken with a Shimadzu UV-1601 UV-VIS double beam spectrophotometer. For measurements with Rhodamine 6G (Rd6G) the maximum absorption of light was determined at a wavelength of 529 nm.

8.3.2.6 Microbiological Tests

The antibacterial activity of the composite fibrous membranes from PLA-PEG-NVCL and PLA-PEG-NVCL-TCH was tested against Gram-negative bacteria (*E. coli*). A solid agar medium was poured into Petri dishes and its surface was inoculated with the bacterial suspension. The composite fibrous membrane was shaped as a disk with a diameter of 10 mm and weight of 2 mg and then placed on the medium surface. After incubation of the Petri dishes (at 37°C for 24 hours) the zone of inhibition was measured. PLA-PEG composite fibrous membranes were used to check fungus cell adhesion on its surface.

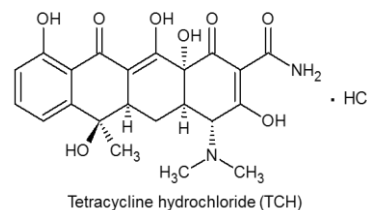
8.3.3 Synthesis of PLA, PLA-PEG and PLA-PEG-NVCL Composite Fibrous Membranes

8 wt% PLA, were dissolved in trichloromethane (TCM) and stirred for 10 hours at room temperature. To this, 8 wt% PEG and 8 wt% NVCL was mixed, to form a PLA-PEG-NVCL composite solution. These samples were filled in a 10 mL plastic syringe equipped with a blunt end stainless steel conducting needle, having a size of $0.80 \times 22 \text{ mm}^2$ ($21 \times 7/8 \text{ G}''$) and connected to the electrospinning unit. For the fabrication of PLA-PEG-NVCL composite fibrous membranes, side-by-side electrospinning apparatus was used as described in section 2.3.3. Table 8.1 shows the parameters used for the electrospinning experiment.

Table 8.1: Summary of electrospinning conditions

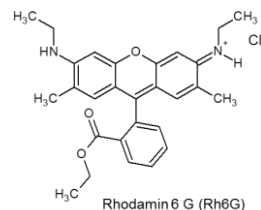
Sample	Concentration [wt %]	Flow rate [mL h^{-1}]	Voltage [kV]	Height [cm]	Rotar speed [m/s]	Mean Diameter [$\mu\text{m} \pm \text{SD}$]
PLA	8	1	12	13	--	6.3 ± 0.13
PLA-PEG	8-8	1	15	15	10	2.1 ± 0.27
PLA-NVCL	8-8	2	18	15	10	--
PLA-PEG-NVCL	8-8-8	2	12	12	10	1.1 ± 0.3

For the antimicrobial experiment, tetracycline hydrochloride (TCH) (0.08 wt %) was first dissolved in methanol. Methanol was chosen as a co-solvent, because it has reported the best encapsulation efficiency [173]. 10g of PLA-PEG-NVCL composite solution was slowly added to the TCH solution and stirred for another 4 hours.



TCH incorporated PLA-PEG-NVCL composite fibrous membranes were prepared by using side-by-side electrospinning apparatus.

For the magnetic stimuli experiments, MagSilica® (3 wt %), as magnetic nanoparticles (See chapter seven) + Rhodamine 6G (0.08 wt %) (Rh6G, as a model drug), were dissolved in methanol. Rh6G is a highly fluorescent dye, which can be easily detected. To this, 10g of PLA-PEG-NVCL composite solution was slowly added. Side-by-side electrospinning apparatus was used for fabricating these composite membranes.



8.4 Results and Discussion of PLA-PEG-NVCL Fibrous Membranes

8.4.1 Scanning Electron Microscopy (SEM)

The SEM images and fiber size distribution of PLA, PLA-PEG, PLA-NVCL and PLA-PEG-NVCL composite fibrous membranes are shown in Figure 8.2. The morphology of the electrospun fibers shows that prepared fibers are porous, bead-free and smooth with almost uniform diameters. Figure 8.2 a revealed that electrospun PLA fibers are porous and cylindrical [152]. The mean diameter of the PLA fiber is $6.3 \pm 0.13 \mu\text{m}$. Figure 8.2 b revealed that PLA- PEG blend fibers with a diameter of $2.1 \pm 0.27 \mu\text{m}$. A significant decrease in fiber diameter is observed as describes in chapter 7.4.1. Figure 8.2 c revealed that the PLA-NVCL composite fibers have losses in the fibers morphology. Here, PLA-NVCL fibers show half-tubes like structure. But it may be possible to fabricate PLA-NVCL membranes with different composition ratios. However, PLA-PEG-NVCL gain the structure of smooth fibers with a mean diameter of $1.1 \pm 0.3 \mu\text{m}$ (Figure 8.2 d), and this may have happened because of the balance of the lacking entropy. It is considered that other factors such as solution, electrical conductivity and viscosity should be changed with the addition of PEG, which could affect the fiber diameter significantly. Figure 8.3 reveals the mean fiber diameter distribution.

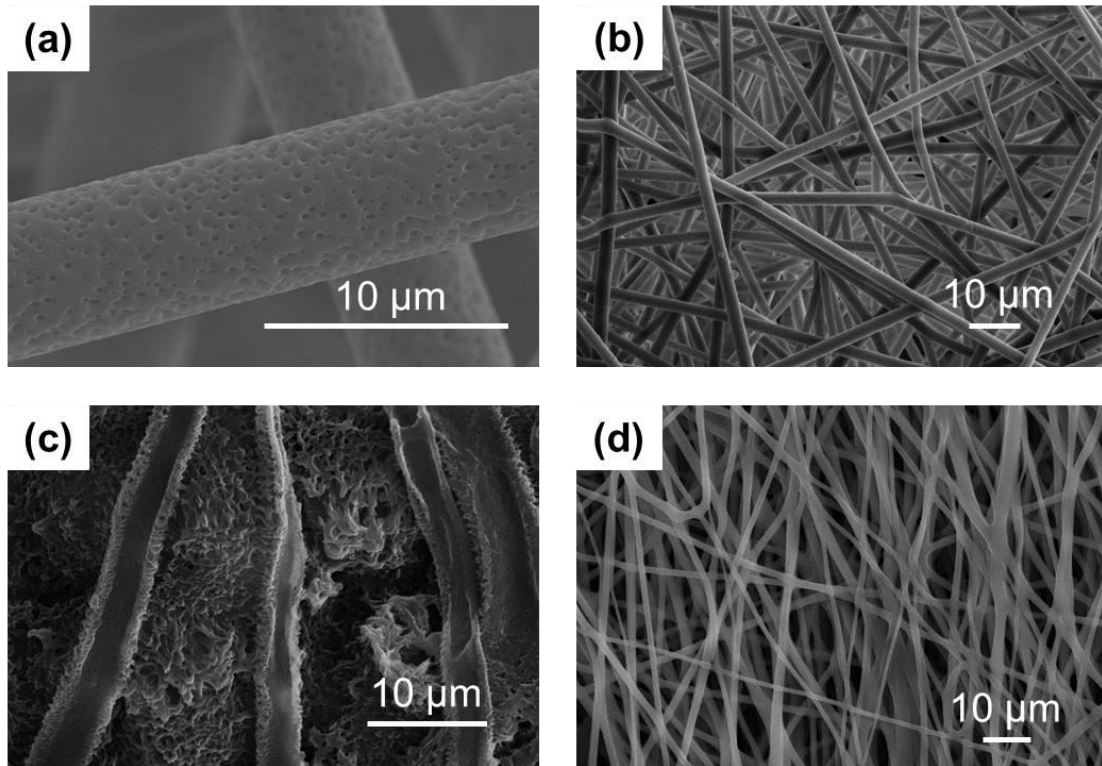


Figure 8.2: Scanning electron micrographs for electrospun fibrous membranes of (a) PLA (b) PLA-PEG (c) PLA-NVCL and (d) PLA-PEG-NVCL composite fibrous membranes

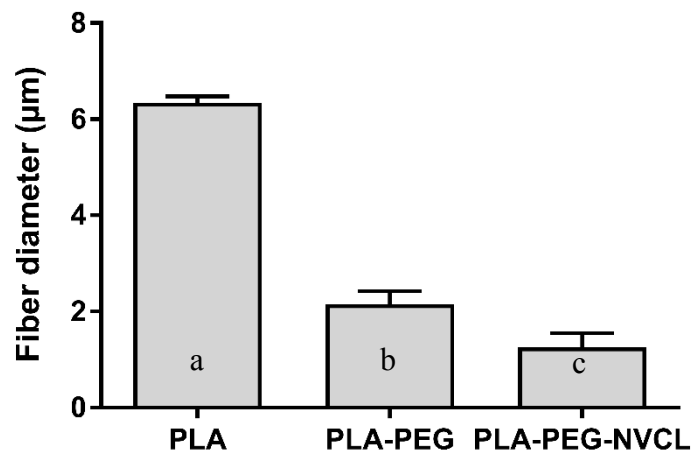


Figure 8.3: Average mean fibers diameter measurements of (a) PLA (b) PLA-PEG and (c) PLA-PEG-NVCL composite fibrous membranes

8.4.2 Micro Raman Spectroscopy (MRS)

Raman is used to investigate the chemical characteristic of the bulk and electrospun composite membrane. Figure 8.4 depicts the Raman spectra of bulk PLA, PEG and NVCL and electrospun PLA, PLA-PEG and PLA-PEG-NVCL composite fibrous membranes. PLA pellets exhibited a characteristic peak at 1450 cm^{-1} (CH_3 asymmetric deformation vibration), 873 cm^{-1} ($\text{C} - \text{COO}$ vibration) [174]. Two other bands appear for PLA near 1130 and 1048 cm^{-1} and are assigned to rCH_3 rocking and C-CH_3 stretching-mode, respectively [175]. PEG bulk pellets revealed characteristic peaks at 1482 cm^{-1} (CH_2 vibration), 1233 cm^{-1} ($\text{C} - \text{C}$ vibration), 1140 cm^{-1} ($\text{C} - \text{O}$ vibration) and 843.5 cm^{-1} (C-O-C vibration) [176][177]. NVCL bulk exhibited characteristic peaks at 1644 cm^{-1} ($\text{C} = \text{N}$ vibration), 1440 cm^{-1} (Amide groups) and 1280 cm^{-1} ($\text{C} - \text{N}$ stretching) [178]. The spectrum of composite fibers revealed minor shifts in the characteristic peaks while the peaks of amide ring are not clearly detected due to the overlap with the spectrum of PLA-PEG composite fibers. The minor shifts can be a result of possible hydrogen bonds between the amide groups of NVCL molecules and PLA-PEG molecules. From this, it can be concluded that substances used, has not undergone any major molecular changes during the electrospinning process (12-18 KV). Molecular reactions are not observed. Only characteristic bonds of the individual substances could be found in the composites. The characteristic peaks exhibited by bulk and electrospun composite fibers are summarized in Table 8.2.

Table 8.2: Comparative study of Raman main characteristic peaks for bulk and electrospun composite fibers as observed in Figure 8.4 and their tentative assignments

Sample	Main peaks at wavenumbers [cm^{-1}]		Tentative assignment
	Bulk (pellets, powder)	Electrospun composite fibers	
PLA	873	873	$\nu(\text{C} - \text{COO})$
PEG	843.5	--	$\nu(\text{C-O-C})$
PLA-PEG	--	844.5	$\nu(\text{C-O-C})$
NVCL	1440	--	$\nu(\text{CN})$
PLA-PEG-NVCL	--	--	
$\nu = \text{Stretching}$			

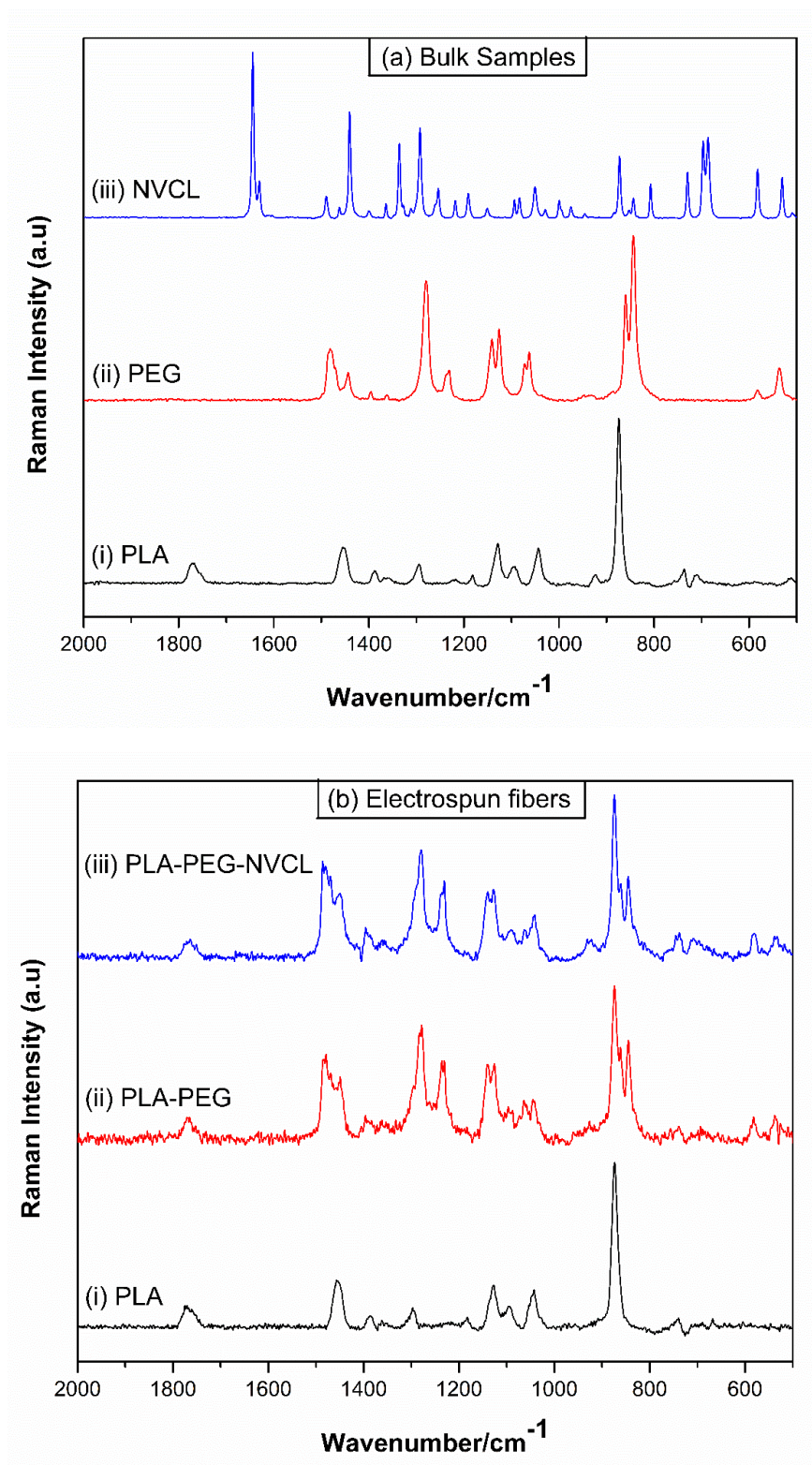


Figure 8.4: Raman spectra of (a) Bulk samples of (i) PLA, (ii) PEG and (iii) NVCL (b) Electrospun (i) PLA, (ii) PLA-PEG and (iii) PLA-PEG-NVCL composite fibrous membranes

8.4.3 Differential Scanning Calorimetry (DSC)

DSC curves are used to determine the thermal stability of the electrospun PLA, PLA-PEG and PLA-PEG-NVCL composite fibrous membranes, as shown in [Figure 8.5](#). [Figure 8.5\(a\)](#) shows DSC curve for PLA fibers membrane with a glass transition temperature of around 75°C. These results are comparable with the existing literature [179][180]. [Figure 8.5\(b\)](#) shows DSC curve for PLA-PEG composite fibrous membrane with a lower glass transition temperature of around 60°C. The probable reason for the reduction in glass- temperature is the plasticizer effect [125]. The micro Raman assay has shown that the functional groups are still present. In this case, the PEG is not covalently bond into the polymer, but interacts with the polymer of its polar groups like hydrogen-hydrogen bonding. This increases the chain mobility, which intern decrease the T_g of composite fibrous membranes.

[Figure 8.5\(c\)](#) shows DSC curve for PLA-PEG-NVCL composite fibrous membrane with further reduced glass transition temperature of around 45.7°C. This could happen because of NVCL molecules presence (melting temperature around 35-38°C), which further reduce the glass transition temperature. All the three composite fibrous membranes were found in the amorphous phase. These DSC data are summarized in [Table 8.3](#).

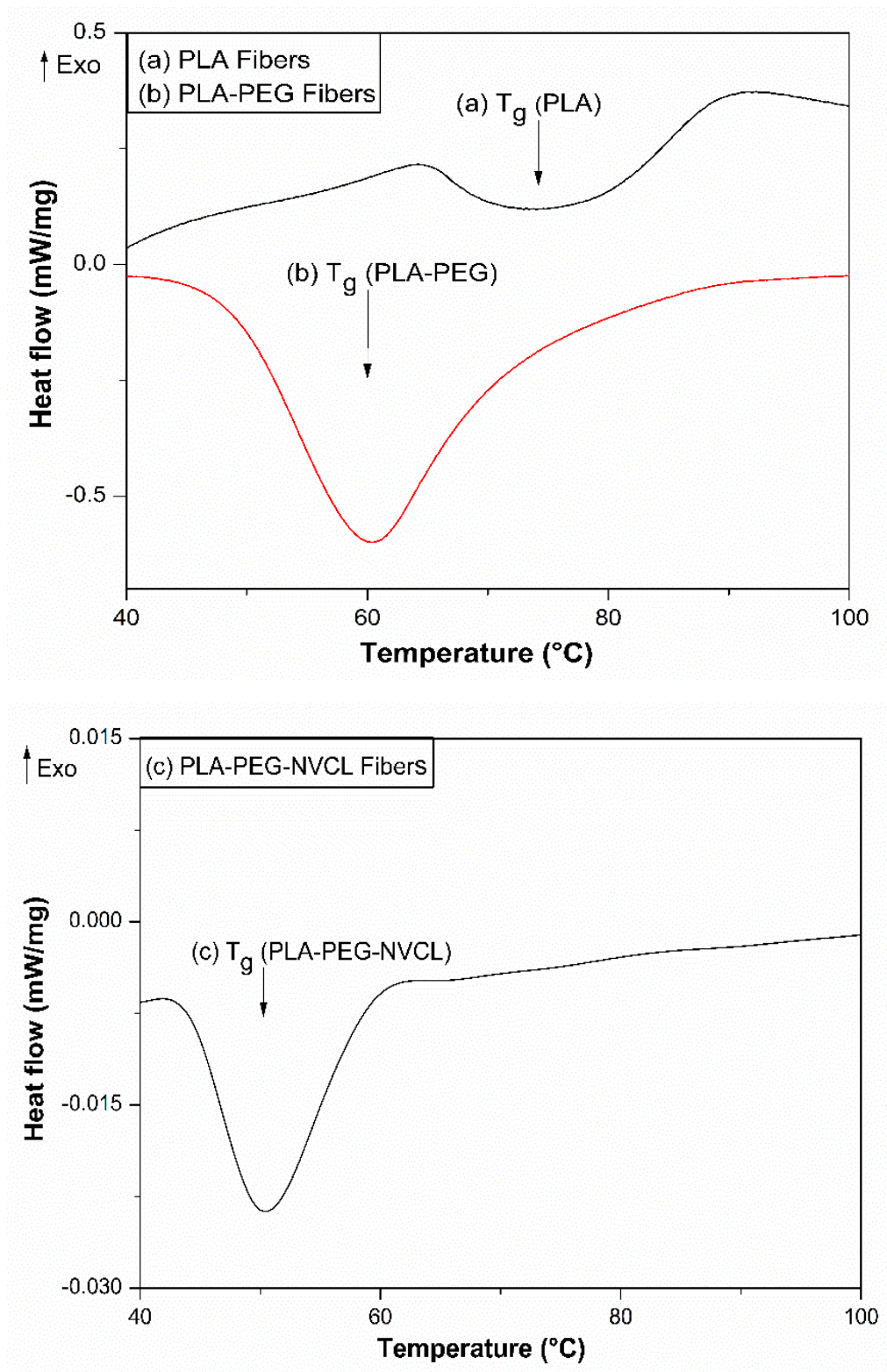
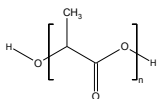
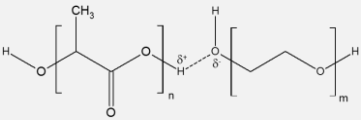
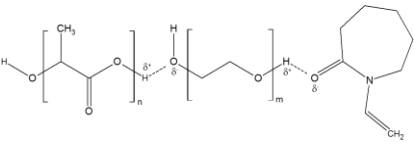


Figure 8.5: DSC curve for electrospun: (a) PLA, (b) PLA-PEG and (c) PLA-PEG-NVCL composite fibrous membrane

Table 8.3: DSC parameters for the thermal transitions of electrospun (a) PLA (b) PLA-PEG and (c) PLA-PEG-NVCL composite fibrous membranes

	Samples	Structures	Orientation	T _g (°C)
(a)	PLA		Aligned	75
(b)	PLA-PEG		Aligned	60
(c)	PLA-PEG-NVCL		Aligned	45.7
T _g = Glass transition temperature				

We can conclude from the Table 8.3, that an addition of PEG and NVCL to PLA membrane reduces glass transition temperatures (T_g).

8.4.4 Contact Angle (CA)

The hydrophobicity of electrospun PLA, and PLA-PEG-NVCL composite fibrous membranes are measured by contact angle goniometer. It is found that PLA fibrous membranes are hydrophobic with a contact angle of 130°, as shown in Figure 8.6(a) [154]. Figure 8.6(b) shows wettability of PLA-PEG-NVCL composite fibers membrane with a lower contact angle of 50.8°. This could happen because PEG and NVCL molecules are water soluble. The chain terminal of hydroxide of PEG and carboxyl of NVCL provide additional hydrophilicity, which results in lower contact angle [181]. All measurements are carried out longitudinal to the fiber and after rotating the membrane by 90° horizontal. From this it can be concluded, that the fiber-direction has no influence to the contact angle.

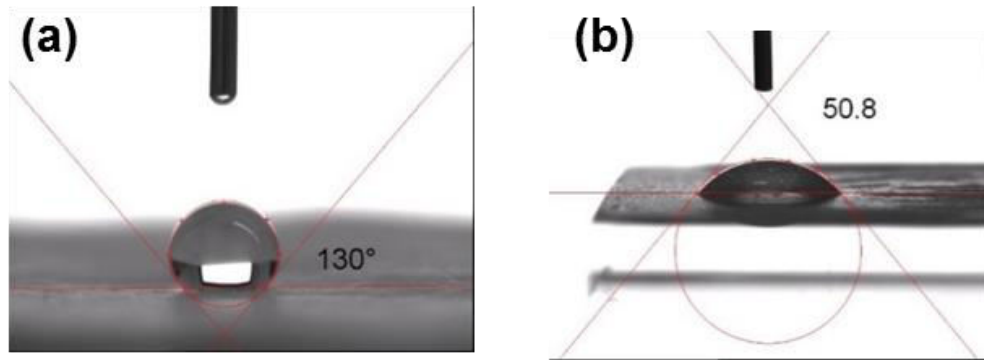


Figure 8.6: Contact angle measurements on electrospun: (a) PLA (b) PLA-PEG-NVCL composite fibrous membranes

8.4.5 Biological Properties of PLA-PEG-NVCL and PLA-PEG-NVCL-TCH Composite Fibrous Membranes

It is known that Tetracycline hydrochloride (TCH) exhibit antibacterial activity against a broad range of pathogenic microorganisms [182]. In this study, the antibacterial activity of the electrospun PLA-PEG-NVCL and PLA-PEG-NVCL-TCH composite fibrous membrane against the Gram-negative bacteria (*E. coli*) is evaluated. As expected, PLA-PEG-NVCL composite fibrous membranes did not exhibit any antibacterial effect as shown in Figure 8.7(a). Figure 8.7(b) shows the antibacterial activity of PLA-PEG-NVCL-TCH composite fibers membrane with the well-defined inhibitory zone. The mean diameter of the inhibitory zone is 2.5 cm. The results obtained are in agreement with previously reported data [183].

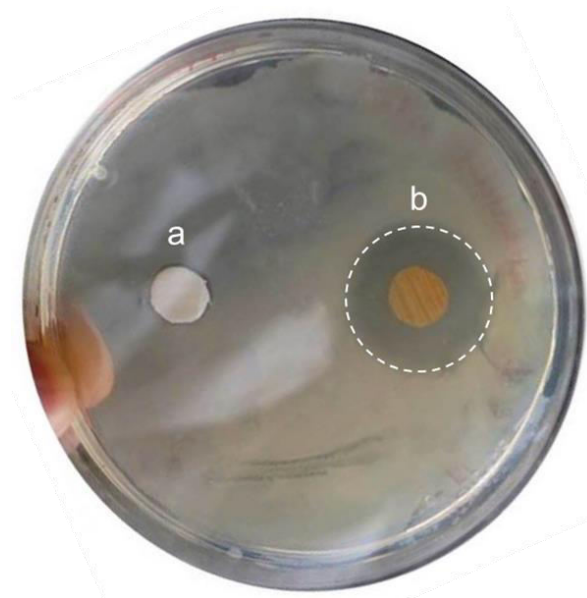


Figure 8.7: Digital images of a test for bacteria inhibition after 24 h contact of the composite membrane with *E.coli*; (a) PLA-PEG-NVCL composite fibrous membranes and (b) PLA-PEG-NVCL-TCH composite fibrous membranes. The inhibitory zone is indicated by a dashed line.

The bacterial cells ability to adhere and form a biofilm on the electrospun composite fibrous membrane surface is estimated. Figure 8.8 shows SEM micrograph after 24 h contact of the membrane with *Trichoderma reesei* (*T. reesei*) fungus suspension. PLA-PEG composite fibrous membranes are a good substrate for the adhesion of fungus cells (*T. reesei*) and the formation of fungal biofilms [184].

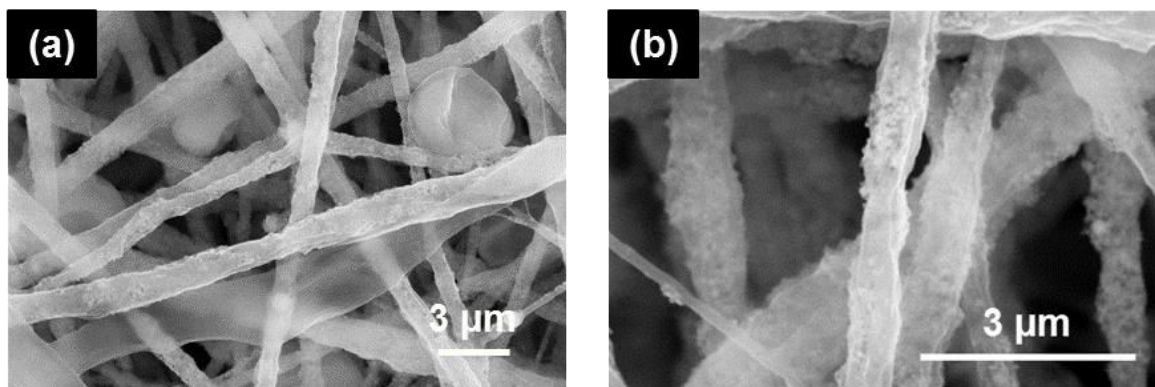


Figure 8.8: Scanning electron micrographs for electrospun PLA-PEG composite fibrous membranes after 24 h contact with the *T. reesei* fungus suspension with different scale of magnification.

8.4.6 Magnetothermally-Triggered Drug Release

In many clinical scenarios, for an effective treatment, drug delivery requires only intermittent drug administration to deal with occasional exacerbation, or pulsatile periodic administration to mimic diurnal variation in drug levels [185]. For this, magnetic fields based delivery systems are very effective approaches for localizing drug in the living body [186], because magnetic forces can be concentrated on a desired region, reducing collateral effects, which do not affect other biological tissues and can be tolerated in the living body [187] [188]. Thus, this local therapy could improve the efficiency of the treatment by reducing adverse toxic effect of drug [189].

The drug carrier composed with MNPs and polymer composite fibrous membranes, should satisfy some conditions for biomedical applications like [190];

- (1) No sedimentation of MNPs;
- (2) Uniform magnetic content;
- (3) No toxicity;
- (4) No iron leakage;
- (5) High selectivity.

Drug directly conjugated with MNPs has some limitations; drug release control and drug loading capacity [191]. To resolve these problems, drug and MNPs have been embedded into PLA-PEG-NVCL composite fibrous membranes. The heat generated by applying an AC magnetic field depends on the properties of MNPs (composition, size) as well as the frequency of the magnetic field [192]. Therefore, MagSilica® nanoparticles (50 nm diameter) were carefully chosen as heating agents for magnetic thermo-drug delivery (see chapter seven). MNPs under AC magnetic field show heating effects due to losses during the magnetization (hysteresis loss, Néel or Brown relaxation and frictional losses) in viscous suspensions [186][193]. Néel relaxation is the reorientation of the magnetic moment within the particles, generating thermal energy by crossing an anisotropy barrier. Brown relaxation is the reorientation of the magnetic particles itself, generating thermal energy by viscous friction with the carrier fluid. This reorientation results in friction between the particles and the medium, hence frictional losses occur generating heat. The heat generated from MNPs is transported by conduction, whereby, drug delivery can be carried out locally. Therefore, AC magnetic field supplies energy and helps the magnetic moments to overcome the energy barrier. This energy is dissipated as heat when the particle moments relax to their equilibrium [194].

In the present experiment, a custom-built setup was used to provide an alternating magnetic field with a maximum frequency of 799 kHz and intensity of 40%. Figure 8.9 shows an illustration of the experiment with magnetic coil inductor.

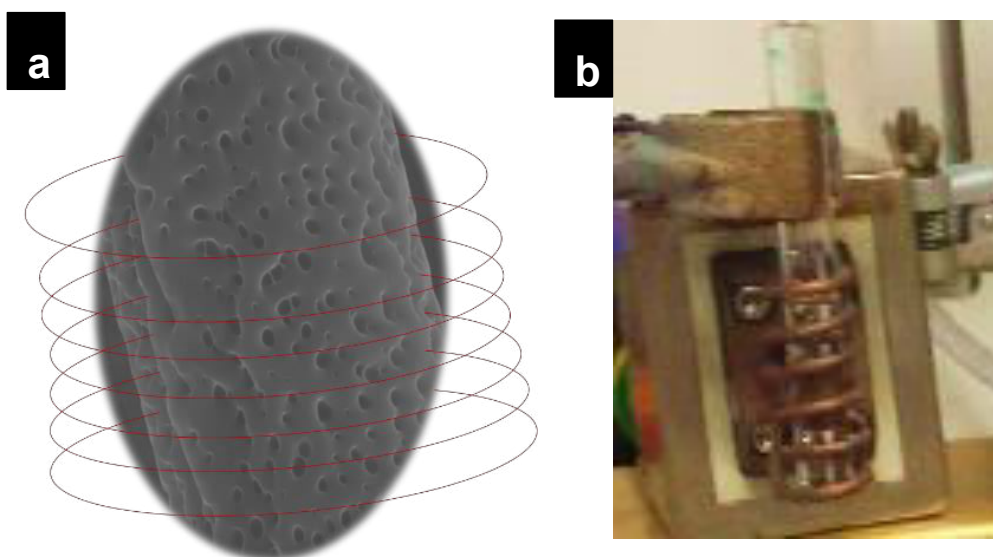


Figure 8.9: Magnetization setup with (a) schematic illustration of of PLA fibrous membrane under magnetic coil (b) photograph of the solenoid (coil-shaped heating station) with fiber inside. (Picture Courtesy: Prof. Kirschning, LUH, Hannover)

Release experiments were performed by placing 10 mg of composite fibers membrane in a test tube containing 10 mL PBS (phosphate buffer saline). This experiment was started by placing the test tube in the setup for 15 minutes at room temperature, then the AC magnetic field was powered on for 10 minutes, then 5 minutes stop – no magnetic field was applied, then for 10 minutes AC magnetic field again. The cumulative release of Rh6G from the composite membranes in on-off condition of magnetic field is shown in Figure 8.10.

Magneto-thermally triggered drug release

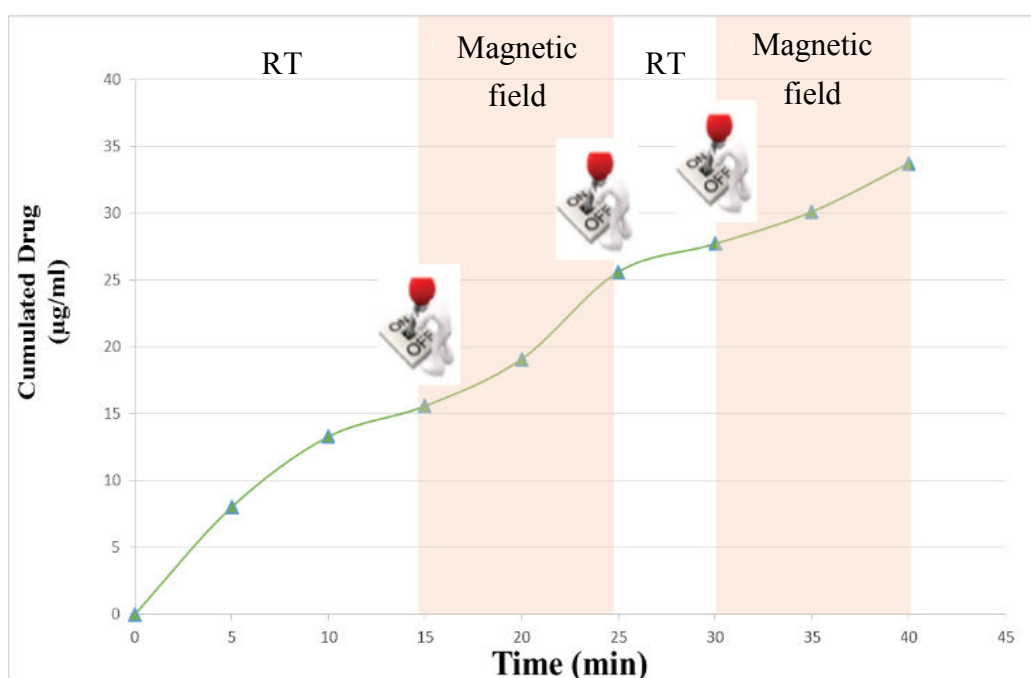


Figure 8.10: The on-demand local Rh6G delivery using PLA-PEG-NVCL-MNPs composite fibrous membrane induced by alternating magnetic field

A quick release (15 µg/ml) from the membrane surface within the first 15 minutes is seen in off condition of magnetic field. On applying magnetic field for 10 minutes, the releasing quantity reached to 25.62 µg/ml in 25 minutes. The release rate became slow in off condition of magnetic field. Only 2.2 µg/ml of Rh6G is released, which makes total release of 27.8 µg/ml. This slow release happens because of hydrogen bonding between atom (O) with strong negativity in Rh6G and hydrogen of OH in PLA. A further apply of magnetic field for other 10 minutes, the releasing quantity again accelerates to 33.7 µg/ml. Heat generated by MNPs, changes membrane property from glassy to rubbery state. It is also assumed, that hydrogen bond is destroyed. These results indicate, that the magnetic field has triggered releasing performance.

The MNPs embedded in the composite membranes (PLA-PEG-NVCL) was heated, when subjected to an external oscillating magnetic field, resulting in power absorption and subsequent magnetic relaxation of MNPs [195]. At the applied magnetic frequency, the membrane in the solution heated by the micro Brownian motion of the MNPs.

In vitro experiments of drug release under external alternating magnetic field, demonstrated that accelerating drug release have been achieved from the composite membranes. After removal of an external oscillating magnetic field, the release rate decreases, demonstrating the switch-ability of the system. This could happen, because of the reversible glass transition temperature switch. This result is in proportion to earlier existing studies [191].

Hence, magnetic thermo-drug delivery from PLA-PEG-NVCL composite fibrous membrane can significantly improve the efficiency of the drug therapy, because it enables the patient or physician to control the dosing of the patient's needs and releases the drug only at the required quantity in the human body. Therefore, patient compliance and efficacy will increase and toxic side effects will decrease.

8.5 Conclusions of PLA-PEG-NVCL Fibrous Membranes

PLA-PEG-NVCL composite fibrous membranes are developed using electrospinning technique. SEM analysis showed, that the fibers mean diameter decreases with blending, PEG to PLA from 6 μ m to 2 μ m, and further blending of NVCL to PLA-PEG decrease the fibers mean diameter from 2 μ m to 1 μ m. DSC study confirmed composite membranes are in an amorphous state. Tetracycline hydrochloride, an antibiotic is embedded within a composite membrane. The fabricated membrane exhibits antibacterial activity. The composite membranes are functionalized with MNPs + model drug and show triggered drug delivery by the production of heat energy using an alternating magnetic field.

9 Preparation of PLA-HPC Thin Film Membranes

9.1 Abstract

This study deals with the development of PLA and cellulose derivatives, especially the temperature-responsive HPC (Hydroxypropyl cellulose) based thin film for drug delivery system. The release of methylene blue (MEB) and tetracycline hydrochloride (TCH) was investigated via UV-VIS spectrophotometry. Two different kinds of cells were used in this work: (i) side-by-side Franz cell and (ii) Franz cell simulating simplified blood pressure conditions.

The blend containing PLA and HPC shows the formation and dispersion of a chiral nematic phase in the matrix. It was possible to notice the formation of mesophase through visual confirmation of the circular dichroism. It may be assumed, that these liquid crystals exhibit anisotropic mechanical properties because the dye release was noticeable under a mechanical stimulus.

9.2 Introduction

With the discovery of new drug, the need for innovating methods to effectively deliver therapeutics has risen. In this regard, the use of *in vitro* diffusion cells has evolved into a major research methodology. The advantages of using Franz-type diffusion cell in comparison to other administration routes are: facilitates avoidance of first pass metabolism, decreased toxicity as well as fewer side effects. In Franz diffusion cell, synthetic membranes are used to model skin tissue as they are easily resourced, less expensive and structurally simpler [196]. The kinetics of skin permeation can be more precisely analyzed by studying the permeation profiles of drug across a synthetic membrane mounted on a Franz diffusion cell.

The Franz cell analysis is an *in-vitro* skin permeation assay used to determine a particular formulation of an active agent through the skin [197]. The Franz cell apparatus consists of two primary chambers separated by a membrane. Two different experimental setups were used, (1) Side-by-side Franz cell (Figure 9.1) (2) Franz cell simulating simplified blood pressure conditions (Figure 9.3).

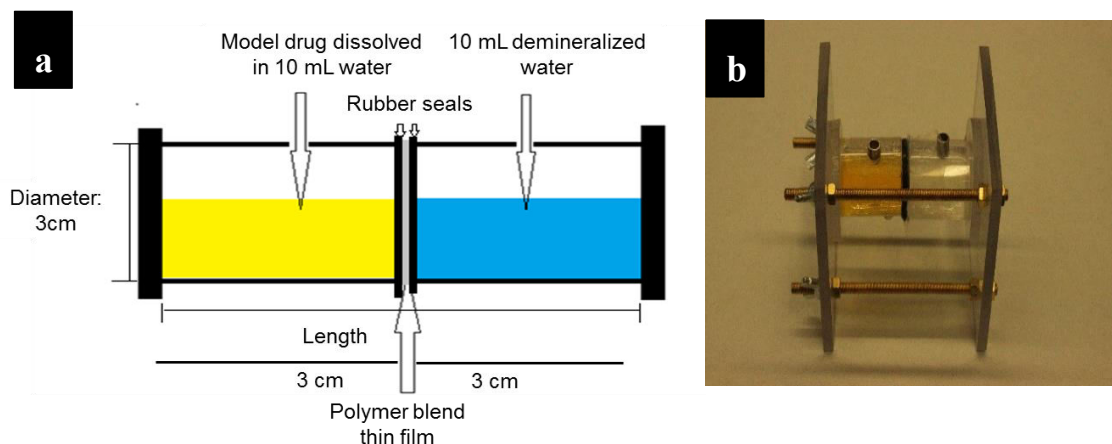
(1) Franz cell

Figure 9.1: Franz horizontal (Side-by-side) diffusion test apparatus (a) Schematic illustration of the horizontal Franz cell (b) lab developed set-up (Pictures: M. Kumar)

Franz cell chambers are made of Poly(methyl methacrylate) (PMMA). It is 6.2 cm in length, 3 cm in diameter. The Franz cell was filled on one side with 10 mL of water or PBS (phosphate buffer saline, receptor chamber) and on the other side (donor chamber) with the same solution containing additionally a dissolved dye, for example methylene blue (0.01 mg/mL). The filling itself was executed almost simultaneously on both sides in order to avoid pressure gradients on the thin film / membrane.

Then the Franz cell was placed in a furnace (Thermo-Fisher Scientific) and heated for a certain amount of time at a specific temperature or kept outside of the furnace at room temperature. After a fixed time interval (30 minutes) the Franz Cell was moved out of the oven and 3 mL of the samples from receptor chamber was taken into UV-VIS cuvettes and the absorbance was measured. Afterwards the receptor chamber was filled again with the same liquid and put again in the oven or left outside at room temperature. This procedure was repeated. Figure 9.2 a shows a cross section sketch of the side-by-side Franz cell and Figure 9.2 b shows digital image of the components of Franz cell.

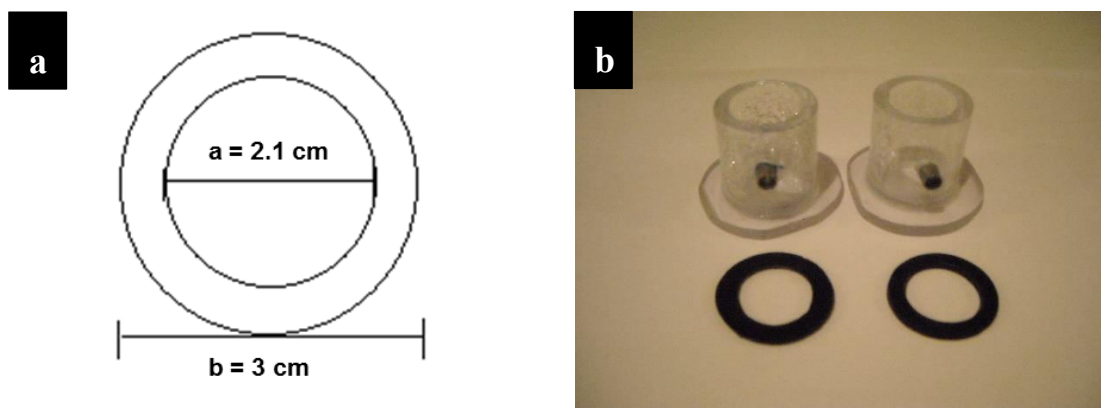


Figure 9.2: (a) Cross section sketch of the side-by Franz cell chamber with the diameters $a = 2.1$ cm and $b = 3$ cm (b) Digital image of the lab developed Franz cell (Picture: K. Smolik).

(2) Modified vertical Franz cell, simulating simplified blood pressure conditions

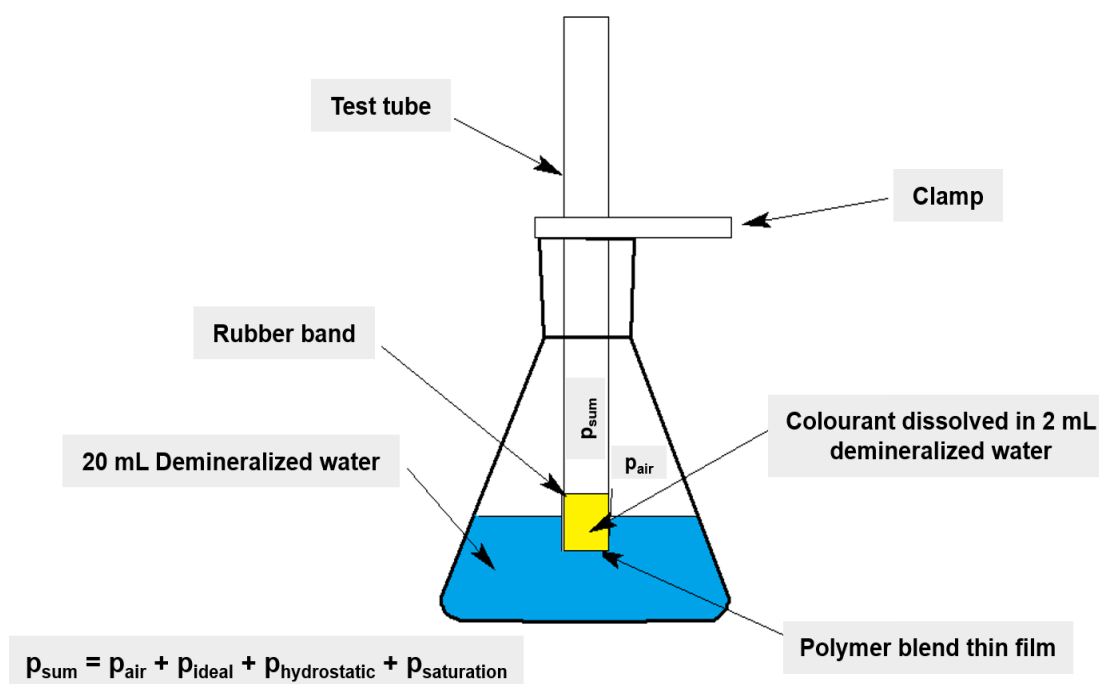


Figure 9.3: Modified vertical pressure cell, simulating blood pressure (Picture: K. Smolik and M. Kumar)

The Erlenmeyer flask was a VWR 214-1171 with a base diameter of 6.4 cm and a neck diameter of 3.4 cm. The height measures 10.5 cm and it has a volume of 100 mL. The test tube / test glass has a height of 12.8 cm and an inner diameter of 1.3 cm. It has a volume of 20 mL and is sealed at the top. This means it is a closed system for the gas. The Erlenmeyer flask was sealed with transparent sheet at the top for measurements in the Thermo Scientific Heratherm drying oven. The test tube had a beading and was placed 0.5 cm below the water surface.

The pressure which is build up in this cell consists mainly of three processes, which can be described in an approximation:

1. Pressure due to the ideal gas law
2. Pressure due to the saturation vapor of water / Clausius-Clapeyron relation
3. Hydrostatic pressure due to Pascal's law

The pressure will be estimated in the following part with the help of above three laws to give an insight about the pressure, i.e. the mechanical stress, which is applied to the thin film or membrane. The author underline that all calculations are just approximations.

1. **Pressure due to the ideal gas law** [198]

$$pV = nRT \quad \text{Equation 9.1}$$

where, p is pressure; V is volume; n is amount of substance; R is universal gas constant and T is temperature.

In the closed system of the test tube the volume V and the amount of substance n are approximately constant because it contains the same volume of air at each time. The pressure can be calculated for different temperatures. This leads to following equation:

$$\frac{p_1}{p_2} = \frac{T_1}{T_2} \quad \text{Equation 9.2}$$

For an air pressure of $p_1=1013$ mbar and at an average room temperature of 25 °C or 298 K, this leads upon heating up to 41 °C or 314 K to a pressure of $p_2=1067$ mbar. Hence the pressure difference Δp is 54 mbar.

2. **Pressure due to saturation vapor of water / Clausius-Clapeyron relation** [198]

The pressure can be estimated by the ideal gas approximation of Clausius-Clapeyron at low temperatures according to equation 9.3 [198]

$$\ln \frac{p_1}{p_2} = -\frac{L}{R} \left(\frac{1}{T_1} - \frac{1}{T_2} \right) \quad \text{Equation 9.3}$$

where, p_1 and p_2 are pressures at specific points; R is universal gas constant; T_1 and T_2 are temperatures at specific points and L is specific latent heat.

For a temperature of $T_1= 298$ K and $T_2= 314$ K it results an additional vapor pressure of water of $p_{\text{max,add}}= 73.8$ mbar (=74 mbar). The vapor pressure of water is in this case the pressure at which the water vapor is in thermodynamic equilibrium with its condensed state.

3. Hydrostatic pressure due to Pascal's law [198]

The hydrostatic pressure applied in this system is low compared to the other processes. It is described by equation 9.4.

$$\Delta p = \rho g(\Delta h) \quad \text{Equation 9.4}$$

where, Δp is hydrostatic pressure; ρ is fluid density; g is standard acceleration due to gravity and Δh is height of fluid above the point of measurement.

If the test glass is filled with 2 mL of solution the hydrostatic pressure is around 2 mbar.

4. Summing up the pressures

$$p_{\text{hydrostatic}} + p_{\text{ideal}} + p_{\text{saturation}} = 2 \text{ mbar} + 54 \text{ mbar} + 74 \text{ mbar} = 130 \text{ mbar}$$

This is the approximated pressure in the system in addition to the air pressure.

130 mbar equates to 95 mmHg. This resides in the range of the human blood pressure, which itself is for example in between 120 mmHg (systolic) to 80 mmHg (diastolic). The force applied to the membrane is according to equation 9.5:

$$F = p \cdot A = 13000 \text{ Pa} \cdot 1.33 \cdot 10^{-4} \text{ m}^2 = 1.72 \text{ N.}$$

$$p = \frac{F}{A} \quad \text{Equation 9.5}$$

The author is aware that there are a lot of disadvantages of the modified vertical cell. For example, no exact pressure is determinable because the pressure is not measurable in this experimental setup or at least it is very hard to measure it. Furthermore, a lot of other processes are involved. One assumption was the use of ideal gas behavior, besides that the system does not contain pure water, but a solution was in some samples also containing a dye and phosphate-buffered saline. Long heating periods were also other problem in the condensation processes. Nevertheless, this experimental setup was used to get a first insight into measurements with a mechanical stress in range of the blood pressure.

This work mainly deals with the distribution of hydrophilic molecules, i.e. simulating drug delivery, across thin films as a basis for a later potential application for a drug release out of electrospun fibers (next chapter). Here, the drug passage across membranes by diffusion is shortly described in order to show the need of on-demand drug release.

9.3 Experimental

9.3.1 Materials Used

All chemicals were of analytical grade and used without prior treatment. Polylactic acid 6202 (PLA) was provided by Prof. Endres, Institute for Bioplastics and Biocomposites (Iffb) Hannover, Germany. Methylene blue, MEB, ($M_w = 319.85$ g/mol) was purchased from company sigma-aldrich, Germany. Tetracycline hydrochloride, TCH, from Roth, Germany. Hydroxypropyl cellulose, HPC, ($M_w \approx 1.150.000$ g/mol, as high molecular weight (HMW-HPC) and $M_w \approx 80.000$ g/mol, as low molecular weight (LMW-HPC) was obtained from Ashland, EF pharm, GF pharm and HF pharm. The solvent used in this study was 2,2,2-Trifluoroethanol (TFE) from Roth, Germany. Potassium chloride, Sodium chloride, Disodium phosphate dehydrate and potassium dihydrogen phosphate, were used to prepare phosphate-buffered saline (PBS) with a pH of 7.4 from company Roth. Distilled deionized water was used throughout the experiments.

9.3.2 Material Characterization

9.3.2.1 UV-VIS Spectrophotometry

Ultraviolet-visible spectrophotometry measurements were taken with a Shimadzu UV-1601 UV-VIS double beam spectrophotometer. For measurements with methylene blue the maximum absorption of light was determined at a wavelength of 664 nm and for tetracycline hydrochloride at 358 nm.

9.3.3 Synthesis of PLA-HPC Thin-film Membranes

Different amount of thermoresponsive polymer, i.e. HMW-HPC, was added to PLA pellets (wt.% based on 1g PLA) and dissolved in 10 mL TFE. After 24 hours in the lab shaker the samples were cast out on a glass plate by using the solvent casting method. If the HPC, especially the HMW-HPC did not dissolve, then the time in the lab shaker was extended (next 24 hour) until the solution was visibly clear. The samples were dried for at least an hour in the fume hood and then at the air for 24 hours. For the casting of the thin films a film applicator of BYK Gardner (cat.no.2041, Ser.No.: 1168280) was used (50 μm , 100 μm , 150 μm , 200 μm). [Figure 9.4](#) shows different colors from a dried PLA-HPC thin film.

HPC was used as liquid crystals to prepare thin film by solvent casting method. Upon evaporation of the solvent, in this work mostly TFE was used, the self-assembly of the HPC chains takes place. The hydrophobic regions of HPC are aligned towards the PLA

which itself is also hydrophobic and the hydrophilic hydroxyl groups initiate the formation of hydrogen bond, probably enforced by TFE.

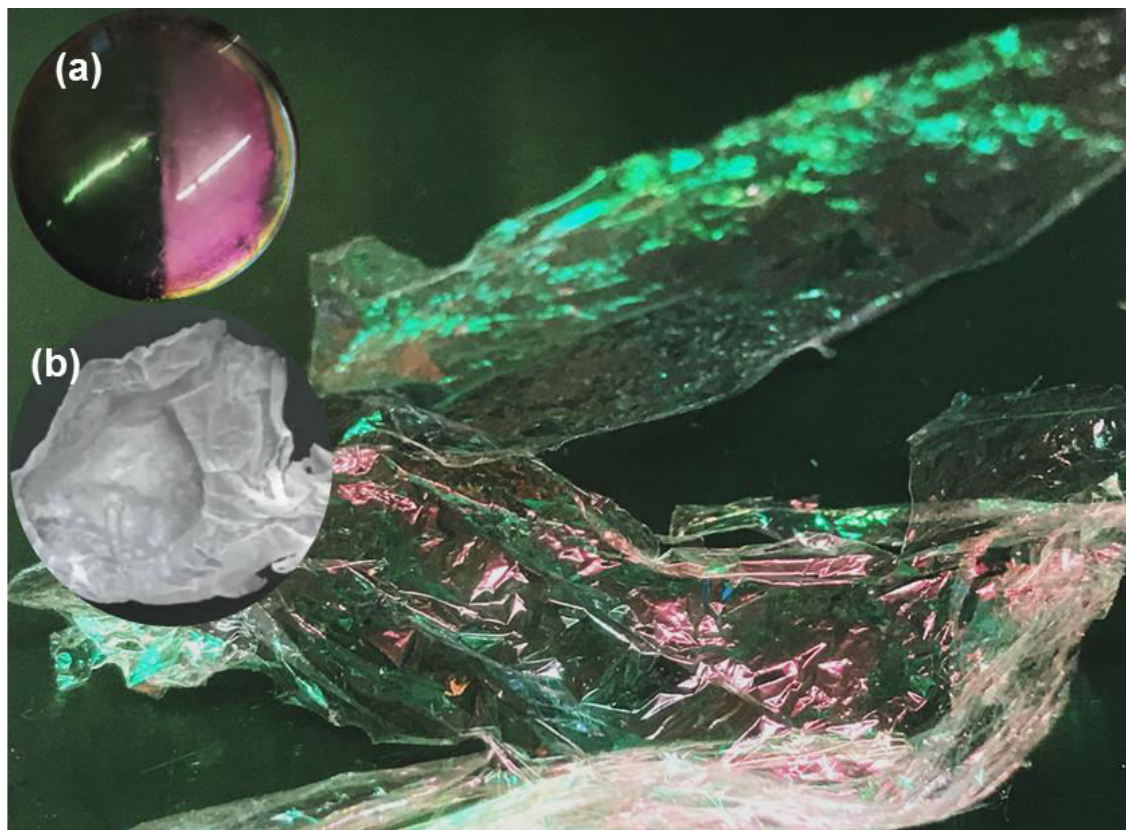


Figure 9.4: PLA-HPC dry thin film shows red/green color (a) shows dark color in the shadow whereas bright color in light (b) thin film shows cloudy or milky appearance at 45°C (Picture: Prof. Dr. F. Renz)

9.4 Results of PLA-HPC Thin-film Membranes

9.4.1 Results from the Side-by-Side Franz Cell

In Figure 9.5 the photometric measurement ($\lambda = 358$ nm) of a tetracycline hydrochloride release through a 200 μm thin film, (94,85 wt.% PLA, 5,15 wt.% HMW-HPC) using a side-by-side Franz Cell is being illustrated. A continuous heating was applied. One explanation for the release through the thin film might be the phase separation between PLA and HMW-HPC leading to aggregates which could be triggered by temperature at or above the LCST.

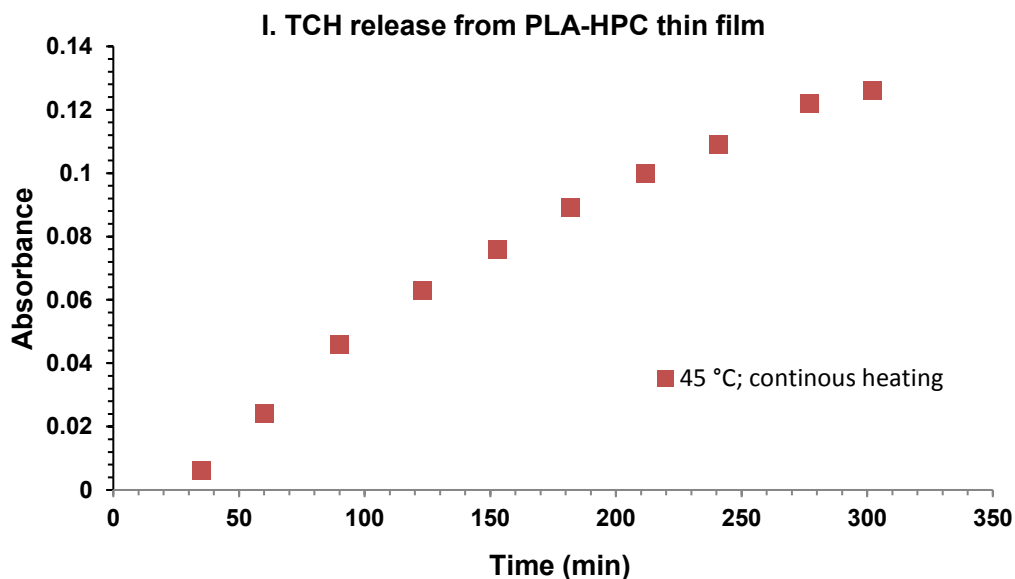


Figure 9.5: Photometric measurements ($\lambda= 358$ nm) of a tetracycline hydrochloride release through a 200 μm thin film (94.85 wt.% PLA, 5.15 wt.% HMW-HPC) using a side-by-side Franz cell

In Figure 9.6 the photometric measurement ($\lambda= 358$ nm) of a tetracycline hydrochloride release through a 200 μm thin film (94.85 wt.% PLA, 5.15 wt.% HMW-HPC) using a side-by-side Franz Cell is shown. The experiment was executed with demineralized water. For 90 minutes samples are measured at 24°C and then it was heated at 45 °C. A strong triggered was notices on providing heat to the samples. The thin films had cloudy or milky appearance (Figure 9.4) at some spots pointing to a phase separation between PLA and HMW-HPC.

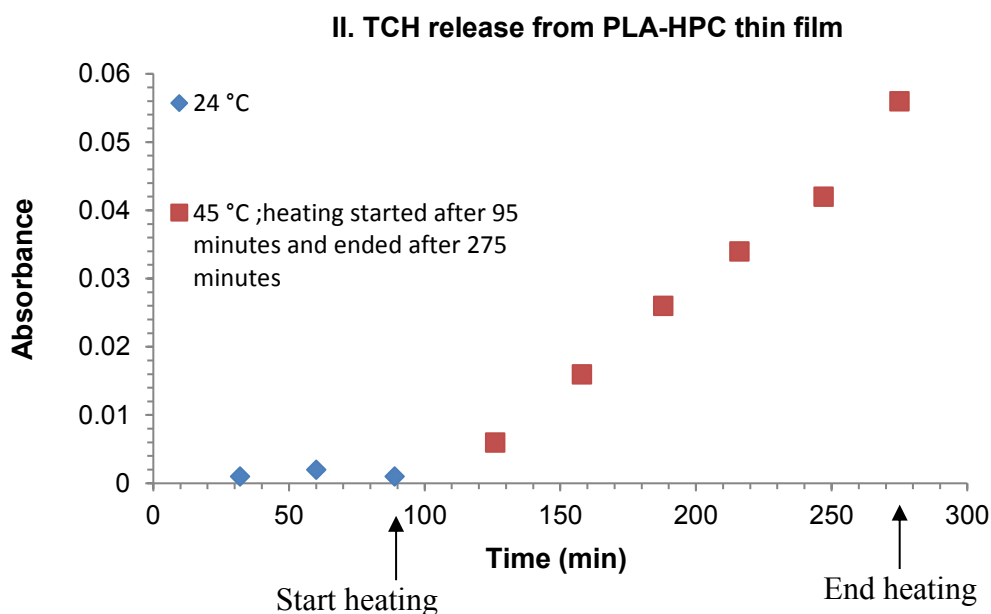


Figure 9.6: Photometric measurements ($\lambda= 358$ nm) of a tetracycline hydrochloride release through a 200 μm thin film (94.85 wt.% PLA, 5.15 wt.% HMW-HPC) using a side-by-side Franz cell

The blend showed as mentioned before a phase separation. Additionally, the LCST behavior was visible by the formation of the white collapsed state of HMW-HPC entangled in the PLA matrix. One explanation might be the rise in hydrophobicity as the LCST was reached. The HMW-HPC changed from a swollen and hydrophilic state to a hydrophobic collapsed state.

9.4.2 Results from the Modified Vertical Franz Cell - Simulating Simplified Blood Pressure Conditions

Figure 9.7 and Figure 9.8 shows result for the modified vertical cell simulating simplified blood pressure conditions. Realistically the human body has in many different regions a pressure available and this should be taken into account besides the body temperature and the occurring pH. HPC is known to be pH-independent which might be helpful because the pH changes in different parts of the human body. The applied pressure in this cell is rather high and near to the arterial blood pressure.

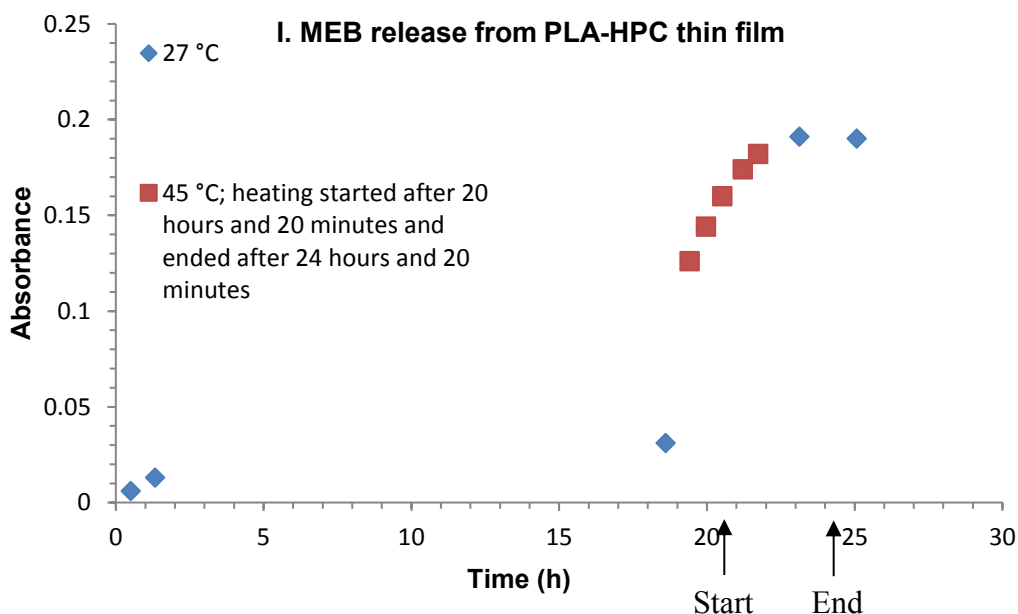


Figure 9.7: Photometric measurements ($\lambda = 664$ nm) of a methylene blue release through a $200 \mu\text{m}$ thin film (98.85 wt.% PLA, 1.15 wt.% HMW-HPC) using a modified vertical Franz cell

The thin films are quite thick ($50 \mu\text{m}$ up to $150 \mu\text{m}$) compared to biological membranes (lipid membranes are 8 nm of thickness). Nonetheless the cell gives a first insight into pressure-related measurements of thin films which are treated like membranes.

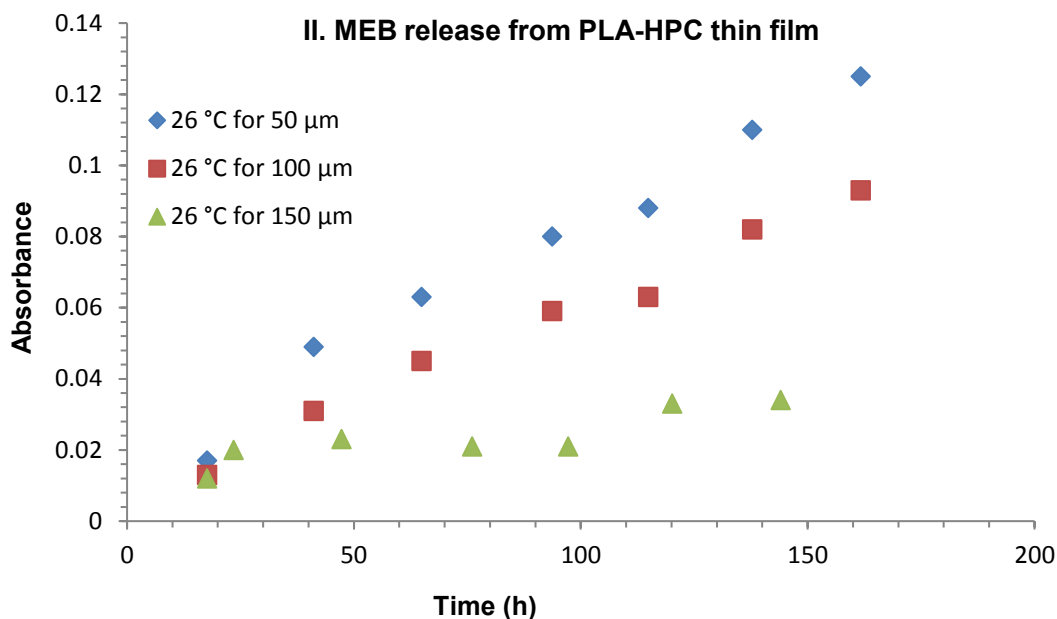


Figure 9.8: Photometric measurements ($\lambda = 664$ nm) of a methylene blue release through a 50, 100 and 150 μm thin film (89.7 wt.% PLA 6202, 10.30 wt.% LMW-HPC) using a modified vertical Franz cell

9.5 Discussion of PLA-HPC Thin-film Membranes

These results indicate a temperature responsive PLA-HPC thin film. A possible mechanism for temperature-responsiveness PLA-HPC thin film membranes could be the LCST- and lyotropic-behavior of HPC. This leads to an induced phase transition from an anisotropic to an isotropic state.

Drug release from PLA-HPC thin film membranes takes place at room temperature (21°C) and highest possible human body temperature (43°C). Drug release rises with the rise in temperature. On lowering the temperature, the drug still gets released but at lower concentration. At change in temperature (from 21°C to 45°C), these membranes show transition from swollen (hydrophilic) to shrink (hydrophobic) state, which increases the release rate.

PLA-HPC thin film membranes used HPC molecules, which show the formation of mesophase (from clear at 21°C to cloudy at 45°C), as change in turbidity in water. Since, the dipole moments of water is 1.85 D, and dipole moment of TFE (Trifluoroethanol) is 2.03 D, which are similar and it is expected that HPC will behave in same manner in TFE solvent as in water.

PLA and HPC is compatible in TFE solvent for the preparation of thin film. There is hydrogen bonding between fluorine from TFE (solvent) and hydroxypropyl group from HPC, which makes HPC stable in the PLA membrane in the thin film preparation. The TFE is integrated in the helix of the hydroxypropyl cellulose.

These PLA-HPC thin film membranes are placed in the side-by-side Franz cell and in the modified vertical Franz cell. An external pressure was not applied in case of side-by-side Franz cell, where in modified vertical Franz cell external pressure were employed. The mechanical stress in form of pressure of 130 mbar (equals 95 mm HG) was applied with the thermic stress. This applied pressure is in the range of the arterial human blood pressure. This force was strong enough to overcome the hydrophobic effect of the PLA and the increased surface hydrophobicity at the LCST of HPC. The model drug (Methylene blue) could bypass the thin films at these conditions and enter the second chamber. This was repeatable until equilibrium for the upper chamber and the chamber below was reached.

The author is aware that both approaches are simplified in comparison to the processes in the human body. The pH, enzymes and the degradation of the PLA matrix and many other factors are not included in this very basic approach. Yet it is still suitable for the development of drug delivery systems and the mechanisms involved.

The thin films used in the experiments had a thickness of 50 μm , 100 μm , 150 μm and 200 μm . The decrease of the thickness might also decrease the pressure which is necessary to overcome the very hydrophobic surface by the dye or the drug. An approximation to the human cell membrane thickness of ca. 8 micrometers could also be achieved by using the multi-responsive system of electrospun nanofibers. This might be one chance to reach the goal, as human-like membranes and might be a first step into a drug release.

The possible existence of circular dichroism or its interference can be seen with the eye (red/green color) (Figure 9.4).

The research on membranes or thin films containing liquid crystals might be interesting in the near future. Lyotropic liquid-crystalline phases are available in living systems like biological membranes. This is often referred to as lipid polymorphism. In addition to that, the membrane is very flexible because these molecules can inter-mingle quite easily but remain still in the membrane due to the fact that much energy would be required for the process to dissolve away. The lipids can vary in shape and therefore also influence the diffusion. This complex and yet very fascinating biological membranes are a good model for the development of drug delivery systems. This partially biomimetic approach in this work was very useful.

9.6 Conclusion of PLA-HPC Thin-film Membranes

In view of drug release mechanisms two different types of approaches were presented. A simple side-by-side Franz cell was used in order to gain insight about diffusion processes. Temperatures between 24°C – 45°C were investigated. Another, more complicated cell, with a pressure gradient was used to examine the drug release in connection with an applied mechanical stress (additional to the thermic stress). The formation of liquid crystals of HPC in a highly hydrophobic PLA environment showed red-green circular dichroism or interference at visible light, which can be observed with eye.

Although HPC is known to have a lower critical solution temperature (LCST) near 41 °C, the diffusion in the horizontal Franz cell was highly hindered, probably due to increased surface hydrophobicity. PLA-HPC membranes show phase transition. The cell with the mechanical stress although showed increased dye release rates while being stable under air pressure. This process was repeatable until the equilibrium was reached in both cell chambers. The PLA-HPC thin films showed phase separation during the formation of the thin films by the solvent casting method leading to a typical morphology.

10 Preparation of PLA-HPC Fibrous Membranes

10.1 Abstract

In this study, Polylactic acid and Hydroxypropyl cellulose (PLA–HPC) fibers were fabricated by electrospinning. Methylene blue (MEB), as a model hydrophilic drug was embedded into PLA–HPC fibrous membranes. SEM results depicted that fibers are smooth, cylindrical, uniform and it confirmed the incorporation of MEB in PLA fibers alter the fibers morphology. Release studies show the on-demand release of drug from PLA–HPC fibrous membranes under temperature stimuli which were absent in membranes manufactured out of PLA. This can be attributed to reversible volume phase transitions of HPC molecules in response to applied external temperature. This study may provide more efficient strategies for developing materials with on-demand drug release capability.

10.2 Introduction

The ongoing efforts to improve drug delivery systems (DDS) for long lasting effects and improved medicinal potential beyond the basic application are receiving a major impetus towards the development of “smart” materials [199][200][201]. When materials are designed for biomedical applications such as drug delivery and biosensors, three important factors have to be taken into account: (1) biocompatibility, (2) surface functionalities and (3) hydrophilicity [157]. Polylactic acid (PLA) is a most common biopolymer used for biomedical application because it is non-toxic, biocompatible and biodegradable [150]. Hydroxypropyl cellulose (HPC) is a non-ionic cellulose derivative, which can also be used in the field of biomedical applications [129], because it is a physiologically inert substance, and is considered to be non-toxic and biocompatible. HPC is mainly used as an excipient in oral solid dosage forms, in which it acts as a disintegrate [202] and as a binder [203]. It is also an ingredient of so-called “artificial tears”, used in the treatment of the dry eye syndrome (i.e., insufficient tear production) and to moisten contact lenses.

An interesting feature of HPC structure is the presence of both hydrophobic and hydrophilic groups. At 42°C, the HPC-molecules display a lower critical solution temperature (LCST) [204]. At room temperature (below LCST), HPC is soluble in water. The solution has a low viscosity and clear appearance. Above the LCST (43°C) its solubility decreases and already dissolved HPC precipitates, as shown in [Figure 10.1](#) [205]. The formation of precipitation is also called “flocculation” and is thermo-reversible

[206]. This property could be utilized in the development of materials with on-demand drug release capability.

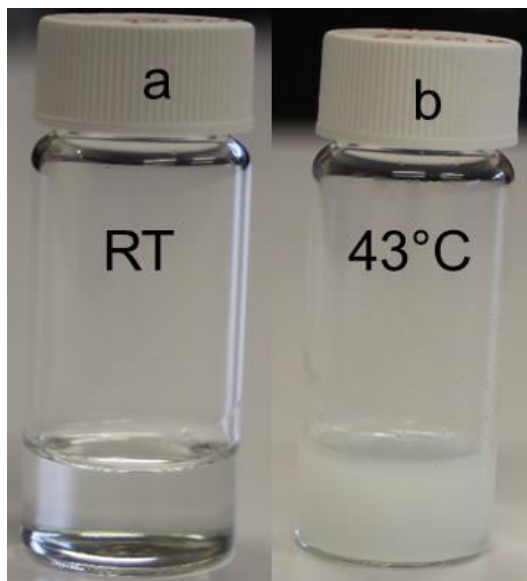


Figure 10.1: Thermal responsiveness of hydroxypropyl cellulose (HPC). (a) Photographs of aqueous solution (5 mg (HPC) / mL (H₂O)) sample at room temperature (RT) (b) and at 43°C (turbidity temperature) [207].

Temperature-responsive release system is an efficient method of delivering drugs to a localized disease site because of their ease control in practical applications [208]. This method can also be applied to fibrous membranes. In fibrous membranes, temperature responsive materials are incorporated within. Such materials show a phase separation at a certain temperature, known as LCST. The LCST is mainly dependent on the hydrogen bonding and hydrophobic interactions between water molecules and the structure of functional units of the polymer [91]. Figure 10.2 shows a symmetric diagram of the thermally induced drug release system. Such smart membranes are proposed to be used for wound healing applications by delivering drug on-demand.

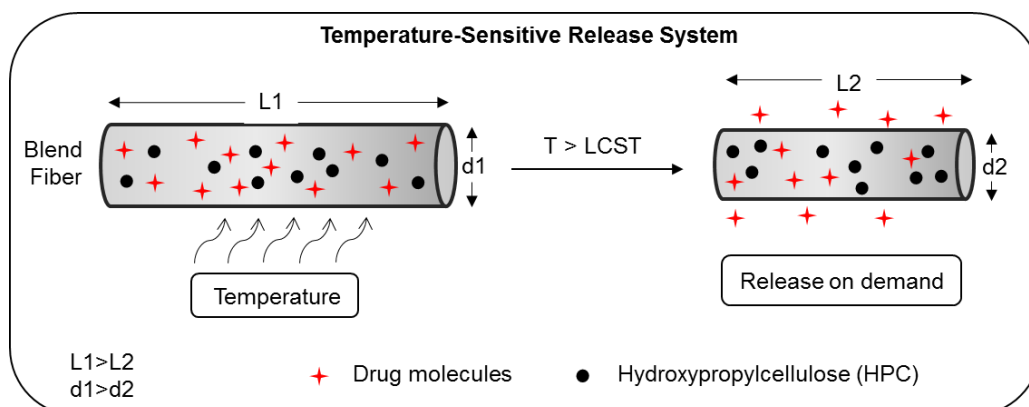


Figure 10.2: A symmetric diagram shows temperature-responsive drug-release system [207].

HPC has a compatibility with another biopolymer such as PLA because of its dual solubility (organic solvents and water). The addition of HPC to PLA fibers improves flexibility, and reduces the water resistance properties of PLA fibers. PLA is chosen as a base material for fiber formation, whereas HPC act as a temperature responsive material. There are a number of studies exists on temperature responsive materials for biomedical applications [208]. Table 10.1 shows a different structure of selective temperature – responsive materials with LCST behavior. However, few studies related to electrospinning of HPC-based composites have been reported [209][210][211]. To date, neither PLA-HPC [212] based electrospun fibrous membranes have not been reported nor tested for drug release.

Table 10.1: A comparative studies on selected temperature-responsive materials with LCST behavior for drug delivery applications [207].

Materials	Structure	LCST (°C)	Ref.
PNIPAAm	Hydrogels	25 – 32	[213]
PDMAAm	Hydrogels	15 – 32	[214]
PNVCL	Hydrogels	32 – 34	[215]
P(PEGMA- <i>co</i> -Boc-Cyst-MMAm)	Particles	20 – 57	[216]
PNIPAAm and PNBAAm	Films	37	[217]
PNIPAAm-PLA	Micelles	38 – 42	[218]
ELPs	peptides	40	[219]
PLA-HPC	Nanofibers	43	This work

PNIPAAm: Poly(*N* -isopropylacrylamide); PDMAAm: Poly(dimethyl acrylamide); PNVCL: Poly(vinyl caprolactam); PEG-MEMA: Poly(ethylene glycol) methyl methacrylate; Boc-Cyst: [[[mono-(*N-tert*-butyloxycarbonyl)amino]ethyl]dithio] ethyl; PLA: Polylactic acid; ELPs: Elastin-like polypeptides; PNBAAm: Poly(*N*-butylacrylamide); HPC: Hydroxypropylcellulose.

Here, the aim was to obtain stable thermo-reversible fibrous membranes in the physiological relevant range of temperatures. The fibrous structure leads to a large surface-to-mass ratio, and would thus enable efficient release of substances [220][221]. For this purpose, PLA-HPC fibers were fabricated by electrospinning. These fabricated fibrous membranes (PLA–HPC) were tested as a carrier for the drug methylene blue (MEB) and applied for on-demand drug delivery systems. The present work reveals that PLA–HPC composite fibrous membranes are thermo-responsive, stable and tuneable and would provide a better control over conventional drug delivery.

10.3 Experimental

10.3.1 Materials Used

All chemicals were of analytical grade and used without prior treatment. Poly(lactic acid) 4043 (PLA) was provided by Prof. Endres, Institute for Bioplastics and Biocomposites (Ifbb) Hannover, Germany. Hydroxypropyl cellulose (HPC) (average molecular weight of 1,000,000 g/mol), and methylene blue (MEB) (average molecular weight of 319.85 g/mol) was obtained from company Sigma-Aldrich. The solvent used in this study were 2,2,2-Trifluoroethanol (TFE) from company Roth, Germany. Di-Sodium hydrogen phosphate dehydrate ($M_w = 178$ g/mol, Roth), Potassium dihydrogen phosphate ($M_w = 136$ g/mol, Roth), Potassium chloride ($M_w = 74.5$ g/mol, Roth), Sodium chloride ($M_w = 58.4$ g/mol, Roth) were purchased and used without any further purification. Distilled – deionized water was used throughout the experiments.

10.3.2 Material Characterizations

10.3.2.1 Scanning Electron Microscopy (SEM)

Scanning Electron Microscopy (SEM) (Zeiss Leo VP 1455) was used to analyze the surface morphology and diameter of the prepared fibers. Three samples were prepared; first sample PLA fibrous mat, second sample PLA-MEB composite fibrous mat, and third sample PLA-MEB-HPC composite fibrous mat. All specimens were vacuum coated with gold/platinum before taking SEM image to minimize sample charging.

10.3.2.2 In vitro Release Profile of MEB

MEB release was performed using phosphate buffer saline (PBS) with pH 7.4 at room temperature (RT) and 43°C. The drug-loaded composite membrane of ca. 10 mg was cut and placed in 10 ml buffer solution. The solution was kept in the shaking incubator (100 rpm). The release kinetic was determined by withdrawing aliquots from the solution at determined time intervals and recorded their absorbance at a wavelength of 665 nm (λ_{max}) using UV-vis Spectroscopy (PerkinElmer Lambda 650 S). The amount of the released MEB over time was calculated using the standard graph (absorbance vs concentration of free drug) with correlation coefficient $R^2 \sim 0.998$.

10.3.3 Synthesis of PLA, PLA-MEB and PLA-MEB-HPC Composite Fibrous Membranes

PLA, PLA-MEB and PLA-MEB-HPC polymer solutions for electrospinning were prepared separately. Firstly, 0.1 g/mL of PLA (Pellets) in 2,2,2-Trifluoroethanol (TFE) was dissolved. To this, 0.01 g/mL MEB (powder) was added into PLA solution, to form PLA-MEB solution and finally, 0.005 g/mL HPC (powder) was incorporated to PLA-MEB solution, to form PLA-MEB-HPC solution. These solutions were stirred (Vortex Genie) until all polymer was dissolved. These three polymer solutions were separately filled in a 10 mL syringe pump and connected to the electrospinning unit [157][159][222]. Electrospinning was performed in a closed chamber (relative humidity = 20 % and chamber temperature, 22°C). For the fabrication of these three-fibrous membranes, side-by-side electrospinning apparatus as described in section 2.3.3 was used. The electrospinning conditions used for these experiments are given in Table 10.2.

Table 10.2: Summary of electrospinning conditions [207]

Sample	Concentration [g/mL]	Flow rate [mL h ⁻¹]	Voltage [kV]	Height [cm]	Rotar speed [m/s]
PLA	0.1	0.15	12	15	15
PLA-MEB	0.1-0.01	0.15	12	15	15
PLA-MEB-HPC	0.1-0.01-0.005	0.15	12	15	15

10.4 Results and Discussion of PLA-HPC Composite Fibrous Membranes

10.4.1 Scanning Electron Microscopy (SEM)

SEM micrographs of the PLA, PLA-MEB and PLA-MEB-HPC nanofibers are shown in Figure 10.3. PLA fibers are beaded and cylindrical and have a mean diameter of $0.4 \pm 0.1 \mu\text{m}$ without bead (Figure 10.3(a)). The bead structure is mainly due to their low concentration effect. The fibers made of PLA-MEB composite are rather homogeneous and have a mean diameter of $0.12 \pm 0.03 \mu\text{m}$, as shown in Figure 10.3(b). A smooth and uniform morphology is observed when MEB model drug is incorporated into the PLA solution by physical blending. The fibers made of PLA-MEB-HPC composite are

cylindrical and have a mean diameter of $0.17 \pm 0.03 \mu\text{m}$ (Figure 10.3(c)). The addition of HPC gradually increases the fiber diameter, due to decrease of uniformity and smoothness [159]. For all samples, 50 fibers were chosen randomly and their mean and standard deviation (SD) of fibers diameter were analyzed using image analysis software (Digimizer, version 4.5). Figure 10.3(d) reveals the mean fibers diameter distribution.

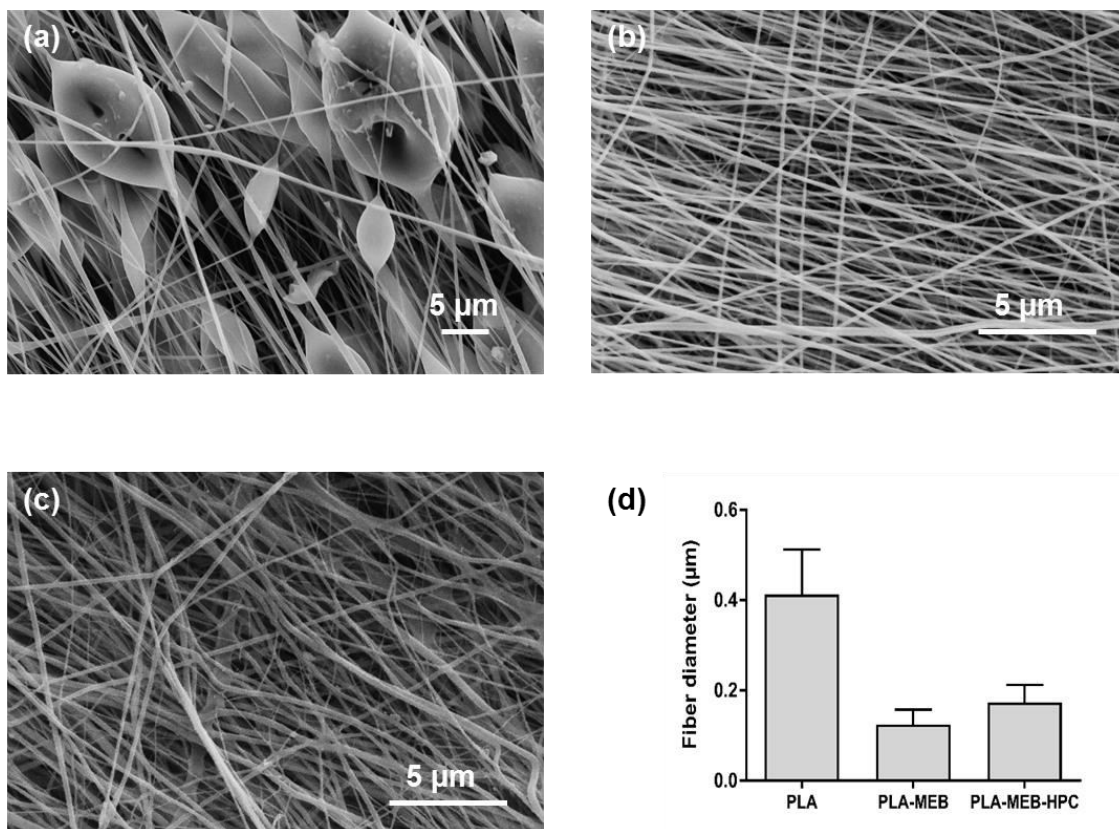


Figure 10.3: Scanning electron micrographs for electrospun (a) PLA (b) PLA-MEB (c) PLA-MEB-HPC composite fibrous membranes and (d) Average mean fibers diameter measurements [207].

10.4.2 In-vitro Release of MEB

The cumulative release profiles of MEB from the PLA and PLA-HPC composite fibrous membranes are shown in Figure 10.4. These membranes (PLA and PLA-HPC) are incubated in PBS environment at $\text{pH} = 7.4$, at room temperature (22°C , below the LCST) and 43°C (above the LCST). The release of MEB from PLA and PLA-HPC composite fibrous membranes depends on many factors, including the solubility, swelling and weight reduction. Both membranes show initial burst release, therefore, composite fibrous membranes were initially washed (5 times, in 10 min) with 10 ml distilled water, so that the surface available drugs are removed. After washing, a sustained release of MEB is achieved from the composite membranes because MEB molecules are hydrophilic. The MEB release is accelerated at the temperature above the LCST, in the case of PLA-HPC

composite fibrous membranes. PLA fibrous membranes show an initial release of 0.75% with the almost negligible release over 1 hour, even under applied temperature (43°C). This is likely due to hydrophobic and semi-crystalline nature of PLA, which limits the diffusion of MEB from the fibrous membranes. The time scale of these release experiments is too short to expect the significant release of MEB, resulting from hydrolysis of PLA. Therefore, it can be expected that Fickian diffusion through the PLA fibrous membranes would be the predominant mechanism [223].

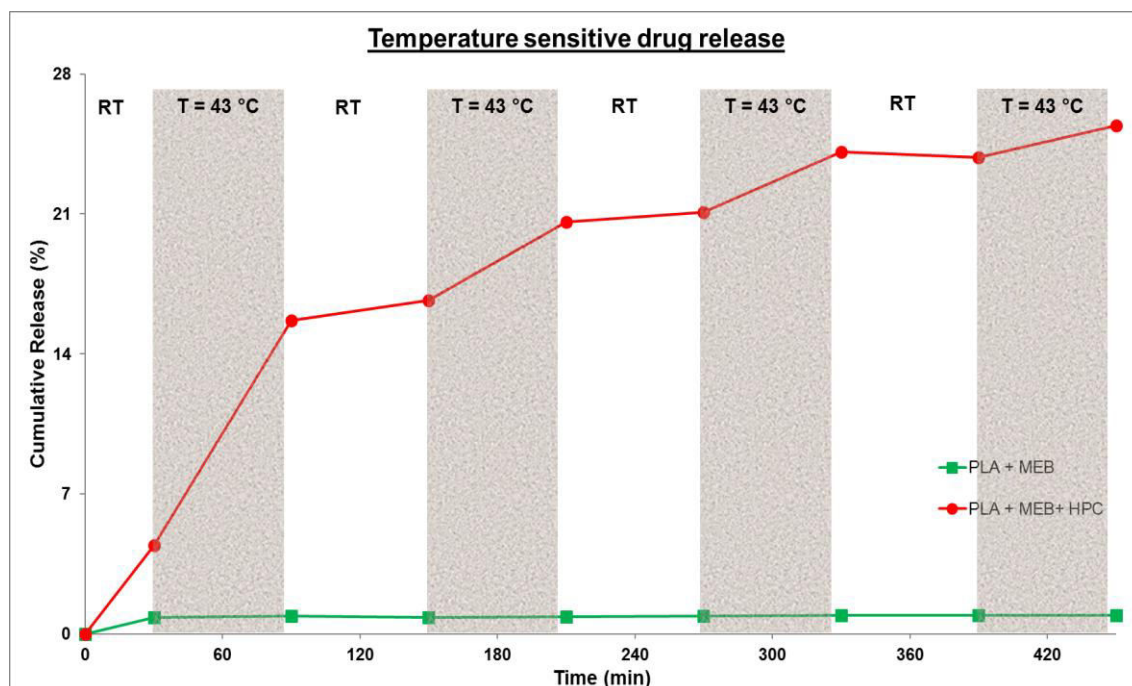


Figure 10.4: Drug release profile showing the cumulative drug release Vs time (min) of drug loaded (a) PLA fibers (b) PLA-HPC composite fibrous membranes [207].

However, a significant variation in MEB release is observed by PLA–HPC fibrous membranes. The initial release of 4.03% is observed, which is much higher than the release by PLA fibrous membranes (0.75%). This may be assigned to the presence of water-soluble HPC molecules in the membranes. The MEB release is accelerated at a temperature above the LCST. HPC molecules show critical solution temperature around which the hydrophobic and hydrophilic interactions between the polymeric chains and aqueous media changes with the temperature [224][225]. When the temperature is below the LCST, the PLA–HPC fibers are stable and therefore, shows slow diffusion of MEB. However, when the temperature is increased to a value above the LCST, hydrophobic interactions in PLA–HPC fibrous membranes are strengthened and thus accelerate MEB diffusion. This happened because of the disruption of intra- and intermolecular electrostatic and hydrophobic interactions and results in chain collapse or expansion (phase transition) [226][227]. The construction or destruction of primary/secondary forces (chain dynamics, i.e. the energy level of the polymer/solvent system, hydrogen

bonding, hydrophobic effects, electrostatic interactions, phase change etc.) are responsible for pulsatile MEB release [228] (Figure 10.5). The maximum 25.4% MEB is released in 7-8 hours in case of PLA–HPC fibrous membranes and in the same time period only 1% MEB released from PLA fibrous membranes. These results show that HPC molecules in the composite fibrous membranes are the cause of MEB release in response to the external temperature.

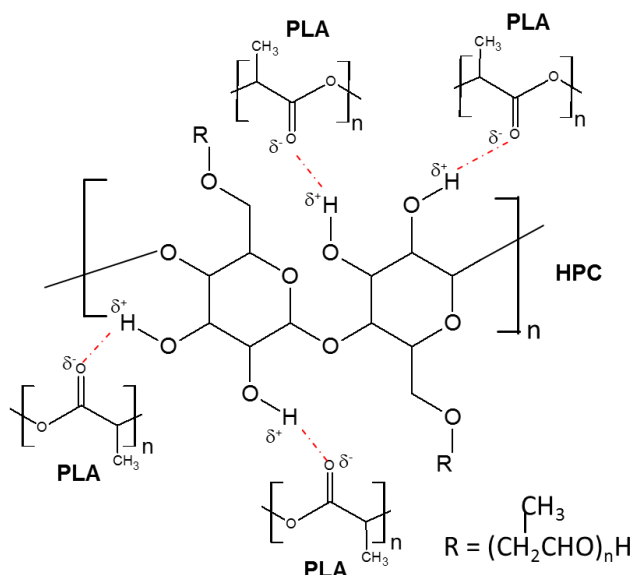


Figure 10.5: Schematics of cellulose repeat chain, showing the proposed hydrogen bonding (dotted line) with PLA.

Thus, in-vitro studies demonstrate that MEB release from PLA–HPC fibrous membranes within the period of 7-8 hours, which is quite good for the acute injuries, where there is an on-demand supply of drug required. Hence, electrospinning approach of drug delivery is quite useful, especially for heat-sensitive drug molecules.

10.5 Conclusions of PLA-HPC Fibrous Membranes

In the present work, temperature sensitive electrospun fibers are developed using PLA and HPC. The morphology of fibers is shown by SEM analysis. A sustained release of the MEB is achieved from the membranes. MEB release from the PLA membranes has no effect on temperature, whereas MEB release from the PLA–HPC membranes has accelerated when the temperature is raised slightly above the LCST. The results are promising for further investigation of biocompatibility, and site specific sustained release (especially for wound care treatments), in order to implement PLA–HPC composite fibrous membranes for a clinical trial.

11 Preparation of PLA-PEG-BSA Fibrous Membranes

Biologically sensitive sensors are a promising technology for detecting pathogens, enzyme, antigen-antibody complexes, and tumor markers. As the state of the art advances, demand for accurate, sensitive, specific, high-throughput and rapid detection methods of molecular identities are increased [229][230][231][232]. To meet these needs, it is proposed to use biotin-avidin complex on the electrospun fibers. The unique advantages of electrospun fibers are large specific surface area, reduced grain size and nanoporosity, which will greatly enhance the performance of the biosensors.

11.1 Biosensors

According to IUPAC recommendations, a biosensor is an independently integrated receptor transducer device, which is capable of providing selective quantitative or semi-quantitative analytical information using a biological recognition element [233][234]. It uses specific biochemical reactions mediated by enzymes, antibody, or whole cell to monitor the presence of various chemical compounds on a substrate usually by chemical, electrical, thermal or optical signals [235]. Its role is to interact specifically with the target analyte and the result of biochemical reaction is consequently transformed through transducer to measurable signal. The basic principle of the biosensor is shown in the [Figure 11.1](#). The ability of biomolecules to react with very low concentrations of substances allows biosensors to be used in various biomedical applications such as in early detection of cancer [236]; in recognition of biological molecules such as enzyme, bacteria, and cholesterol [237][238][239]; and biosensors with microelectrodes are used to examine nerve signal in brain [240].

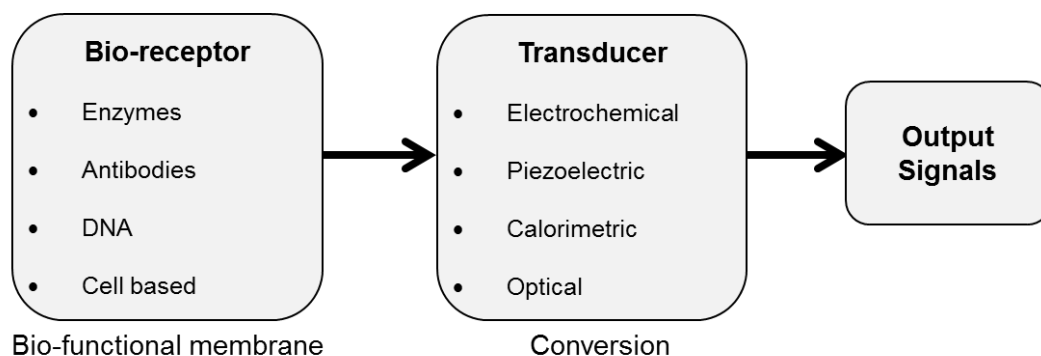


Figure 11.1: The principles of the biosensors

11.2 Avidin-Biotin

Avidin is a tetrameric protein recognized as a biological factor in egg white [241]. It has two-fold symmetry, i.e. the binding sites being arranged in two pairs on opposed faces of the molecules (as shown in Figure 11.2 and Figure 11.3). It has a remarkable strength of the interaction with the vitamin biotin. The extraordinary affinity between avidin-biotin system is characterized by an association constant (K_a) of the order of $10^{15} M^{-1}$. This value corresponds to a free energy of association of about 21 kcal/mol, a staggeringly large value for the noncovalent interaction of a protein with a molecule as small as biotin [242]. The interaction between avidin-biotin is so strong that even chemically modified and any biologically active compound with biotin can be attached. The four biotin-binding sites of avidin, provide the possibility of cross-linking between different biotin molecules, which could be used for signal amplifications, diagnostics and even selective eliminations.

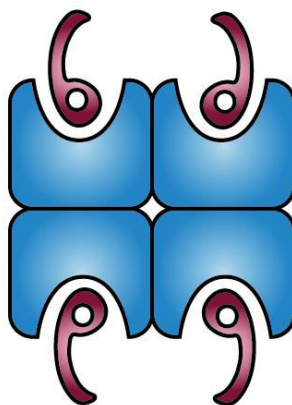


Figure 11.2: Schematic illustration of an avidin molecule (2-fold symmetry) complexed with four biotins [157]

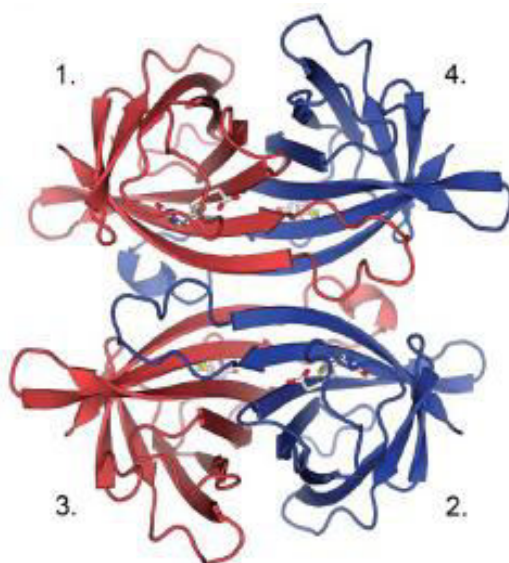


Figure 11.3: Avidin tetramer with subunit is colored to red and blue according to dual chain avidin subunits [243]

11.3 Advantages of Avidin-Biotin

Avidin-biotin offers several advantages, some are as follows [242]:

1. Avidin-biotin has high affinity of interaction and stability.
2. Biotin can be used to attach binders and probes to avidin and, biotinylation, does not affect the biological activity and physical characteristics.
3. Tetrameric structure of avidin allows signal amplification.
4. A wide spectrum of different biotinylated chemicals, reagents and avidin-containing probes are available.
5. The system is highly versatile, i.e molecular interaction can be analyzed by various means.

11.4 Challenges

The typical problems of biosensors are stability, sensitivity, low analyte-antigen concentrations (\sim nM), lifetime of biological components and limited dynamic ranges. In addition to this, reversibility may be a problem. Therefore, the growth condition such as culture age, temperature and population can affect the response of the biosensors. In this regard, biosensor developed by electrospinning technique could be greatly benefited from the availability of high surface area and miniaturized size (ultimately nanoscale), which allows one to easily decouple excitation and signal emission. Sensors with such technology will improve sensitivity, detection limit, response time and selectivity.

11.5 Results of PLA-PEG-BSA Fibrous Membrane

Mixture of PLA-PEG and Biotinylated Albumin enables Immobilization of Avidins on Electrospun Fibers

Manish Kumar, Rolle Rahikainen, Daniel Unruh, Vesa P. Hytönen, Cesare Delbrück, Ralf Sindelar, Franz Renz

J. Biomed. Mater. Res. Part A, (2017):105A:356-362.

DOI: 10.1002/jbm.a.35920

Web link: <http://onlinelibrary.wiley.com/doi/10.1002/jbm.a.35920/full>

“Winner of the Society for Biomaterials Student Award in the Undergraduate Category, Charlotte, NC”.

The publication is reprinted from Journal of Biomedical Materials Research Part A, Copyright (2017), WILEY-VCH Verlag GmbH & Co.



My Orders > Orders > All Orders

License Details

This Agreement between Leibniz University Hannover ("You") and John Wiley and Sons ("John Wiley and Sons") consists of your license details and the terms and conditions provided by John Wiley and Sons and Copyright Clearance Center.

[printable details](#)

License Number	4175300483820
License date	Aug 24, 2017
Licensed Content Publisher	John Wiley and Sons
Licensed Content Publication	Journal of Biomedical Materials Research
Licensed Content Title	Mixture of PLA-PEG and biotinylated albumin enables immobilization of avidins on electrospun fibers
Licensed Content Author	Manish Kumar,Rolle Rahikainen,Daniel Unruh,Vesa P. Hytönen,Cesare Delbrück,Ralf Sindelar,Franz Renz
Licensed Content Date	Oct 21, 2016
Licensed Content Pages	7
Type of Use	Dissertation/Thesis
Requestor type	Author of this Wiley article
Format	Print and electronic
Portion	Full article
Will you be translating?	No
Title of your thesis / dissertation	Energy transfer and -conversion by functionalized nano-bio-fibers for biomedical applications
Expected completion date	Nov 2017
Expected size (number of pages)	150
Requestor Location	Leibniz University Hannover Institut f. Anorganische Chemie Leibniz Universität Hannover Callinstr. 9, D-30167 Hannover Hannover, 30167 Germany Attn: Leibniz University Hannover EU826007151
Publisher Tax ID	
Billing Type	Invoice
Billing address	Leibniz University Hannover Laboratory of Nano & Quantum Engineering Leibniz Universität Hannover Schneiderberg 39 Hannover, Germany 30167 Attn: Leibniz Universität Hannover
Total	0.00 EUR

[BACK](#)



Winner of the Society for Biomaterials Student Award in the Undergraduate Category, Charlotte, NC

Mixture of PLA-PEG and biotinylated albumin enables immobilization of avidins on electrospun fibers

Manish Kumar,^{1,2} Rolle Rahikainen,^{3,4} Daniel Unruh,⁵ Vesa P. Hytönen,^{3,4} Cesare Delbrück,⁵ Ralf Sindelar,¹ Franz Renz⁵

¹Department of Material Science Faculty II, University of Applied Science and Arts, Ricklinger Stadtweg 120, Hannover, 30459, Germany

²Laboratorium of Nano and Quantum Engineering, Leibniz Universität Hannover, Schneiderberg 39, Hannover, 30167, Germany

³BioMediTech University of Tampere, Lääkärikatu 1, Tampere, Finland 33520

⁴Fimlab Laboratories, Biokatu 4, Tampere, Finland 33520

⁵Institute of Inorganic Chemistry Leibniz Universität Hannover, Callinstraße 9, Hannover, 30167, Germany

Received 23 June 2016; revised 14 September 2016; accepted 16 September 2016

Published online 21 October 2016 in Wiley Online Library (wileyonlinelibrary.com). DOI: 10.1002/jbm.a.35920

Abstract: The application of nanotechnology in biomedical field has enormous potential in basic and applied research. Micro or nanofibers produced by electrospinning technique offer excellent properties because of large specific surface area, high porosity, and ability to incorporate functional additives. Here we embedded biotinylated bovine serum albumin into polylactic acid (PLA)-polyethylene glycol (PEG) fibers, which enabled specific immobilization of fluorescently labelled avidin. An alkaline phosphatase enzyme was immobilized via biotin-streptavidin interaction on the hybrid nanofibers,

demonstrating the suitability of the material for biosensing applications. These functional nanofibers provide a promising platform for development of biosensors and other biofunctional materials utilizing avidin-biotin as a generic and robust immobilization method. © 2016 Wiley Periodicals, Inc. *J Biomed Mater Res Part A*: 105A: 356–362, 2017.

Key Words: electrospinning, polylactic acid (PLA), polyethylene glycol (PEG), biotinylated BSA, avidin, functional fibers

How to cite this article: Kumar M, Rahikainen R, Unruh D, Hytönen VP, Delbrück C, Sindelar R, Renz F. 2017. Mixture of PLA-PEG and biotinylated albumin enables immobilization of avidins on electrospun fibers. *J Biomed Mater Res Part A* 2017:105A:356–362.

INTRODUCTION

Electrospinning is a straight-forward approach for creating highly functional continuous one-dimensional nanofibers.^{1–5} Electrospun polymeric micro- and nanofibers provide unique properties, such as inherently high surface area-to-volume ratio, high interconnectivity, porous structure, and high flexibility in surface functionality. Fibers with complex architecture such as randomly oriented, aligned fibers, core-shell fibers, hollow fibers, porous fibers, side-by-side structures can be easily produced with this technique.^{6,7} These fibers have desirable properties for advanced biomedical applications such as biosensors, controlled drug delivery, tissue engineering, enzyme carriers, and much more.^{8–12} During electrospinning, one of the important challenges is the control of the morphology and the geometry of the nanofibers. All in all, nanofibers open the door to dramatically improve the performance of existing technologies/devices.

When fibers are considered for biosensing applications, there are three important factors to be considered^{13,14}: (1) hydrophilicity, (2) surface functionalities, and (3) biocompatibility. The hydrophilicity of the fibers must be balanced to avoid aqueous degradation. The fiber surface must be functional which provides the ability to interact with bioactive surface. And it must be biocompatible to avoid injurious effects on the living body. For this purpose, we have chosen bio-absorbable, bio-degradable, bio-based polymer; polylactic acid (PLA), as a base material for functionalization using avidin-biotin interaction. Avidin-biotin was selected because of its high specificity, greater availability of the suitable functionalization tools (biotinylated antibodies, nucleic acids, nanoparticles, and so forth), and also because genetically engineered avidins¹⁵ makes it possible to meet more specific needs in biofunctionalization.

Correspondence to: F. Renz; Leibniz Universität Hannover, Institute of Inorganic Chemistry, Callinstraße 9, Hannover, Lower Saxony 30167, Germany; e-mail: franz.renz@acd.uni-hannover.de

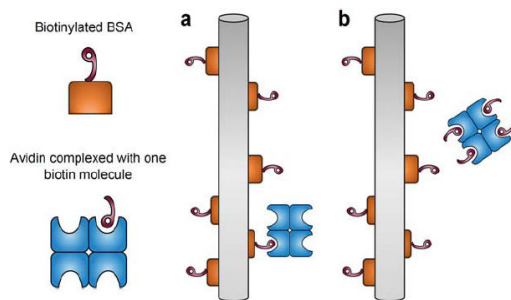


FIGURE 1. Immobilization of avidin on biotinylated fiber. (a) Avidin immobilized on biotinylated fiber. (b) Free ligand-binding sites of avidin are blocked by an excess of free biotin.

PLA represents the front-runner bio-based polymer because of its attractive features such as renewability, biocompatibility, and high thermo-mechanical properties,^{16–18} which brings a large set of applications from biosensor to packaging. However, there are some shortcomings to be addressed, especially for biosensor applications, high hydrophobicity being one of the important challenges.¹⁹ A range of modifications, including chemical, physical, biological, and nanotechnology techniques are therefore proposed to improve the characteristics of PLA.²⁰ A simple method is physical blending with hydrophilic polymer such as polyethylene glycol (PEG).^{21,22} The addition of PEG to PLA is mainly to decrease the hydrophobicity, which improves the wettability of the final fibers.²³ PEG is chosen as plasticizer which increases the free volume of the polymer/plasticizer system by augmenting the space between polymer chains and thus causing them to spread apart. During the electrospinning process, PEG in copolymers of PLA-PEG has been found to become segregated, leading to a fiber with hydrophilic PEG at the surface.²⁴ This results in fibers with higher homogeneity and wettability as compared to fibers made of PLA alone.

Biotin (244.3 g/mol) is chemically inert, water-soluble, and optically inactive B-vitamin, also called vitamin H. Avidin is a homotetrameric protein known to bind biotin with high affinity ($K_d \sim 10^{-16} M$). This protein–ligand pair has been widely utilized in applications ranging from biosensors to targeting of gene therapy. One promising application for avidin–biotin is a cancer therapy method called pretargeting radioimmunotherapy.²⁵ In addition to avidin isolated from chicken eggs, there are improved genetically modified versions of avidin available. For example, so called chimeric avidin has been found thermostable, resistant for proteolysis, and suitable for biofunctionalization of various materials, while retaining high affinity ligand binding.²⁶ Chimeric avidin remains stable during long periods of storage and provides cost-effective manufacturing of biochips and biosensors. Another example of engineered avidins is switchavidin, which can be removed from biotinylated surfaces with mild treatment, enabling re-use of the biotinylated device.²⁷ Because of four biotin-binding sites per avidin, this protein–ligand pair used as a signal-amplifier to sandwich molecules responsible for specific binding and detection.

Binding between biotin and avidin is very tight, and several studies have demonstrated that usually sufficient conditions for protein denaturation are failing to weaken the

binding between avidin and biotin complexes.²⁸ It is also possible to independently control individual binding sites and alter their affinity for the ligands.²⁹ Once the avidin–biotin complex is formed, it is unaffected by wide extremes of pH (between 2 and 13), high temperature (melting point around 120°C), organic solvents, or other denaturing agents. Avidin retains its ability to bind to biotin at room temperature (RT) in the presence of common surfactant such as SDS, SDBS, and Triton X-100. This protein–ligand pair has proved ideal for immobilization of single-stranded DNA (ssDNA) or double-stranded DNA (dsDNA). Figure 1 shows a schematic diagram of avidin immobilization on biotinylated fibers and their blocking with free biotin.

In the present investigation, we successfully synthesized biotinylated bovine serum albumin (BSA) embedded PLA-PEG as blend fiber membrane. These blend fiber membranes were able to immobilize chimeric avidin. In contrast, excess of free biotin blocked the binding sites of avidin and prevented binding to fibers, confirming the specificity of the interaction. Furthermore, fibers produced without biotinylated BSA showed no binding of avidin. We also used enzymatic assay to demonstrate the accessibility of the biotin groups on the nanofibers for suitable attachment of streptavidin-functionalized alkaline phosphatase enzyme.

MATERIALS AND METHODS

All chemicals are of analytical grade and used without prior treatment. PLA 6202 was provided by Prof. Endres, Institute for Bioplastics and Biocomposites (IFBB) Hannover, Germany. Biotinamidohehexanoyl-6-aminohexanoic acid N-hydroxysuccinimide ester (Biotin-X-X-NHS) and BSA were obtained from Sigma-Aldrich. PEG 1500 was purchased from abcr, and chloroform (CLF) 99.8% (UV/IR-Grade) from Roth. Deionized water was used throughout the process.

Chemical coupling of biotinylated BSA

Biotinylated BSA was produced by chemically coupling biotin on the amino groups of BSA. To prepare this, 2.95 g of BSA was dissolved in 28.5 mL of 50 mM sodium phosphate buffer containing 100 mM NaCl (pH 7). In the separate flask, 25 mg of biotin-X-X-NHS was dissolved in 1 mL of DMF. The biotin-X-X-NHS solution was directly added to the BSA solution. The mixture was incubated 1 h at RT on a shaker. Biotinylated BSA was then dialyzed against 50 mM sodium phosphate, 100 mM NaCl (pH 7) o/n and stored $-20^{\circ}C$ in aliquots.

Synthesis of PLA, PLA-PEG, and biotinylated PLA-PEG nanofibers

Three homogeneous electrospinning solution sets were prepared, in one set, 8 wt % PLA are dissolved in chloroform ($CHCl_3$) solvent and stirred for 10 h to obtain (a uniform) viscous solution. Chloroform was chosen as solvent because it improves the dispersion of biotinylated BSA.³⁰ In the second set, PEG (1:1 wt %) added to the prepared PLA solution. The addition of PEG was mainly to decrease the hydrophobicity and increase the stability and flexibility of the fibers.²³ And in the third set, biotinylated BSA (0.01 wt %) was slowly dispersed to the prepared PLA-PEG blend solution and ultrasonicated (Bandelin Electronic) for 10 min

TABLE I. Summary of Electrospinning Conditions

Sample	Concentration [wt %]	Flow rate [mL h ⁻¹]	Voltage [kV]	Height [cm]	Mean diameter [μm]
PLA	8	1	12	13	5.98 ± 0.33
PLA-PEG	8-8	1	12	15	1.92 ± 0.30
Biotinylated PLA-PEG	8-8-0.01	1	18	13	1.32 ± 0.49

in 1 min interval to get a clear dispersion. All the three sets of sample, that is, ⁽¹⁾ 8 wt % PLA, ⁽²⁾ 8-8 wt % PLA-PEG blend, and ⁽³⁾ 8-8-0.01 wt % PLA-PEG-biotinylated BSA blend (referred later as "biotinylated PLA-PEG") was separately filled in a 5 mL plastic syringe equipped with a blunt end stainless steel needle having a size of 0.80 × 22 mm² (21 × 7/8 G"). During electrospinning at RT, a positive high voltage was maintained between needle (as a positive terminal) and stainless steel flat surface covered with aluminum foil (as negative terminal). Under this applied electrostatic field, the polymeric hemi-sphere droplet surface gets elongated to form a "Taylor cone" and when it reaches the critical point, the repulsive force overcomes the surface tension of the polymeric solution. Hence, the charged jet was emitted to from the end of Taylor cone and converted into a web of fibrous material which is collected on the grounded substrate.³¹ This electrospun membrane was then peeled off from the collector and kept for drying at RT to remove the residual solvent. Table I shows the parameters used for the electrospinning experiment.

MATERIAL CHARACTERIZATION

Scanning electron microscopy (SEM)

The surface morphology and diameter of the prepared fibers were observed by scanning electron microscope (SEM) Zeiss Leo VP 1455. Three samples were prepared; (1) PLA fibrous membrane, (2) PLA-PEG blend fibrous membrane, and (3) biotinylated PLA-PEG fibrous membrane. A thin layer of gold/platinum was sputtered before taking SEM image to make the fiber conductive. The mean fiber diameters were analysed using digimizer software (Digimizer, version 4.5), with an error bar (standard deviation).

Determination of the availability of the biotin using fluorescence microscopy

For fluorescent microscopy, individual PLA-PEG blend fibers and PLA-PEG blend fibers containing biotinylated BSA were used to detect the biotin molecules on the fiber surface. This blend fiber membranes were shred into pieces by using tweezers and immersed into 0.05% PBS-Tween (pH 7.4). First, the samples were incubated for 30 min in 0.5% BSA in PBS-Tween to minimize non-specific binding. For fluorescent staining, the samples were incubated for 120 min in 150 nM of neutralized chimeric avidin²⁶ labeled with amino-reactive AlexaFluor-488 (Life Technologies). For negative samples, 150 μM biotin was added to the avidin solution 10 min before the sample incubation. All samples were washed three times (5 min + 30 min + 30 min) with PBS-

Tween and mounted between coverslips by using Prolong Gold mounting media (Life Technologies).

Stained samples were imaged by using Zeiss LSM780 laser scanning confocal microscope equipped with 63x/NA 1.4 oil immersion objective. For each field, a Z-stack of 50 μm was imaged at 2 μm intervals. The imaged field size was 224 μm × 224 μm. Bright field image was captured by using a transmitted light PMT detector. All imaging parameters were kept constant for all samples.

Demonstration of enzymatic assay on biotinylated nanofibers

To demonstrate the suitability of the biotinylated fibers for enzymatic assays, streptavidin-alkaline phosphatase was used as a probe. For this, three different fiber membranes of a 0.5 mg piece (app. 3 mm × 3 mm) were cut: (1) PLA fibers, (2) PLA-PEG blends fibers, and (3) biotinylated PLA-PEG blend fibers. All the samples were analyzed in duplicate.

For convenient sample handling, the protocol was performed in 96-well microplate. The samples were first immersed in PBS (10 mM phosphate buffer; 140 mM NaCl, 2.7 mM KCl pH 7.4) containing 1 mg/mL BSA for 1 h and then washed three times with PBS. Streptavidin-alkaline phosphatase (SA-AP) solution were prepared by diluting SA-AP (Roche prod. no. 11 093 266 910) 1:3000 in PBS containing 0.1 mg/mL BSA. The negative control solution was prepared by including 17 μg/mL biotin (Sigma B-4501) to the diluted SA-AP, followed by 1 h incubation. The SA-AP solutions were applied on the fiber membrane samples for 1 h, followed by three washes with PBS. After moving the samples to new microwells, the samples were again washed three times with PBS. A substrate solution for AP was applied to the samples. After 30 min incubation, the substrate solution was transferred to empty wells and the absorbance was measured at 405 nm. All the measurements were performed at RT. A substrate solution in empty microwell was used as a reference sample.

RESULTS

Fiber morphology studies by scanning electron microscopy (SEM)

SEM image shows that prepared fibers were randomly orientated, porous, beadles, smooth, and interconnected. Figure 2(a) revealed that electrospun PLA fiber membrane was porous and cylindrical,³² this could happen because of rapid evaporation of solvent (CHCl₃) during electrospinning. The mean diameter of the fibers was 5.9 ± 0.3 μm. Figure 2(b) shows PLA-PEG blend fibers with diameter 1.9 ± 0.3 μm.

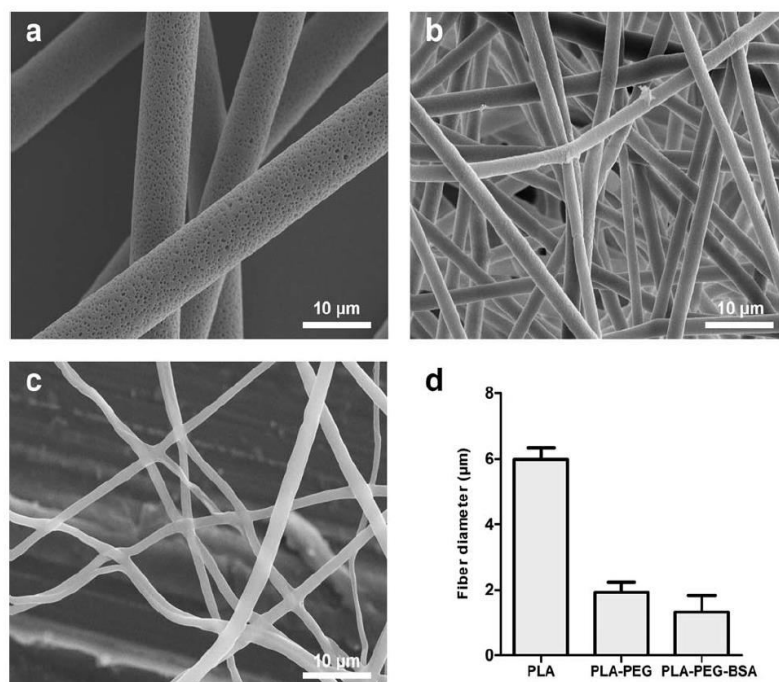


FIGURE 2. Scanning electron micrographs for electrospun (a) PLA fibers, (b) PLA-PEG blend fibers, (c) Biotinylated PLA-PEG blend fibers, and (d) and their average diameter distribution.

Figure 2(c) shows biotinylated BSA dispersed PLA-PEG blend fibers which reveal that the fibers were still cylindrical and smooth with a mean diameter $1.3 \pm 0.4 \mu\text{m}$. We observed that the addition of biotin-BSA to the spinning dope did not affect the final morphology Fig. 2(d) shows mean fiber diameter for various mixtures used.

Enzymatic detection of the biotin

As biotinylated BSA molecules were distributed throughout the fiber surface, enzymatic assays were performed to demonstrate the biotin availability at the surface of fibers. The method consisted of adding 0.5 mg (app. 3 mm x 3 mm) fiber membrane into a streptavidin-alkaline phosphatase (SA-AP) solution. Binding of the enzyme was detected by measuring the immobilized enzymatic activity with the chromogenic substrate at 405 nm. When a fiber membrane containing biotin was added to the SA-AP solution, clear enzymatic activity was observed because of fiber-immobilized enzymes. We also observed that no SA-AP immobilization on PLA and PLA-PEG fibers took place. This confirms that the presence of biotin at the fiber surface caused the immobilization of the enzyme.

Wettability is one of the important parameter which influenced the enzymatic assays¹³, therefore we had incorporated PEG to PLA, which makes SA-AP solution easier to penetrate. This (incorporation of PEG to PLA) also increased the surface area of the membrane from 2.1 to 5.0 m²/g (Table II) which improved the accessible surface area and

possibly also enhanced migration of the biotin to the fiber surface.

Fibers for avidin immobilization

The biotinylated BSA incorporated PLA-PEG blends fibers were conjugated with neutralized chimeric avidin using a simple single-step binding assay. Two sets of experiments were performed. In the first set, PLA-PEG blend fibers were cut and incubated with 150 nM AlexaFluor-488 labeled neutralized chimeric avidin for 120 min at RT. In the second step avidin-biotin interaction was blocked with excess of free biotin. The same experiment was also performed for biotinylated PLA-PEG blend fibers.

Our result shows immobilization of chimeric avidin on biotinylated PLA-PEG blend fibers via adsorption onto the fiber surface membrane. In contrast, no immobilization of avidin molecules on PLA-PEG fibers were observed. This was expected because PLA-PEG fibrous membrane does not contain biotin. These results shed promise for the use of the material for biosensor applications. This is also studied by Frey et al.^{30,33} and Lu et al.³⁴

TABLE II. The BET Surface Area of PLA and PLA-PEG Blend Fibrous Membrane

Sample	Surface area of the fiber (m ² /g)
PLA	2.1
PLA-PEG	5.0

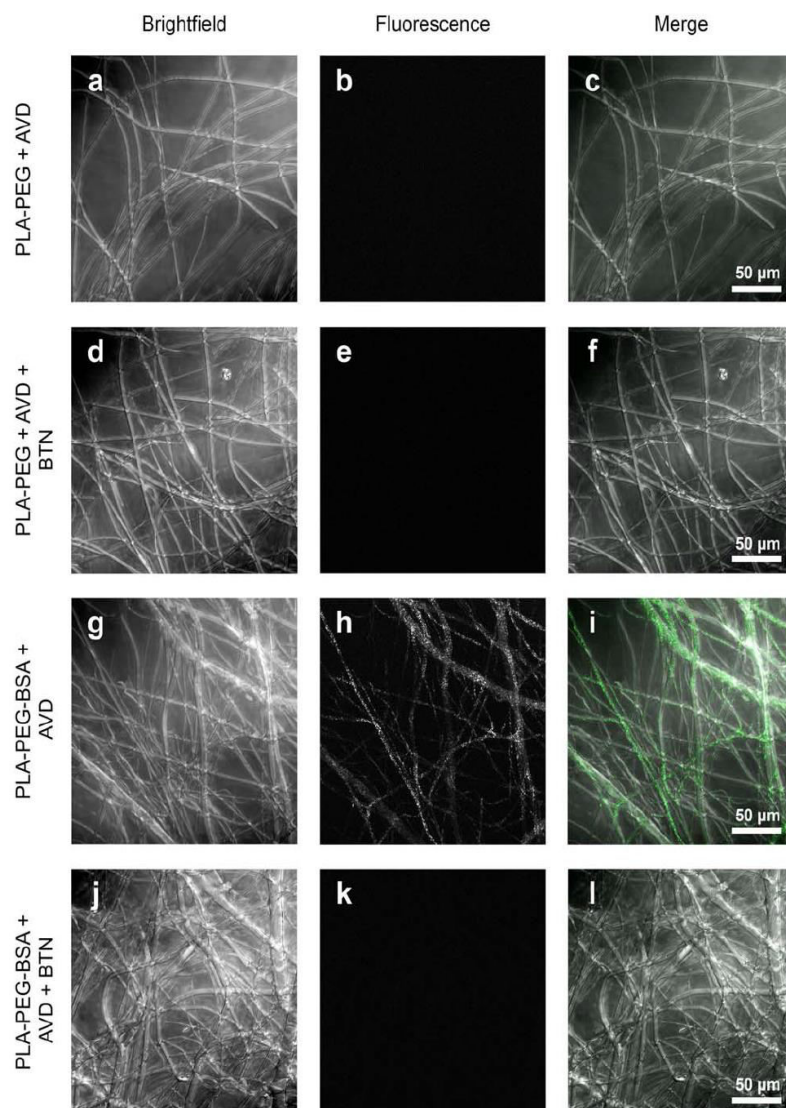


FIGURE 3. (a) Shows a fluorescent confocal microscopy image of the PLA-PEG fibers. (b) The same fibers were immersed in fluorescently labelled avidin solution and fluorescence at 488 nm was measured. (c) PLA-PEG fibers merged with fluorescently labelled avidin, which clearly indicate no immobilization of avidin on the PLA-PEG fibers because the biotin binding sites in avidin were not present. (d–f) The non avidin immobilized PLA-PEG fibers were treated with excess of biotin. There were no blocking occurred because of unavailability of avidin molecules. (g–l) The same analysis as in (a–f) was conducted for PLA-PEG fibers containing biotinylated BSA, which clearly indicate immobilization of avidin on fibers. (j–l) indicates the same analysis, where the immobilized avidins are blocked with excess of free biotin.

After immobilization of avidin molecules on fiber surface [Fig. 3(i)], the binding specificity was proven by blocking the binding by preincubation of avidin in the presence of excess of free biotin [Fig. 3(l)]. Figure 4 shows histogram analysis of the samples, including biotin binding. From this we could conclude that avidin molecules were only immobilized on biotinylated PLA-PEG fibrous membrane and no immobilization on PLA-PEG fibrous membrane was observed.

DISCUSSION

Electrospun fibers have unique properties, such as high aspect ratio, high surface area, high porosity, and outstanding properties,³⁵ which make them suitable material for designing biosensors. We observed a significant decrease in fiber diameter when PEG copolymer was added to PLA solution. This was expected because PEG works as a plasticizer which create points of attraction with the polymer chains and leave an unattached portion. Indeed, this

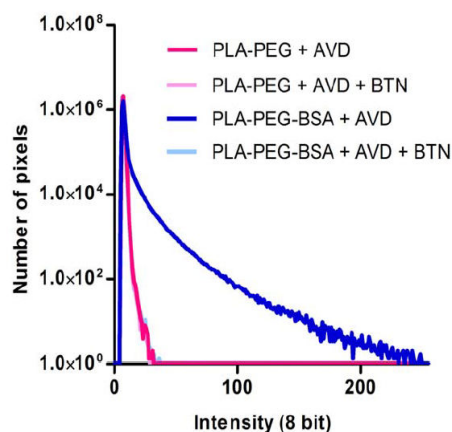


FIGURE 4. Fluorescence histogram analysis of avidin immobilization on biotinylated PLA-PEG blend fiber (dark blue). Biotinylated PLA-PEG blend fibers treated with avidin blocked with excess of free biotin (biotin-blocked negative control; light blue). PLA-PEG blend fibers show no binding (negative control; red). PLA-PEG blend fibers without biotin functionalization treated with biotin-blocked avidin studied as a comparison (pink).

increase in free volume of the system by augmenting the space between polymer chains in spreading them apart.¹² It is considered that the addition of the flexible PEG chains decrease the solution electrical conductivity, viscosity, and surface tension of the spinning solution, results in a decreased fiber diameter.³⁶

We also found that the biotinylated electrospun PLA-PEG fibers could be functionalized with neutralized chimeric avidin (also called as nChiAvid) and this can be blocked by treating with an excess of free biotin. Functionalization via genetically engineered avidins leads to new and improved properties when compared to conventional micro or nanofibers. The observed phase separation of biotin-BSA toward the fiber surface membrane were happened most probably because of applied electric voltage during fiber formation process³³ and also because of lack of entropy during polymer mixing,³⁷ which results in more biotin at the surface of fiber membrane. The resulting fibrous membrane shows fast immobilization of avidin molecules, which open the door for paper-based biosensors.^{38–40} Recently, avidin enabling release from biotinylated materials has been described, offering a potential way to develop regenerable biosensors.^{27,41,42}

In conclusion, biotinylated BSA surface functionalized PLA-PEG blend fibers were successfully prepared by electrospinning technique. PLA fibers showed porous, beadless and interconnected structure. PLA-PEG blend fibers showed a decreased fiber diameter with smooth morphology. Biotinylated PLA-PEG blend fibers also showed uniform morphology. In addition, biotinylated BSA at the fiber surface was used to couple fluorescent avidin molecules. This biotin-avidin binding on fiber surface could be blocked by excess of free biotin. This functional hydrophilic fiber shows potential application for biosensor applications.

ACKNOWLEDGMENTS

The authors gratefully thank Dr. Jenni Leppiniemi for preparation of biotinylated BSA. Folke Dencker is acknowledged for his support with the scanning electron microscopy (SEM) and Marc Krey for Brunauer Emmett Teller (BET) analysis. The work was supported by grants from Hannover School for Nanotechnology, Germany and from Academy of Finland.

REFERENCES

- Greiner A, Wendorff JH. Electrospinning: A fascinating method for the preparation of ultrathin fibers. *Angew Chemie Int Ed* 2007; 46:5670–5703.
- Reneker DH, Yarin AL. Electrospinning jets and polymer nanofibers. *Polymer* 2008;49:2387–2425.
- Agarwal S, Greiner A, Wendorff JH. Functional materials by electrospinning of polymers. *Prog Polym Sci* 2013;38:963–991.
- Subbiah T, Bhat GS, Tock RW, Parameswaran S, Ramkumar SS. Electrospinning of nanofibers. *J Appl Polym Sci* 2005;96:557–569.
- Li D, Xia Y. Electrospinning of nanofibers: Reinventing the wheel?. *Adv Mater* 2004;16:1151–1170.
- Valizadeh A, Mussa Farkhani S. Electrospinning and electrospun nanofibers. *IET Nanobiotechnol* 2014;8:83–92.
- Senthilram T, Mary LA, Venugopal JR, Nagarajan L, Ramakrishna S, Dev VRG. Self crimped and aligned fibers. *Mater Today* 2011; 14:226–229.
- Ramaseshan R, Ganesh VK. *Polymer Nanofibers for Biosensor Applications*. Springer; 2007.377392.
- Yoo HS, Kim TG, Park TG. Surface-functionalized electrospun nanofibers for tissue engineering and drug delivery. *Adv Drug Deliv Rev* 2009;61:1033–1042.
- Fang J, Niu H, Lin T, Wang X. Applications of electrospun nanofibers. *Chin Sci Bull* 2008;53:2265–2286.
- Fang J, Wang X, Lin T. Functional Applications of Electrospun Nanofibers. *Nanofibers Prod Prop Funct Appl* 2011;287–326.
- Ramakrishna S, Fujihara K, Teo WE, Yong T, Ma Z, Ramaseshan R. Electrospun nanofibers: Solving global issues. *Mater Today* 2006;9:40–50.
- Menzies KL, Jones L. The impact of contact angle on the biocompatibility of biomaterials. *Optom Vis Sci* 2010;87:387–399.
- Kim TG, Park TG. Surface functionalized electrospun biodegradable nanofibers for immobilization of bioactive molecules. *Bio-technol Prog* 2006;22:1108–1113.
- Laitinen OH, Hytönen VP, Nordlund HR, Kulomaa MS. Genetically engineered avidins and streptavidins. *Cell Mol Life Sci* 2006;63: 2992–3017.
- Jamshidian M, Tehrani EA, Imran M, Jacquot M, Desobry S. Poly-Lactic Acid: Production, applications, nanocomposites, and release studies. *Compr Rev Food Sci Food Saf* 2010;9:552–571.
- Ikada Y, Tsuji H. Biodegradable polyesters for medical and ecological applications. *Macromol Rapid Commun* 2000;21:117–132.
- Gupta B, Revagade N, Hilborn J. Poly(lactic acid) fiber: An overview. *Prog Polym Sci* 2007;32:455–482.
- Li L, Ding S, Zhou C. Preparation and degradation of PLA/Chitosan composite materials. *J Appl Polym Sci* 2004;91:274–277.
- Wei Q. *Functional Nanofibers and their Applications*. Woodhead Publishing Limited; 2012. 92p.
- Toncheva A, Mincheva R, Kancheva M, Manolova N, Rashkov I, Dubois P, Markova N. Antibacterial PLA/PEG electrospun fibers: Comparative study between grafting and blending PEG. *Eur Polym J* 2016;75:223–233.
- Sheth M, Kumar RA, Dave V, Gross AR, McCarthy PS. Biodegradable Polymer Blends of Poly (lactic acid) and Poly (ethylene glycol). *J Appl Polym Sci* 1996;66:1495–1505.
- Javadian M, Rostamizadeh K, Danafar H. Preparation and characterization of electrospinning PEG-PLA nanofibers for sustained release of tamoxifen. *Pharm Sci* 2012;7:S235.
- González E, Shepherd LM, Saunders L, Frey MW. Surface Functional Poly (lactic Acid) Electrospun Nanofibers for Biosensor Applications. *Materials* 2016;9:47.

25. Walter RB, Press OW, Pagel JM. Pretargeted radioimmunotherapy for hematologic and other malignancies. *Cancer Biother Radiopharm* 2010;25:125–142.
26. Määttä JAE, Eisenberg-Domovich Y, Nordlund HR, Hayouka R, Kulomaa MS, Livnah O, Hytönen VP. Chimeric avidin shows stability against harsh chemical conditions-biochemical analysis and 3D structure. *Biotechnol Bioeng* 2011;108:481–490.
27. Pollheimer P, Taskinen B, Scherfler A, Gusenkov S, Creus M, Wiesauer P, Zauner D, Schöfberger W, Schwarzinger C, Ebner A, Tampé R, Stutz H, Hytönen VP, Gruber HJ. Reversible biofunctionalization of surfaces with a switchable mutant of avidin. *Bioconjug Chem* 2013;24:1656–1668.
28. Morag E, Bayer EA, Wilchek M. Reversibility of biotin-binding by selective modification of tyrosine in avidin. *Biochem J* 1996;316:193–199.
29. Leppiniemi J, Määttä JAE, Hammaren H, Soikkeli M, Laitaoja M, Jänis J, Kulomaa MS, Hytönen VP. Bifunctional avidin with covalently modifiable ligand binding site. *PLoS One* 2011;6:e16576.
30. Li D, Frey MW, Bäumner AJ. Electrospun polylactic acid nanofiber membranes as substrates for biosensor assemblies. *J Membr Sci* 2006;279:354–363.
31. Wang H-S, Fu G-D, Li X-S. Functional polymeric nanofibers from electrospinning. *Recent Pat Nanotechnol* 2009;3:21–31.
32. Wagner A, Poursorkhabi V, Mohanty AK, Misra M. Analysis of Porous Electrospun Fibers from Poly(L-lactic acid)/Poly(3-hydroxybutyrate-co-3-hydroxyvalerate) Blends. *ACS Sustain Chem Eng* 2014;2:1976–1982.
33. Li D, Frey MW, Vynias D, Bäumner AJ. Availability of biotin incorporated in electrospun PLA fibers for streptavidin binding. *Polymer* 2007;48:6340–6347.
34. Lu T, Chen X, Shi Q, Wang Y, Zhang P, Jing X. The immobilization of proteins on biodegradable fibers via biotin-streptavidin bridges. *Acta Biomater* 2008;4:1770–1777.
35. Tsou P-H, Chou C-K, Saldana SM, Hung M-C, Kameoka J. The fabrication and testing of electrospun silica nanofiber membranes for the detection of proteins. *Nanotechnology* 2008;19:445714.
36. Buttaro LM, Druvva E, Frey MW. Phase separation to create hydrophilic yet non-water soluble PLA/PLA-b-PEG fibers via electrospinning. *J Appl Polym Sci* 2014;131:7.
37. Reddy MR, Erion MD. Free Energy Calculations in Rational Drug Design; 2001;384. Available from: <http://www.lavoisier.fr/notice/frMWOLXXAKXWO2O.html>
38. Grant BD, Smith CA, Karvonen K, Richards-Kortum R. Highly sensitive two-dimensional paper network incorporating biotin-streptavidin for the detection of malaria. *Anal Chem* 2016;88:2553–2557.
39. Reinholt SJ, Sonnenfeldt a, Naik a, Frey MW, Bäumner a. J. Developing new materials for paper-based diagnostics using electrospun nanofibers. *Anal Bioanal Chem* 2013;406:3297–3304.
40. Dupont-Filliard A, Billon M, Livache T, Guillerez S. Biotin/avidin system for the generation of fully renewable DNA sensor based on biotinylated polypyrrole film. *Anal Chim Acta* 2004;515:271–277.
41. Taskinen B, Zauner D, Lehtonen SI, Koskinen M, Thomson C, Kähkönen N, Kukkurainen S, Määttä JAE, Ihalainen TO, Kulomaa MS, Gruber HJ, Hytönen VP. Switchavidin: Reversible biotin-avidin-biotin bridges with high affinity and specificity. *Bioconjug Chem* 2014;25:2233–2243.
42. Zauner D, Taskinen B, Eichinger D, Flattinger C, Ruttman B, Knoglinger C, Traxler L, Ebner A, Gruber HJ, Hytönen VP. Regenerative biosensor chips based on switchable mutants of avidin-A systematic study. *Sens Actuators B Chem* 2016;229:646–654.

12 Conclusions

Electrospinning (ESP) has become a popular polymer processing technique to produce functional nano-bio-fibers for many biomedical applications (e.g., drug delivery, antibacterial, and biosensors). Uniquely tunable qualities such as high surface to volume ratio, degradability, and porosity is the major advantage of electrospun nano-bio-fibers, which greatly enhances their response rate, selectivity and sensitivity.

This thesis addresses several structural and functional features of polylactic acid (PLA) and its composite fibrous membrane. For the first objective, PLA fibers were obtained using a single solvent (DCM, TCM, or THF). By varying ESP parameters, PLA fibers of different diameters and surface porosities were produced. The degree of crystallinity of PLA fibers were compared with the native PLA pellets. PLA was blended with Polyethylene glycol (PEG) and magnetic nanoparticles (MNPs) and was converted into fibers. PLA-PEG-MNPs nanocomposite fibrous membranes showed proportionally reduced saturation magnetization compared to pure magnetic nanoparticles and therefore promise the possibility for temperature effects, such as hyperthermia treatment.

For the second objective, PLA was blended with PEG and N-Vinylcaprolactam (NVCL). This blend solution was converted to fibers. Tetracycline hydrochloride (TCH) was embedded into these composite fibrous membranes, and the antibacterial activity was proved. Further, MNPs were embedded into these composite fibrous membranes. These composite membranes (PLA-PEG-NVCL-MNPs) showed on-demand drug release under switch on-off condition of magnetic field.

For the third objective, the smart thin-film and fibrous membranes were developed using PLA and Hydroxypropylcellulose (HPC) and were used for on-demand drug delivery under temperature stimuli. A switch on-off behavior of drug release was established. These smart membranes allow a local chemotherapy without causing other collateral damage to the patient's body. Hence, the developed system will offer significant advantages in contrast to conventional delivery systems, in terms of increased efficiency in drug delivery applications. Due to decreased drug concentration throughout the body (local application with the use of the nanofibers), many drugs where the therapeutic dosage is above the toxic level for the human body may now find its application. In general side-effects of drugs will be significantly reduced.

For the fourth objective, biotinylated bovine serum albumin was embedded into PLA-PEG fibers, these enabled specific immobilization of fluorescently labelled avidin. An alkaline phosphatase enzyme was immobilized via biotin-streptavidin interaction on the hybrid nanofibers, demonstrating the suitability of the material for biosensing applications.

There are still plenty of challenges which need to be addressed. The stimuli may differ from one patient condition to another, providing difficulty in benchmarking, reproducibility and potential cytotoxicity in vivo is also not fully understood. Extensive research and developments are still needed in order to make a bond between materials and biological environment, so that clinical applications could be done.

It is firmly believed that, with sustained effort and enough time from the scientific and engineering community, electrospun functional nano-bio-fibers will become one of the most promising tools for fabricating high performance advanced materials with a broad range of functionalities and applications in multidisciplinary areas of biomedicine in the near future.

Literature Cited

- [1] I. Vikholm-Lundin *et al.*, “Cysteine-tagged chimeric avidin forms high binding capacity layers directly on gold,” *Sensors Actuators, B Chem.*, vol. 171–172, pp. 440–448, 2012.
- [2] N. M. Neves, *Electrospinning for Advanced Biomedical Applications and Therapies*. Smithers Rapra Technology Ltd, 2012.
- [3] V. Labhasetwar and D. L. Leslie-Pelecky, *Biomedical Applications of Nanotechnology*. John Wiley & Sons, Inc., 2007.
- [4] N. H. Malsch, *Biomedical Nanotechnology*. Taylor & Francis Group, 2005.
- [5] C. S. R. Kumar, “Nanodevice for the lifescience.” Wiley-VCH Verlag GmbH & Co. KGaA, p. 240, 2006.
- [6] J. B.-H. Tok, *Nano and Microsensors for Chemical and Biological Terrorism Surveillance*. Royal Society of Chemistry, 2008.
- [7] A. Tiwari and A. Tiwari, *Nanomaterials in Drug Delivery, Imaging, and Tissue Engineering*. Scrivener Publishing, 2013.
- [8] E. Jabbari and A. Khademhosseini, *Biologically-responsive Hybrid Biomaterials*. World Scientific Publishing Co. Pte. Ltd., Singapore, 2010.
- [9] M. Valizadeh, S. A. H. Ravandi, and S. Ramakrishna, “Recent advances in electrospinning of some selected biopolymers,” *J. Text. Polym.*, vol. 1, no. 2, pp. 70–84, 2013.
- [10] A. S. Hoffman and P. S. Stayton, “Bioconjugates of smart polymers and proteins: Synthesis and applications,” in *Macromolecular Symposia*, 2004, vol. 207, pp. 139–151.
- [11] X. Hu, S. Liu, G. Zhou, Y. Huang, Z. Xie, and X. Jing, “Electrospinning of polymeric nanofibers for drug delivery applications,” *Journal of Controlled Release*, vol. 185, no. 1, pp. 12–21, 2014.
- [12] J. K. Chen and C. J. Chang, “Fabrications and applications of stimulus-responsive polymer films and patterns on surfaces: A review,” *Materials*, vol. 7, no. 2, pp. 805–875, 2014.
- [13] R. Lehner, X. Wang, M. Wolf, and P. Hunziker, “Designing switchable nanosystems for medical application,” *Journal of Controlled Release*, vol. 161, no. 2, pp. 307–316, 2012.
- [14] Y. Li, H. Dong, K. Wang, D. Shi, X. Zhang, and R. Zhuo, “Stimulus-responsive polymeric nanoparticles for biomedical applications,” *Sci. China Chem.*, vol. 53, no. 3, pp. 447–457, 2010.
- [15] P. K. Deshmukh *et al.*, “Stimuli-sensitive layer-by-layer (LbL) self-assembly systems: Targeting and biosensory applications,” *Journal of Controlled Release*, vol. 166, no. 3, pp. 294–306, 2013.
- [16] A. Kikuchi and T. Okano, “Intelligent thermoresponsive polymeric stationary phases for aqueous chromatography of biological compounds,” *Progress in Polymer Science (Oxford)*, vol. 27, no. 6, pp. 1165–1193, 2002.
- [17] T. Ware, D. Simon, R. L. Rennaker, and W. Voit, “Smart Polymers for Neural Interfaces,” *Polym. Rev.*, vol. 53, no. 1, pp. 108–129, 2013.
- [18] K. L. Hamner, C. M. Alexander, K. Coopersmith, D. Reishofer, C. Provenza, and M. M. Maye, “Using temperature-sensitive smart polymers to regulate DNA-mediated nanoassembly and encoded nanocarrier drug release,” *ACS Nano*, vol. 7, no. 8, pp. 7011–7020, 2013.
- [19] Y. Qiu and K. Park, “Environment-sensitive hydrogels for drug delivery,”

- Advanced Drug Delivery Reviews*, vol. 64, no. SUPPL. pp. 49–60, 2012.
- [20] N. Islam and K. Miyazaki, “An empirical analysis of nanotechnology research domains,” *Technovation*, vol. 30, no. 4, pp. 229–237, 2010.
- [21] A. N. Nakagaito and H. Yano, “Novel high-strength biocomposites based on microfibrillated cellulose having nano-order-unit web-like network structure,” *Appl. Phys. A Mater. Sci. Process.*, vol. 80, no. 1, pp. 155–159, 2005.
- [22] N. Reddy and Y. Yang, “Biofibers from agricultural byproducts for industrial applications,” *Trends Biotechnol.*, vol. 23, no. 1, pp. 22–27, 2005.
- [23] A. Iwatake, M. Nogi, and H. Yano, “Cellulose nanofiber-reinforced polylactic acid,” *Compos. Sci. Technol.*, vol. 68, no. 9, pp. 2103–2106, 2008.
- [24] A. Bhatnagar and M. Sain, “Processing of Cellulose Nanofiber-reinforced Composites,” *J. Reinf. Plast. Compos.*, vol. 24, no. 12, pp. 1259–1268, 2005.
- [25] I. Siro and D. Plackett, “Microfibrillated cellulose and new nanocomposite materials: A review,” *Cellulose*, vol. 17, no. 3, pp. 459–494, 2010.
- [26] D. Li and Y. Xia, “Electrospinning of nanofibers: Reinventing the wheel?,” *Adv. Mater.*, vol. 16, no. 14, pp. 1151–1170, 2004.
- [27] D. H. Reneker and I. Chun, “Nanometre diameter fibres of polymer, produced by electrospinning,” *Nanotechnology*, vol. 7, no. 3, pp. 216–223, 1996.
- [28] W. E. Teo and S. Ramakrishna, “A review on electrospinning design and nanofibre assemblies,” *Nanotechnology*, vol. 17, no. 14, pp. R89–R106, 2006.
- [29] S. Ramakrishna, K. Fujihara, W. Teo, T. Lim, and Z. Ma., *An Introduction to Electrospinning and Nanofibers*. World Scientific Publishing Co. Pte. Ltd., Singapore, 2005.
- [30] A. Formhals, “Process and apparatus for preparing artificial threads,” 1934.
- [31] A. Formhals, “Method and apparatus for spinning,” *US Pat.*, vol. 2160962, 1939.
- [32] A. Formhals, “Artificial thread and method of producing same,” 1940.
- [33] A. Formhals, “Production of artificial fibers from fiber forming liquids,” 1943.
- [34] A. Formhals, “Method and apparatus for spinning,” 1944.
- [35] B. Vonnegut and R. L. Neubauer, “Production of monodisperse liquid particles by electrical atomization,” *J. Colloid Sci.*, vol. 7, no. 6, pp. 616–622, 1952.
- [36] V. G. Drozin, “The electrical dispersion of liquids as aerosols,” *J. Colloid Sci.*, vol. 10, no. 2, pp. 158–164, 1955.
- [37] S. G. F. R. S. Taylor, “Electrically driven jets,” *Proc. R. Soc. London*, vol. 313, pp. 453–475, 1969.
- [38] H. Simons, “Process and apparatus for producing patterned non-woven fabrics,” pp. 3, 280, 229, 1966.
- [39] P. K. Baumgarten, “Electrostatic spinning of acrylic microfibers,” *J. Colloid Interface Sci.*, vol. 36, no. 1, pp. 71–79, 1971.
- [40] J. J. Feng, “The stretching of an electrified non-Newtonian jet: A model for electrospinning,” *Phys. Fluids*, vol. 14, no. 11, pp. 3912–3926, 2002.
- [41] M. M. Hohman, M. Shin, G. Rutledge, and M. P. Brenner, “Electrospinning and electrically forced jets. I. stability theory,” *Phys. Fluids*, vol. 13, no. 8, pp. 2221–2236, 2001.
- [42] C. J. Thompson, G. G. Chase, A. L. Yarin, and D. H. Reneker, “Effects of parameters on nanofiber diameter determined from electrospinning model,” *Polymer (Guildf.)*, vol. 48, no. 23, pp. 6913–6922, 2007.
- [43] J. H. He, Y. Wu, and W. W. Zuo, “Critical length of straight jet in electrospinning,” *Polymer (Guildf.)*, vol. 46, no. 26, pp. 12637–12640, 2005.
- [44] D. Sun, C. Chang, S. Li, and L. Lin, “Near-field electrospinning,” *Nano Lett.*, vol.

- 6, no. 4, pp. 839–842, 2006.
- [45] D. H. Reneker, A. L. Yarin, H. Fong, and S. Koombhongse, “Bending instability of electrically charged liquid jets of polymer solutions in electrospinning,” *J. Appl. Phys.*, vol. 87, no. 9, pp. 4531–4547, 2000.
- [46] S. G. F. R. S. Taylor, “Disintegration of water drops in an electric field,” *Proc. R. Soc. London*, vol. 268, p. 527, 1962.
- [47] A. L. Andrady, *Science and Technology of Polymer Nanofibers*. A John Wiley & Sons, Inc., Publication, 2008.
- [48] D. H. Reneker and H. Fong, “Polymeric nanofibers: Introduction,” *A.C.S. Symp. Ser.*, vol. 918, pp. 1–6, 2006.
- [49] S. Y. Chew, Y. Wen, and Y. D. and K. W. Leong, “The Role of Electrospinning in the Emerging Field of Nanomedicine,” *Current Pharmaceutical Design*, vol. 12, no. 36, pp. 4751–4770, 2006.
- [50] S. Agarwal, J. H. Wendorff, and A. Greiner, “Use of electrospinning technique for biomedical applications,” *Polymer (Guildf.)*, vol. 49, no. 26, pp. 5603–5621, 2008.
- [51] A. L. Yarin, “Coaxial electrospinning and emulsion electrospinning of core-shell fibers,” *Polym. Adv. Technol.*, vol. 22, no. 3, pp. 310–317, 2011.
- [52] Z. Sun, E. Zussman, A. L. Yarin, J. H. Wendorff, and A. Greiner, “Compound Core-Shell Polymer Nanofibers by Co-Electrospinning,” *Adv. Mater.*, vol. 15, no. 22, pp. 1929–1932, 2003.
- [53] R. Khajavi and M. Abbasipour, “Electrospinning as a versatile method for fabricating coreshell, hollow and porous nanofibers,” *Sci. Iran.*, vol. 19, no. 6, pp. 2029–2034, Dec. 2012.
- [54] C. He, Z. Huang, X. Han, L. Liu, H. Zhang, and L. Chen, “Coaxial Electrospun Poly(L-Lactic Acid) Ultrafine Fibers for Sustained Drug Delivery,” *J. Macromol. Sci. Part B*, vol. 45, no. 4, pp. 515–524, 2006.
- [55] H. Kriel, R. D. Sanderson, and E. Smit, “Coaxial electrospinning of miscible PLLA-core and PDLLA-shell solutions and indirect visualisation of the core-shell fibres obtained,” *Fibres Text. East. Eur.*, vol. 91, no. 2, pp. 28–33, 2012.
- [56] Y. Dror *et al.*, “One-step production of polymeric microtubes by co-electrospinning,” *Small*, vol. 3, no. 6, pp. 1064–1073, 2007.
- [57] E. Biber, G. Gündüz, B. Mavis, and U. Colak, “Effects of electrospinning process parameters on nanofibers obtained from Nylon 6 and poly (ethylene-n-butyl acrylate-maleic anhydride) elastomer blends using Johnson SB statistical distribution function,” *Appl. Phys. A Mater. Sci. Process.*, vol. 99, no. 2, pp. 477–487, 2010.
- [58] J. Malašauskiene and R. Milašius, “Investigation and Estimation of Structure of Web from Electrospun Nanofibres,” *J. Nanomater.*, vol. 2013, 2013.
- [59] S. Koombhongse, W. Liu, and D. H. Reneker, “Flat Polymer Ribbons and Other Shapes by Electrospinning,” *J. Polym. Sci. Part B Polym. Phys.*, vol. 39, no. 1, pp. 2363–2377, 2001.
- [60] K. H. Lee, H. Y. Kim, H. J. Bang, Y. H. Jung, and S. G. Lee, “The change of bead morphology formed on electrospun polystyrene fibers,” *Polymer (Guildf.)*, vol. 44, no. 14, pp. 4029–4034, Jun. 2003.
- [61] M. Zafar *et al.*, “Potential of electrospun nanofibers for biomedical and dental applications,” *Materials (Basel)*, vol. 9, no. 2, pp. 1–21, 2016.
- [62] “<http://www.bccresearch.com/market-research/pharmaceuticals/advanced-drug-delivery-systems-tech-markets-report-phm006k.html>.
- [63] N. I. of B. I. and Bioengineering, “Drug Delivery Systems,” *Natl. Institutes Heal.*,

- no. July, pp. 1–2, 2013.
- [64] C. M. Agrawal, J. L. Ong, M. R. Appleford, and G. Mani, “Introduction to biomaterials,” *Cambridge Univ. Press*, 2014.
- [65] J. Zeng *et al.*, “Biodegradable electrospun fibers for drug delivery,” *J. Control. Release*, vol. 92, no. 3, pp. 227–231, 2003.
- [66] D. J. Brayden, “Controlled release technologies for drug delivery,” *Drug Discov. Today*, vol. 8, no. 21, pp. 976–978, 2003.
- [67] D. W. Grainger, “The Williams dictionary of biomaterials,” *Mater. Today*, vol. 2, no. 3, p. 29, 1999.
- [68] C. P. McCoy *et al.*, “Triggered drug delivery from biomaterials,” *Expert Opin. Drug Deliv.*, vol. 7, no. 5, pp. 605–616, 2010.
- [69] W. a Goddard, D. W. Brenner, S. E. Lyshevski, and G. J. Lafrate, *Handbook of Nanoscience, Engineering and Technology*. CRC Press, Taylor & Francis Group, 2007.
- [70] H. Wen and K. Park, *Oral controlled release formulation design and drug delivery: theory to practice*. John Wiley & Sons Hoboken, NJ., 2010.
- [71] Z. Xie and G. B. Diller, “Electrospun Poly(D,L-lactide) Fibers for Drug Delivery: The Influence of Cosolvent and the Mechanism of Drug Release,” *J. Appl. Polym. Sci.*, vol. 115, pp. 1–8, 2010.
- [72] J. Y. Park and I. H. Lee, “Controlled release of ketoprofen from electrospun porous polylactic acid (PLA) nanofibers,” *J. Polym. Res.*, vol. 18, no. 6, pp. 1287–1291, 2011.
- [73] C. Shasteen and Y. Bin Choy, “Controlling degradation rate of poly(lactic acid) for its biomedical applications,” *Biomed. Eng. Lett.*, vol. 1, no. 3, pp. 163–167, 2011.
- [74] J. Crank, *The mathematics of Diffusion*. Oxford University Press London, 1975.
- [75] Y. W. Chien, *Novel drug delivery systems*. CRC Press, Taylor & Francis Group, 1992.
- [76] R. W. Korsmeyer, R. Gurny, E. Doelker, P. Buri, and N. A. Peppas, “Mechanisms of solute release from porous hydrophilic polymers,” *Int. J. Pharm.*, vol. 15, no. 1, pp. 25–35, 1983.
- [77] P. L. Ritger and N. A. Peppas, “A simple equation for description of solute release II. Fickian and anomalous release from swellable devices,” *J. Control. Release*, vol. 5, no. 1, pp. 37–42, 1987.
- [78] A. Szentivanyi, T. Chakradeo, H. Zernetsch, and B. Glasmacher, “Electrospun cellular microenvironments: Understanding controlled release and scaffold structure,” *Adv. Drug Deliv. Rev.*, vol. 63, no. 4, pp. 209–220, 2011.
- [79] M. Brandl, G. Eide Flaten, and A. Bauer-Brandl, “Passive Diffusion Across Membranes,” *Wiley Encycl. Chem. Biol.*, pp. 1–10, 2008.
- [80] G. S. Banker and C. T. Rhodes, *Modern pharmaceuticals*, no. 121. 2002.
- [81] H. Tian, Z. Tang, X. Zhuang, X. Chen, and X. Jing, “Biodegradable synthetic polymers: Preparation, functionalization and biomedical application,” *Prog. Polym. Sci.*, vol. 37, no. 2, pp. 237–280, 2012.
- [82] I. Y. Galaev and B. Mattiasson, “Smart polymers and what they could do in biotechnology and medicine,” *Trends Biotechnol.*, vol. 17, pp. 335–340, 1999.
- [83] M. Chen, Y.-F. Li, and F. Besenbacher, “Electrospun Nanofibers-Mediated On-Demand Drug Release,” *Adv. Healthc. Mater.*, vol. 3, no. 11, pp. 1721–1732, 2014.
- [84] C. de Las Heras Alarcon, S. Pennadam, and C. Alexander, “Stimuli responsive polymers for biomedical applications,” *Chem. Soc. Rev.*, vol. 34, no. 3, pp. 276–

- 285, 2005.
- [85] B. Priya and Et Al., “Stimuli-responsive polymers and their applications in drug delivery,” vol. 4, p. 22001, 2009.
- [86] K. S. Soppimath, T. M. Aminabhavi, a. M. Dave, S. G. Kumbar, and W. E. Rudzinski, “Stimulus-Responsive ‘Smart’ Hydrogels as Novel Drug Delivery Systems,” *Drug Dev. Ind. Pharm.*, vol. 28, no. 8, pp. 957–974, 2002.
- [87] P. Guardia *et al.*, “Water-soluble iron oxide nanocubes with high values of specific absorption rate for cancer cell hyperthermia treatment,” *ACS Nano*, vol. 6, no. 4, pp. 3080–3091, 2012.
- [88] A. Gupta, R. S. Kane, and D. A. Borca-Tasciuc, “Local temperature measurement in the vicinity of electromagnetically heated magnetite and gold nanoparticles,” *J. Appl. Phys.*, vol. 108, no. 6, 2010.
- [89] D. Roy, W. L. Brooks, and B. S. Sumerlin, “New directions in thermoresponsive polymers,” *Chem Soc Rev*, vol. 42, no. 17, pp. 7214–7243, 2013.
- [90] A. Gandhi, A. Paul, S. O. Sen, and K. K. Sen, “Studies on thermoresponsive polymers: Phase behaviour, drug delivery and biomedical applications,” *Asian J. Pharm. Sci.*, vol. 10, no. 2, pp. 99–107, 2015.
- [91] M. Shibayama and T. Tanaka, “Volume phase transition and related phenomena of polymer gels,” *Adv. Polym. Sci.*, vol. 109, pp. 1–62, 1993.
- [92] T. Baltes, F. Garret-Flaudy, and R. Freitag, “Investigation of the LCST of polyacrylamides as a function of molecular parameters and the solvent composition,” *J. Polym. Sci. Part A Polym. Chem.*, vol. 37, no. 15, pp. 2977–2989, 1999.
- [93] T. Hellmuth, *Microscopy, in the Optics Encyclopedia*. Wiley-VCH Verlag GmbH & Co. KGaA, 2007.
- [94] R. G. Lieckfield, *Analytical Methods, in Patty’s Industrial Hygiene*. John Wiley & Sons, Inc., 2001.
- [95] G. Gauglitz, *Ultraviolet and Visible Spectroscopy, in Ullmann’s Encyclopedia of Industrial Chemistry*. Wiley-VCH Verlag GmbH & Co. KGaA, 2000.
- [96] J. Nicholson, *The Chemistry of Polymers. 3rd ed.* The Royal Society of Chemistry Publishing, 2006.
- [97] S. B. Warrington and G. W. H. Höhne, *Thermal Analysis and Calorimetry, in Ullmann’s Encyclopedia of Industrial Chemistry*. Wiley-VCH Verlag GmbH & Co. KGaA, 2000.
- [98] D. Garlotta, “A Literature Review of Poly (Lactic Acid),” *J. Polym. Environ.*, vol. 9, no. 2, pp. 63–84, 2002.
- [99] S. Sinha Ray, K. Yamada, M. Okamoto, and K. Ueda, “New polylactide-layered silicate nanocomposites. 2. Concurrent improvements of material properties, biodegradability and melt rheology,” *Polymer (Guildf)*, vol. 44, no. 3, pp. 857–866, 2002.
- [100] H. G. M. Edwards, *Spectroscopy, Raman, in The Optics Encyclopedia*. Wiley-VCH Verlag GmbH & Co. KGaA, 2007.
- [101] A. H. Kuptsov and G. N. Zhizhin, “Important advantages of Raman spectroscopy,” *Phys. Sci. Data, Elsevier*, pp. xii–xiv, 1998.
- [102] J. G. Vos, R. J. Forster, and T. E. Keyes, *Methods of Analysis, in Interfacial Supramolecular Assemblies*. John Wiley & Sons, Ltd., 2003.
- [103] H.-J. Endres and A. Siebert-Raths, *Engineering biopolymers: markets, manufacturing, properties, and applications*. Hanser Publications, 2011.
- [104] L. Avérous and E. Pollet, “Biodegradable Polymers,” *Green Energy Technol.*, vol.

- 50, 2012.
- [105] L. Avérous, "Biodegradable Multiphase Systems Based on Plasticized Starch: A Review," *J. Macromol. Sci. Part C Polym. Rev.*, vol. 44, no. 3, pp. 231–274, 2004.
- [106] R. Auras, B. Harte, and S. Selke, "An overview of polylactides as packaging materials," *Macromol. Biosci.*, vol. 4, no. 9, pp. 835–864, 2004.
- [107] L. S. Nair and C. T. Laurencin, "Biodegradable polymers as biomaterials," *Prog. Polym. Sci.*, vol. 32, no. 8–9, pp. 762–798, 2007.
- [108] A. J. Domb, J. Kost, and D. M. Wiseman, *Handbook of biodegradable polymers*. CRC Press, Taylor & Francis Group, 1997.
- [109] J. Lunt, "Large-scale production, properties and commercial applications of polylactic acid polymers," *Polym. Degrad. Stab.*, vol. 59, no. 1–3, pp. 145–152, 1998.
- [110] H. Korhonen, A. Helminen, and J. V. Seppälä, "Synthesis of polylactides in the presence of co-initiators with different numbers of hydroxyl groups," *Polymer (Guildf.)*, vol. 42, no. 18, pp. 7541–7549, 2001.
- [111] G. Schwach, J. Coudane, R. Engel, and M. Vert, "Zn lactate as initiator of DL-lactide ring opening polymerization and comparison with Sn octoate," *Polym. Bull.*, vol. 37, pp. 119–126, 1996.
- [112] P. Degée, P. Dubois, and R. Jérôme, "Bulk polymerization of lactides initiated by aluminum isopropoxide. I. Mechanism and kinetics," in *Macromolecular Symposia*, 1997, vol. 123, no. 1, pp. 67–84.
- [113] G. Schwach, J. Coudane, R. Engel, and M. Vert, "More about the polymerization of lactides in the presence of stannous octoate," *J. Polym. Sci. Part A Polym. Chem.*, vol. 35, no. 16, pp. 3431–3440, 1997.
- [114] M. Möller, R. Känge, and J. L. Hedrick, "Sn(OTf)₂ and Sc(OTf)₃: Efficient and versatile catalysts for the controlled polymerization of lactones," *J. Polym. Sci. Part A Polym. Chem.*, vol. 38, no. 11, pp. 2067–2074, 2000.
- [115] H. R. Kricheldorf, I. Kreiser-Saunders, and C. Boettcher, "Polylactones: 31. Sn(II)octoate-initiated polymerization of L-lactide: a mechanistic study," *Polymer (Guildf.)*, vol. 36, no. 6, pp. 1253–1259, 1995.
- [116] M. Jamshidian, E. A. Tehrany, M. Imran, M. Jacquot, and S. Desobry, "Poly-Lactic Acid: Production, applications, nanocomposites, and release studies," *Compr. Rev. Food Sci. Food Saf.*, vol. 9, no. 5, pp. 552–571, 2010.
- [117] D. Briassoulis, "An overview on the mechanical behaviour of biodegradable agricultural films," *J. Polym. Environ.*, vol. 12, no. 2, pp. 65–81, 2004.
- [118] K. Madhavan Nampoothiri, N. R. Nair, and R. P. John, "An overview of the recent developments in polylactide (PLA) research," *Bioresour. Technol.*, vol. 101, no. 22, pp. 8493–8501, 2010.
- [119] F. E. Bailey and J. K. Koleske, *Ullmann's encyclopedia of industrial chemistry*. Wiley-VCH, Weinheim, Germany, 2003.
- [120] S. Zalipsky, "Chemistry of polyethylene glycol conjugates with biologically active molecules," *Adv. Drug Deliv. Rev.*, vol. 16, no. 2–3, pp. 157–182, 1995.
- [121] A. Abuchowski, T. van Es, N. C. Palczuk, and F. F. Davis, "Alteration of Immunological Properties of Bovine Serum Albumin by Covalent Attachment of Polyethylene Glycol," *Journal*, vol. 252, no. 11, pp. 3578–3581, 1977.
- [122] N. V. Katre, "The conjugation of proteins with polyethylene glycol and other polymers," *Adv. Drug Deliv. Rev.*, vol. 10, pp. 91–114, 1993.
- [123] M. C. Woodle, C. M. Engbers, and S. Zalipsky, "New amphipatic polymer-lipid conjugates forming long-circulating reticuloendothelial system-evading

- liposomes.," *Bioconjug. Chem.*, vol. 5, no. 6, pp. 493–496, 1994.
- [124] S. Saeki, N. Kuwahara, M. Nakata, and M. Kaneko, "Upper and lower critical solution temperatures in poly (ethylene glycol) solutions," *Polymer (Guildf.)*, vol. 17, no. 8, pp. 685–689, 1976.
- [125] M. Javadian, K. Rostamizadeh, and H. Danafar, "Preparation and characterization of electrospinning PEG-PLA nanofibers for sustained release of tamoxifen," *Pharm. Sci.*, vol. 7, no. 5, p. 2012, 2012.
- [126] V. I. Lozinsky *et al.*, "Synthesis of N-vinylcaprolactam polymers in water-containing media," *Polymer (Guildf.)*, vol. 41, no. 17, pp. 6507–6518, 2000.
- [127] F. Shubo, L. Shuyuan, H. Cunfeng, Z. Erli, and T. Xinliang, "Synthesis of N-vinyl caprolactam," *Catal. Today*, vol. 140, no. 3–4, pp. 169–173, 2009.
- [128] J.-H. Guo, G. . Skinner, W. . Harcum, and P. . Barnum, "Pharmaceutical applications of naturally occurring water-soluble polymers," *Pharm. Sci. Technol. Today*, vol. 1, no. 6, pp. 254–261, 1998.
- [129] Y. Bai *et al.*, "Novel thermo- and pH-responsive hydroxypropyl cellulose- and poly (l-glutamic acid)-based microgels for oral insulin controlled release," *Carbohydr. Polym.*, vol. 89, no. 4, pp. 1207–1214, 2012.
- [130] A. Abdelbary, A. H. Elshafeey, and G. Zidan, "Comparative effects of different cellulosic-based directly compressed orodispersable tablets on oral bioavailability of famotidine," *Carbohydr. Polym.*, vol. 77, no. 4, pp. 799–806, 2009.
- [131] "<https://de.wikipedia.org/wiki/Hydroxypropylcellulose>."
- [132] "Ashland Inc. (2012) Hydroxypropylcellulose (Klucel, Aerowhip)." [Online]. Available: <http://www.ashland.com/products/aerowhip-hydroxypropylcellulose>.
- [133] A. Södergård and M. Stolt, "Properties of lactic acid based polymers and their correlation with composition," *Prog. Polym. Sci.*, vol. 27, no. 6, pp. 1123–1163, 2002.
- [134] H. Auras, Rafael; Tak Lim Loong; Selke, S.E.M.; Tsuji, *Poly (lactic acid): Synthesis, Structures, Properties, Processing, and Applications*. John Wiley & Sons., 2010.
- [135] M. Bogntizki *et al.*, "Preparation of Fibers with nanoscaled morphologies - ES of Polymer Blends," *Polym. Eng. Sci.*, vol. 41, no. 6, pp. 982–989, 2001.
- [136] Z. Qi, H. Yu, Y. Chen, and M. Zhu, "Highly porous fibers prepared by electrospinning a ternary system of nonsolvent/solvent/poly(l-lactic acid)," *Mater. Lett.*, vol. 63, no. 3–4, pp. 415–418, 2009.
- [137] R. Casasola, N. L. Thomas, and S. Georgiadou, "Electrospinning of poly(lactic acid): Theoretical approach for the solvent selection to produce defect-free nanofibers," *J. Polym. Sci. Part B Polym. Phys.*, vol. 54, no. 15, pp. 1483–1498, 2016.
- [138] D. T., Waclaw; S., Wojciech; S., Marek; K., Michal; C., "Simple Methods Influencing on Properties of Electrospun Fibrous Mats," *Polym. Polym. Compos.*, vol. 21, no. 7, pp. 449–456, 2013.
- [139] A. R. K. Sasikala, A. R. Unnithan, Y. H. Yun, C. H. Park, and C. S. Kim, "An implantable smart magnetic nanofiber device for endoscopic hyperthermia treatment and tumor-triggered controlled drug release," *Acta Biomater.*, vol. 31, pp. 122–133, 2016.
- [140] Y. Luo *et al.*, "Novel biosensor based on electrospun nanofiber and magnetic nanoparticles for the detection of E. coli O157:H7," *IEEE Trans. Nanotechnol.*, vol. 11, no. 4, pp. 676–681, 2012.
- [141] G. Ding, Y. Guo, Y. Lv, X. Liu, L. Xu, and X. Zhang, "A double-targeted magnetic

- nanocarrier with potential application in hydrophobic drug delivery,” *Colloids Surfaces B Biointerfaces*, vol. 91, no. 1, pp. 68–76, 2012.
- [142] T. Hoare *et al.*, “A magnetically triggered composite membrane for on-demand drug delivery,” *Nano Lett.*, vol. 9, no. 10, pp. 3651–3657, 2009.
- [143] R. Saadat and F. Renz, “Simultaneous cancer control and diagnosis with magnetic nanohybrid materials,” *Beilstein J. Nanotechnol.*, vol. 7, no. Figure 1, pp. 121–125, 2016.
- [144] M. Saravanan, K. Bhaskar, G. Maharajan, and K. S. Pillai, “Ultrasonically controlled release and targeted delivery of diclofenac sodium via gelatin magnetic microspheres,” *Int. J. Pharm.*, vol. 283, no. 1–2, pp. 71–82, 2004.
- [145] J. L. Arias, M. A. Ruiz, V. Gallardo, and A. V. Delgado, “Tegafur loading and release properties of magnetite/poly(alkylcyanoacrylate) (core/shell) nanoparticles,” *J. Control. Release*, vol. 125, no. 1, pp. 50–58, 2008.
- [146] T. Meyer *et al.*, “Electrospun complexes - functionalised nanofibres,” *Hyperfine Interact.*, vol. 237, no. 1, pp. 1–11, 2016.
- [147] J. M. Holzwarth and P. X. Ma, “Biomimetic nanofibrous scaffolds for bone tissue engineering,” *Biomaterials*, vol. 32, no. 36, pp. 9622–9629, 2011.
- [148] S. Khansari, S. Sinha-ray, A. L. Yarin, and B. Pourdeyhimi, “Biopolymer-Based Nano fiber Mats and Their Mechanical Characterization,” 2013.
- [149] E. Y. Gómez-Pachón, R. Vera-Graziano, and R. M. Campos, “Structure of poly(lactic-acid) PLA nanofibers scaffolds prepared by electrospinning,” *IOP Conf. Ser. Mater. Sci. Eng.*, vol. 59, p. 12003, 2014.
- [150] Y. Ikada and H. Tsuji, “Biodegradable polyesters for medical and ecological applications,” *Macromol. Rapid Commun.*, vol. 21, no. 3, pp. 117–132, 2000.
- [151] D. E. Henton, P. Gruber, J. Lunt, and J. Randall, “Polylactic Acid Technology,” vol. 48674, no. 23, pp. 1841–1846, 2000.
- [152] A. Wagner, V. Poursorkhabi, A. K. Mohanty, and M. Misra, “Analysis of Porous Electrospun Fibers from Poly(L -lactic acid)/Poly(3-hydroxybutyrate- co -3-hydroxyvalerate) Blends,” *ACS Sustain. Chem. Eng.*, vol. 2, no. 8, pp. 1976–1982, 2014.
- [153] Y. Wan, W. Chen, J. Yang, J. Bei, and S. Wang, “Biodegradable poly(L-lactide)-poly(ethylene glycol) multiblock copolymer: Synthesis and evaluation of cell affinity,” *Biomaterials*, vol. 24, no. 13, pp. 2195–2203, 2003.
- [154] E. Hendrick and M. Frey, “Increasing Surface Hydrophilicity in Poly (Lactic Acid) Electrospun Fibers by Addition of Pla-b-Peg Co-Polymers.,” *J. Eng. Fabr. Fibers*, vol. 9, no. 2, pp. 153–164, 2014.
- [155] A. Ulman, “Formation and Structure of Self-Assembled Monolayers,” *Chem. Rev.*, vol. 96, no. 4, pp. 1533–1554, 1996.
- [156] G. Wallace, D. De Rossi, Y. Wu, K.-T. Lau, and S. Coyle, “Smart Nanotextiles: A Review of Materials and Applications,” *MRS Bull.*, vol. 32, no. 5, pp. 434–442, 2007.
- [157] M. Kumar *et al.*, “Mixture of PLA-PEG and biotinylated albumin enables immobilization of avidins on electrospun fibers,” *J. Biomed. Mater. Res. - Part A*, vol. 105A, no. 105A, pp. 356–362, 2017.
- [158] S. Rana, A. Gallo, R. S. Srivastava, and R. D. K. Misra, “On the suitability of nanocrystalline ferrites as a magnetic carrier for drug delivery: Functionalization, conjugation and drug release kinetics,” *Acta Biomater.*, vol. 3, no. 2, pp. 233–242, 2007.
- [159] M. Kumar, D. Unruh, R. Sindelar, and F. Renz, “Preparation of Magnetic

- Poly(lactic acid) Fiber Mats by Electrospinning,” *Nano Hybrids Compos.*, vol. 14, pp. 39–47, 2017.
- [160] M. Liu *et al.*, “Preparation and characterization of TiO₂ nanofibers via using poly(lactic acid) as template,” *J. Appl. Polym. Sci.*, vol. 128, no. 2, pp. 1095–1100, 2013.
- [161] K. Kim *et al.*, “Control of degradation rate and hydrophilicity in electrospun non-woven poly(D,L-lactide) nanofiber scaffolds for biomedical applications,” *Biomaterials*, vol. 24, no. 27, pp. 4977–4985, 2003.
- [162] H. J. Lee *et al.*, “Biomedical applications of magnetically functionalized organic/inorganic hybrid nanofibers,” *Int. J. Mol. Sci.*, vol. 16, no. 6, pp. 13661–13677, 2015.
- [163] B. D. Cullity and C. D. Graham, *Introduction to magnetic materials*. A John Wiley & Sons, Inc., Publication, 2009.
- [164] M. A. M. Gijs, F. Lacharme, and U. Lehmann, “Microfluidic applications of magnetic particles for biological analysis and catalysis,” *Chem. Rev.*, vol. 110, no. 3, pp. 1518–1563, 2010.
- [165] R. K. Singh *et al.*, “Potential of magnetic nanofiber scaffolds with mechanical and biological properties applicable for bone regeneration,” *PLoS One*, vol. 9, no. 4, 2014.
- [166] T. Y. Liu, S. H. Hu, T. Y. Liu, D. M. Liu, and S. Y. Chen, “Magnetic-sensitive behavior of intelligent ferrogels for controlled release of drug,” *Langmuir*, vol. 22, no. 14, pp. 5974–5978, 2006.
- [167] J. M. Shen, T. Yin, X. Z. Tian, F. Y. Gao, and S. Xu, “Surface charge-switchable polymeric magnetic nanoparticles for the controlled release of anticancer drug,” *ACS Appl. Mater. Interfaces*, vol. 5, no. 15, pp. 7014–7024, 2013.
- [168] L. Hosseini, K. Mahboobnia, and M. Irani, “Fabrication of PLA/MWCNT/Fe₃O₄ composite nanofibers for leukemia cancer cells,” *Int. J. Polym. Mater. Polym. Biomater.*, vol. 65, no. 4, pp. 176–182, 2016.
- [169] E. P. Goldberg, A. R. Hadba, B. a Almond, and J. S. Marotta, “Intratumoral cancer chemotherapy and immunotherapy: opportunities for nonsystemic preoperative drug delivery,” *J. Pharm. Pharmacol.*, vol. 54, no. 2, pp. 159–180, 2002.
- [170] R. K. Jain, “Delivery of molecular medicine to solid tumors: Lessons from in vivo imaging of gene expression and function,” in *Journal of Controlled Release*, 2001, vol. 74, no. 1–3, pp. 7–25.
- [171] T. U. Eindhoven, *Magnetically induced localized on-demand drug delivery*. 2010.
- [172] Y. E. Kirsh, “Water-soluble poly (n-vinylamidess): Microstructure, solvation, conformational state and complex formation in aqueous solutions,” *Prog. Polym. Sci.*, vol. 18, no. 3, pp. 519–542, 1993.
- [173] C. Witschi and E. Doelker, “Influence of the microencapsulation method and peptide loading on poly(lactic acid) and poly(lactic-co-glycolic acid) degradation during in vitro testing,” *J. Control. Release*, vol. 51, no. 2–3, pp. 327–341, 1998.
- [174] G. Kister, G. Cassanas, and M. Vert, “Effects of morphology, conformation and configuration on the IR and Raman spectra of various poly(lactic acid)s,” *Polymer (Guildf)*, vol. 39, no. 2, pp. 267–273, 1998.
- [175] G. Kister, G. Cassanas, M. Vert, B. Pauvert, and A. Terol, “Vibrational Analysis of Poly(L-lactic acid),” *J. RAMAN Spectrosc.*, vol. 26, pp. 307–311, 1995.
- [176] L. Koenig and a C. Angood, “Spectra of Poly(ethylene Glycols) in Solution,” *J. Polym. Sci.*, vol. 8, pp. 1787–1796, 1970.
- [177] M. Kozielski, M. Mühle, Z. Błaszczak, and M. Szybowicz, “Raman and Rayleigh

- scattering study of crystalline polyoxyethyleneglycols,” *Cryst. Res. Technol.*, vol. 40, no. 4–5, pp. 466–470, 2005.
- [178] A. Moshaverinia, N. Roohpour, J. A. Darr, and I. U. Rehman, “Synthesis and characterization of a novel N-vinylcaprolactam-containing acrylic acid terpolymer for applications in glass-ionomer dental cements,” *Acta Biomater.*, vol. 5, no. 6, pp. 2101–2108, 2009.
- [179] E. Y. Gómez-Pachón, R. Vera-Graziano, and R. M. Campos, “Structure of poly(lactic-acid) PLA nanofibers scaffolds prepared by electrospinning,” *IOP Conf. Ser. Mater. Sci. Eng.*, vol. 59, p. 12003, 2014.
- [180] R. P. Gonçalves *et al.*, “Morphology and Thermal Properties of Core-Shell PVA/PLA Ultrafine Fibers Produced by Coaxial Electrospinning,” *Mater. Sci. Appl.*, vol. 6, no. 2, pp. 189–199, 2015.
- [181] M. Webster *et al.*, “Tunable thermo-responsive poly(N-vinylcaprolactam) cellulose nanofibers: Synthesis, characterization, and fabrication,” *Macromol. Mater. Eng.*, vol. 298, no. 4, pp. 447–453, 2013.
- [182] I. Chopra and M. Roberts, “Tetracycline Antibiotics: Mode of Action, Applications, Molecular Biology, and Epidemiology of Bacterial Resistance,” *Microbiol. Mol. Biol. Rev.*, vol. 65, no. 2, pp. 232–260, 2001.
- [183] R. Qi, R. Guo, F. Zheng, H. Liu, J. Yu, and X. Shi, “Controlled release and antibacterial activity of antibiotic-loaded electrospun halloysite/poly(lactic-co-glycolic acid) composite nanofibers,” *Colloids Surfaces B Biointerfaces*, vol. 110, pp. 148–155, 2013.
- [184] M. A. Jabra-Rizk, W. A. Falkler, and T. F. Meiller, “Fungal Biofilms and Drug Resistance,” *Emerg. Infect. Dis.*, vol. 10, no. 1, pp. 14–19, 2004.
- [185] E. R. Edelman and R. Langer, “Optimization of release from magnetically controlled polymeric drug release devices,” *Biomaterials*, vol. 14, no. 8, pp. 621–626, 1993.
- [186] W. Andrä and H. Nowak, *Magnetism in Medicine*. Wiley-VCH Verlag GmbH & Co. KGaA, 2007.
- [187] B. B. Yellen *et al.*, “Targeted drug delivery to magnetic implants for therapeutic applications,” in *Journal of Magnetism and Magnetic Materials*, 2005, vol. 293, no. 1, pp. 647–654.
- [188] A. Iannone *et al.*, “Blood Clearance of Dextran Magnetite Particles Determined by a noninvasive in vivo ESR method,” *Magn. Reson. Med.*, vol. 22, no. 2, pp. 435–442, 1991.
- [189] R. Fernandez-Pacheco *et al.*, “Magnetic nanoparticles for local drug delivery using magnetic implants,” *J. Magn. Magn. Mater.*, vol. 311, no. 1 SPEC. ISS., pp. 318–322, 2007.
- [190] K. Landfester and L. P. Ramirez, “Encapsulated magnetite particles for biomedical application,” *J. Phys. Condens. Matter*, vol. 15, no. 15, pp. S1345–S1361, 2003.
- [191] J. Yang, H. Lee, W. Hyung, S.-B. Park, and S. Haam, “Magnetic PECA nanoparticles as drug carriers for targeted delivery: synthesis and release characteristics,” *J. Microencapsul.*, vol. 23, no. 2, pp. 203–212, 2006.
- [192] D. H. Kim, D. E. Nikles, D. T. Johnson, and C. S. Brazel, “Heat generation of aqueously dispersed CoFe₂O₄ nanoparticles as heating agents for magnetically activated drug delivery and hyperthermia,” *J. Magn. Magn. Mater.*, vol. 320, no. 19, pp. 2390–2396, 2008.
- [193] M. Shinkai, “Functional magnetic particles for medical application,” *J. Biosci. Bioeng.*, vol. 94, no. 6, pp. 606–613, Dec. 2002.

- [194] L. Néel, "Influence des fluctuations thermiques sur l'aimantation de grains ferromagnétiques très fins," *Comptes Rendus Hebd. Des Seances L Acad. Des Sci.*, vol. 228, no. 8, pp. 664–666, 1949.
- [195] D. K. Jackson, "Power electronic drives for magnetically triggered gels," *IEEE Trans. Ind. Electron.*, vol. 44, no. 2, pp. 217–225, 1997.
- [196] S.-F. Ng, J. J. Rouse, F. D. Sanderson, V. Meidan, and G. M. Eccleston, "Validation of a Static Franz Diffusion Cell System for In Vitro Permeation Studies," *AAPS PharmSciTech*, vol. 11, no. 3, pp. 1432–1441, 2010.
- [197] T. J. Franz, "Percutaneous Absorption. On the Relevance of in Vitro Data," *J. Invest. Dermatol.*, vol. 64, no. 3, pp. 190–195, Mar. 1975.
- [198] P. W. Atkins, J. de Paula, S. Michael, H. Anna, and Carsten, *Physikalische Chemie, 4. vollständig überarbeitete Auflage*. New York: Wiley-VCH, Weinheim, 2006.
- [199] H. Priya James, R. John, and A. Alex, "Smart polymers for the controlled delivery of drugs – a concise overview," *Acta Pharm. Sin. B*, vol. 4, no. 2, pp. 120–127, 2014.
- [200] P. Bawa, V. Pillay, Y. E. Choonara, and L. C. du Toit, "Stimuli-responsive polymers and their applications in drug delivery," *Biomed. Mater.*, vol. 4, no. 22001, pp. 1–15, 2009.
- [201] E. Cabane, X. Zhang, K. Langowska, C. G. Palivan, and W. Meier, "Stimuli-responsive polymers and their applications in nanomedicine," *Biointerphases*, vol. 7, no. 1–4, pp. 1–27, 2012.
- [202] Y. Machida and T. Nagai, "Directly Compressed Tablets Containing Hydroxypropyl Cellulose in Addition to Starch or Lactose," *Chem. Pharm. Bull.*, vol. 14, pp. 369–375, 1966.
- [203] G. W. Skinner, W. W. Harcum, P. E. Barnum, and J.-H. Guo, "The Evaluation of Fine-Particle Hydroxypropylcellulose as a Roller Compaction Binder in Pharmaceutical Applications," *Drug Dev. Ind. Pharm.*, vol. 25, no. 10, pp. 1121–1128, 1999.
- [204] J. Gao, G. Haidar, X. Lu, and Z. Hu, "Self-association of hydroxypropylcellulose in water," *Macromolecules*, vol. 34, no. 7, pp. 2242–2247, 2001.
- [205] D. Bielska *et al.*, "Self-organized thermo-responsive hydroxypropyl cellulose nanoparticles for curcumin delivery," *Eur. Polym. J.*, vol. 49, no. 9, pp. 2485–2494, 2013.
- [206] T. Wüstenberg, *Cellulose and cellulose derivatives in the food industry*. Wiley-VCH Verlag GmbH & Co. KGaA, 2015.
- [207] M. Kumar, D. Wengerowsky, F. Böttcher, R. Sindelar, V. P. Hytönen, and F. Renz, "PLA-HPC Fibrous Membranes for Temperature-Responsive Drug Release," *Nano Hybrids Compos.*, vol. 18, pp. 34–41, 2017.
- [208] M. Bikram and J. L. West, "Thermo-responsive systems for controlled drug delivery," *Taylor Fr.*, vol. 5, no. 10, pp. 1077–1091, 2008.
- [209] S. Shukla, E. Brinley, H. J. Cho, and S. Seal, "Electrospinning of hydroxypropyl cellulose fibers and their application in synthesis of nano and submicron tin oxide fibers," *Polymer (Guildf)*, vol. 46, no. 26, pp. 12130–12145, 2005.
- [210] V. Periasamy, K. Devarayan, M. Hachisu, J. Araki, and K. Ohkawa, "Chemical Modifications of Electrospun Non-woven Hydroxypropyl Cellulose Fabrics for Immobilization of Aminoacylase-I," *J. Fiber Bioeng. Informatics*, vol. 5, no. 2, pp. 191–205, 2012.
- [211] L. Francis, A. Balakrishnan, K. P. Sanosh, and E. Marsano, "Characterization and tensile strength of HPC–PEO composite fibers produced by electrospinning,"

- 2010.
- [212] D. Chen and B. Sun, "New tissue engineering material copolymers of derivatives of cellulose and lactide: their synthesis and characterization," *Mater. Sci. Eng. C*, vol. 11, no. 1, pp. 57–60, 2000.
- [213] A. Gutowska, Y. H. Bae, H. Jacobs, S. W. Kim, and J. Feijen, "Thermosensitive Interpenetrating Polymer Networks: Synthesis, Characterization, and Macromolecular Release," *Macromolecules*, vol. 27, no. 15, pp. 4167–4175, 1994.
- [214] M. Carenza, F. Martellini, H. I. Mei, and J. L. Bali, "Water and drug transport in radiation-crosslinked poly (2-methoxyethylacrylate- co -dimethyl acrylamide) and poly (2-methoxyethylacrylate- co -acrylamide) hydrogels," *Radiat. Phys. Chem.*, vol. 66, pp. 155–159, 2003.
- [215] K. Rao, K. Rao, and C.-S. Ha, "Stimuli Responsive Poly(Vinyl Caprolactam) Gels for Biomedical Applications," *Gels*, vol. 2, no. 1, p. 6, 2016.
- [216] L. Li, X. Jiang, and R. Zhuo, "Synthesis and Characterization of Thermoresponsive Polymers Containing Reduction-Sensitive Disulfide Linkage," *J. Polym. Sci.*, vol. 47, pp. 5989–5997, 2009.
- [217] K. B. Doorty *et al.*, "Poly(N-isopropylacrylamide) co-polymer films as potential vehicles for delivery of an antimetabolic agent to vascular smooth muscle cells," *Cardiovasc. Pathol.*, vol. 12, no. 2, pp. 105–110, Mar. 2003.
- [218] M. Nakayama, T. Okano, T. Miyazaki, F. Kohori, K. Sakai, and M. Yokoyama, "Molecular design of biodegradable polymeric micelles for temperature-responsive drug release," *J. Control. Release*, vol. 115, no. 1, pp. 46–56, 2006.
- [219] D. Y. Furgeson, M. R. Dreher, and A. Chilkoti, "Structural optimization of a 'smart' doxorubicin-polypeptide conjugate for thermally targeted delivery to solid tumors," *J. Control. Release*, vol. 110, no. 2, pp. 362–369, 2006.
- [220] M. Chen, Y. F. Li, and F. Besenbacher, "Electrospun Nanofibers-Mediated On-Demand Drug Release," *Adv. Healthc. Mater.*, vol. 3, no. 11, pp. 1721–1732, 2014.
- [221] Z. M. Huang, Y. Z. Zhang, M. Kotaki, and S. Ramakrishna, "A review on polymer nanofibers by electrospinning and their applications in nanocomposites," *Compos. Sci. Technol.*, vol. 63, no. 15, pp. 2223–2253, 2003.
- [222] M. Kumar *et al.*, "Electrospinning synthesis and characterization of PLA-PEG-MNPs composite fibrous membranes," *Hyperfine Interact.*, vol. 238, no. 1, p. 66, 2017.
- [223] E. R. Kenawy *et al.*, "Release of tetracycline hydrochloride from electrospun poly(ethylene-co-vinylacetate), poly(lactic acid), and a blend," *J. Control. Release*, vol. 81, no. 1–2, pp. 57–64, 2002.
- [224] K. A. Heitfeld, T. Guo, G. Yang, and D. W. Schaefer, "Temperature responsive hydroxypropyl cellulose for encapsulation," *Mater. Sci. Eng. C*, vol. 28, no. 3, pp. 374–379, 2008.
- [225] M. Shibayama and T. Tanaka, "Volume phase transition and related phenomena of polymer gels," in *Responsive Gels: Volume Transitions I*, K. Dušek, Ed. Berlin, Heidelberg: Springer Berlin Heidelberg, 1993, pp. 1–62.
- [226] X. Lu, Z. Hu, and J. Gao, "Synthesis and light scattering study of hydroxypropyl cellulose microgels," *Macromolecules*, vol. 33, no. 23, pp. 8698–8702, 2000.
- [227] T. Baltes, F. Garret-Flaudy, and R. Freitag, "Investigation of the LCST of polyacrylamides as a function of molecular parameters and the solvent composition," *J. Polym. Sci. Part A Polym. Chem.*, vol. 37, no. 15, pp. 2977–2989, 1999.
- [228] B. Priya and Et Al., "Stimuli-responsive polymers and their applications in drug

- delivery,” vol. 4, p. 22001, 2009.
- [229] E. Stern *et al.*, “Label-free biomarker detection from whole blood,” *ICSICT-2010 - 2010 10th IEEE Int. Conf. Solid-State Integr. Circuit Technol. Proc.*, vol. 5, no. 2, pp. 1392–1393, 2010.
- [230] W. D. Wilson, “Analyzing biomolecular interactions,” *Science (80-.)*, vol. 295, no. March, pp. 2103–2105, 2002.
- [231] F. Patolsky and C. M. Lieber, “Nanowire nanosensors,” *Mater. Today*, vol. 8, no. 4, pp. 20–28, 2005.
- [232] N. Ramachandran *et al.*, “Self-Assembling Protein Microarrays,” vol. 305, no. July, pp. 86–91, 2004.
- [233] D. R. Thévenot, K. Toth, R. A. Durst, and G. S. Wilson, “Electrochemical biosensors: Recommended definitions and classification,” *Biosens. Bioelectron.*, vol. 16, no. 1–2, pp. 121–131, 2001.
- [234] V. Perumal and U. Hashim, “Advances in biosensors: Principle, architecture and applications,” *J. Appl. Biomed.*, vol. 12, no. 1, pp. 1–15, 2014.
- [235] R. Ramaseshan and V. K. Ganesh, “Polymer Nanofibers for Biosensor Applications,” *Polymer (Guildf)*, pp. 377–392.
- [236] B. Bohunicky and S. A. Mousa, “Biosensors: The new wave in cancer diagnosis,” *Nanotechnol. Sci. Appl.*, vol. 4, no. 1, pp. 1–10, 2011.
- [237] A. Mueller, “Enzyme electrodes for medical sensors.,” *Mini Rev. Med. Chem.*, vol. 5, no. 3, pp. 231–9, 2005.
- [238] J. P. Smith, “Medical and biological sensors: a technical and commercial review,” *Sens. Rev.*, vol. 25, no. 4, pp. 241–245, 2005.
- [239] S. K. Arya, M. Datta, and B. D. Malhotra, “Recent advances in cholesterol biosensor,” *Biosens. Bioelectron.*, vol. 23, no. 7, pp. 1083–1100, 2008.
- [240] N. Dale, S. Hatz, F. Tian, and E. Llaudet, “Listening to the brain: Microelectrode biosensors for neurochemicals,” *Trends in Biotechnology*, vol. 23, no. 8. pp. 420–428, 2005.
- [241] F. Kögl and B. Tönnes, “Über das Bios-Problem.20. Mitteilung über pflanzliche Wachstumsstoffe,” *Hoppe-Seyler’ s Zeitschrift für Physiol. Chemie*, vol. 242, no. 1–2, pp. 43–73, 1936.
- [242] M. Wilchek and E. A. Bayer, “Introduction to avidin-biotin technology,” *Methods in Enzymology*, vol. 184. pp. 5–13, 1990.
- [243] J. Leppiniemi *et al.*, “Bifunctional avidin with covalently modifiable ligand binding site,” *PLoS One*, vol. 6, no. 1, 2011.
- [244] T. Furukawa *et al.*, “Structure, dispersibility, and crystallinity of poly(hydroxybutyrate)/ poly(L-lactic acid) blends studied by FT-IR microspectroscopy and differential scanning calorimetry,” *Macromolecules*, vol. 38, no. 15, pp. 6445–6454, 2005.
- [245] X. Zong, S. Ran, K. Kim, D. Fang, B. S. Hsiao, and B. Chu, “Structure and Morphology Changes during in Vitro Degradation of Electrospun Poly (glycolide-co-lactide) Nanofiber Membrane,” *Biomacromolecules*, vol. 4, pp. 416–423, 2003.
- [246] Y. You, B. M. Min, S. J. Lee, T. S. Lee, and W. H. Park, “In vitro degradation behavior of electrospun polyglycolide, polylactide, and poly(lactide-co-glycolide),” *J. Appl. Polym. Sci.*, vol. 95, no. 2, pp. 193–200, 2005.
- [247] H. Tsuji, M. Nakano, M. Hashimoto, and K. Takashima, “Electrospinning of Poly (lactic acid) Stereocomplex Nanofibers,” *Biomacromolecules*, vol. 7, pp. 3316–3320, 2006.
- [248] H. W. Kim, H. S. Yu, and H. H. Lee, “Nanofibrous matrices of poly(lactic acid)

- and gelatin polymeric blends for the improvement of cellular responses,” *J. Biomed. Mater. Res. - Part A*, vol. 87, no. 1, pp. 25–32, 2008.
- [249] D. Ishii *et al.*, “In Vivo Tissue Response and Degradation Behavior of PLLA and Stereocomplexed PLA Nanofibers In Vivo Tissue Response and Degradation Behavior of PLLA and Stereocomplexed PLA Nanofibers,” *Biomacromolecules*, vol. 10, pp. 237–242, 2009.
- [250] K.-T. Noh, H.-Y. Lee, U.-S. Shin, and H.-W. Kim, “Composite nanofiber of bioactive glass nanofiller incorporated poly(lactic acid) for bone regeneration,” *Mater. Lett.*, vol. 64, no. 7, pp. 802–805, Apr. 2010.
- [251] F. Peng, X. Yu, and M. Wei, “In vitro cell performance on hydroxyapatite particles/poly(L-lactic acid) nanofibrous scaffolds with an excellent particle along nanofiber orientation,” *Acta Biomater.*, vol. 7, no. 6, pp. 2585–2592, 2011.
- [252] T. T. Trang Mai *et al.*, “A novel nanofiber Cur-loaded polylactic acid constructed by electrospinning,” *Adv. Nat. Sci. Nanosci. Nanotechnol.*, vol. 3, no. 2, p. 25014, 2012.
- [253] T. Wang *et al.*, “Fabrication and Characterization of Heparin-Grafted Poly-L-lactic acid–Chitosan Core–Shell Nanofibers Scaffold for Vascular Gasket,” *Am. Chem. Soc.*, vol. 5, pp. 3757–3763, 2013.
- [254] S. J. Lee, A. P. Arun, and K. J. Kim, “Piezoelectric properties of electrospun poly(l-lactic acid) nanofiber web,” *Mater. Lett.*, vol. 148, pp. 58–62, Jun. 2015.
- [255] Y. Goh, M. Akram, A. Alshemary, and R. Hussain, “Antibacterial polylactic acid/chitosan nanofibers decorated with bioactive glass,” *Appl. Surf. Sci.*, vol. 387, pp. 1–7, Nov. 2016.

Symbols and Abbreviations

Symbols and abbreviations are listed in the following notation:

Symbols and Abbreviations	Descriptions
μm	Micrometer
CEs	Cellulose ethers
cm	Centimeter
DCM	Dichloromethane
DDS	Drug Delivery Systems
DSC	Differential scanning calorimetry
E. coli	Escherichia coli
ESP	Electrospinning
FTIR	Fourier transform infrared
g	Gram
h	Hour
HPC	Hydroxypropyl cellulose
kV	Kilovolt
kV	Kilovolt
LCST	Lower critical solution temperature
MEB	Methylene blue
mg	Milligram
min	Minute
mL	Milliliter
M_n	Number-average molecular weight
M_w	Mass average molar mass
M_w	Weight-average molecular weight
nm	Nanometer

Symbols and Abbreviations

NVCL	N-Vinylcaprolactam
PBS	Phosphate buffered saline
PCL	Poly- ϵ -caprolactam
PEG	Polyethylene glycol
PLA	Poly(lactic acid)
PNIPAm	Poly(N-isopropyl acrylamide)
R	Universal gas constant
RT	Room temperature
SEM	Scanning electron microscopy
TCM	Trichloromethane
TFE	2,2,2-Trifluoroethanol
T_g	Glass transition temperature
TGA	Thermogravimetric analysis
THF	Tetrahydrofuran
T_m	Melting temperature
UCST	Upper critical solution temperature
UV-VIS	Ultraviolet-visible
V	Volume
wt%	Weight percentage
wt. %	Percentage by weight
XRD	X-ray diffraction
ΔG	Gibbs Free Energy
ΔH	Enthalpy term
ΔS	Entropy term
λ	Wavelength

Figures List

Figure 1.1: Schematic illustration of the energy transfer and –conversion scheme. First functional nanofibers with tailored properties are fabricated by electrospinning technique. After this, the functionalized nanofibers are treated with an external energy source and stimulated (on-demand) therapeutic release is measured. The functionalized nanofibers are treated with biological samples [1] and their binding ability is demonstrated (Picture: M. Kumar).	1
Figure 1.2: Number of publication related to nanofibers for biomedical applications (Source: Web of Science accessed on 6 March 2017).	3
Figure 1.3: From raw materials to functional nano-bio-fibrous membranes by electrospinning technique and their potential biomedical applications (Picture: M. Kumar).	5
Figure 1.4: Working package for the development of functional nano-bio-fibrous membranes and their potential biomedical applications (Picture: M. Kumar).	5
Figure 2.1: Electrospinning lab set-up (Picture:F. Böttcher and M. Kumar).	7
Figure 2.2: Some of the advanced biomedical applications of electrospun nanofibers (Picture: M. Kumar).	11
Figure 2.3: (a) Schematic illustration of single nozzle electrospinning setup and (b) designed lab apparatus displaying the single nozzle system (Pictures: M. Kumar).	12
Figure 2.4: (a) Schematic illustration of coaxial electrospinning setup and (b) designed lab apparatus displaying the core-shell system (Pictures: M. Kumar).	13
Figure 2.5: (a) Schematic illustration of side-by-side electrospinning setup (b) designed lab apparatus displaying the two side on single collector (Pictures: M. Kumar)	14
Figure 2.6: SEM micrographs of electrospun PLA fibers fabricated by using (a) Single nozzle spinning (b) coaxial spinning [Cellulose acetate (core) – PLA (shell)] (c) side-by-side spinning [PLA (one side) – cellulose acetate (second side)]. (Pictures: F. Dencker).	15
Figure 2.7: SEM micrographs of different morphologies of fibers (a) beaded PLA fibers (b) circular PLA fibers (c) porous PLA fibers (d) core-shell (Cellulose acetate-PLA) fibers (e) ribbon-like cellulose acetate fibers (f) hollow PLA fibers. (Pictures: F. Dencker)	16
Figure 3.1: Drug concentration level in blood showing conventional release system (Multiple dosing at regular intervals leads to oscillating drug concentrations, which may fall outside the therapeutic range for significant time periods). (Picture: M. Kumar). ..	19

Figure 3.2: Drug concentration level in blood showing (a) controlled release system (drug concentration in blood lies within the therapeutic range, which is bounded below by the minimum toxic concentration and above by the minimum effective concentration) and (b) triggered release system. (Pictures: M. Kumar).....	21
Figure 3.3: Different mechanisms of drug release.....	22
Figure 3.4: Classification of stimuli of stimuli-responsive polymers (Picture: M. Kumar)	25
Figure 3.5: A symmetric diagram shows a stimuli-responsive drug-release system (Picture: M. Kumar).....	26
Figure 3.6: Symmetric diagram shows magnetically-sensitive release system (Picture: M. Kumar).....	29
Figure 3.7: Schematic illustration of phase diagram for polymer/solvent mixture (a) lower critical solution temperature (LCST) behavior and (b) upper critical solution temperature (UCST) behavior (Pictures: M. Kumar).	30
Figure 4.1: Schematic illustration of the contact angle measurements on fibrous membranes (Picture: M. Kumar)	38
Figure 5.1: Number of scientific papers published on biopolymers (Source: Web of Science accessed on 6 March 2017)	39
Figure 5.2: A broad classification of biopolymers	40
Figure 5.3: Classification of the biodegradable polymers (Adapted from Reference [105].)	40
Figure 5.4: Structures of mono D-, L- and DL-lactic acid	41
Figure 5.5: PLA life cycle.....	42
Figure 5.6: Current production steps for PLA.	43
Figure 5.7: Some of the biomedical applications of PLA (Source: Web of Science accessed on 20 Dec 2016).....	44
Figure 5.8: PLA 6202 pellets (Picture: M. Kumar).	44
Figure 5.9: Polyethylene glycol preparation by using ethylene oxide polymerization ..	46
Figure 5.10: Mechanism for the preparation of NVCL (Adapted from Reference [127])	47
Figure 5.11: Structure of Hydroxypropyl cellulose (HPC) (Adapted from Reference [131])	48

Figure 6.1: 3D image of PLA electrospun fibrous membrane (Picture: M. Kumar).....	52
Figure 6.2: SEM image of single PLA fiber in chloroform solvent (Picture: F. Dencker).....	52
Figure 6.3: SEM micrograph of PLA electrospun fiber in (a) DCM solvent and (b) THF solvent.....	53
Figure 6.4: SEM micrograph shows electrospun fiber of (a) 8 wt% PLA in DCM (b) 8 wt% PLA in TCM (c) 20 wt% PLA in TCM and (d) 0.1 g/mL PLA in TFE solvent	53
Figure 6.5: Average fibers diameter distribution v/s concentration of PLA	54
Figure 6.6: Average fibers diameter distribution v/s applied voltage for PLA	55
Figure 6.7: Average fiber diameter distribution v/s PLA flow rate.....	55
Figure 6.8: Surface modification technique applied on PLA electrospun fibers (A, C) Co-electrospinning and (B) Plasma treatment (Picture: M. Kumar)	56
Figure 6.9: SEM micrograph of PLA electrospun fibers (a) before plasma treatment and (b) after plasma treatment	57
Figure 6.10: BET surface area of PLA (a) Pellets, (b) PLA fibers and (c) PLA-PEG composite fibers.....	57
Figure 6.11: XRD spectrum of PLA fibers show amorphous nature whereas PLA pellet show semi-crystalline	58
Figure 7.1: PLA-PEG-MNPs3 composite fibrous membrane in distilled water shows the magnetic attraction by the lab magnet [155]	60
Figure 7.2: Scanning electron micrographs for electrospun (a) PLA fibers (b) PLA-PEG blend fibers (c) PLA-PEG-MNPs1 blend fibers (d) PLA-PEG-MNPs2 blend fibers and (e) PLA-PEG-MNPs3 blend fibers [159].	63
Figure 7.3: Average mean fibers diameter measurement of (a) PLA fibers (b) PLA-PEG blend fibers (c) PLA-PEG-MNPs1 blend fibers (d) PLA-PEG-MNPs2 blend fibers and (e) PLA-PEG-MNPs3 blend fibers [159].	64
Figure 7.4: Energy dispersive x-ray micrographs for electrospun PLA-PEG-MNPs1 composite fibers.....	64
Figure 7.5: Thermal degradation of (a) PLA fibers (b) PLA-PEG blend fibers as measured through TGA [159]......	65
Figure 7.6: XRD pattern of (a) pure MNPs (b) PLA-PEG-MNPs1 composite fibers (c) PLA-PEG-MNPs2 composite fibers and (d) PLA-PEG-MNPs3 composite fibrous membrane.....	66

Figure 7.7: Magnetization curves measured at room temperature for (a) PLA-PEG-MNPs1 (b) PLA-PEG-MNPs2 (c) PLA-PEG-MNPs3 and (d) Pure MNPs [159].	67
Figure 8.1: Effect of phase transition temperature on the polymer fiber volume and drug delivery (Picture: M. Kumar).	70
Figure 8.2: Scanning electron micrographs for electrospun fibrous membranes of (a) PLA (b) PLA-PEG (c) PLA-NVCL and (d) PLA-PEG-NVCL composite fibrous membranes	74
Figure 8.3: Average mean fibers diameter measurements of (a) PLA (b) PLA-PEG and (c) PLA-PEG-NVCL composite fibrous membranes	74
Figure 8.4: Raman spectra of (a) Bulk samples of (i) PLA, (ii) PEG and (iii) NVCL (b) Electrospun (i) PLA, (ii) PLA-PEG and (iii) PLA-PEG-NVCL composite fibrous membranes	76
Figure 8.5: DSC curve for electrospun: (a) PLA, (b) PLA-PEG and (c) PLA-PEG-NVCL composite fibrous membrane	78
Figure 8.6: Contact angle measurements on electrospun: (a) PLA (b) PLA-PEG-NVCL composite fibrous membranes	80
Figure 8.7: Digital images of a test for bacteria inhibition after 24 h contact of the composite membrane with E.coli; (a) PLA-PEG-NVCL composite fibrous membranes and (b) PLA-PEG-NVCL-TCH composite fibrous membranes. The inhibitory zone is indicated by a dashed line.	80
Figure 8.8: Scanning electron micrographs for electrospun PLA-PEG composite fibrous membranes after 24 h contact with the T. reesei fungus suspension with different scale of magnification.	81
Figure 8.9: Magnetization setup with (a) schematic illustration of of PLA fibrous membrane under magnetic coil (b) photograph of the solenoid (coil-shaped heating station) with fiber inside. (Picture Courtesy: Prof. Kirschning, LUH, Hannover)	82
Figure 8.10: The on-demand local Rh6G delivery using PLA-PEG-NVCL-MNPs composite fibrous membrane induced by alternating magnetic field	83
Figure 9.1: Franz horizontal (Side-by-side) diffusion test apparatus (a) Schematic illustration of the horizontal Franz cell (b) lab developed set-up (Pictures: M. Kumar)	86
Figure 9.2: (a) Cross section sketch of the side-by Franz cell chamber with the diameters $a = 2.1$ cm and $b = 3$ cm (b) Digital image of the lab developed Franz cell (Picture: K. Smolik).	87

Figure 9.3: Modified vertical pressure cell, simulating blood pressure (Picture: K. Smolik and M. Kumar).....	87
Figure 9.4: PLA-HPC dry thin film shows red/green color (a) shows dark color in the shadow whereas bright color in light (b) thin film shows cloudy or milky appearance at 45°C (Picture: Prof. Dr. F. Renz)	91
Figure 9.5: Photometric measurements ($\lambda= 358$ nm) of a tetracycline hydrochloride release through a 200 μm thin film (94.85 wt.% PLA, 5.15 wt.% HMW-HPC) using a side-by-side Franz cell.....	92
Figure 9.6: Photometric measurements ($\lambda= 358$ nm) of a tetracycline hydrochloride release through a 200 μm thin film (94.85 wt.% PLA, 5.15 wt.% HMW-HPC) using a side-by-side Franz cell.....	92
Figure 9.7: Photometric measurements ($\lambda= 664$ nm) of a methylene blue release through a 200 μm thin film (98.85 wt.% PLA, 1.15 wt.% HMW-HPC) using a modified vertical Franz cell.....	93
Figure 9.8: Photometric measurements ($\lambda= 664$ nm) of a methylene blue release through a 50,100 and 150 μm thin film (89.7 wt.% PLA 6202, 10.30 wt.% LMW-HPC) using a modified vertical Franz cell.....	94
Figure 10.1: Thermal responsiveness of hydroxypropyl cellulose (HPC). (a) Photographs of aqueous solution (5 mg (HPC) / mL (H ₂ O)) sample at room temperature (RT) (b) and at 43°C (turbidity temperature) [207]......	98
Figure 10.2: A symmetric diagram shows temperature-responsive drug-release system [207]......	98
Figure 10.3: Scanning electron micrographs for electrospun (a) PLA (b) PLA-MEB (c) PLA-MEB-HPC composite fibrous membranes and (d) Average mean fibers diameter measurements [207]......	102
Figure 10.4: Drug release profile showing the cumulative drug release Vs time (min) of drug loaded (a) PLA fibers (b) PLA-HPC composite fibrous membranes [207]......	103
Figure 10.5: Schematics of cellulose repeat chain, showing the proposed hydrogen bonding (dotted line) with PLA.	104
Figure 11.1: The principles of the biosensors.....	105
Figure 11.2: Schematic illustration of an avidin molecule (2-fold symmetry) complexed with four biotins [157].....	106
Figure 11.3: Avidin tetramer with subunit is colored to red and blue according to dual chain avidin subunits [243]......	106

Tables List

Table 2.1: Some of the electrospun production sites.....	6
Table 2.2: History of electrospinning.....	8
Table 2.3: Important parameters for electrospinning experiments.....	9
Table 2.4: List of variable parameters affecting the characteristics of electrospun fibers.....	17
Table 2.5: Typical problems and their solutions during electrospun fiber formation	18
Table 3.1: Analysis of diffusional release mechanisms [75].....	24
Table 3.2: Some effects of various external stimuli, release mechanisms, advantages, limitations and examples.....	27
Table 4.1: Utilized chemicals, their abbreviation used and suppliers.....	32
Table 5.1: Characteristics of N-Vinylcaprolactam NVCL.....	48
Table 5.2: Characteristics of Hydroxypropyl cellulose (HPC).....	49
Table 6.1: Solubility of PLA with different solvent.....	50
Table 6.2: Miscibility of PLA (6202) with other biopolymers.....	51
Table 7.1: Summary of electrospinning conditions.....	62
Table 7.2: Thermogravimetric data table for PLA and PLA-PEG blend fibers [157]....	66
Table 7.3: Some materials based on magnetic polymer composites and their potential medical applications.....	68
Table 8.1: Summary of electrospinning conditions.....	72
Table 8.2: Comparative study of Raman main characteristic peaks for bulk and electrospun composite fibers as observed in Figure 8.4 and their tentative assignments	75
Table 8.3: DSC parameters for the thermal transitions of electrospun (a) PLA (b) PLA-PEG and (c) PLA-PEG-NVCL composite fibrous membranes.....	79
Table 10.1: A comparative studies on selected temperature-responsive materials with LCST behaviour for drug delivery applications.....	99
Table 10.2: Summary of electrospinning conditions.....	99

List of Journal Publications (2013-2017)

- I **M. Kumar**, A. Subramania and K. Balakrishnan, "Preparation of Electrospun Co_3O_4 Nanofibers as Electrode Material for High Performance Asymmetric Supercapacitors", *Electrochimica Acta*, (2014), 149, 152-158.
- II K. Balakrishnan, **M. Kumar**, A. Subramania, "Synthesis of Polythiophene and its Carbonaceous Nanofibers as Electrode Materials for Asymmetric Supercapacitors", *Advanced Materials Research*, (2014), 938, 151-157.
- III D. Unruh, P. Homenya, **M. Kumar**, R. Sindelar, Y. Garcia and F. Renz, "Spin State Switching of Metal Complexes by Visible Light or Hard X-Rays", *Dalton Transactions*, (2016), 45, 14008-14018.
- IV **M. Kumar**, R. Rahikainen, D. Unruh, V. P. Hytönen, C. Delbrück, R. Sindelar and F. Renz, "Mixture of PLA-PEG and Biotinylated Albumin enables Immobilization of Avidins on Electrospun Fibers", *J. Biomed. Mater. Res. Part A*, (2017):105A:356-362. **"Winner of the Society for Biomaterials Student Award in the Undergraduate Category, Charlotte, NC"**.
- V **M. Kumar**, D. Unruh, R. Sindelar and F. Renz, "Preparation of Magnetic Polylactic Acid Fiber Mats by Electrospinning", *Nano Hybrids and Composites*, (2017), 14, 39-47.
- VI **M. Kumar**, S. Klimke, A. Preiss, D. Unruh, D. Wengerowsky, R. Lehmann, R. Sindelar, G. Klingelhöfer, R. Boča, and F. Renz, "Electrospinning synthesis and characterization of PLA-PEG-MNPs composite fibrous membranes", *Hyperfine Interact* (2017), 238:66.
- VII **M. Kumar**, D. Wengerowsky, F. Böttcher, R. Sindelar, V. P. Hytönen, and F. Renz, "PLA-HPC Fibrous Membranes for Temperature-Responsive Drug Release", *Nano Hybrids and Composites*, (2017), 18, 34-41.

- VIII R. Lehmann, D. Wengerowsky, H. J. Schmidt, **M. Kumar**, A. A. Niebur, B.F.O. Costa, F. Dencker, G. Klingelhöfer, R. Sindelar and F. Renz; “Klimt Artwork: Red-Pigment Material Investigation by Backscattering Fe-57 Mössbauer Spectroscopy”, SEM and p-XRF, *Science and Technology of Archaeological Research*, (2017), <https://doi.org/10.1080/20548923.2017.1399332>.

Part of this work has been presented by the author:

Oral Presentations

Slovak University of Technology,

M. Kumar, R. Sindelar, F. Renz

2 – 3 Dec. 2014, *Bratislava, Slovakia; supported by PPP Slovakia – DAAD, 2014.*

Title: Preparation and characterization of stimuli responsive nanofibers

Tampere University of Applied Sciences,

M. Kumar, R. Sindelar, F. Renz

11th Dec. 2014, *Tampere, Finland; supported by HSN – LUH, 2014.*

Title: Stimuli responsive nanofibers and their biomedical applications

ICMM (2016), The University of Tokyo,

F. Renz, **M. Kumar**, R. Saadat, R. Sindelar, and G. Klingelhöfer

9 – 10 Sep. 2016, *Tokyo, Japan; supported by MWK – Japan, 2016.*

Title: Stimuli-Responsive Drug Release

PDSTM (2016), The University of Valencia,

F. Renz, **M. Kumar**, R. Sindelar, et al.

27 – 30 Nov. 2016, *Valencia, Spain*

Title: Stimuli-Responsive Drug Release: Selectivity via Vitamin K

Slovak University of Technology,

M. Kumar, R. Sindelar, F. Renz

10 – 15 Dec. 2016, *Bratislava; supported by PPP Slovakia – DAAD, 2016.*

Title: Energy Transfer and –conversion by Functionalized Nano-Bio-Fibers

Poster Presentations

Hannover Messe,

M. Kumar, R. Sindelar, F. Renz

7 – 11 Apr. 2014, *Hannover, Germany*

Title: Biopolymer Nanofibers

NanoDay 2015,

M. Kumar, D.Unruh, R. Sindelar, F. Renz, et al.

1st Oct. 2015, *Hannover, Germany*

Title: Surface Functionalized Electrospun Magnetic Nano-Bio-Fibers

International Conference Applied Natural Sciences 2015,

D.Unruh, **M.Kumar**, L.Heyer, F. Renz, et al.

30 Sep. – 2 Oct. 2015, *Jasná, Slovak Republic*

Title: Switching and Addressing of Molecular Switches in Magnetic Nanoparticles in Nanoscopic Fibers

The International Chemical Congress of Pacific Basin Societies,

D.Unruh, **M.Kumar**, L.Heyer, T.Meyer, B.Dreyer, F. Renz and R.Sindelar

15 – 20 Dec. 2015, *Honolulu, Hawaii, USA*

Title: Optical Switching and Addressing of Molecular Switches in Nanoscopic Fiber

Engineering and Life (Volkswagen Foundation),

M. Kumar, V.P. Hytönen, R. Sindelar, F. Renz

19 – 21 Oct. 2016, *Hannover, Germany*

Title: Electrospun Biofibrous Membrane for Biosensor Applications

The International Conference on the Applications of the Mössbauer Effect,

M. Kumar, A. Preiss, D. Wengerowsky, R. Sindelar, G. Klingelhöfer, F. Renz

03 – 08 Sep. 2017, *St. Petersburg, Russia*

Title: Magnetic polylactic acid fibrous membrane studied via Mössbauer spectroscopy for biomedical applications

Supporting Information

Confocal microscopy

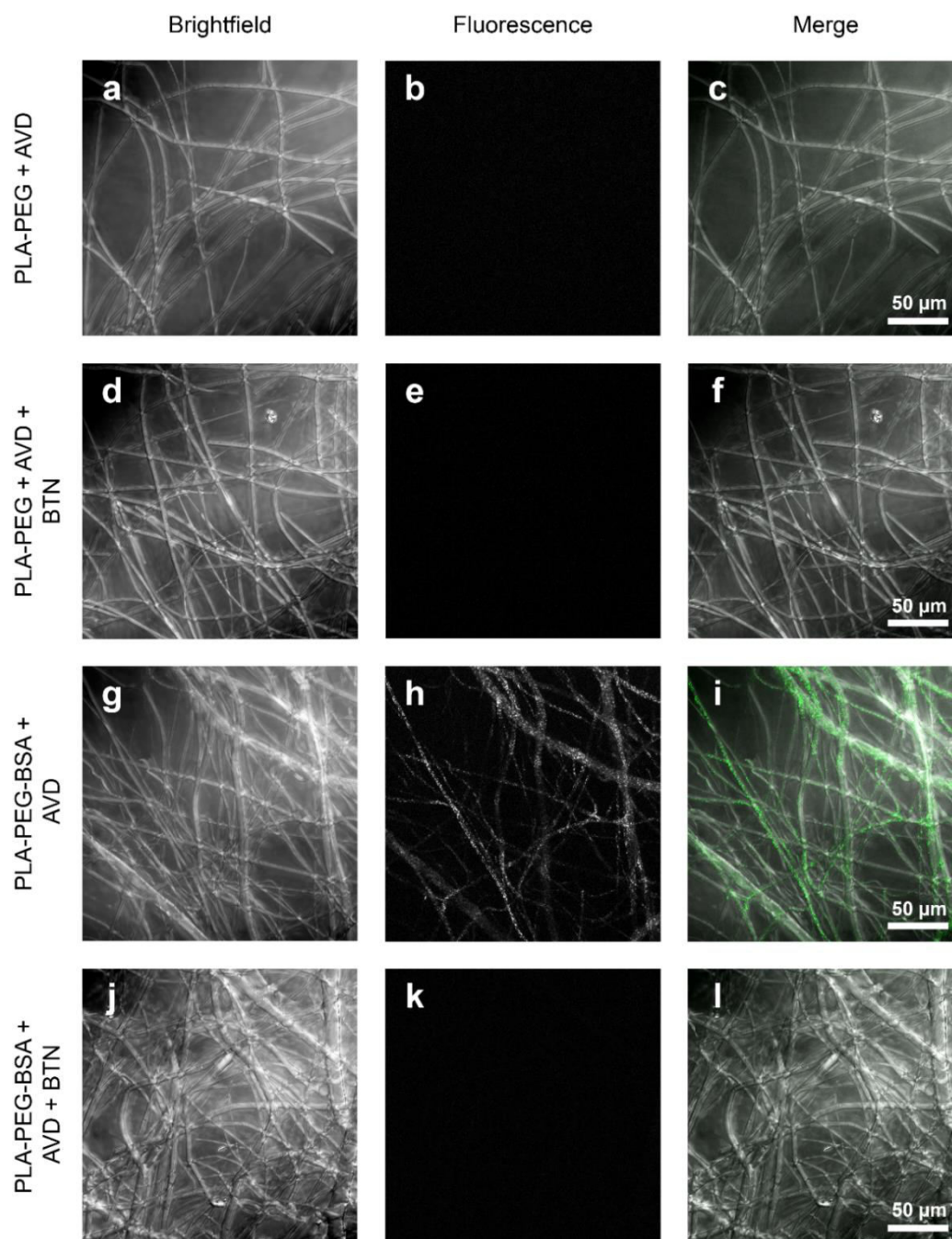


Figure I (a) Shows a fluorescent confocal microscopy image of the PLA-PEG fibers. (b) The same fibers were immersed in fluorescently labelled avidin solution and fluorescence at 488 nm was measured. (c) PLAPEG fibers merged with fluorescently labelled avidin, which clearly indicate no immobilization of avidin on the PLA-PEG fibers because the biotin binding sites in avidin were not present. (d-f) The non avidin immobilized PLA-PEG fibers were treated with excess of biotin. There were no blocking occurred due to unavailability of avidin molecules. (g-l) The same analysis as in (a-f) was conducted for PLA-PEG fibers containing biotinylated BSA, which clearly indicate immobilization of avidin on fibers. (j-l) indicates the same analysis, where the immobilized avidins are blocked with excess of free biotin.

Franz Cell Apparatus

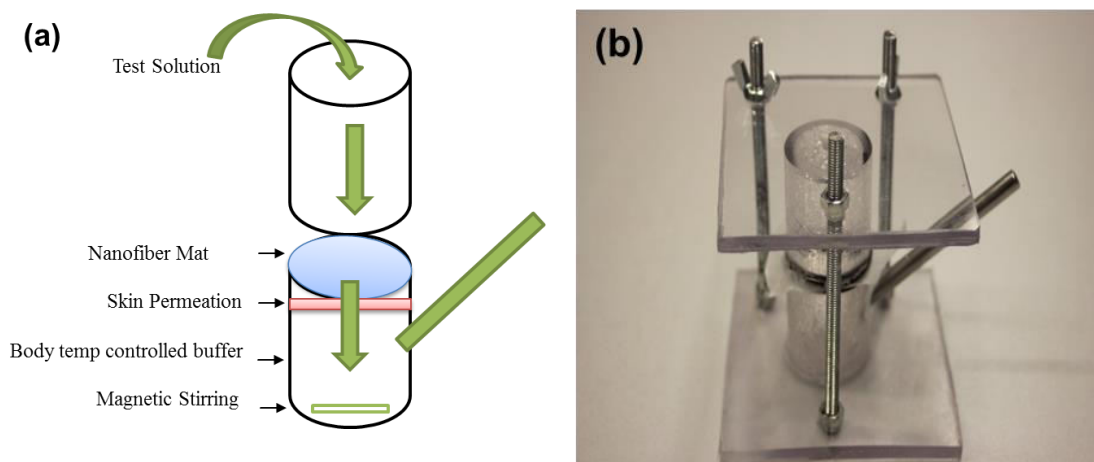


Figure II: Franz diffusion cell (a) basic model (b) lab developed apparatus (Pictures: M. Kumar)

FTIR spectral studies of PLA fibers

The infrared spectrum of PLA fibrous membranes was determined by Fourier Transform Infrared (FT-IR) as shown in Figure 2. Table 1, shows a comparison of PLA fibers data with the data published in the review paper by Auras et al. and by Furukawa et al.

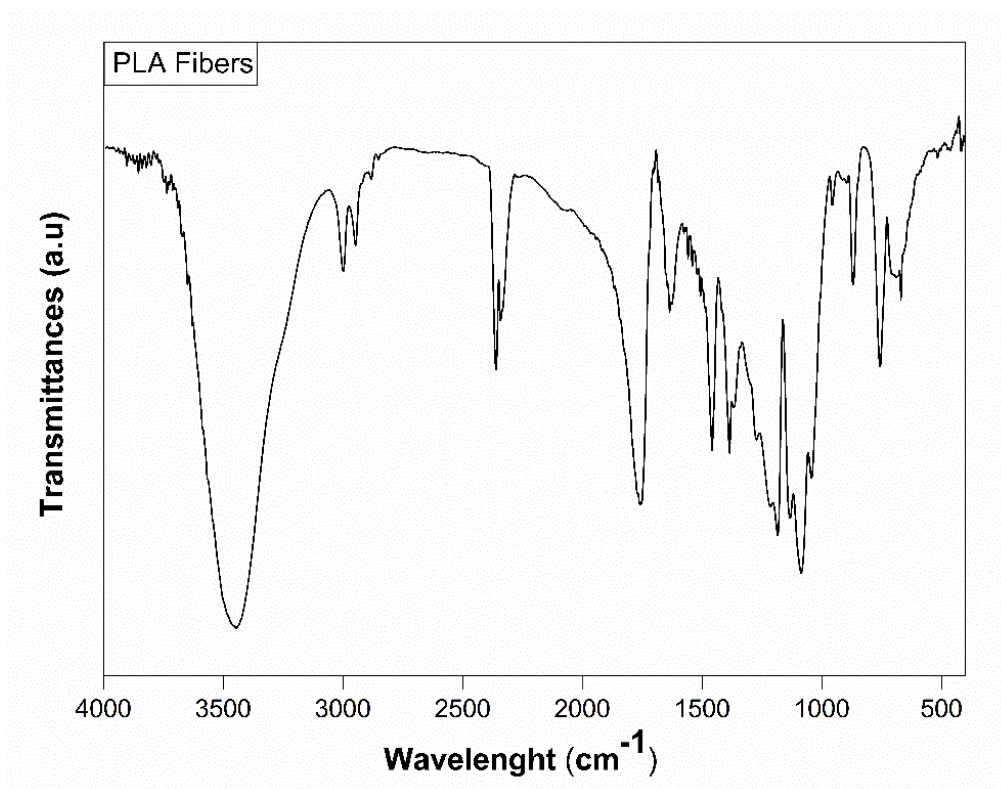


Figure III: FTIR absorption spectrum of PLA fibrous membranes

Table I: Comparative studies of infrared spectroscopy peak band assignment for PLA and its fibers

Assignment	Peak Position (cm ⁻¹)		
	Furukawa et al. [244]	Auras et al. [106]	PLA fibers
-OH stretch (free)		3571	3453
-CH-stretch		2997 (asym), 2946 (sym), 2877	2996 (asym), 2944 (sym), 2880
-C=O carbonyl stretch	1752 (C), 1744 (A)	1748	1756
-CH ₃ bend	1450 (asym), 1380 (sym), 1356 (sym, C)	1456	1458
-CH- deformation (symmetric and asymmetric bend)	1356, 1256 (A)	1382, 1365	1384
-C=O bend		1225	
-C-O- stretch	1265, 1210 (C), 1179, 1080	1194, 1130, 1093	1184
-OH bend		1047	1090
-CH ₃ rocking modes	1125	956, 921	
-C-C- stretch	1044	926, 868	874

C= Crystalline; A= Amorphous.

Liquid crystal (LCs)

Liquid crystal (LCs) is a state of matter that is intermediate between the solid crystalline and the ordinary (isotropic) liquid phases. It is also known as mesomorphic state (meaning intermediate form) or liquid crystals.

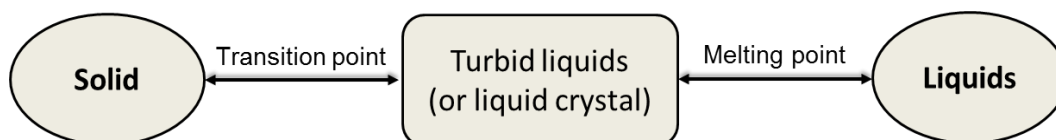


Figure IV: Liquid crystals lies between solid and liquid

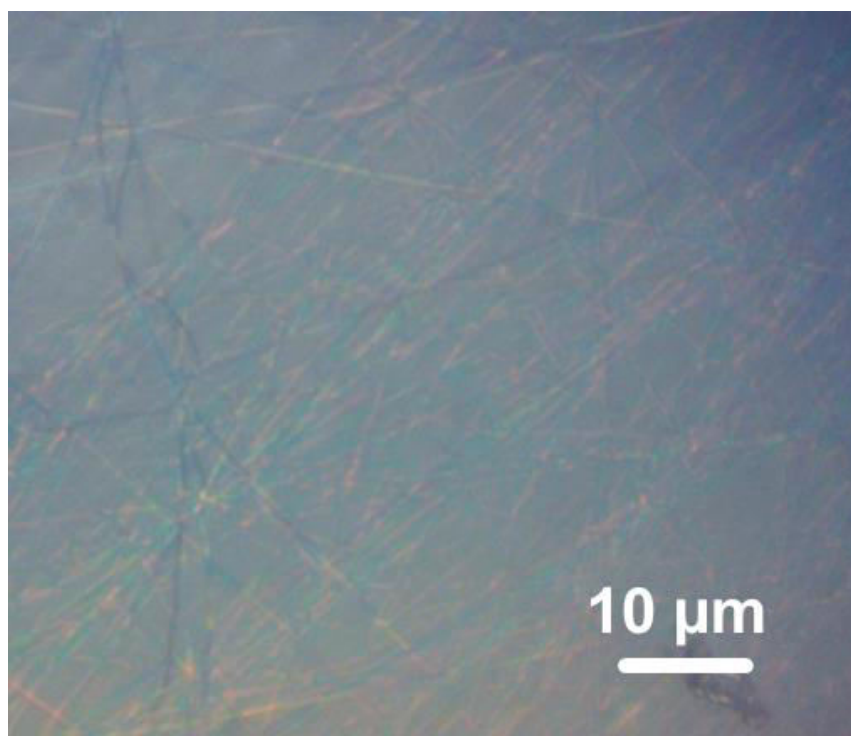


Figure V: Optical micrograph image of PLA-HPC fibrous membranes. The dichroism caused by the optical activity of the HPC can be seen.

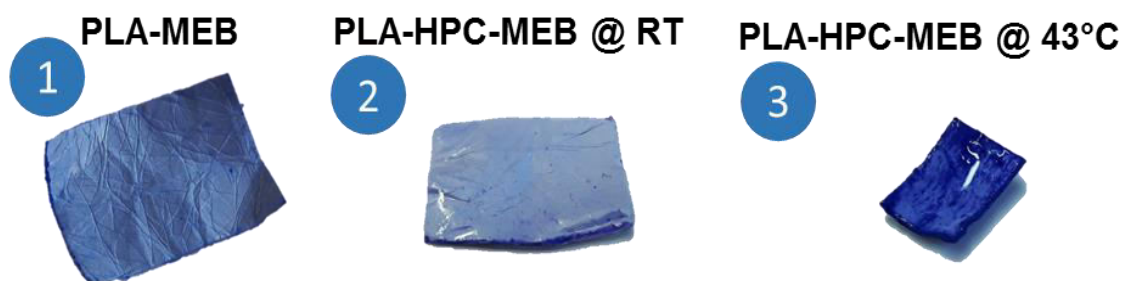


Figure VI: Digital image of (1) PLA-MEB fibrous membrane (2) PLA-HPC-MEB fibrous membrane at room temperature and (3) PLA-HPC-MEB fibrous membrane at 43°C.

SEM image of Cellulose acetate - PLA core-shell fibrous membranes

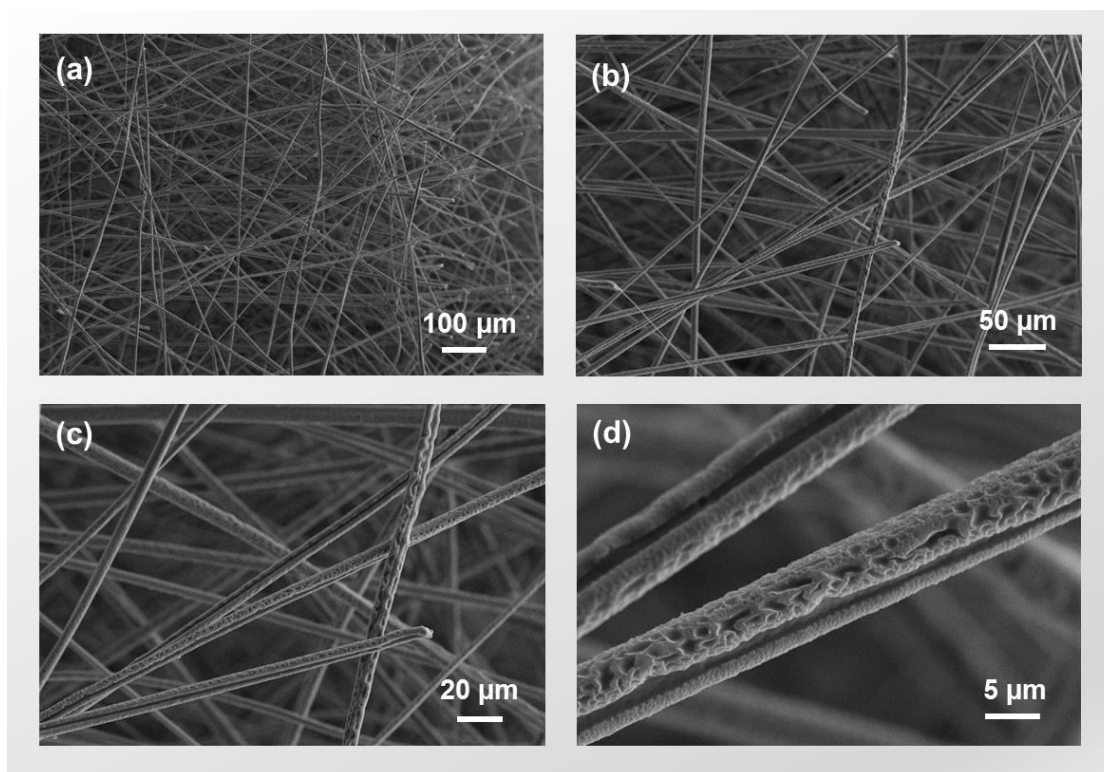


Figure VII: Morphology of the cellulose acetate - PLA core-shell fibrous membranes with different magnifications

SEM image of magnetic PLA fibrous membranes

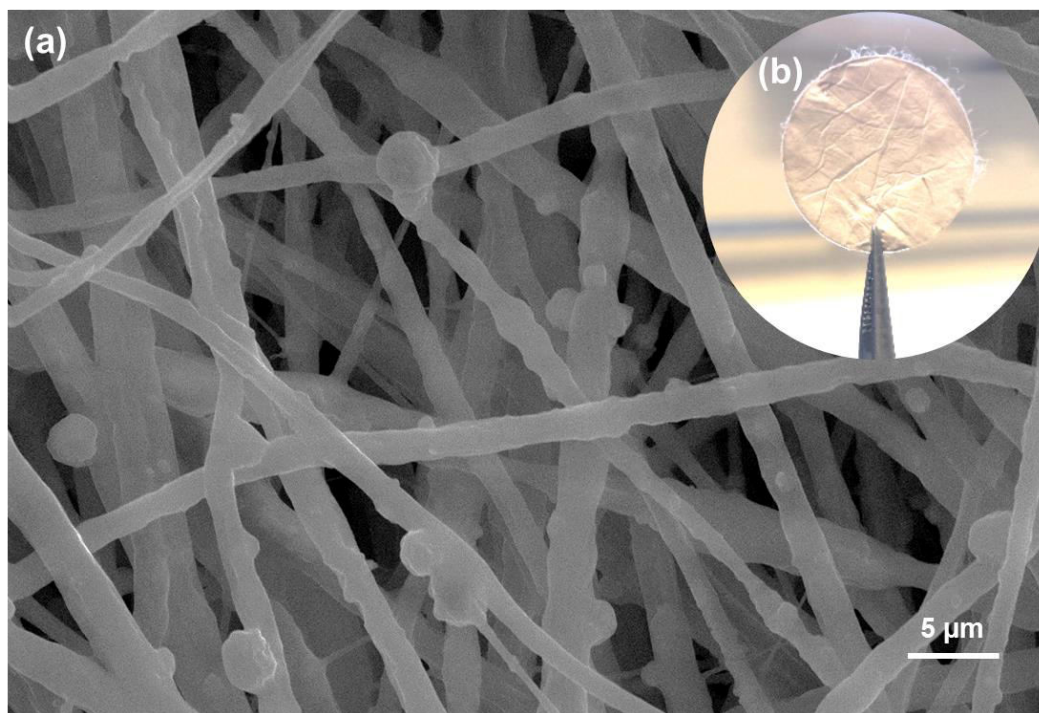


Figure VIII: Morphology of the magnetic PLA fibrous membranes (a) SEM images (b) digital images of the membranes.

Preparation of Phosphate Buffered Saline (PBS)

PBS has many applications since the solution is isotonic and not harmful to cells. It can be used to dilute the substance for drug delivery application.

1. Dissolve the following chemicals in 800ml distilled H₂O.

8.0g of NaCl
0.2g of KCl
1.44g of Na₂HPO₄
0.24g of KH₂PO₄

Table 2 shows a literature review on PLA based electrospun fiber membrane mainly for biomedical applications.

Tetracycline hydrochloride (TCH) release from PLA-HPC thinfilm membrane

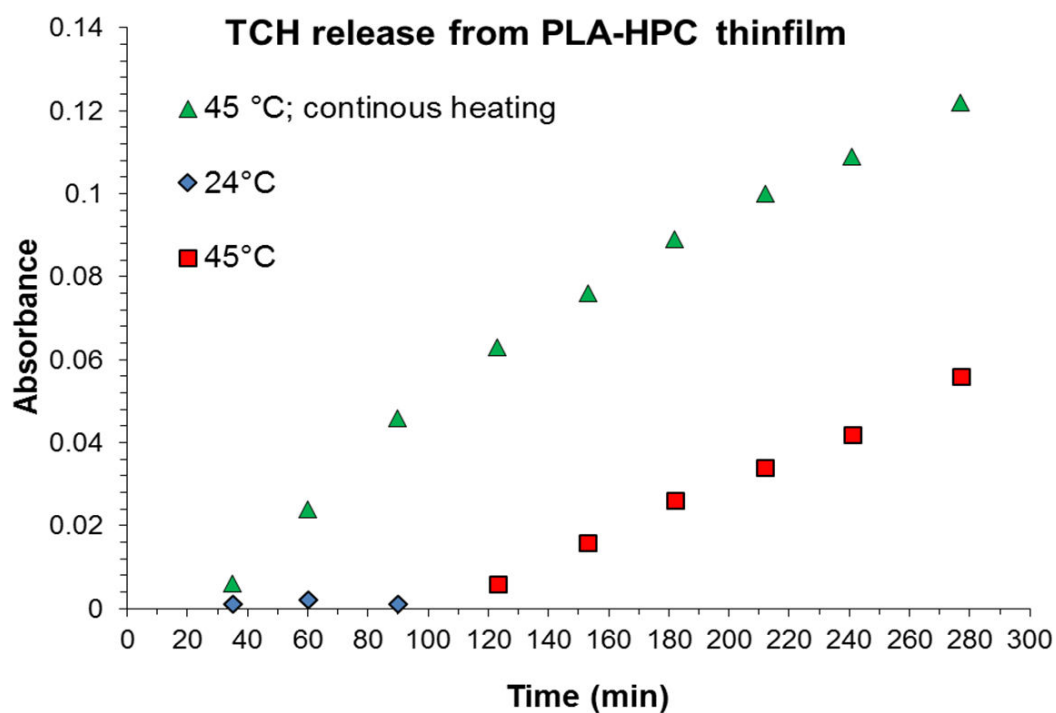


Figure IX: TCH release or transport from donor compartment to receptors compartments (Franz Cell) through PLA-HPC thin film membrane at 24°C, 45°C and changing between them (24 – 45 °C).

Mössbauer analysis

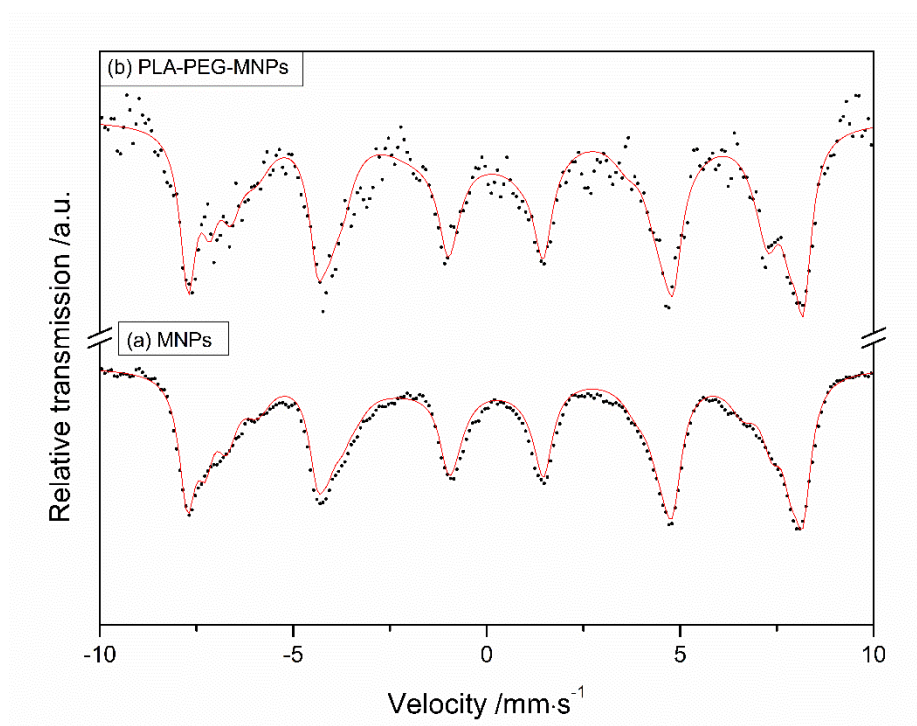


Figure X: Mössbauer spectra of (a) Magnetic nanoparticles (MNPs) and (b) PLA-PEG-MNPs composite fibrous membranes measured at room temperature [222].

Table II: Literature review on PLA electrospun fibers, year workers and process highlight

Year	Researchers	Process highlight
2002	Kenawy et al. [223]	Fibers electrospun from chloroform solutions containing a small amount of methanol to solubilize drug
2003	Zong et al. [245]	A mechanism of structure, morphology and property changes during in vitro degradation of electrospun PLGA nanofibers was proposed
2005	You et al. [246]	Fabrication of nanofiber matrices. Optimum solution concentration for fiber formation is 5 wt%
2006	Tsuji et al. [247]	Stereocomplex nanofibers of high molecular weight PLLA/PDLA = 1:1 was prepared and suppresses the formation of homo-crystallites

2007	Kim et al. [248]	Produce blending nanofibers made of PLA and gelatin to improve the cellular responses of PLA
2008	Iwatake et al. [23]	Green-composites of PLA/cellulose nanofibers were reported. Mechanical and thermo-mechanical properties were studied
2009	Ishii et al. [249]	PLLA and stereocomplexed PLA nanofibers was implanted in rats for 4 – 12 weeks. stereocomplexed PLA nanofiber caused milder inflammatory reaction than PLLA nanofiber
2010	Noh et al. [250]	Small concentration of the bioactive glass was incorporated in PLA nanofibers. Osteoblastic cells were demonstrated to adhere on composite nanofibers
2011	Peng et al. [251]	Highly porous hydroxyapatite (HA)/PLLA nanofibers were fabricated. Cell morphology viability and alkaline phosphatase (ALP) activity were examined.
2012	Mai et al. [252]	Curcumin incorporated (5 wt%) PLA nanofibers were fabricated and used for biomedical application
2013	Wang et al. [253]	PLA/chitosan core/shell nanofibers were fabricated and potentially be used as vascular gasket
2014	Wagner et al. [152]	Blends of PLLA and PHBV in chloroform/DMF were electrospun and optimal electrospinning conditions were determined.
2015	Lee et al. [254]	PLA nanofiber was used as a piezoelectric sensor material to operate LEDs.
2016	Goh et al. [255]	PLA/Chitosan nanofibers were coated with functional bioglass and used for <i>in-vitro</i> bioactivity
2017	This work [159] [157] [222] [207]	PLA, PEG, HPC, NVCL and BSA based composite fibrous membranes were fabricated and used for biomedical applications

Declaration

Herewith, I confirm that I have written the present PhD thesis myself and independently, and that I have not submitted it at any other university worldwide. All used sources have been cited.

Hannover, 30 May 2017

Curriculum Vitae

Manish Kumar

Biographical Information

Date of birth 8 - January - 1990
Nationality Indian

Education and Professional Experience

10/2013 – 10/2017 Doctor of Natural Sciences (PhD) at the Institute for
Inorganic Chemistry, Gottfried Wilhelm Leibniz Universität
Hannover in the group of Prof. Dr. Franz Renz

Title: “Energy Transfer and -Conversion by Functionalized
Nano-Bio-Fibers for Biomedical Applications

07/2011 – 05/2013 Master of Technology (**Distinction**)

Pondicherry University, Puducherry, India

International Cooperation

12/2014 University of Tampere, BioMediTech, Lääkärintätkatu 1,
Finland in the group of Associate Prof. Vesa Hytönen

Award

**“Winner of the Society for Biomaterials Student Award in the Undergraduate
Category, Charlotte, NC” USA.**